2038-5625

Italian Journal of Agrometeorology

Rivista Italiana di Agrometeorologia

n. 2 – 2025

Italian Journal of Agrometeorology

n. 2 - 2025

Firenze University Press

The ***Italian Journal of Agrometeorology*** (***IJAm - Rivista Italiana di Agrometeorologia***) is the official periodical of the Italian Association of Agrometeorology (AIAM) and aims to publish original scientific contributions in English on agrometerology, as a science that studies the interactions of hydrological and meteorological factors with the agricultural and forest ecosystems, and with agriculture in its broadest sense (including livestock and fisheries).

https://riviste.fupress.net/index.php/IJAm
ISSN 2038-5625 (print) | ISSN 3103-1722 (online)

Italian Association of Agrometeorology (AIAM)
Presidente: Simone Orlandini (simone.orlandini@unifi.it)
Vicepresidente: Gabriele Cola
Consiglieri: Marina Baldi, Claudio Cassardo, Carmelo Maucieri, Federico Spanna, Danilo Tognetti, Leonardo Verdi
Revisori dei conti: Andrea Cicogna, Marco Secondo Gerardi, Emanuele Scalcione
Segreteria: Simone Falzoi, Emanuela Forni, Tiziana La Iacona, Mattia Sanna, Irene Vercellino
e-mail AIAM: segreteria@agrometeorologia.it
Sede legale: via Caproni, 8 - 50144 Firenze
web: www.agrometeorologia.it
e-mail Italian Journal of Agrometeorology: ijagrometeorology@agrometeorologia.it

SUBSCRIPTION INFORMATION
IJAm articles are freely available online, but print editions are available to paying subscribers. Subscription rates are in Eur and are applicable worldwide.
Annual Subscription: € 50,00 Single Issue: € 25,00

CONTACT INFORMATION
Please contact ordini@fupress.com, if you have any questions about your subscription or if you would like to place an order for the print edition. Information on payment methods will be provided after your initial correspondence.

Published by Firenze University Press

Firenze University Press
Università degli Studi di Firenze
via Cittadella, 7, 50144 Firenze, Italy
www.fupress.com

Italian Journal of Agrometeorology
Rivista Italiana di Agrometeorologia

Firenze University Press
https://riviste.fupress.net/index.php/IJAm

OPEN ACCESS

Citation: Parisi, S. G., Alimonti, G., & Mariani, L. (2025). Mean and extreme precipitation regime in North and Central Italy – between stability and change. *Italian Journal of Agrometeorology* (2): 3-22. doi: 10.36253/ijam-3315

Received: February 8, 2025

Accepted: August 7, 2025

Published: December 31, 2025

Data Availability Statement: All relevant data are within the paper and its Supporting Information files.

Competing Interests: The Author(s) declare(s) no conflict of interest.

ORCID:
GA: 0000-0002-7128-9046

Mean and extreme precipitation regime in North and Central Italy – between stability and change

Simone Gabriele Parisi[1,*], Gianluca Alimonti[2], Luigi Mariani[3]

[1] *DIAGRAM S.p.A, Via Cavicchini 9, 44037 Jolanda di Savoia (FE), Italy*
[2] *INFN, Dipartimento di Fisica, Università degli Studi di Milano, Via Celoria 16, 20133 Milano, Italy*
[3] *DICATAM, Università degli Studi di Brescia, Via Branze, 43, 25123 Brescia*
*Corrisponding author. E-mail: s.parisi@diagramgroup.it

Abstract. The work was carried out on the gridded precipitation dataset of the ARCIS consortium (hereafter ARCIS) that was produced spatializing a daily dataset of 1762 stations coming from 7 regions of Northern Italy and three regions of Central Italy for the period 1961-2023, with a pixel of 4.7 x 4.7 km. The mean yearly precipitation value from 1961 to 2023 shows a large interannual variability. On the other hand, the trend in frequency and intensity of extreme events (daily events above 50 mm) exhibit high space and time variability. Highlighting areas with significant or not significant trends is crucial for designing hydraulic infrastructures and managing the impacts of natural risks such as floods and landslides. Overall, results reveal that 83% and 86% of the areas do not show significant increases respectively in frequency and intensity while 11% and 15% show significant increases and 2% and 3% show significant decreases. Moreover, the spatial pattern of the areas affected by increasing frequency and intensity, highlights the presence of some regions characterized by increasing trend in North Italy at the beta mesoscale (20-200 km) which is the theatre of phenomena like mesocyclones or low-level jets. Finally, it should be noted that the 1991-2023 analysis of seasonal variations highlights a frequency increase of extreme phenomena in autumn (from October to December with a more marked increase in November), a weak decrease from January to April and a marked decrease in August. These variations can be interpreted as the result of the interaction of the synoptic circulation with mesoscale effects triggered by orography and sea surface temperature.

Keywords: extreme events, precipitation climatology, gridded precipitation dataset, frequency and intensity trends.

INTRODUCTION

Jacqueline Katz, the 2022-2023 Albert Einstein Distinguished Educator Fellow at the Library of Congress, wrote in a 2023 post that "*In all scientific disciplines, there are examples of stability and change. Stability refers to the tendency of an object or system to stay the same, while change occurs when objects or systems become different. Changes that occur in the various scientific disciplines can happen over extremely short or long-time intervals*" (Katz,

2023). In climatology, which is the science of the climate system, this very general consideration refers to climate variability and change as products of the internal system variability or the response to changes in natural and anthropogenic forcings. In this context, variations in mean and extreme precipitation regime are a relevant aspect, due to their strong impacts on natural and anthropized ecosystems. In fact, precipitation related phenomena like floods, erosional processes and landslides result in strong damage to populations and human activities like agriculture, industry, transportation and tourism (IPCC, 2023).

Italy pertains to the Mediterranean basin and has more than 8000 km of coasts. Therefore, the sea influence on the area precipitation framework is mighty. It should be mentioned that the analysis of trends in maximum values for stations in the Mediterranean basin carried out by Sun et al. (2021) indicate that about 4% of the stations in the area have a significant upward trend in absolute yearly maxima while about 4% manifest a significant decrease. Basically, a relative stationarity is seen in extreme rainfall events, which is also highlighted by the IPCC future scenarios where it is stated: "*Observations have a seasonal and regional pattern consistent with projected increase of precipitation in winter in Northern Europe. A precipitation decrease is projected in summer in the Mediterranean extending to northward regions. Extreme precipitation and pluvial flooding are projected to increase at global warming levels exceeding 1.5°C in all regions except the Mediterranean (high confidence).*" (IPCC_AR6_WGI_Regional_Fact_Sheet_Europe.pdf).

Climatological analysis of precipitation is typically performed using rainfall stations time series. As an example of this approach, we can cite the analysis of a large dataset of daily rainfall data from stations in the Euro-Mediterranean area for the period 1973-2010 carried out by Mariani and Parisi (2013). The authors, using the analysis scheme proposed by Alpert et al. (2002), demonstrated the groundlessness of "*the paradoxical increase of Mediterranean extreme daily rainfall in spite of decrease in total values*" inferred by Alpert et al. (2002).

On the Italian area, a very detailed work was carried out by a research group at Politecnico di Torino on more than 4500 rainfall stations spanning the period between 1916 and 2014 (Libertino et al., 2018). The analysis of trends on 1-, 3-, 6-, 12- and 24-hour precipitation dataset highlighted that: "*increasing rainfall extremes remains elusive at large spatial scales*" (Libertino et al. 2019). More specifically, on the frequency, the outcomes show that all the observed trends are not significant, that is compatible with the hypothesis of stationary climate. Meantime, concerning the intensities of the events, a clear trend in extreme rainfall values cannot be detected at the country-scale. It's worth noting that trends are significant in some specific areas and periods. The abovementioned paper has received considerable attention from the scientific community, and it is cited in the AR6 (IPCC, 2023).

Fatichi and Caporali (2009), working on the rainfall time series of 785 stations in Tuscany for the period 1916-2003, highlighted the absence of trends in the mean rainfall regime and intensity of 3-, 6- and 12-h extreme events in almost all the stations analyzed. This conclusion agrees with Pinna (2014) which worked on extreme rainfall for stations of the Mediterranean area and Tuscany.

Bassi et al. (2011), working on 45 stations of the ARPA network and 47 stations of the former SIMN network, analyzed heavy rainfall for Piemonte (Italy) over the time period 1930-2004 and for durations of 1-,3-,6-, 12- and 24-h. Results highlight that spatial distribution shows no significant variations with main maxima in the northern alpine and pre-alpine sectors and secondary maxima in the southern mountain ranges. About the intensity trend, the 47 SIMN stations showed a clear predominance of negative trends for durations of 1 hour and a slight predominance of positive trends for durations of 24 hours while for durations of 3,6 and 12 hours the trends were about 50% negative and 50% positive. On the other hand, the 45 ARPA stations showed negative trends for more than 50 percent of the stations. Overall, the analysis conducted by Bassi et al. (2011) didn't highlight preferential areas where positive or negative trends dominate.

Brunetti et al. (2010) analyzed daily extreme precipitation trends for 129 stations in Calabria (1920-2005) and showed a precipitation decrease in the higher intensity categories and an increase in the lower categories, especially in the winter period. These trends were highly dependent on the subperiod considered, with negative trends prevailing after 1950.

It should also be reminded that the Italian territory is by nature exposed to a lot of synoptic and mesoscale factors favorable to extreme precipitation events: the high frequency of synoptic blocking patterns (Barton et al., 2022) and the closeness of regions sources of cold (Polar Continental, Polar Maritime, Arctic Continental and Arctic Maritime). Moreover, it must be considered the Mediterranean basin, source of humid air masses, and the presence of the complex geomorphology of the Alps and the Apennines that is favorable to the convergence and rise of air masses.

Doswell et al. (1996) gave an effective description of mesoscale factors favorable to continued high

rates rainfall events. In turn, "high precipitation intensity" involves the rapid ascent of low-level air containing substantial water vapor and depends on the precipitation efficiency (ratio of the amount of rainfall that reaches the ground to the amount of rainfall formed in the storm). Moreover, the "long duration" of an event is associated with its movement speed and the size of the system causing the event along the direction of system movement. This naturally leads us to explore the meteorological processes that combine these fundamental elements to generate weather events. Describing these processes and the types of storms that produce heavy precipitation, reveals the many different ways such events can occur. Since the right mixture of these ingredients can be found in a wide variety of synoptic and mesoscale situations, it is necessary to know which of the ingredients is critical in any given case. For example, in the specific case of the flood that hit the surroundings of Valencia (Spain) on 29 October 2024 (Pucik, 2024) with a 14 hours rainfall peak of 771.8 mm reached at Turis (26 km South-west of the city center of Valencia).

The precipitation intensity of the event was enhanced by the following forcing factors:

- high absolute moisture content in the lower troposphere rapidly advected towards the coast due to wind speeds up to 25 m/s in the bottom 500 m (low level jet).
- High potential for rapid vertical flux of moisture due to high Convective Available Potential Energy (CAPE)

On the other hand, "precipitation efficiency" (defined as the precipitate over precipitable water ratio) was enhanced by:

- low-cloud bases, and high relative humidity in the low to mid-troposphere, resulting in a low potential for rainfall evaporation
- relevant depth of the cloud available for the growth of raindrops through collision and coalescence, given by the large distance between the lifted condensation level and the 0° isotherm (the so-called deep warm cloud depth).

Bauer and Scherrer (2024) analyzed the long-term (1901-2023) evolution of daily and multi-day heavy precipitation intensity and frequency in Swiss, finding that daily maximum precipitation and the frequency of precipitation events exceeding the 99th all-day percentile have increased since 1901 with a peak in the 1980s and decreases thereafter. For the recent period 1981 –2023, positive trends in summer heavy precipitation intensity are detected for short (10-min to 3-h) events, but no changes are found for the frequency of these moderate extreme events. For longer (1- to 5-day) events on the other hand, decreases in intensity and frequency are found, especially for the winter half-year. This work highlights the importance of the reference period in trend analysis and the fact that precipitation trends are not only influenced by thermodynamics (increase in global temperatures) but also by the dynamics of circulation phenomena at different scales (Bauer and Scherrer, 2024).

It is worth noting that average or extreme precipitation analysis can now be performed with the aid of gridded datasets with variable spatial resolutions. Sun et al. (2017) carried out a comprehensive review of some global precipitation gridded data sets, with pixel ranging from 0.5x0.5 to 5x5 degrees. Gridded datasets covering the Italian area are the Alpine area dataset described by Isotta et al (2013) or the ARCIS gridded dataset, covering North Italy and part of Central Italy (Toscana, Umbria and Marche administrative regions) (Pavan et al., 2013).

In this work we aim to analyze the spatial distribution and trends in 24-hour extreme precipitation recorded in North and Central Italy in the period 1961-2023 and collected by the ARCIS daily dataset with the purpose of providing useful insights for land use management.

DATA & METHODS

The work was done analyzing data from the Climatological Archive for North and Central Italy by the ARCIS consortium (https://www.arcis.it/wp/). This archive is the result of an agreement between some regional meteorological services belonging to the following public bodies: ARPA Piemonte, ARPAL, ARPA Emilia Romagna, ARPA Lombardia, ARPA Veneto, Provincia Autonoma di Trento, Provincia Autonoma di Bolzano, Regione Autonoma Valle D'Aosta, ARPA Friuli-Venezia Giulia (Fig. 16). This agreement aimed to the establishment and management of an historical daily precipitation database (Pavan et al., 2013). The ARCIS database contains daily precipitation data from 1961 to 2023, spatialized on 4.7 x 4.7 km cells for a total of 7605 cells and it is an effective tool for understanding the precipitation evolution over North-Central Italy.

As indicated by Pavan et al. (2018), the data come from 1762 stations located in the ARCIS consortium areas, from stations belonging to 11 Italian administrative regions (Piemonte, Valle d'Aosta, Liguria, Lombardia, Emilia Romagna, Veneto, Trentino Alto Adige, Friuli Venezia Giulia, Toscana, Umbria, and Marche), and from stations close to the Italian borders belonging to foreign national meteorological services. The ARCIS area covers 189343 km^2 and there is one station every 107.47 km^2 on average, despite the presence of significant

inhomogeneities in the stations spatial distribution. The ARCIS data collection is frequently updated and at present spans from 1961 to 2023.

The time series was constructed by joining several stations that did not overlap in time, selecting stations that cover at least 80 percent of the analysis period. The Italian data come partly from the former National Hydrographic Service and subsequently from various local and regional services.

Precipitation data were interpolated on a regular grid of 4.7 x 4.7 km using a method based on a modified Shepard algorithm (Antolini et al., 2015) that considers topographic distances between stations and the interpolation error was evaluated using a cross-validation technique.

Errors were analyzed according to season and altitude. Low-intensity events tend to be overestimated in low-elevation areas, while high-intensity events are often underestimated, especially in winter. The final product has improved performance in mountainous areas and regions with high station density.

The whole process allowed the construction of a homogeneous and consistent database suitable for describing not only average precipitation values, but also their spatial and temporal variability, which is essential for climate and impact studies.

This paper analyzes precipitations on the Arcis area to obtain an updated climatology referred to average, variability and extreme values for the whole dataset. Moreover, the extreme precipitation temporal trend over the ARCIS area has been analyzed, including the calculation of significantly positive and negative trends at the general level and pixel by pixel. More specifically:

- The intensity trend referred to yearly absolute maximum daily precipitation
- The frequency trend of the number of days per year when daily precipitation exceeds the 50 mm threshold, which can be considered a benchmark for extreme daily precipitation (Fig. 2.34 from: https://archive.ipcc.ch/ipccreports/tar/wg1/090.htm?).

Trend analysis was performed using the Mann Kendall test (Gilbert, 1987) that is a nonparametric methodology that allows trends to be analyzed without making assumptions about the data distribution.

This was supplemented by an analysis of the frequency and intensity percentage changes that occurred during 1991-2023 (33 years) compared with the 30-year period 1961-1990 by highlighting them in map products and frequency histograms. The choice of the two subperiods was dictated by the fact that 1961-1990 is still recommended by WMO for the computation and tracking global climate anomalies relative to a fixed and common reference period (World Meteorological Organization, 2021 - a) while the 1991-2023 subperiod is after the macroscale circulatory change of the ’80s, which global features are described by Reid et al., (2016) while European effects on selected crops are described in Mariani et al. (2012).

The significance of the differences in frequencies of different classes of precipitation in the subperiods 1961-90 e 1991-2023 has been evaluated using the Chi square test “SciPy-stats” library of Python (Skipper et al., 2010).

DATA ANALYSIS

Mean climatology

The total yearly average precipitation (period 1961-2023) of the ARCIS area is shown in Fig. 1. The map reveals the heavy influence of topography on the precipitation field. It is worth noting that mountainous regions (pre-Alpine areas and North Apennines) receive the highest rainfall, while plains, the interior of the Alps and coastal areas, experience lower precipitation. The mean yearly precipitation pattern is substantially stable over time, as demonstrated by the evident similarity to maps referred to previous periods 1921-50 (Mori, 1964), 1921-70 (Cati, 1981) and 1971-1990 (Frei and Schar, 1998). This is relevant to meet the water needs of agriculture and other socio-economic sectors.

The map in Fig. 2 shows the spatial distribution of standard deviation of yearly precipitation calculated for each pixel. The visual analysis shows the consistency with the mean values represented in Fig. 1: areas of maximum Alpine and Apennine rainfall are also those affected by a higher variability. By performing a correlation analysis between mean values and standard deviation of yearly precipitation, as a matter of fact we obtain a Pearson correlation coefficient of 0.8887 and a p-value less than 0.01 (highly significant).

The coherence between mean and standard deviation is also highlighted by the diagram in Fig. 3 which shows that the years with the highest mean precipitation are also those with the highest standard deviation. Both time series are stationary, as stated by the Mann Kendall test for mean (S : -133; Z : -0.7829; p (no trend): 0.43368) and standard deviation (S : 35; Z: 0.20166; p (no trend): 0.84018). The stationarity in an index of central tendency and variability allows to exclude the presence of signals of change in annual precipitation in the area.

The diagram in Fig. 3 shows also that four rainy years (1963, 2002, 2010 and 2014) exceed the 95th percentile, while four dry years are below the 5th percentile. This interannual variability is influenced by a wide range of precipitation-driving factors operating at different spatial and temporal scales. Among these factors a crucial

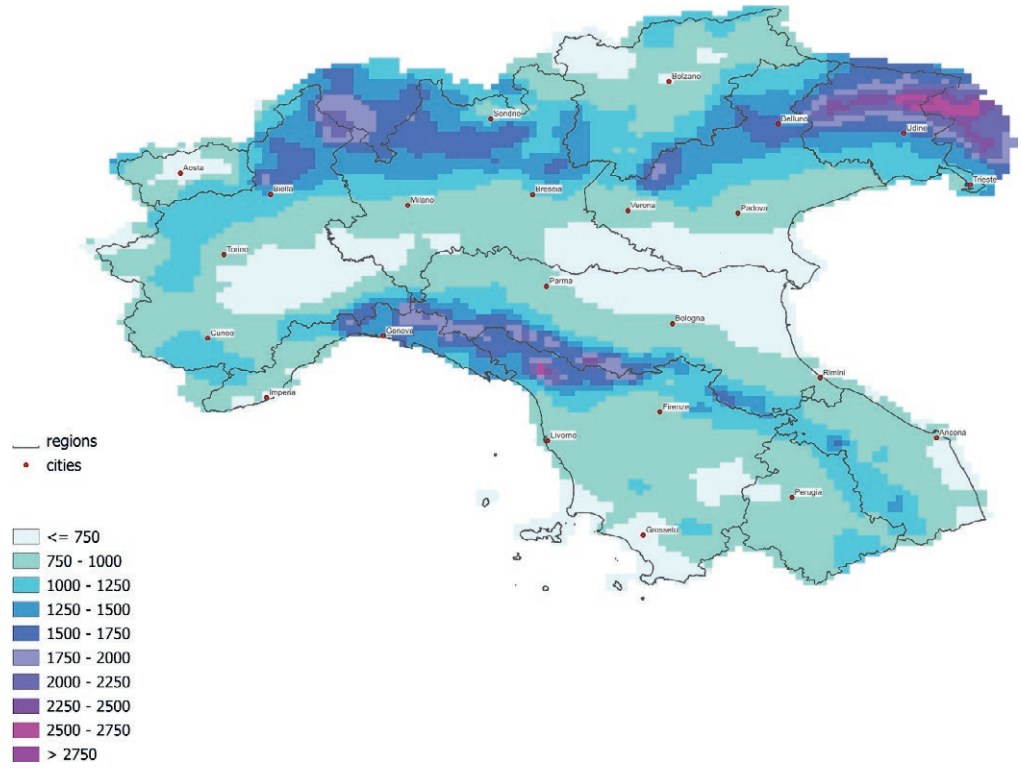

Figure 1. Map of the mean annual precipitation on the period 1961-2023.

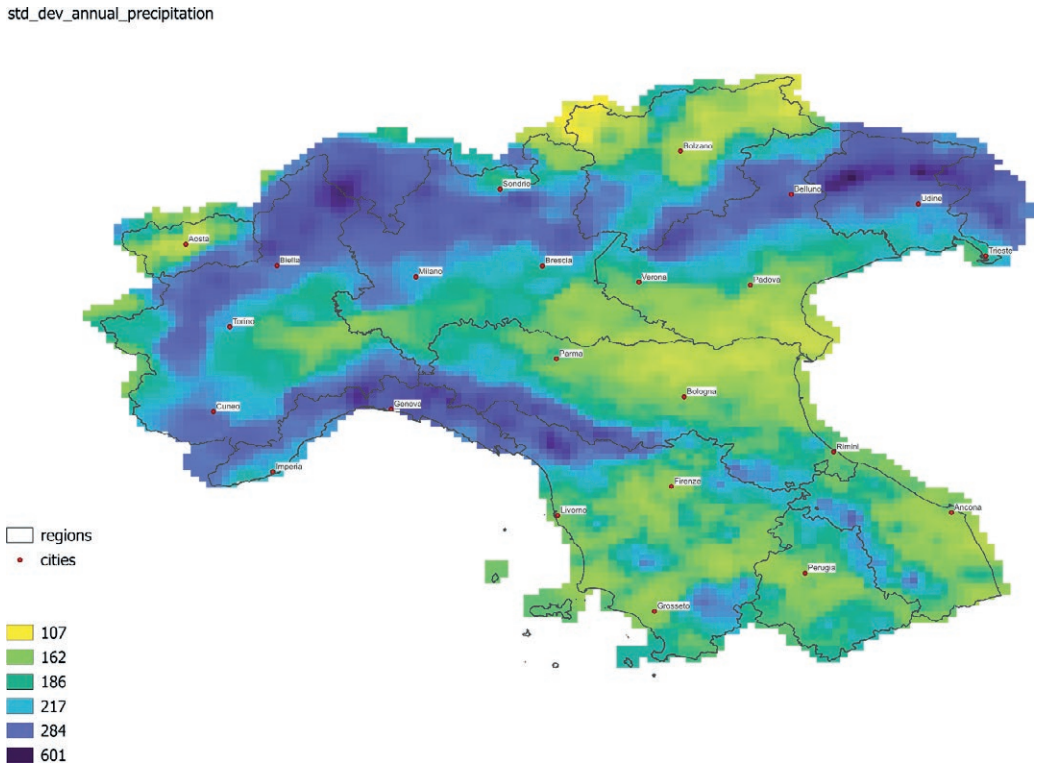

Figure 2. Map of the standard deviation that illustrates precipitation variability on the period 1961-2023.

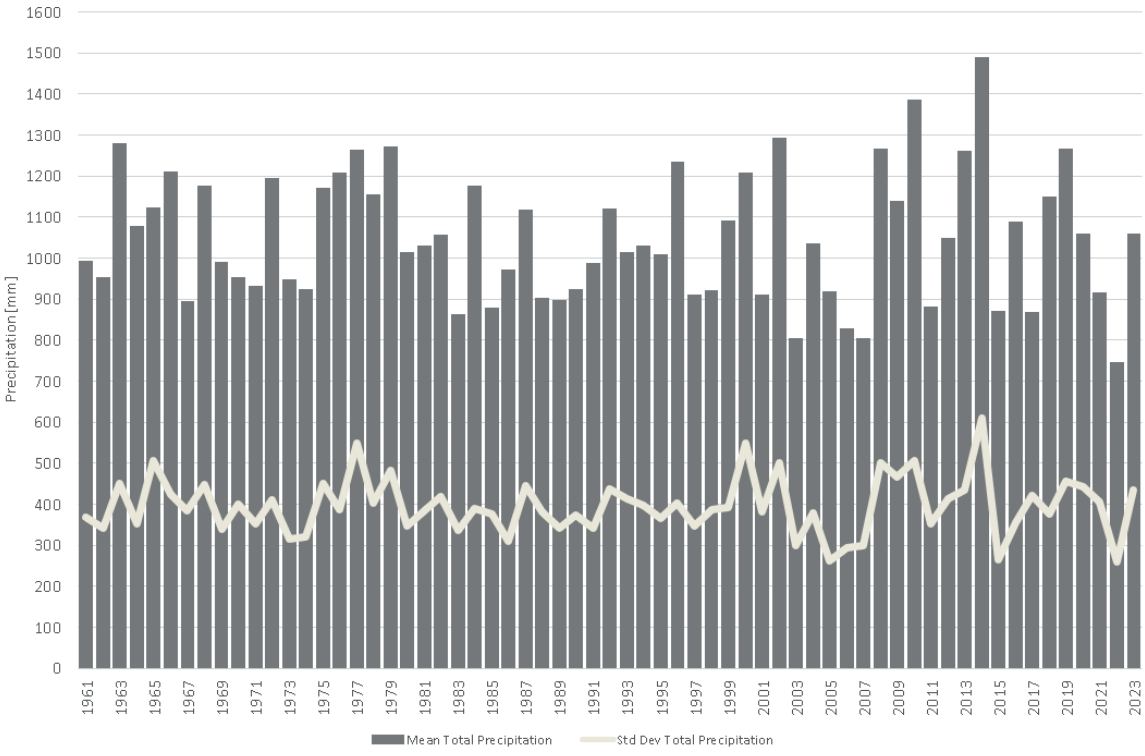

Figure 3. Plot of the total mean yearly precipitation and standard deviation on the whole ARCIS dataset area from 1961 to 2023. The two time series according to Mann-Kendall test have no significant trend.

role is played by the frequency and persistence variability of different macro- and mesoscale circulation weather types (Piotrowicz and Ciaranek, 2020). The weather at mid latitudes of our Planet is ruled by the annular circulation (westerlies) that produces a rapid alternation of anticyclonic (stable weather) and cyclonic weather types (perturbed weather). In this variability context, prolonged rainy phases or total absence of precipitation are also observable, which are the result of the periodic establishment of long-persistence blocking systems over the Euro-Atlantic area. An adaptation to this precipitation interannual variability is obtained by irrigation facilities that fed a complex system of irrigation channels and water storages dams in the Alpine and Apennine areas or natural reservoirs (pre-Alpine lakes: i.e. Maggiore, Como, Iseo, Idro and Garda) or rivers like Po, which storage capacity is enhanced by artificial barriers.

It is also interesting to note that human settlements in the ARCIS area, often very ancient, were established and developed with careful consideration about the spatial and temporal precipitation distribution, which has always imposed significant constraints on human life and activities. For example, the main urban centers in the ARCIS area are typically located in zones with moderate rainfall and near rivers, which are fed by areas with more intense and persistent precipitation from the surrounding highlands.

Regarding the mean precipitation climatology, the ARCIS dataset offers many possibilities for investigation at monthly and seasonal scales that could be the subject of future contributions. Focusing solely on the agricultural sector, consider, for example, the potential for studying water limitations for agriculture using water balance techniques (Lebon et al., 2003), or examining thermal resources and their limitations for crops (Mariani et al., 2012). However, in the next part of this work we will focus our attention on the frequency and intensity of extreme rainfall events characteristic of the ARCIS area.

Extreme precipitation events

The diagram of the annual absolute maximum daily rainfall values from 1961 to 2023 for the whole ARCIS area (Fig. 4) shows high inter-annual variability with maxima not infrequently exceeding 400 mm. The whole time series shows a positive trend that is very close to the 95% threshold of significance (Mann - Kendall test: S :331; Z:1.9573; p (no trend): 0.050309).

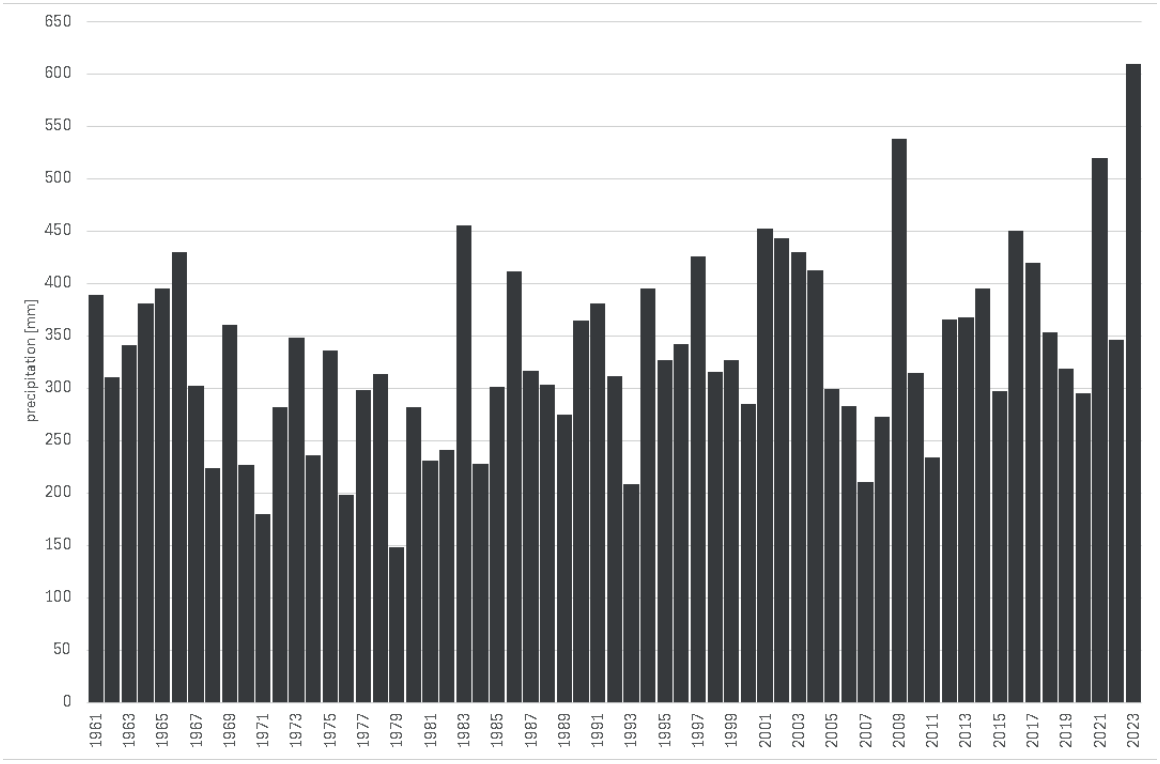

Figure 4. Diagram of yearly absolute maximum daily precipitation in the whole ARCIS dataset area.

The diagram of the total number of events exceeding the 50 mm threshold for the whole ARCIS area (Fig. 5) shows high inter-annual variability. The visual analysis highlights that the number of events over 50 mm is stationary until 2007 with the exceptions of 2000 and 2002; an increase is instead observed since 2008. The whole time series shows a positive but not-significant trend (Mann - Kendall test: S : 205; Z :1.2099; p (no trend): 0.2263). Note also that the absolute maximum of 28524 yearly events exceeding 50 mm is reached in 2014 which is the year with maximum yearly mean precipitation (1489 mm) and that was the consequence of a strong precipitation in January, February, July and November.

The map in Fig. 6 shows the absolute maximum daily precipitation over the whole period covered by ARCIS dataset (1961-2023) while the map in Fig. 7 shows the total number of daily events with precipitation > 50 mm. These two maps highlight the areas potentially most exposed to extreme rainfall events. Obviously, the risk of catastrophic events (landslides, floods) is the result not only of the danger of extreme rainfall events, but also of the vulnerability of the region, which is strictly related to its geo-morphological features and of the exposure to risk of populations and infrastructures. From this point of view, it should be considered that extreme events occurring in locations characterized by high average annual precipitations generally have a lower impact than extreme events of the same magnitude occurring in areas with low average annual precipitation (Libertino et al., 2016).

The map in Fig. 8 illustrates the significant positive and negative trends over the period 1961-2023 in the maximum daily precipitation recorded each year for each pixel, providing a representation of the areas where the most extreme events have intensified or weakened in a statistically significant way (p-value < 0.05, 95 % significance according to the Mann - Kendall test). Note that the pixels with significant decrease in intensity are isolated and without spatially coherent aggregations. On the contrary, pixels subject to intensification tend to predominate in some spatially coherent areas (hereafter named increase nuclei) affecting namely the area of the Apennines surrounding the Genoa Gulf, the area of the High Plain and the Prealps of Piemonte, the area of central-eastern Lombardia and the area of Alto Adige. The pixels affected by intensification are instead isolated and scarcely frequent in Emilia Romagna, Veneto, Friuli Venezia Giulia and the 3 regions of Central Italy (Toscana, Umbria and Marche).

Tab. 1 shows that the 83.42% of the cells illustrated in Fig. 8 do not show any significant trend, while 14.66%

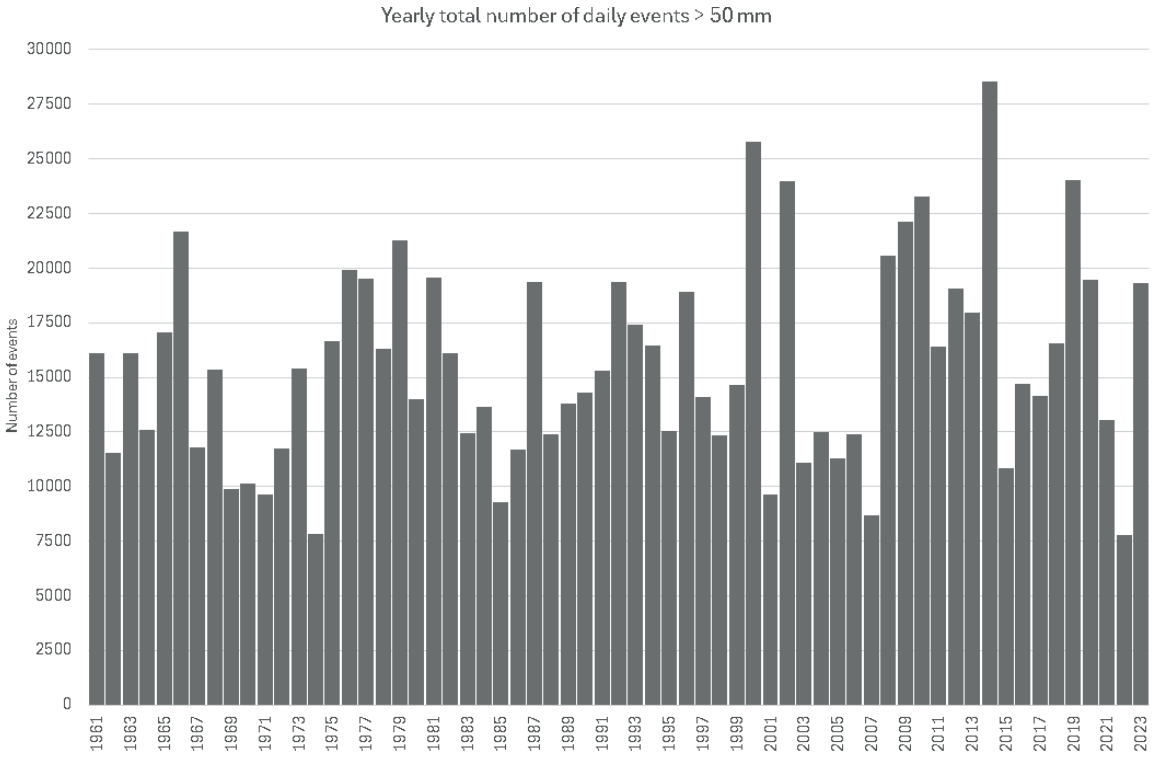

Figure 5. Diagram of Yearly number of total events > 50 mm in the whole ARCIS dataset area.

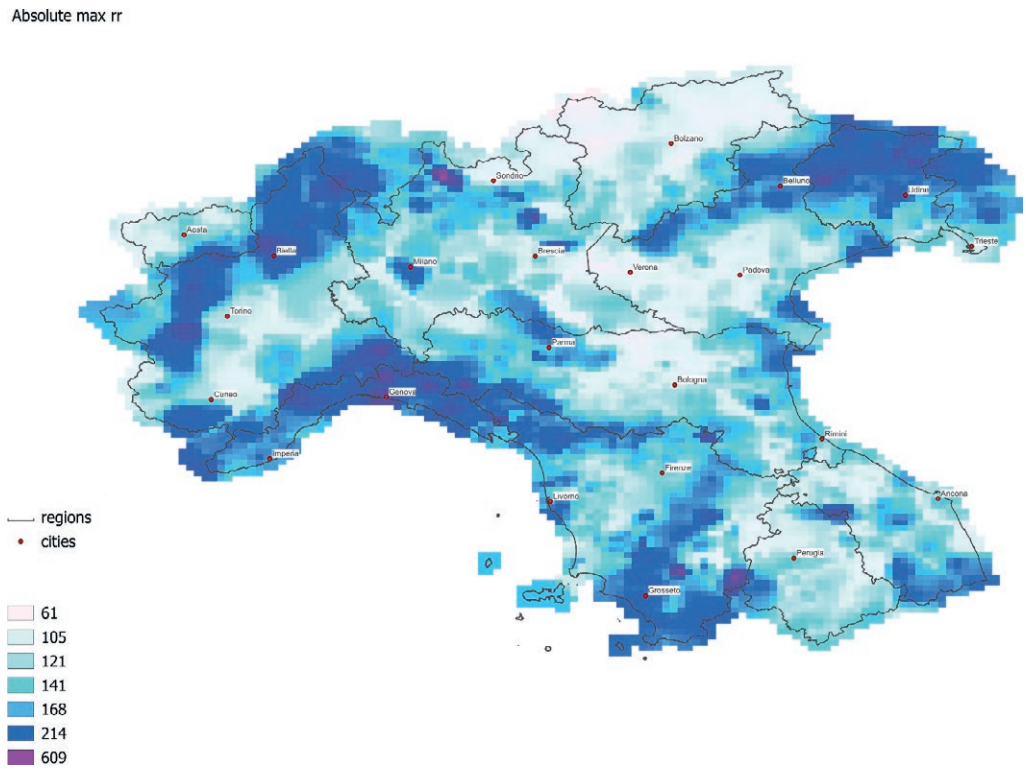

Figure 6. Map of absolute maximum daily precipitation for the period 1961. 2023. The color scale is based on 7 classes percentile values.

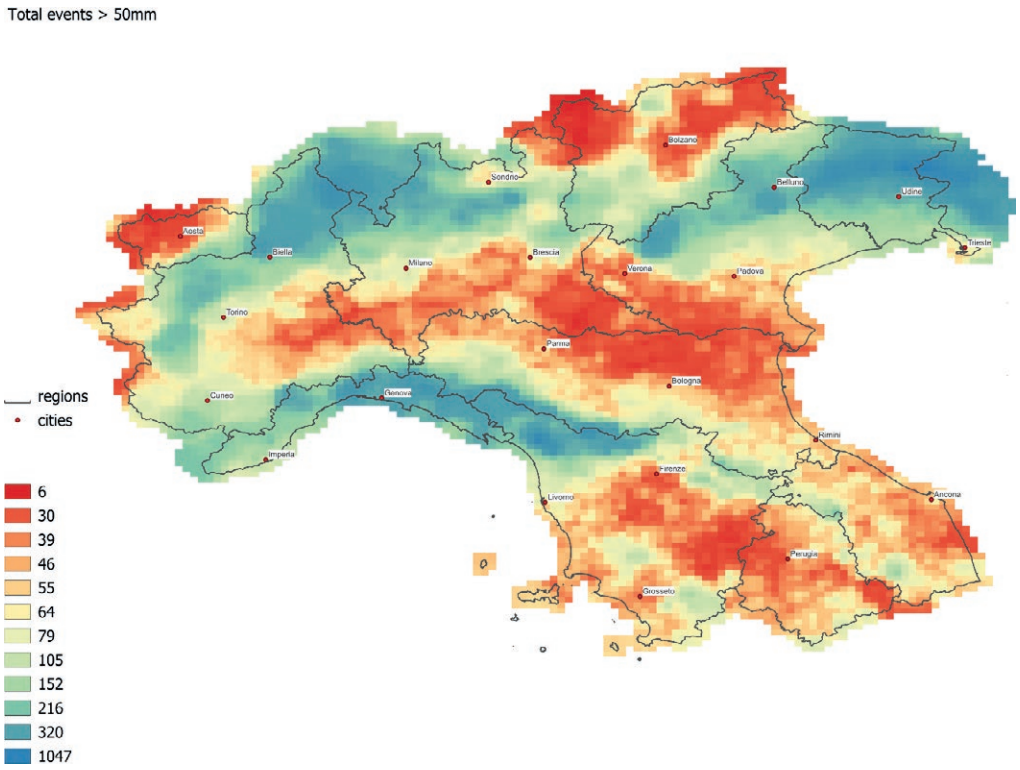

Figure 7. Map of the total number of daily rainfall events exceeding 50 mm for the period 1961. 2023. The color scale is based on 12 classes percentiles values.

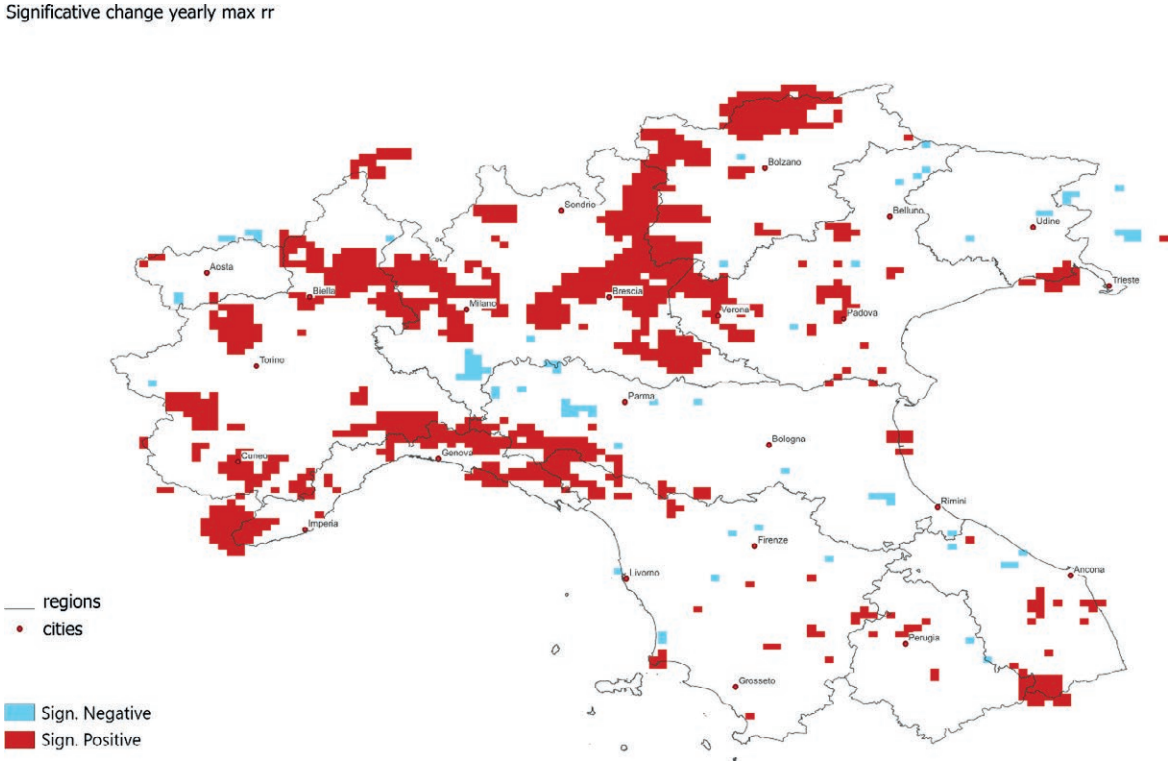

Figure 8. Map illustrating the pixels for which the Mann Kendall test highlights a 95% significant trend over the period 1961-2023 for annual maximum daily precipitation. The areas with a positive trend are in red, and those with a negative trend are in light blue.

show an increasing trend and 1.92% show a decreasing trend. Most of the positive trends are concentrated in 5 regions (Liguria with 34,58 of its territory, Lombardia with 31.4%, Trentino-Alto Adige with 25.4%, Piemonte with 23.1% and Veneto with 9.6%). At the opposite side are Friuli Venezia Giulia, with only 1.25% of territory affected by positive trends, Valle d'Aosta with 1.56%, Emilia Romagna with 3.69% and the three regions of the Central Italy (Toscana, Marche, Umbria) with 4-6% of the territory affected by positive trends.

The map in Fig. 9 illustrates the yearly number of daily events greater than 50 mm significant positive or negative trends for each pixel. As already highlighted for the trends of the annual absolute maximums, it is noted that the pixels subject to a frequency decrease are isolated and never show spatially coherent aggregations. On the contrary, the pixels subject to frequency increase tend to predominate in some spatially coherent hotspots mainly affecting Lombardia, Veneto and Alto Adige.

Tab. 1 reports that 85.83% of the cells illustrated in Fig. 9 do not show significant trends while 11.66% show increasing trends and 2.51% show decreasing trends. The main part of the positive trends is concentrated in 3 administrative regions: Lombardia with 30.32% of its territory, Trentino-Alto Adige with 24.33% and Veneto with 20.67%. At the opposite are Emilia Romagna with 1.01%, Piemonte with 2.23% and Valle d'Aosta with 3.91%. The three regions of the Central Italy (Toscana, Marche, Umbria) show the 3-8% of the territory affected by positive trends. It is also interesting to highlight the marked difference between the percentage of pixels with positive trends in events over 50 mm and in the absolute annual maxima in Piemonte (the percentage of the territory with increasing absolute maximums exceeds the percentage with increasing number of events over 50 mm) and Veneto (the opposite). It should also be noted that in Piemonte, Emilia Romagna and Umbria the percentage of negative trends exceeds the percentage of positive ones.

Fig. 10 shows the percentage change in absolute rainfall maxima between the two subperiods 1961-1990 and 1991-2023. The map was obtained by calculating for the two subperiods the multiyear average of annual absolute maximum daily precipitation for each pixel and the following calculation was used to obtain the percentage variation:

Percentage change = ((mean(1991-2023) - mean (1961-1990) / mean (1961-1990)) * 100

It is worth noting the good visual correlation existing between the areas in Fig. 10 with strong positive changes and the areas in Fig. 8 affected by significant positive trends in maximum yearly events.

To disentangle the scale effects associated with the extreme precipitation intensity and frequency, it is useful to investigate the correlation of average yearly precipitation (Rmed) with the absolute maximum precipitation (RX_abs) (scatterplot in Fig. 14) and the number of annual events exceeding 50 mm (R>50), the latter represented in the scatterplot in Fig. 15.

The correlations under examination are both highly significant: R = 0.3726, p-Value = 0.002636 for Rmed vs. RX_abs, and R = 0.8011, p-Value = 0.002636 for Rmed vs. R>50. However, the determination coefficient (R^2) highlights important differences in the explained vari-

Table 1. Regional percentage of pixels with significantly positive / negative trend on number of days with precipitation > 50 mm, and maximum annual precipitation in the period 1961-2023.

Administrative Regions	% significative positive pixels (maximum events)	% significative negative pixels (maximum events)	% non significative	% significative positive pixels (events > 50 mm)	% significative negative pixels (events > 50 mm)	% non significative
Piemonte	23.08	0.39	76.53	2.23	6.40	91.37
Valle d'Aosta	1.56	3.13	95.31	3.91	1.56	94.53
Lombardia	31.36	2.70	65.94	30.32	1.66	68.02
Trentino-Alto Adige	25.40	0.71	73.89	24.33	0.00	75.67
Veneto	9.60	1.60	88.8	20.67	0.53	78.8
Friuli-Venezia Giulia	1.25	1.88	96.87	7.19	0.63	92.18
Liguria	34.58	0.00	65.42	9.35	0.93	89.72
Emilia-Romagna	3.69	4.92	91.39	1.01	2.68	96.31
Toscana	4.69	1.34	93.97	5.14	1.79	93.07
Umbria	4.26	0.61	95.13	3.65	6.69	89.66
Marche	6.22	2.70	91.08	8.38	2.16	89.46
Tot Area ARCIS	14.66	1.92	83.42	11.66	2.51	85.83

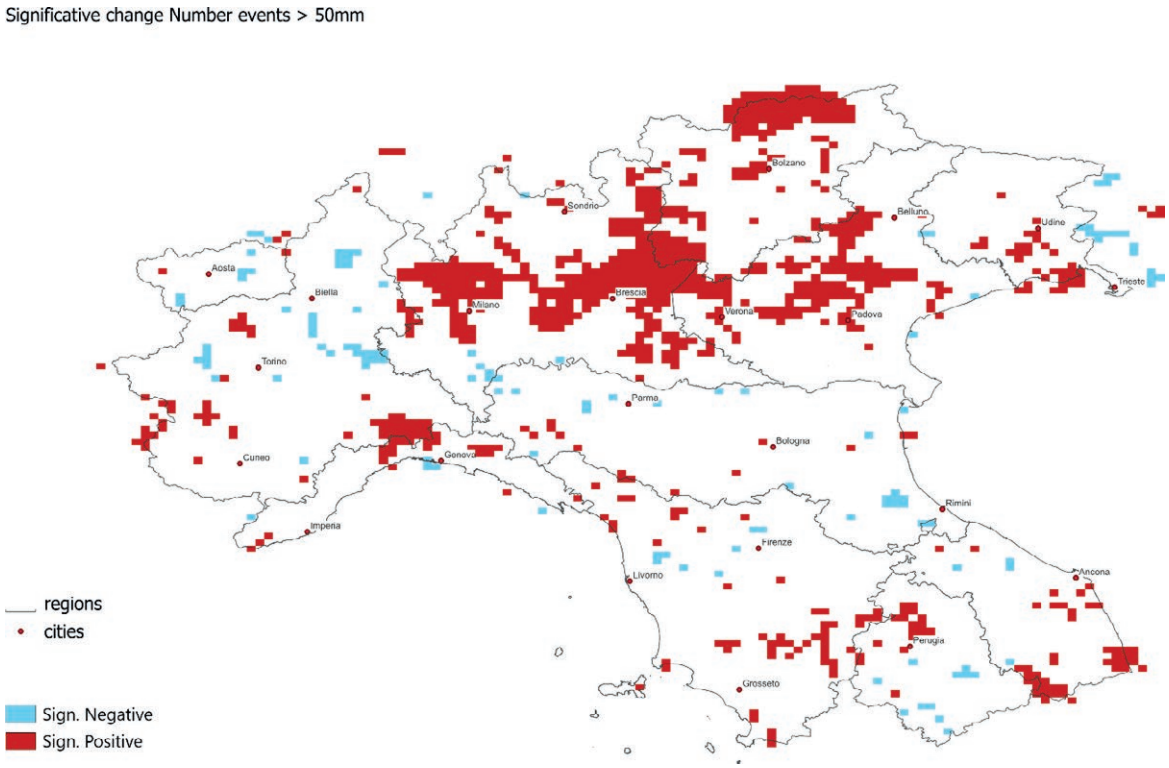

Figure 9. Map illustrating the pixels for which the Mann Kendall test highlights a 95% significant trend over the period 1961-2023 for daily precipitation exceeding 50 mm. The areas with a positive trend are in red, and those with a negative trend are in light blue.

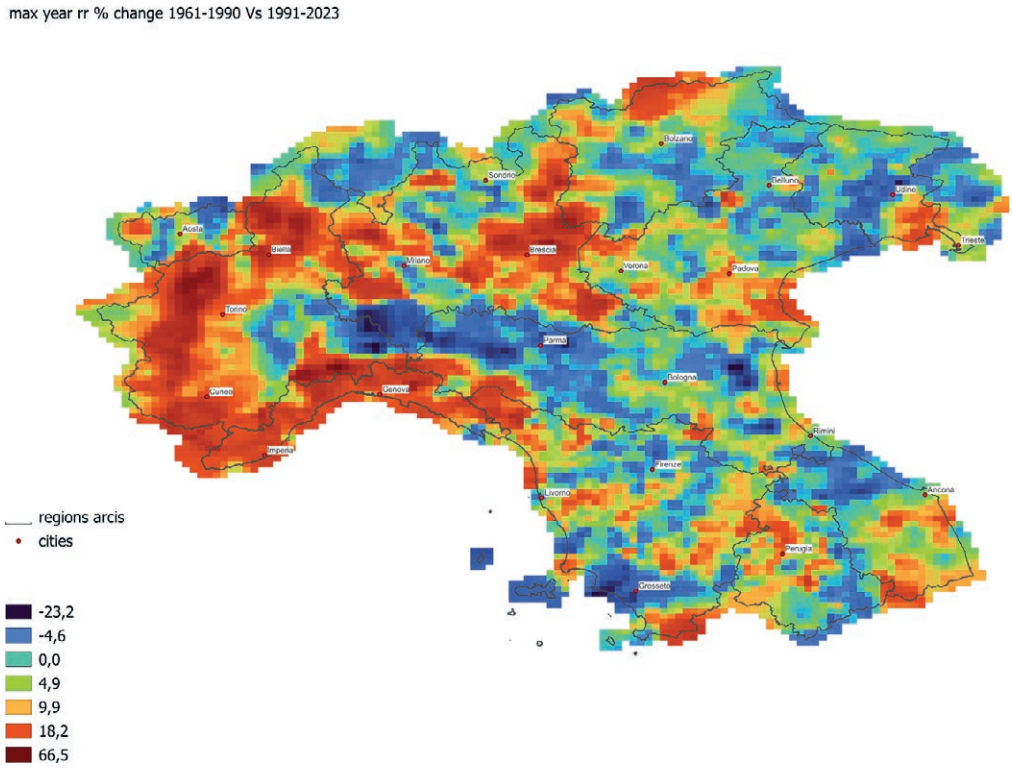

Figure 10. Map of the percentage change in absolute rainfall maximums between the period 1961-1990 and 1991-2023. The color scale is based on 7 classes percentiles values.

ance: R^2 = 0.1389 for Rmed vs. RX_abs, and R^2 = 0.6418 (highly significant) for Rmed vs. R>50.

This suggests that the share of variance explained by mean precipitation is much more limited for RX_abs than for R>50. In our view, this can be attributed to the fact that R>50 is primarily driven by macroscale and mesoscale phenomena, while RX_abs is predominantly influenced by local-scale (beta mesoscale) factors, such as the triggering mechanisms of storm events that lead to high-intensity precipitation.

Fig. 11 shows the percentage change in the number of days with rainfall greater than 50 mm between the periods 1961-1990 and 1991-2023, calculated using the same approach described for Fig. 10. It is important to note the good visual correlation existing between areas in Fig. 11 with strong positive changes and areas in Fig. 10 affected by significant positive trends in yearly events greater than 50 mm. On the other hand, the areas with negative trends in Fig. 10 (light blue) correspond to areas of more than 50% reduction in that number of days.

The correlation analysis performed between the percentage change in the number of days with rainfall greater than 50 mm and the percentage change in absolute maximum values evidence a Pearson correlation coefficient of 0. 5165 and a p-value less than 0.01 (highly significant).

Fig. 12 plots the average daily frequency of events > 50 mm on the period 1961-2023, where there is a clear dominance of events during October/November periods.

Fig. 13 shows the monthly frequency of events > 50 mm (1991-2023 vs 1961-1990). Note that the frequency increases in the autumn and early winter period, with a growth peak in November. A significant frequency drop is recorded in August and smaller drops are observed from January to April.

In summary, the diagram of frequency monthly variation highlights the increasing frequency of intense precipitation events in the autumn as already shown by Grazzini et al. (2019).

Increased frequency in autumn, mainly in November, could be possibly associated with changes in atmospheric circulation and with the increase of surface temperatures of Mediterranean sea which is the main source of humidity for precipitating systems that affect the Italian area although there is a significant contribution from Atlantic humidity in Central Northern Italy (Giustini et al., 2016).

Finally Tab. 2 presents a comparison of numerical distributions of rainfall events between two time peri-

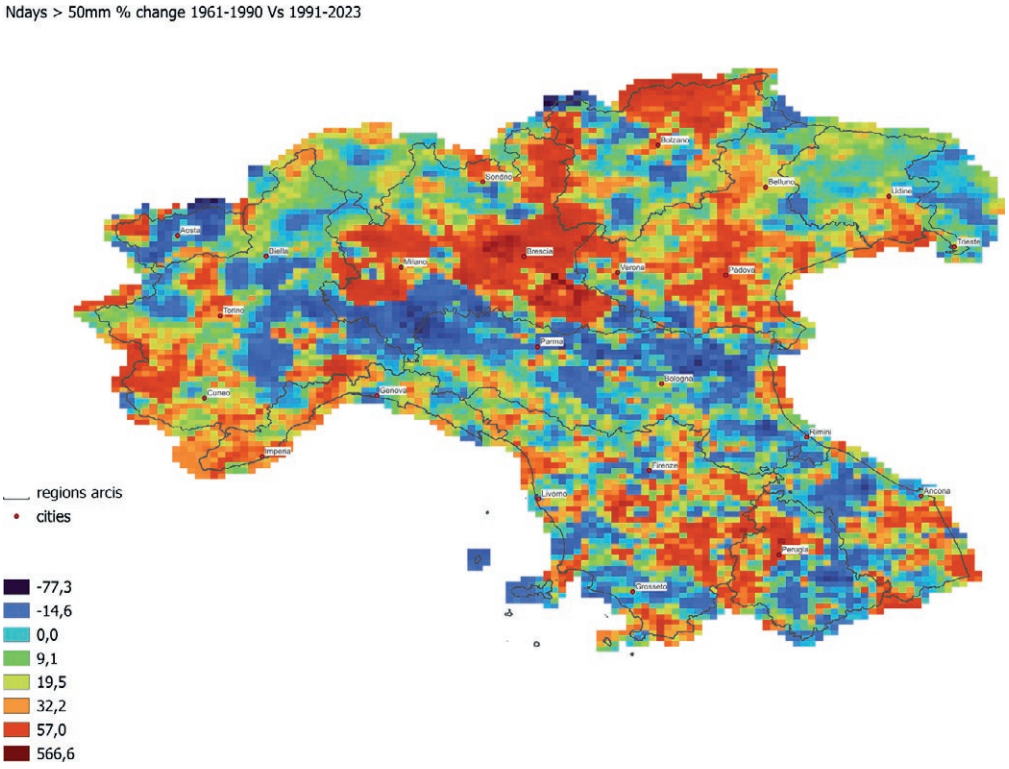

Figure 11. Map of the percentage change in the annual average of the number of days with maximum rainfall exceeding 50 mm in the period 1961-1990 compared to those in 1991-2023. The color scale is based on 8 classes percentage values.

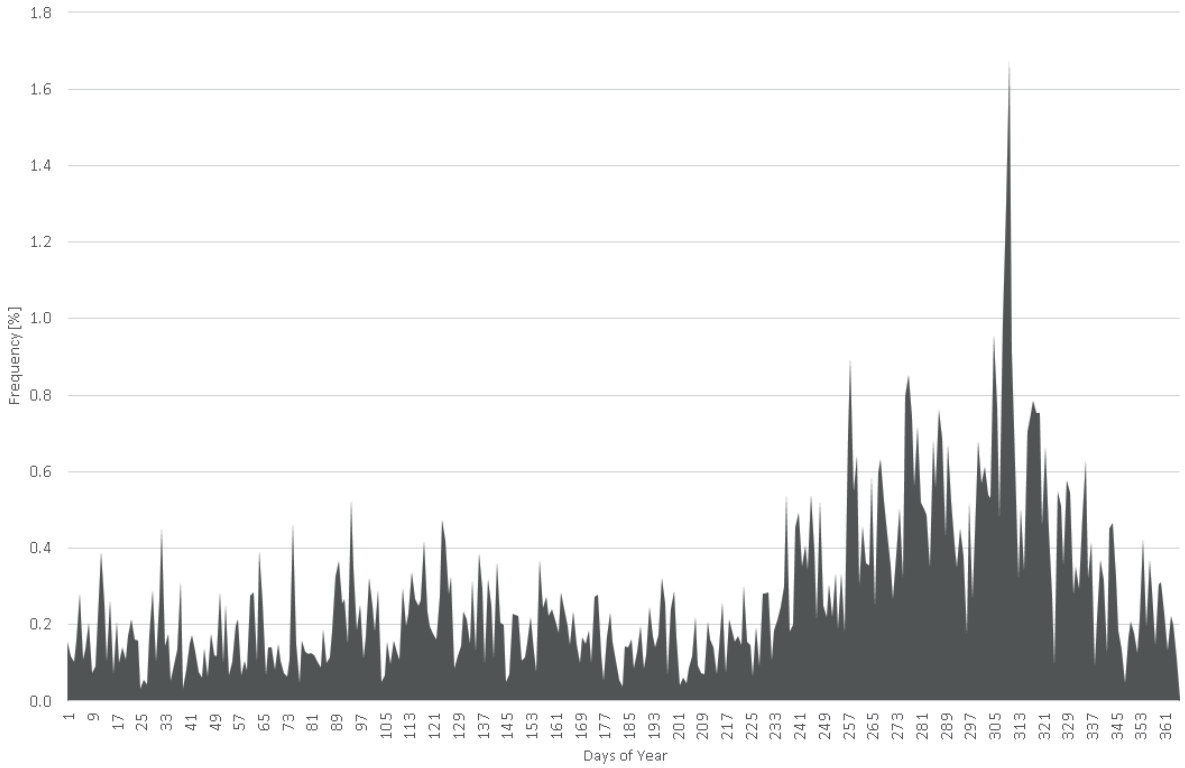

Figure 12. Frequency histogram of the daily occurrence of the events greater than 50 mm in the period 1961-2023.

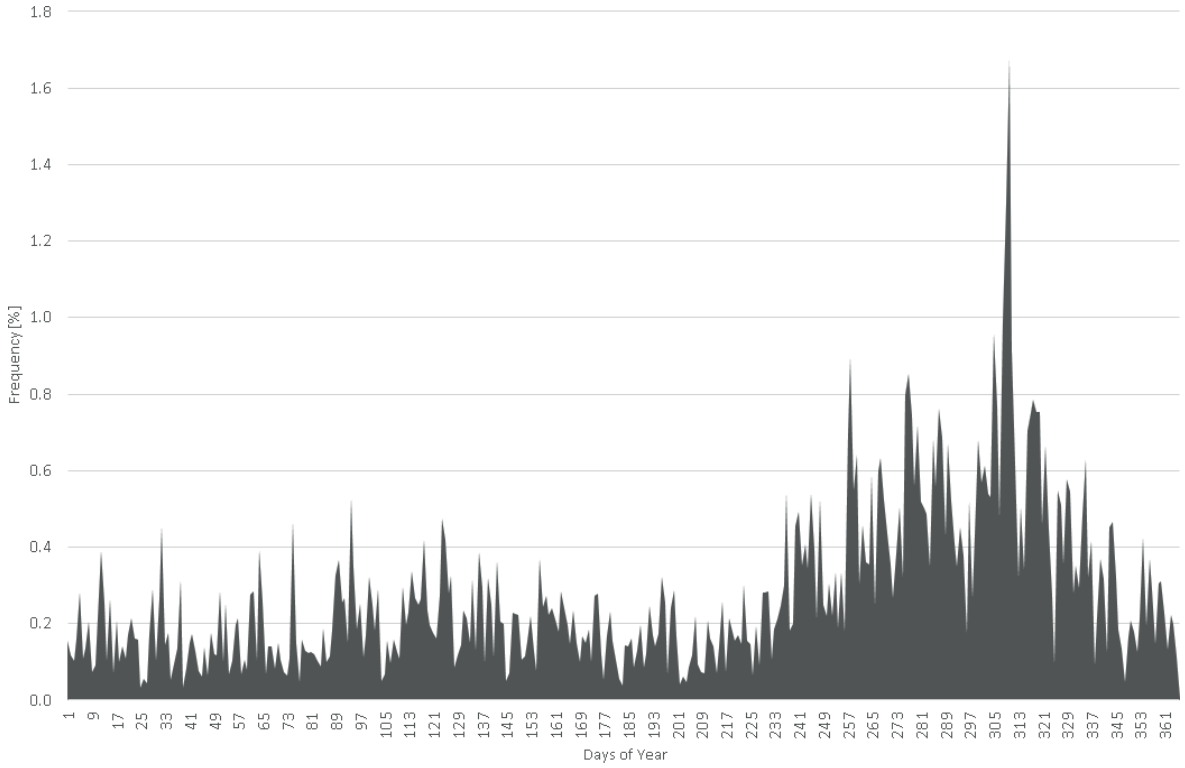

Figure 13. Change in monthly frequency of events > 50 mm (1991-2023 Vs 1961.90).

Table 2. Number of events divided by classes in the two subperiods, the period (1991-2023) *has been also normalized to 30 years. The last column show the percentage of variation between the two subperiods , considering the normalized one.

Class	Total num (1961-1990)	Total num (1991-2023)	Total num (1991-2023) *	Variation (%)
0-25	20440061	21395771	19450701	-4.8
25-50	1724348	1929040	1753673	1.7
50-75	318995	382545	347768	9.0
75-100	80935	103922	94475	16.7
100-125	23836	35305	32095	34.6
125-150	8960	13868	12607	40.7
150-175	3692	6016	5469	48.1
175-200	1681	2800	2545	51.4
200-625	1618	2793	2539	56.9

Table 3. Results of the chi-squared test on the data at tab. 2. , for the period (1991-2023), has been considered the normalized one.

Class	Chi2 Statistic	P-Value	Significant trend
0-25	24537.8464	0.0000E+00	Negative
25-50	247.2497	1.0329E-55	Positive
50-75	1241.6642	5.3781E-272	Positive
75-100	1045.0930	2.8372E-229	Positive
100-125	1219.6820	3.2202E-267	Positive
125-150	616.7956	3.7214E-136	Positive
150-175	344.7245	5.9702E-77	Positive
175-200	176.8105	2.4090E-40	Positive
200-625	204.0871	2.6791E-46	Positive

ods: 1991-2023 (33 years) and 1961-1990 (30 years), the longer one has been normalized to 30 years multiplying values for (30/33). To evaluate the significance of the difference of number events per classes of daily precipitation intensities was performed the chi-squared test which results are reported in Tab. 3. As can be notified, all p-values are extremely small (close to 0) indicating that the differences between the two periods are highly significant. The significance of the changes has been identified for all the classes. Specifically, only for the class (0-25) , the lower one, there is a significant decrease in the events, for all the other higher classes there is a significant increase in the events.

DISCUSSION

The analysis of North-Central Italy extreme precipitations over the period 1961-2023 from the ARCIS daily precipitation dataset, allows to obtain an updated precipitation climatology compliant with the WMO reference standards for the current climate.

Furthermore, with reference to extreme events, the dataset allows to have updated information on the status and variability of heavy rainfall, both in terms of intensity and frequency. The presented maps, which illustrate absolute rainfall maxima, number of days with precipitation greater than 50 mm and percentage changes between the two periods (1961-1990 and 1991-2023), provide a detailed picture of such phenomena.

From the analysis carried out it emerges that changes in the regime of precipitation extremes highlighted by ARCIS dataset are not evenly distributed. In fact, the signal of intensification mainly concerns specific areas of some North Italy regions (Piemonte, Lombardia, Liguria, Trentino Alto Adige e Veneto) while Friuli Venezia Giulia, Emilia Romagna and the Central Italy regions show an overall absence of trends.

The absence of a generalized increase highlights the importance of analyzing phenomena at beta (20-200 km) and gamma mesoscale (2-20 km), to fully understand the local impacts and the associated risks. The absence of trends in precipitation maxima for Toscana region obtained from ARCIS dataset agrees with the results of Fatichi and Caporali (2009) and Pinna (2014); results for Piemonte region are in agreement with those obtained by Bassi et al. (2011) while results for Lombardia are in agreement with Parisi et al (2014).

Moreover, it is worth noting that the areas experiencing the two absolute annual precipitation maxima in Italy – the Carnia region in Friuli Venezia Giulia (with over 3000 mm/year) and the northern shore of Lake Maggiore (2400 mm/year) (Mori, 1964; Frei and Schär, 1998) – exhibit overall stationarity in extreme precipitation.

This phenomenon is particularly fascinating because these maxima result from the interaction between the Alpine orography and the synoptic circulation. Therefore, the temporal variability of extreme precipitation in these areas can be regarded as an important indica-

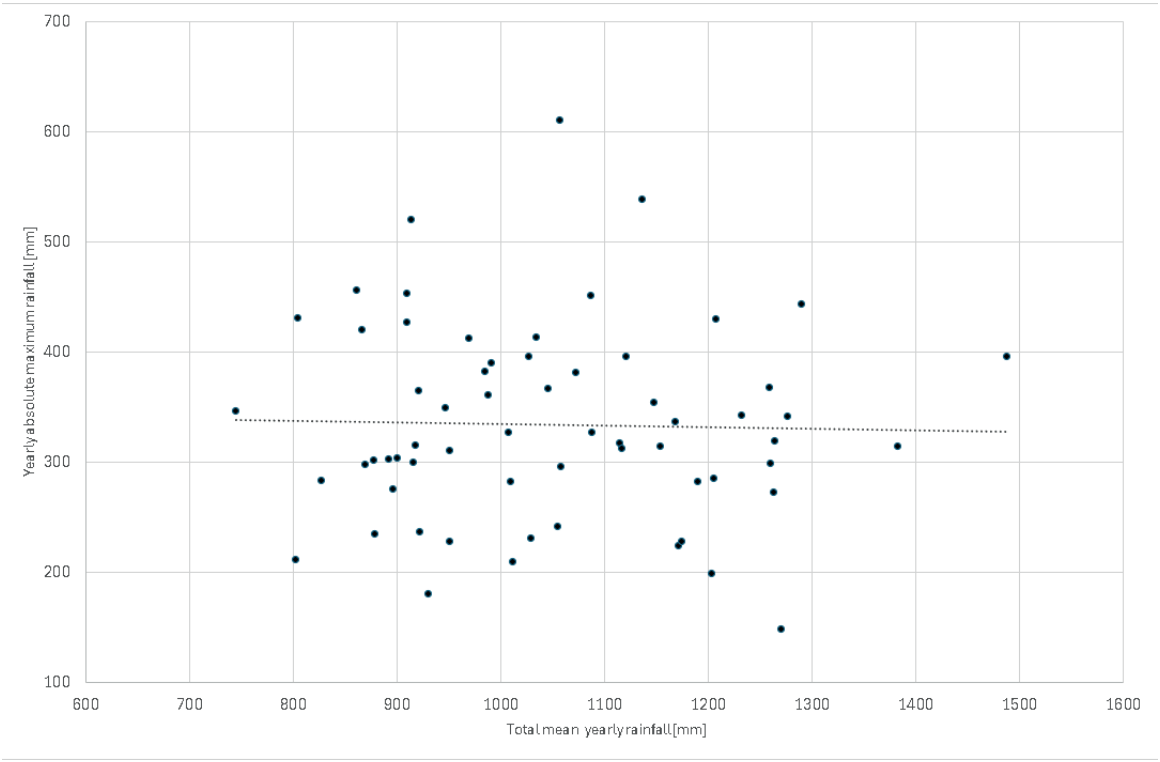

Figure 14. Scatterplot of the yearly absolute maximum rainfall Vs. Total mean yearly rainfall.

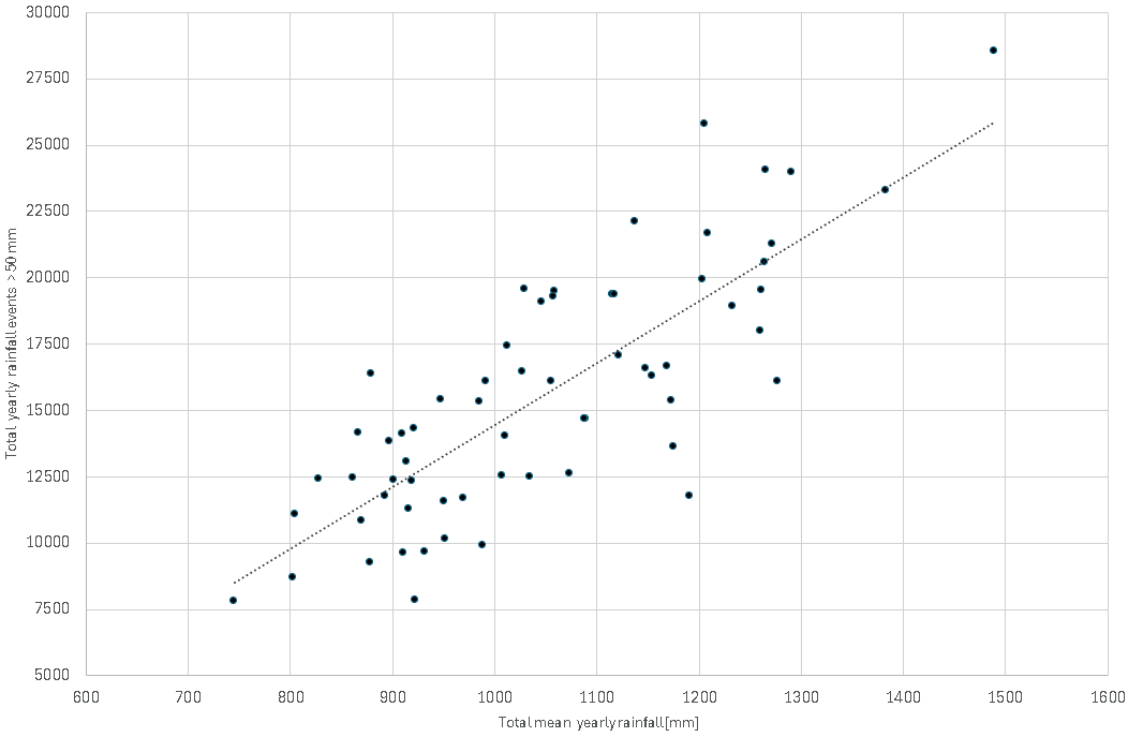

Figure 15. Scatterplot of the total yearly rainfall events > 50 mm Vs. Total mean yearly rainfall.

Figure 16. Italian Regions interested by ARCIS Dataset.

tor of the influence of synoptic-scale signals on the mesoscale climate. Another interesting phenomenon evident in Northern Italy is the presence of areas showing an increase in the frequency or intensity of precipitation adjacent to areas that exhibit no change, or even a decrease. This reflects one of the most remarkable characteristics of the climate system: its variability across all temporal and spatial scales (Franzke et al., 2020).

Based on our experience with local-scale analysis and forecasting in the Po Valley, we hypothesize that these observed trends result from mesoscale processes triggered by interactions with both larger-scale processes (e.g., synoptic circulation and air mass advection) and smaller-scale processes (e.g., boundary layer dynamics). This aligns with the idea of the Po Valley as a "laboratory for mesoscale meteorological processes," a concept recently demonstrated in the context of tornado development (De Martin et al., 2024).

Precipitation is inherently a complex phenomenon, driven by causal factors across a wide range of scales, from macro- to microscale. At the macroscale, factors include westerlies and large blocking systems; at the mesoscale, phenomena such as foehn-stau mechanisms dominate; and at the microscale, processes such as boundary layer dynamics contribute energy and condensation nuclei to precipitating systems. Consequently, in our specific case, the frequency and intensity of extreme precipitation are influenced by a range of processes, including:

a) Mediterranean Sea temperature, which directly affects the flow of sensible and latent heat, warming and moistening the overlying air mass.
b) Temperature of cold air masses (polar continental, maritime, or Arctic) that reach the Mediterranean region from specific source regions.
c) Cyclogenetic activity within the basin, such as lee cyclogenesis in the Gulf of Genoa and the Balearic area, or the cutoff of Atlantic baroclinic waves (Mariani and Parisi, 2013; Carniel et al., 2024).
d) Synoptic disturbances (e.g., Atlantic baroclinic waves) reaching the basin (Carniel et al., 2024).
e) Orographic precipitation processes, particularly significant for the Mediterranean region due to the surrounding mountain ranges, including the Pyrenees, Alps, Apennines, and Atlas Mountains (Rotunno and Houze, 2007).
f) Other factors, such as convection organization, thermal and moisture stratification, precipitation efficiency, air-stream ascent mechanisms, interactions with orography, proximity to the sea, and vertical wind shear. The Mediterranean, with its warm sea (especially in autumn) and surrounding high orography, provides an ideal setting to study these phenomena (Khodayar et al., 2018).

About the above processes, only one subset currently shows indications of trends. For instance, with reference to point (a), Mediterranean Sea surface temperatures are rising, with the fastest warming occurring in the eastern Mediterranean and the northern half of the western Mediterranean, while the trend is weaker on the south part of Italy (Bonacci and Vrsalovi´c, 2022). This warming increases the potential moisture supply for precipitating systems, especially in autumn, when the temperature difference between the sea surface and the overlying air is greatest (Grazzini et al., 2019; Lavers and Villarini, 2015).

On the other hand, several studies identify large-scale precursors of Mediterranean extreme precipitation events. An upper-level trough (Rossby wave) often induces a warm, moist southerly airflow over the western Mediterranean (Pinto et al., 2013). More than half of these moist airflows are classified as Warm Conveyor Belts (WCB), highlighting the roles of baroclinic instability and large-scale lifting (Raveh-Rubin and Wernli, 2015).

Air trajectory analysis emphasizes the importance of large-scale transport and local sources of water vapour for precipitation systems, particularly during convective events. Remote origins, such as the North and subtropical Atlantic, contribute significantly to stratiform precipitation, while local sources like Mediterranean evaporation are more influential for convective systems (Winschall et al., 2014). Within extratropical cyclones' WCB, moisture advection often occurs via atmospheric rivers – narrow filaments of high integrated water vapor – which

are precursors to heavy precipitation in mountainous regions, including Europe (Lavers and Villarini, 2013).

With reference to point (b) Nygard et al (2023), working on the 1979-2020 November to March period, stated that the extremeness of cold air masses reaching the Mediterranean basin from polar and arctic area has not decreased at the same rate with the warming climate, although the Arctic source areas of cold air masses have experienced Arctic amplification. Therefore, the thermal contrast with the warm air overlying the Mediterranean basin remains high and this translates into a greater potential supply for precipitating systems.

With reference to point (c), Carniel et al. (2024), analysing the frequency of explosive cyclones (ECs) in the Mediterranean from 1979 to 2020, highlighted that no clear linear trend is discernible in the data, as the number of ECs fluctuates significantly over the years. Periods of high activity, such as in the early 1980s and between 2009 and 2012, contrast with years of reduced or no activity, underscoring the variability in EC occurrences rather than a consistent increase or decrease over time.

The local nature of the intensity increase that emerges from the analysis of the ARCIS dataset translates into the fact that areas with significant increases in both the intensity of maximum precipitation and the frequency of extreme events, are often close to neighbouring areas that show a reduction in such phenomena. This leads us to wonder what the normal climatic conditions are to adopt for the planning of adaptation works to extreme rainfall. On this topic, the debate remains open; however, in our opinion, it would be essential to adopt an approach based on sufficiently large areas, such as those defined in the past by the National Hydrographic Service. In a publication dedicated to maximum precipitation over 1 to 5 days for the period 1921–1950, Northern Italy was divided into six homogeneous areas (Cati, 1981)

In any case, we believe that daily rainfall data from the last 50-70 years can provide valuable insights for planning adaptation activities. However, relying solely on 24-hour cumulative rainfall data is insufficient; it is essential to analyse shorter intervals (e.g., 1, 3, 6, and 12 hours) to gain a more detailed understanding. The ARCIS database, with its spatial coverage, offers a valuable tool for analyzing such phenomena, but it will be necessary to continue collecting high-quality data to identify any new trends or anomalies. This will be crucial for proper planning and to address any future changes in the rainfall regime.

In conclusion, precipitation extremes in North-Central Italy show strong local variability, rather than a homogeneous increase on a large scale. This highlights the need for flexible and targeted strategies of adaptation for climate risk management in its hazard, exposure, and vulnerability components. Infrastructure adaptive capacity and water resources planning will need to consider the geographic specificities of each area to ensure an effective response to climate change, protecting communities and minimizing damage caused by extreme events.

A final element worth of discussion is the issue of data quality, which is a critical element in gridded datasets. Such datasets are based on the data reconstruction in individual cells extreme precipitation events that are characterized by very high spatial and temporal variability.

In this context, it is worth noting that Sun et al. (2017) conducted a comprehensive review of data sources and estimation methods used in 30 currently available precipitation gridded datasets, which are based on rain gauges, satellite data, and reanalysis data. Their discrepancies analysis among these datasets revealed significant differences in both the magnitude and variability of precipitation estimates, with annual precipitation estimates differing by as much as 300 mm/year across the products.

Additionally, Mallakpour et al. (2022) conducted an analysis of six gridded precipitation datasets for the United States, focusing on the period from 1983 to 2017. Their study highlighted substantial discrepancies in the observed changes in the characteristics of both extreme and non-extreme precipitation events. In the specific ARCIS case, data validation was performed via:

- checks to eliminate spurious zero rainfall periods (no rainfall where other stations report rainfall) due to data digitization errors
- tests for statistical homogeneity (such as SNHT and Craddock-Vincent test) to eliminate data that did not meet the criteria
- synchronicity tests to ensure that all stations were aligned over the same observation period. In some cases, it was necessary to move the data by one day to synchronize the recording periods.

On the other hand, it is important to acknowledge that a significant source of inhomogeneity in worldwide rainfall measurement time series rises from the radical changes in observation technology that occurred mostly between 1980 and 2000. This period saw the transition from older manual or automatic stations with mechanical transduction to modern automatic stations with electronic transduction (WMO, 2021b). This technological shift was often accompanied by changes in measurement locations, introducing biases due to inconsistencies in meteorological instruments and sampling points.

From a broader perspective, it is crucial to recognize that inhomogeneities in meteorological measurements can result from various factors, including changes

in measurement locations, observing technology (hardware), radiation shields, or the software algorithms used to convert instrument signals into meteorological variable values. To address such issues, the WMO recommends that data from automatic weather stations (AWS) be processed and adjusted before the discontinuation of manual measurements (Lukasova et al., 2024). However, this recommendation has been followed in only a limited number of cases, such as the Swiss meteorological network (Heimo et al., 2003).

In contrast, many weather station networks (mesonets) lack national and international coordination, suffer from poor maintenance, inadequate data quality and redundancy, as noted by Silvestri et al. (2022)

CONCLUSIONS

The work was carried on ARCIS dataset which refers to data from Northern Italy and from some regions (three) of Central Italy. This analysis was referred to some average precipitation characteristics for the period 1961-2023 and highlighted that precipitation patterns are stationary despite the presence of a significant interannual variability. The analysis was then extended to intensity and frequency trends of extreme precipitation and highlighted that 83% and 86% of the area does not show significant increases in frequency and intensity respectively, while 11% and 15% show significant increases and 2% and 3% show significant decreases. Finally, regarding seasonality, it was highlighted an extreme phenomena frequency increase in autumn (from October to December with a more marked increase in November), a weak decrease from January to April and a marked decrease in August. The obtained indications have significant implications in terms of agricultural and hydro-geological management.

Finally, we would like to point out that it would be important that the activities will expand also to the remaining part of the Italian Country to have a meteorological data homogeneous gathering system coming from Italian weather station networks (mesonets).

ACKNOWLEDGEMENT

The authors thank the ARCIS researchers' group for their precious volunteers-based work and in particular Dr. Valentina Pavan for her tempestive and kind reply to our requests on dataset metadata.

REFERENCES

Alpert P., Ben-Gai T., Baharad A., Benjamini Y., Yekutieli D., Colacino M., Diodato L., Ramis C., Homar V., Romero R., Michaelides S., Manes A., 2002. The paradoxical increase of Mediterranean extreme daily rainfall in spite of decrease in total values. Geophysical Research Letters 29(11): 301-314

Antolini G., Auteri L., Pavan V., Tomei F., 2015. A daily high-resolution gridded climatic data set for Emilia-Romagna, Italy, during 1961-2010. International Journal of Climatology, August 2015, https://doi.org/10.1002/joc.4473

Barton Y., Rivoire P., Koh J., Ali M. Kopp J., Martius O., 2022. On the temporal clustering of European extreme precipitation events and its relationship to persistent and transient large-scale atmospheric drivers. Weather and Climate Extremes, Volume 38, December 2022, 100518.

Bassi M., Colombino G., Cremonini R., Masciocco L., 2011. Analisi delle piogge estreme in Piemonte. Atti del convegno Le modificazioni climatiche ed i rischi naturali, 53-58.

Bauer, V. M., & Scherrer, S. C. (2024). The observed evolution of sub-daily to multi-day heavy precipitation in Switzerland. Atmospheric Science Letters 25(9): e1240. https://doi.org/10.1002/asl.1240

Bonacci, O.; Vrsalovi´c, A., 2022. Differences in Air and Sea Surface Temperatures in the Northern and Southern Part of the Adriatic Sea. Atmosphere 2022, 13: 1158. https://doi.org/10.3390/atmos13071158

Brunetti M., Caloiero T., Coscarelli R., Gullà G., Nanni T., Simolo C., 2010. Precipitation variability and change in the Calabria region (Italy) from a high resolution daily dataset. https://doi.org/10.1002/joc.2233

Carniel C.E., Ricchi A., Ferretti R., Curci G., Miglietta M.M., Reale M., Serafini P., Wellmeyer E.D., Davolio S., Zardi D., Kantha L., 2024. A high-resolution climatological study of explosive cyclones in the Mediterranean region: Frequency, intensity and synoptic drivers. Q J R Meteorol Soc. 150: 5561–5582.

Cati L., 1981. Idrografia e idrologia del Po, Roma, Istituto Poligrafico e Zecca dello Stato, 310 pp.

De Martin F., Davolio S., Miglietta M.M., Levizzani V., 2024. A Conceptual Model for the Development of Tornadoes in the Complex Orography of the Po Valley. Monthly Weather Review 152(6): 1357-1377.

Doswell III C.A., Brooks H.E., Maddox R.A., 1996. Flash Flood Forecasting: An Ingredients-Based Methodology. Weather and forecasting 11(4): 560-581.

Fatichi S., Caporali E., 2009. A comprehensive analysis of changes in precipitation regime in Tuscany. Interna-

tional Journal of Climatology 29(13): 1883-1893.

Franzke C.L.E., Barbosa S., Blender R., Fredriksen H.-B., Laepple T., Lambert F., 2020. The structure of climate variability across scales. Reviews of Geophysics 58: e2019RG000657. https://doi.org/10.1029/2019RG000657

Frei C., Schär C., 1998. A precipitation climatology of the Alps from high-resolution rain-gauge observations. Int. J. Clim. 18(8): 873-900.

Gilbert R.O, 1987. Statistical methods for environmental pollution monitoring. Van Nostrand Reinhold, New York, 321 pp.

Giustini F., Brilli M. and Patera A., 2016. Mapping oxygen stable. isotopes of precipitation in Italy. Journal of Hydrology: Regional Studies 8(2016): 162-181.

Grazzini F., Craig G.C., Keil C.,Antolini G., Pavan V., 2019. Extreme precipitation events over northern Italy. Part I: A systematic classification with machine-learning techniques. Q J R Meteorol Soc. 146: 69-85. https://doi.org/10.1002/qj.3635

Heimo A. , Konzelmann T., 2003. SwissMetNet: Renewal of the Swiss Meteorological Networks. Proceedings of the International Conference on the Experiences with Automatic Weather Stations, Torremolinos, Spain, 19-21 February, 2003.

IPCC, 2023. Sections. In: Climate Change 2023: Synthesis Report. Contribution of Working Groups I, II and III to the Sixth Assessment Report of the Intergovernmental Panel on Climate Change [Core Writing Team, H. Lee and J. Romero (eds.)]. IPCC, Geneva, Switzerland, pp. 35-115, https://doi.org/10.59327/IPCC/AR6-9789291691647

Isotta F.A., Frei C., Weilguni V., Percec Tadic M., Lassegues P., Rudolf B., Pavan V., Cacciamani C., Antolini G., Ratto S.M., Munari M., Micheletti S., Bonati V., Lussana C., Ronchi C., Panettieri E., Marigo G., Vertacnik G., 2013. The climate of daily precipitation in the Alps: development and analysis of a high-resolution grid dataset from pan-Alpine rain-gauge data. Int J Climatol. 34(5): 1657-1675.

Katz J., 2023. Concepts across the Sciences: Stability and Change, USA Library of congress, https://blogs.loc.gov/teachers/2023/03/concepts-across-the-sciences-stability-and-change/

Khodayar S., Kalthoff N. , Kottmeier C. ,2018. Atmospheric conditions associated with heavy precipitation events in comparison to seasonal means in the western Mediterranean region. Climate Dynamics 51(3): 951-967.

Lavers D.A. , Villarini G., 2013. The nexus between atmospheric rivers and extreme precipitation across Europe. Geophysical Research Letters 40: 3259-3264. https://doi.org/10.1002/grl.50636

Lavers D.A. , Villarini G., 2015. The relationship between daily European precipitation and measures of atmospheric water vapour transport. International Journal of Climatology 35: 2187-2192. https://doi.org/10.1002/joc.4119

Lebon E., Dumas V., Pieri P., Schultz H.R. , 2003. Modelling the seasonal dynamics of the soil water balance of vineyards. Funct. Plant Biol. 30: 699-710.

Libertino A., Macchia S., Claps P., 2016. Nubifragi eccezionali in Italia: analisi preliminare di rilevanza sugli eventi 1920-2000, Atti del XXXV Convegno Nazionale di Idraulica e Costruzioni Idrauliche, Bologna, 14-16 Settembre 2016, 4 pp. (in Italian)

Libertino A., Ganora D., Claps P., 2018 Technical note: Space–time analysis of rainfall extremes in Italy - clues from a reconciled dataset. Hydrol. Earth Syst. Sci. 22: 2705-2715. https://doi.org/10.5194/hess-22-2705-2018

Libertino A., Ganora D., Claps P., 2019. Evidence for increasing rainfall extremes remains elusive at large spatial scales: the case of Italy. Geophysical Research Letters https://doi.org/10.1029/2019GL083371

Lukasova V., Varsova S., Onderka M., Bilcik D., Buchholcerov A., Nejedl P., 2024. Continuity of long-term climate data series after the transition from manual to automatic weather station. Contributions to Geophysics and Geodesy 54(3): 251-266.

Mallakpour I., Sadeghi M., Mosaffa H., Akbari Asanjan A., Sadegh M., Nguyen P., Sorooshian S., and Agha-Kouchak A., 2022. Discrepancies in changes in precipitation characteristics over the contiguous United States based on six daily gridded precipitation datasets. Weather Clim. Extrem. 36: 100433. https://doi.org/10.1016/j.wace.2022.100433

Mariani L., Parisi S., 2013. Extreme rainfalls in the Mediterranean area, in Storminess and environmental changes: climate forcing and responses in Mediterranean region. Diodato and Bellocchi (Eds.), Springer.

Mariani L. , Parisi S. , Cola G. , Failla O., 2012. Climate change in Europe and effects on thermal resources for crops. International Journal of Biometeorology 56: 1123-1134. https://doi.org/10.1007/s00484-012-0528-8

Mori A., 1964. Carta delle precipitazioni medie annue in Italia (trentennio 1921-1950), CNR, Istituto di geografia dell'Università di Pisa, Roma, Cartografia Riccardi (in Italian).

Nygard T., Papritz L., Naakka T., Vihma T., 2023. Cold wintertime air masses over Europe: where do they come from and how do they form? Weather Clim. Dynam. 4: 943-961. https://doi.org/10.5194/wcd-4-943-2023

Parisi S.G., Mariani L., Cola G., 2014. Extreme rainfall in the Lombardy region. Italian Journal of Agrometeorology 1: 19-28.

Pavan V., G.Antolini, G.Agrillo, L. Auteri, R. Barbiero, V. Bonati, F. Brunier, C.Cacciamani, O. Cazzuli, A. Cicogna, C. De Luigi, L. Maraldo, G. Marigo, R. Millini, E. Panettieri, S. Ratto, C. Ronchi, S. Saibanti, A. Sulis, F. Tomei, R. Tomozeiu, I. Torlai, G. Villani, 2013. The ARCIS Project. Italian Journal of Agrometeorology 2: 51-55.

Pavan V., Antolini G., Barbiero R., Berni N., Brunier F. Cacciamani C. Cagnati A., Cazzuli O., Cicogna A., De Luigi C., Di Carlo E., Francioni M., Maraldo L., Marigo G., Micheletti S. Onorato L., Panettieri E., Pellegrini U., Pelosini R., Piccinini D., 2018. High resolution climate precipitation analysis for north-central Italy, 1961–2015'. Climate Dynamics 52: 1-19.

Pinna S., 2014. La falsa teoria del clima impazzito, 158 pp. (in italian)

Pinto J.G., Ulbrich S., Parodi A., Rudari R., Boni G., Ulbrich U., 2013. Identification and ranking of extraordinary rainfall events over northwest Italy: the role of Atlantic moisture. Journal of Geophysical Research: Atmospheres 118: 2085-2097. https://doi.org/10.1002/jgrd.50179

Piotrowicz K., Ciaranek D., 2020. A selection of weather type classification systems and examples of their application. Theoretical and Applied Climatology 140: 719-730. https://doi.org/10.1007/s00704-020-03118-2

Pucik T., 2024. Meteorological analysis of extreme flash flood situation in the Valencia region, https://www.essl.org/cms/meteorological-analysis-of-extreme-flash-flood-situation-in-the-valencia-region/ (site visited at 27 June 2025)

Raveh-Rubin S., Wernli H., 2015. Large-scale wind and precipitation extremes in the Mediterranean – a climatological analysis for 1979-2012. Quarterly Journal of the Royal Meteorological Society 141: 2404-2417. https://doi.org/10.1002/qj.2531

Reid P.C., Hari R.E., Beaugrand G., Livingstone D.M., Marty C., Straile D., Barichivich J., Goberville E., Adrian R., Aono Y., Brown R., Foster J., Groisman P., Hélaouët P., Hsu H.H., Kirby R., Knight J., Kraberg A., Li J., Lo T.T., Myneni R.B., North R.P., Pounds J.A., Sparks T., Stübi R., Tian Y., Wiltshire K.H., Xiao D., Zhu Z., 2015. Global impacts of the 1980s regime shift. Glob Chang Biol. 22(2): 682-703. https://doi.org/10.1111/gcb.13106

Rotunno R., Houze R.A., 2007. Lessons on orographic precipitation from the Mesoscale Alpine Programme. Q. J. R. Meteorol. Soc. 133: 811-830.

Silvestri L., Saraceni M., Bongioannini Cerlini P., 2022. Quality management system and design of an integrated mesoscale meteorological network in Central Italy. Meteorological Applications 29: e2060. https://doi.org/10.1002/met.2060

Skipper S., Perktold J., 2010. Statsmodels: Econometric and statistical modeling with python. Proceedings of the 9th Python in Science Conference.

Sun Q., Miao C., Duan Q., Ashouri H.,Sorooshian S., Hsu K.-L., 2017. A review of global precipitation data sets: Data sources, estimation, and inter-comparisons. Reviews of Geophysics 56: 79-107. https://doi.org/10.1002/2017RG000574

Sun Q., Zhang X., Zwiers F., Westra S., Alexander L.V., 2021. A Global, Continental, and Regional Analysis of Changes in Extreme Precipitation. Journal of Climate 1 Jan 2021: 243-258. https://doi.org/10.1175/JCLI-D-19-0892.1

Winschall A., Sodemann H., Pfahl S. , Wernli H., 2014. How important is intensified evaporation for Mediterranean precipitation extremes? Journal of Geophysical Research: Atmospheres 119: 5240-5256. https://doi.org/10.1002/2013JD021175

World Meteorological Organization, 2021a. Updated 30-year reference period reflects changing climate, https://wmo.int/media/news/updated-30-year-reference-period-reflects-changing-climate (site visited the 3 January 2025)

World Meteorological Organization, 2021b. Guide to meteorological instruments and methods of observation (WMO guide n. 8), Geneva, CH, https://community.wmo.int/en/activity-areas/imop/wmo-no_8

Italian Journal of Agrometeorology
Rivista Italiana di Agrometeorologia

Firenze University Press
https://riviste.fupress.net/index.php/IJAm

OPEN ACCESS

Citation: Surmaini, E., Misnawati, Ramadhani, F., Dewi, E. R., Sarvina, Y., Syahputra, M. R., Estiningtyas, W., Apriyana, Y., Susanti, E., & Aziz, A. (2025). A new spatial-temporal modelling approach for predicting rice drought in Indonesia using the Standardized Precipitation Index. *Italian Journal of Agrometeorology* (2): 23-37. doi: 10.36253/ijam-3677

Received: July 24, 2025

Accepted: October 25, 2025

Published: December 31, 2025

Data Availability Statement: All relevant data are within the paper and its Supporting Information files.

Competing Interests: The Author(s) declare(s) no conflict of interest.

ORCID:
ES: 0000-0002-2540-6504
M: 0009-0006-3356-3223
FR: 0000-0003-1642-9234
ERD: 0000-0001-8991-7613
YS: 0000-0002-9185-2596
MRS: 0000-0002-0146-4099
WE: 0000-0002-5514-2132
YA: 0000-0003-1809-6103
ES: 0009-0007-8295-9651
AA: 0000-0001-6685-5165

A new spatial-temporal modelling approach for predicting rice drought in Indonesia using the Standardized Precipitation Index

Elza Surmaini[1,*], Misnawati[1], Fadhlullah Ramadhani[2], Elsa Rakhmi Dewi[1], Yeli Sarvina[1], Muhammad Ridho Syahputra[3], Woro Estiningtyas[1], Yayan Apriyana[1], Erni Susanti[1], Amiral Aziz[4]

[1] *Research Center for Climate and Atmosphere, National Research and Innovation Agency (BRIN), Jl. Raya Puspiptek 60, Tangerang Selatan 15310. Indonesia*
[2] *Research Center for Geoinformatics, National Research and Innovation Agency (BRIN), Raya Jakarta-Bogor KM 46, Cibinong, Indonesia*
[3] *Faculty of Earth Sciences and Technology, Bandung Institute of Technology, Jl Ganesha no 10. Bandung, Indonesia*
[4] *Research Center for Energy Conversion Technology, National Research and Innovation Agency (BRIN), Jl. Raya Puspiptek 60, Tangerang Selatan 15310. Indonesia*
*Corresponding author. E-mail: elza001@brin.go.id

Abstract. Agricultural drought poses a major threat to rice production in Indonesia, highlighting the need for dynamic prediction to support timely and effective management strategies. This study aims to develop a new approach for predicting rice drought stress that incorporates the characteristics of SPI3, emphasizing onset and trends, and to evaluate the model's accuracy in predicting rice drought. The onset of SPI3 denotes conditions at the start of the planting season, while the SPI3 trend represents the four-month gradient from planting to harvest. The Normalized Difference Vegetation Index (NDVI) derived from MODIS was utilized to validate the spatial and temporal predictions of rice drought using the Proportion Correct (PC) method. The model performs most reliably in capturing severe droughts during the dry season, with accuracies in the very high drought category ranging from 60% to 85%. Performance declines in March and August, highlighting challenges during the transitions between wet and dry seasons. During the El Niño year, predictions aligned with observed very high drought (PC: 59–77%), whereas in the La Niña year, they matched the low drought category (PC: 72–76%). Comparable prediction accuracies in Indramayu and Bone indicate the feasibility of developing a generalized model for Indonesia's diverse rice-producing areas. Future improvements should integrate higher-resolution data and machine learning, account for local irrigation practices, and expand validation across regions to enhance model transferability and comprehensively assess its performance.

Keywords: drought, rice, prediction, SPI3, NDVI.

HIGHLIGHTS

- Rice production in Indonesia is highly susceptible to drought, with the damaged areas increasing sharply during El Niño years.
- The onset and trend of the 3-month Standardized Precipitation Index (SPI3) reflect drought risk across the growing season, making it a reliable predictor of rice drought.
- Negative SPI3 trends correspond to lower yields, while positive trends indicate higher yields, demonstrating SPI3's predictive value for yield variability.
- The higher accuracy in predicting severe rice drought enhances early warning systems and enables proactive drought mitigation.

INTRODUCTION

Drought, as a natural disaster, demonstrates a complex and cascading nature, leading to more severe impacts compared to single-disaster events. Agriculture is significantly affected by drought hazards, which are a primary cause of crop failures and pose a substantial threat to global food security (FAO, 2012; Zinat et al., 2020). Prior studies indicate that the duration and intensity of droughts are expected to increase significantly in the future (Zhou et al., 2023; Li et al., 2024). These findings confirm that drought represents a considerable future threat, underscoring the necessity of understanding its patterns and intensity for effective anticipatory action.

Rice serves as the staple food for over 280 million people in Indonesia. Rice fields cover approximately 7.4 million hectares across various regions of the country (BPS [Statistics Indonesia], 2024). Planting generally occurs twice a year, namely during the wet season planting (WSP) and the first dry-season planting (DSP1), with the possibility of a third planting in irrigated areas when water resources are sufficient (the second dry-season planting, DSP2). Rice production in Indonesia is highly susceptible to drought, particularly during the dry-season plantings (Naylor et al., 2007; Surmaini et al., 2015). El Niño events are often associated with droughts that significantly reduce rice production in Indonesia (D'Arrigo and Wilson, 2008; Surmaini et al., 2015; Boer and Surmaini, 2020). Data from the Ministry of Agriculture of the Republic of Indonesia indicate that prolonged droughts caused by moderate to strong El Niño events between 1990 and 2020 resulted in annual rice production losses ranging from approximately 500,000 to 1.7 million tons.

Droughts are typically classified according to their duration and impacts on various ecological and social contexts (Mishra and Singh, 2010). Consequently, they are generally categorized into four types: meteorological, agricultural, hydrological, and socio-economic droughts. The transition from meteorological drought to agricultural drought is particularly crucial for developing effective early warning systems for agricultural drought (Xu et al., 2023). Drought propagation refers to the transition from meteorological drought to other types of drought (Bhardwaj et al., 2020). Typically, droughts begin with insufficient precipitation, which subsequently reduces soil moisture and decreases surface and groundwater availability (Hao & Singh, 2015), ultimately leading to adverse effects on crops (Wu et al., 2020; Li et al., 2024).

The Standardized Precipitation Index (SPI) is widely recognized as one of the most the straightforward method for drought analysis and monitoring (McKee et al., 1993). Its widespread adoption can be attributed to its interpretability, comparability, standardized calculation methods (Zipper et al., 2016; Leng and Hall, 2019), flexibility, simplicity, and accessibility of data (Dai et al., 2020). In addition, SPI is easy to compute and demonstrates strong adaptability across both temporal and spatial scales (Pei et al., 2020). The SPI at a 3-month scale (SPI3) is particularly suitable for agricultural drought monitoring because it captures short to medium term precipitation deficits that directly affect soil moisture and crop growth (McKee et al., 1993; Zargar et al., 2011). Tsige et al. (2019) identified a strong relationship between SPI3 and agricultural drought, making it a valuable indicator for monitoring agricultural drought (Dai et al., 2020).

Although the SPI is a well-established and widely applied indicator for drought assessment, it frequently categorizes drought events based on static thresholds or classifications. This study introduces a novel interpretive framework by focusing on the gradual onset and trend dynamics of SPI3 as a predictive indicator for rice drought. Our approach emphasizes the temporal pattern and directionality of SPI3, monitoring how its values evolve before a drought fully manifests. To our knowledge, few studies examine SPI3 in this dynamic, trend-oriented manner specifically tailored for agronomic drought prediction in rice systems. The primary ratio for employing this index as a drought predictor is the recognition that rice growth and yield are influenced not only by conditions at the onset of planting but also throughout the entire growing period. By capturing the gradual escalation and directional shifts of SPI3 values, our method offers earlier detection of emerging drought stress aligned with critical rice growth stages, enabling

a more sensitive and agronomically relevant early-warning tool. The objective of this study is to develop a rice drought prediction model that incorporates combined SPI3 characteristics, with an emphasis on the onset and trend dynamics, and to evaluate the model's accuracy in predicting rice drought.

MATERIALS AND METHODS

Study area

The model was constructed using data from two districts, namely Indramayu in West Java Province, representing the monsoon rainfall pattern, and Bone in South Sulawesi Province, exemplifying the local rainfall pattern. These regions serve as key centers of rice production and are vulnerable to drought occurrences. Indramayu is located in the western region of Indonesia, whereas Bone is situated in the central region (Figure 1).

Data

Meteorological data

Daily meteorological data from 38 rain gauge stations in Indramayu and Bone, including rainfall, minimum and maximum temperatures, and solar radiation, were collected for the period 1982–2009. The spatial distribution of the rain gauge stations used in this study is shown in Figure 1. In addition, gridded rainfall data from the Climate Hazards Group InfraRed Precipitation with Station (CHIRPS) dataset for the years 2010–2019 were used for the SPI3 model application.

Soil data

Soil data samples were collected from study fields in each sub-district of Indramayu and Bone. The data included drainage class, runoff potential, slope, soil layers, texture, organic carbon, pH, nitrogen content, bulk density, and cation exchange capacity.

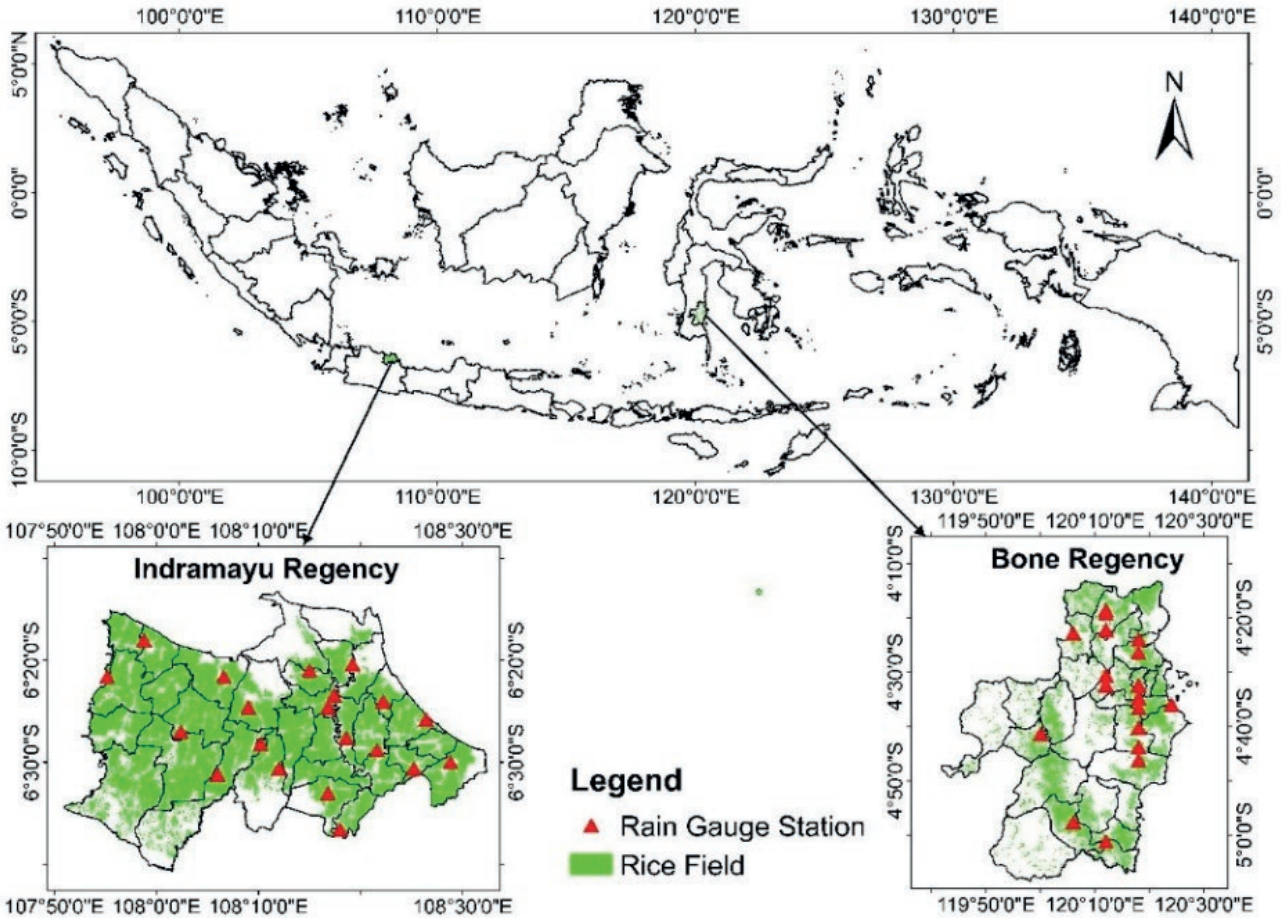

Figure 1. Study region and distribution of rain gauges.

Management practice data

In this study, management practices data were obtained through interviews with farmers. The data included sowing date, sowing density, row width, transplanting date, fertilizer application rates and dates, as well as irrigation application dates and amounts.

Crop phenology

Data on crop phenology were obtained from *the Book of Variety Description of Rice* published by the Indonesian Center for Food Crops Research and Development (ICFORD). The data included crop varieties, emergence, flowering, maturity, heat units, biomass at each stage, and yield.

Vegetation index

The Normalized Difference Vegetation Index (NDVI) was generated from MOD13Q1.061 Terra Vegetation Indices of MODIS TERRA, with a spatial resolution of 250 m and a temporal resolution of 16 days. The MODIS data underwent atmospheric correction to ensure reliable measurements of vegetation indices over time (de Oliveira and Epiphanio, 2012).

Methods

The method begins with the simulation of probable rice yields using the Decision Support System for Agro-technology Transfer (DSSAT) and the development of the SPI3–rice yield model. The model is implemented with SPI3, informed by gridded rainfall data from CHIRPS, to assess the spatial prediction of rice drought. The final step involves validating rice drought predictions using NDVI obtained from MODIS TERRA and evaluating prediction skill with the Proportion Correct (PC) method. Figure 2 presents the analysis flowchart.

Crop simulation scenario

The CERES-Rice model, a component of DSSAT (Hoogenboom et al., 2023; Jones et al., 2003), was used to simulate rice yield. The model has been validated and shown to provide high accuracy for the Indonesian region (Boer and Surmaini, 2020), with simulated rice yield results of R^2-adj = 88% ($P<0.01$). Planting date scenarios were established at 10-day intervals during the dry season, specifically on the 5th, 15th, and 25th of February, March, April, and May in Indramayu, and in May, June, July, and August in Bone for the period 1982–2009. The rice variety used was Ciherang, with a common fertilizer application of 200 kg/ha of urea, applied twice at 10 and 40 days after planting. Planting distance

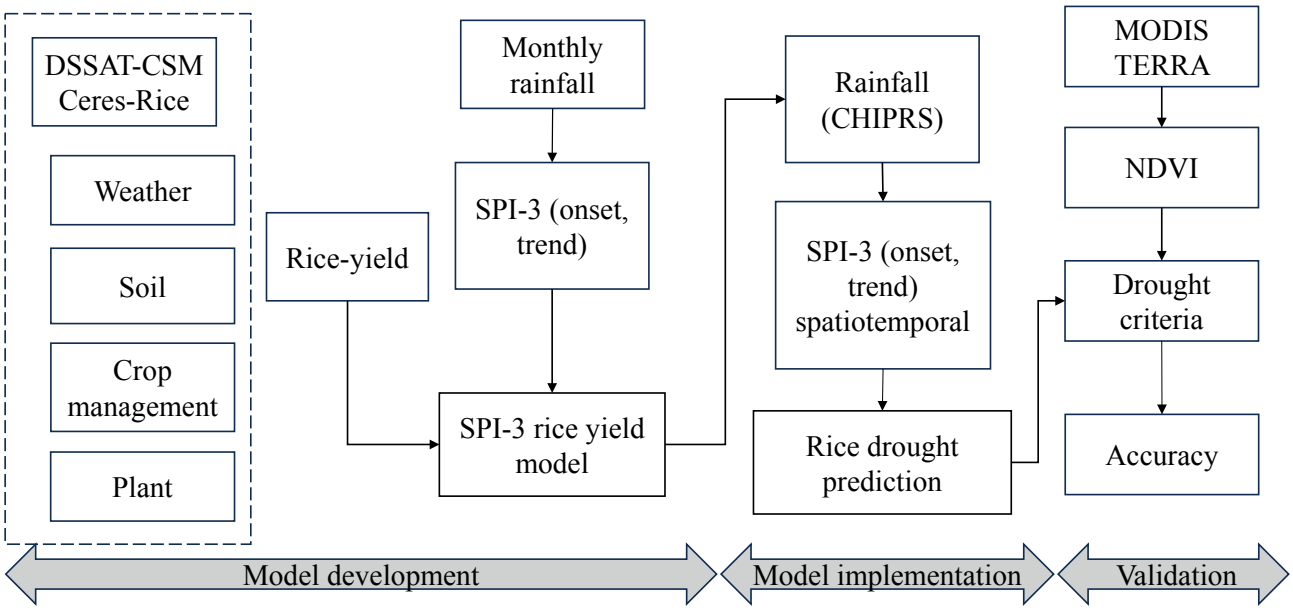

Figure 2. Flowchart outlining the development process of the rice drought prediction model.

was set at 25 × 20 cm, and transplanting was conducted 21 days after seedling emergence.

The Onset and Trend of SPI3

The SPI3 is calculated using the formula proposed by McKee et al. (1993). The SPI3 compares precipitation over a specific three-month period with historical records for the same period. The onset of SPI3 denotes its value at the beginning of the planting season. The SPI3 trend is defined by the gradient of SPI3 over four months, spanning from planting initiation to harvest, as shown in Figure 3. Rice yield predictions were generated one month prior to planting, providing an early warning of potential yield losses due to drought.

Linkage between the onset and trend SPI3 and rice yield

The Cartesian plane quadrants were utilized to examine the relationships between the onset and trend of SPI3 and rice yield (Figure 4). Quadrant (Q) I indicates the emergence of a positive SPI3 accompanied by an upward trend. Q II demonstrates the commencement of a positive SPI3, albeit with a declining trend. Q III depicts the onset of a negative SPI3, yet shows an upward trend. Finally, Q IV denotes the onset of a negative SPI3 with a declining trend. The SPI3 trend further provides insights into moisture dynamics, where a positive trend indicates an increase in moisture levels over time, whereas a negative trend signifies decreasing moisture levels.

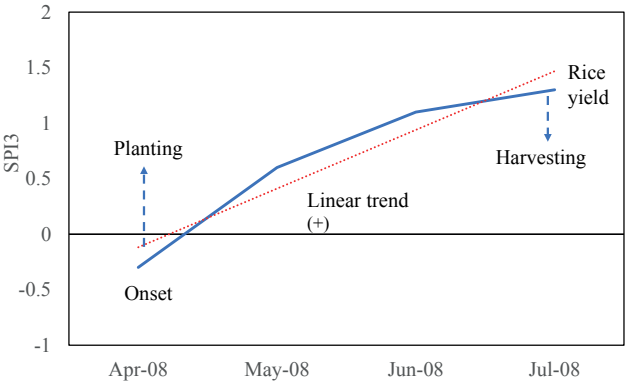

Figure 3. Plot of SPI3 onset and trend associated with planting and harvesting between April and July. As illustrated, the onset of SPI3, defined three months in advance (April 2008), is –0.3, while the SPI3 trend from April to July shows a gradient of +0.4.

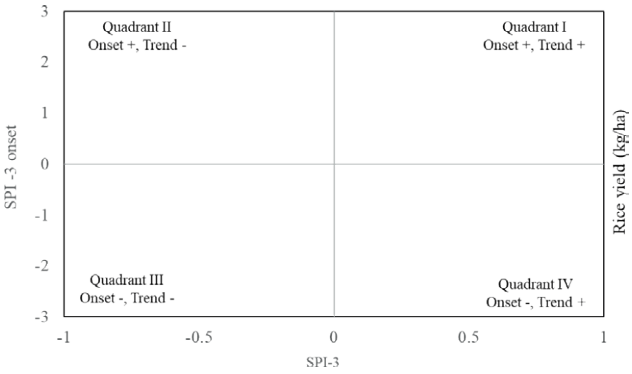

Figure 4. The quadrant illustrates the relationship between SPI3 onset (y-axis), SPI3 trend (x-axis), and rice yield.

Validation of rice drought prediction

This study employed NDVI to validate the spatial and temporal patterns of rice drought. In rice cultivation, which is particularly sensitive to variations in water availability, NDVI is instrumental in detecting early indicators of drought stress (Thapa et al., 2019). The dataset comprises two primary near-infrared (NIR) bands, which were employed to calculate NDVI following the formulation in Equation (1):

$$\mathbf{NDVI} = \frac{\mathbf{NIR}-\mathbf{Red}}{\mathbf{NIR}+\mathbf{Red}} \quad (1)$$

NDVI anomalies were calculated by comparing the monthly NDVI values for each year with a baseline period from 2014 to 2020. Negative anomalies indicated vegetation health below normal levels, suggesting the occurrence of water stress (Nanzad et al., 2019). The formula for NDVI anomaly is defined by Equation (2):

$$\mathbf{NDVIAnomaly} = \mathbf{NDVI_{Observed}} - \mathbf{NDVI_{baseline}} \quad (2)$$

Where: $NDVI_{observed}$ is the monthly median NDVI value for a specific time period. $NDVI_{baseline}$ is the monthly median NDVI value over a baseline period.

Vegetation anomalies were classified into four severity levels based on NDVI anomaly values, determined by predefined thresholds, as shown in Table 1.

Performance measures

Proportion of Correct (PC) is recognized as the most straightforward for assessing the accuracy of categorical forecast systems. Its simplicity and ease of interpretation make it a useful baseline for evaluating model performance, particularly when class distributions are

Table 1. NDVI anomaly ranges for drought hazard classification.

Class	NDVI Anomaly Range	Drought level	Description
Class 1	Anomaly > 0.05	Low	Above-normal vegetation growth, likely resulting from surplus water availability
Class 2	-0.05 ≤ Anomaly ≤ 0.05	Moderate	Absence of significant water stress or drought conditions
Class 3	-0.1 ≤ Anomaly < -0.05	High	Minor drought conditions, characterized by vegetation experiencing moderate water stress
Class 4	Anomaly < -0.1	Very High	Signify severe drought conditions

balanced (Nurmi, 2003; Wilks, 2019), and it has been widely used in drought prediction systems where ease of communication to stakeholders is critical (Wilks, 2019). This measure is derived by calculating the ratio of accurate predictions to the total number of predictions, as described by Equation (3). The schematic contingency for categorical forecasts is detailed in Table 2.

$$\mathbf{PC} = \frac{\mathbf{a+d}}{\mathbf{n}} \quad (3)$$

The PC methods commonly applied to analyze categorical data are based on contingency tables (Mason, 2012). The elements of equation 3 and Table 2 are defined as a (hits) represents the number of true positives, where the model predicted drought and drought was observed, b (false alarms) indicates the number of false positive, where the model predicted drought, although no drought was observed, c (misses) represents the number of false negative, where the model predicted no drought, but drought was occurred, d (correct rejections) indicates the number of true negatives, where the model correctly predicted no drought and no drought was observed, and n expresses the total number of observations.

The model was developed using historical data from 1982 to 2009, which served as the model construction. The validation process was conducted using an independent dataset covering the period 2014 to 2020, applied at monthly intervals. The choice of these periods was determined by the availability and consistency of reliable data, while the gap years (2010-2013) were excluded due to data incompleteness. This approach ensured that the model's performance could be rigorously evaluated under independent conditions, thereby strengthening the reliability of its predictive capability. Additional validation was conducted for specific months in DSP1 (June) and DSP2 (October) during Neutral (2014), El Niño (2015), and La Niña (2017) years.

Table 2. Schematic contingency table for categorical forecasts of binary events.

Forecast	Observed		
	Yes	No	Total
Yes	a (Hits)	b (False alarms)	a+b
No	c (Misses)	d (Correct rejections)	c+d
Total	a+c	b+d	a+b+c+d= n

RESULTS

Association between SPI3 and rice yield

Figure 5 illustrates that the temporal patterns of SPI3 and rice yield anomalies show that periods of negative and positive rice yield anomalies are interspersed with dry and wet conditions throughout the study years. In Indramayu, notable drought events, indicated by negative SPI3 values, were recorded in 1982, 1991, and 1997. During these years, rice yield anomalies were markedly lower than average, reflecting a significant reduction in actual rice yields compared to typical levels. These events are associated with reduced WSP periods and production, consistent with the lower-than-average yield anomalies we observe in those years (Siswanto et al., 2022). In contrast, in Bone, yield declines occur only during extreme or prolonged drought, reflecting local hydroclimatic and management differences (Sunusi et al., 2024). This spatial heterogeneity in drought–yield relationships highlights a broader pattern seen across Indonesia, where rice yield responses to SPI-based drought indicators vary considerably depending on local agroclimatic conditions (Hendrawan et al., 2023).

The onset and trend SPI3 - rice yield model

Figure 6 was generated by combining data from the two study areas, Indramayu and Bone. These data were used to develop a prediction model designed to robustly capture agricultural drought events in distinct rainfall regimes, specifically the monsoonal rainfall in Indramayu and the local rainfall in Bone.

This figure reveals a clear association between the onset and trend of SPI3 and rice yields. Rice yields below

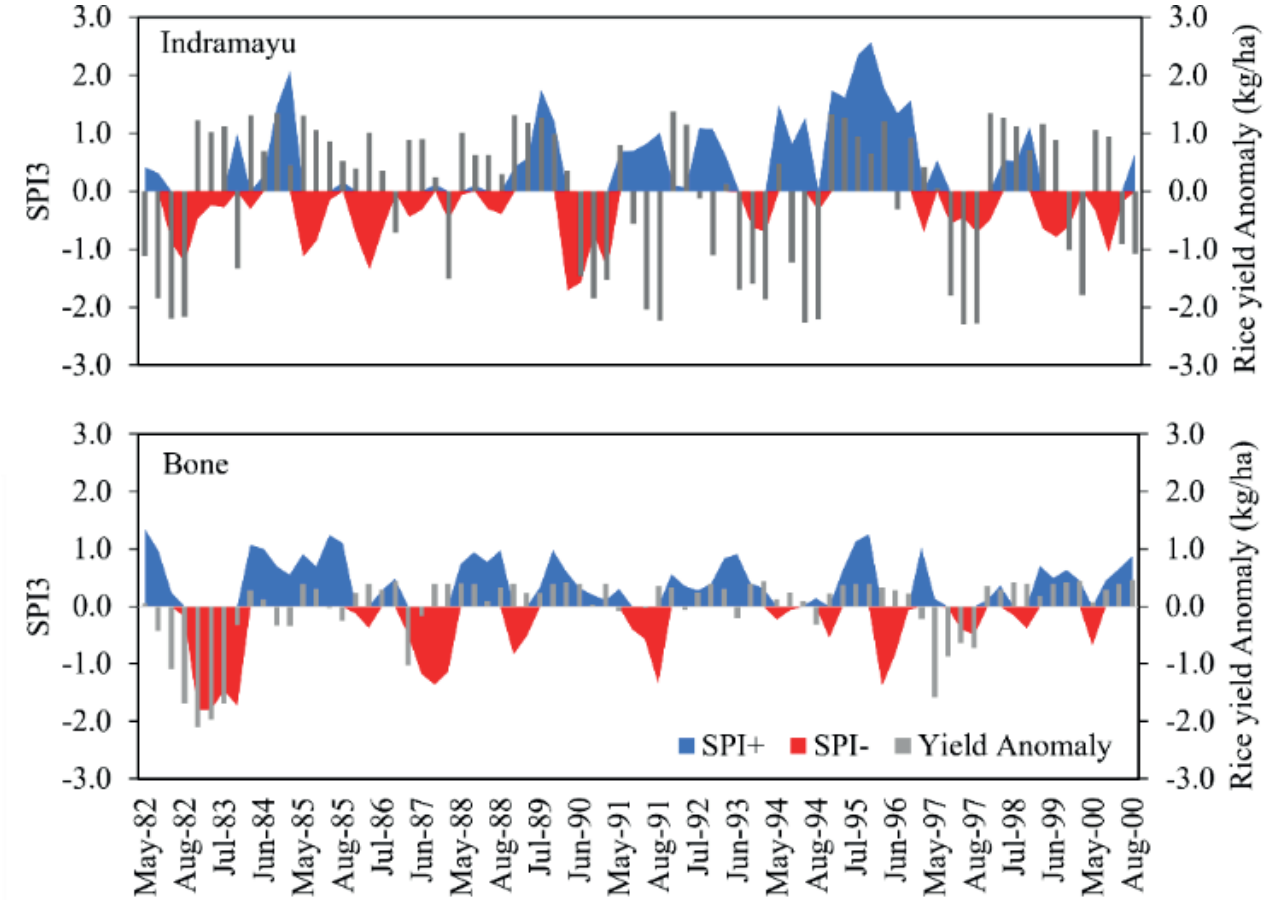

Figure 5. Evolution of SPI3 from 1982 to 2000, with a comparison to rice yield anomalies in Indramayu and Bone.

2 t/ha appear more frequently in Quadrants II and III, which are characterized by negative SPI3 trends indicating drier conditions during the growing season, consistent with other regional findings that SPI3 effectively captures drought-induced reductions in rice productivity (Surmaini et al., 2019). In contrast, Quadrants I and IV - marked by positive SPI3 trends and therefore wetter conditions show a higher incidence of rice yields exceeding 4 t/ha, suggesting improved moisture availability significantly mitigates drought-induced yield losses.

The Cumulative Distribution Function (CDF) offers a compelling visualization of the probability distribution of rice yields under the corresponding conditions in each quadrant. Figure 7 shows the CDF curves for QII and QIII, which demonstrate a gradual increase up to less than 4 t/ha, indicating that lower rice yields are more prevalent when both SPI3 trends are negative. In contrast, in QI and QIV, the CDF curves exhibit a steep increase once rice yields exceed 4 t/ha, suggesting that higher rice yields are more common when both the onset and trend of SPI3 are positive.

The rice drought category in each quadrant is assessed using a score based on a rice yield threshold of 2 t/ha, under the assumption that drought conditions result in yields falling below this level. The score is calculated by multiplying the percentage of rice yields below 2 t/ha in each quadrant by the probability of these yields occurring in that quadrant, relative to the total sample across all quadrants. The rice drought categories are classified into four levels, as presented in Table 3.

Skill of rice drought prediction

The performance of rice drought prediction across four drought categories from 2014 to 2020 is shown in Figure 8. The analysis was conducted monthly from January to December, comparing the model's predictions with observed conditions using NDVI data from the MOD13Q1 product.

Figure 8 (a) displays rice drought predictions in Indramayu. In the low drought category, accuracy

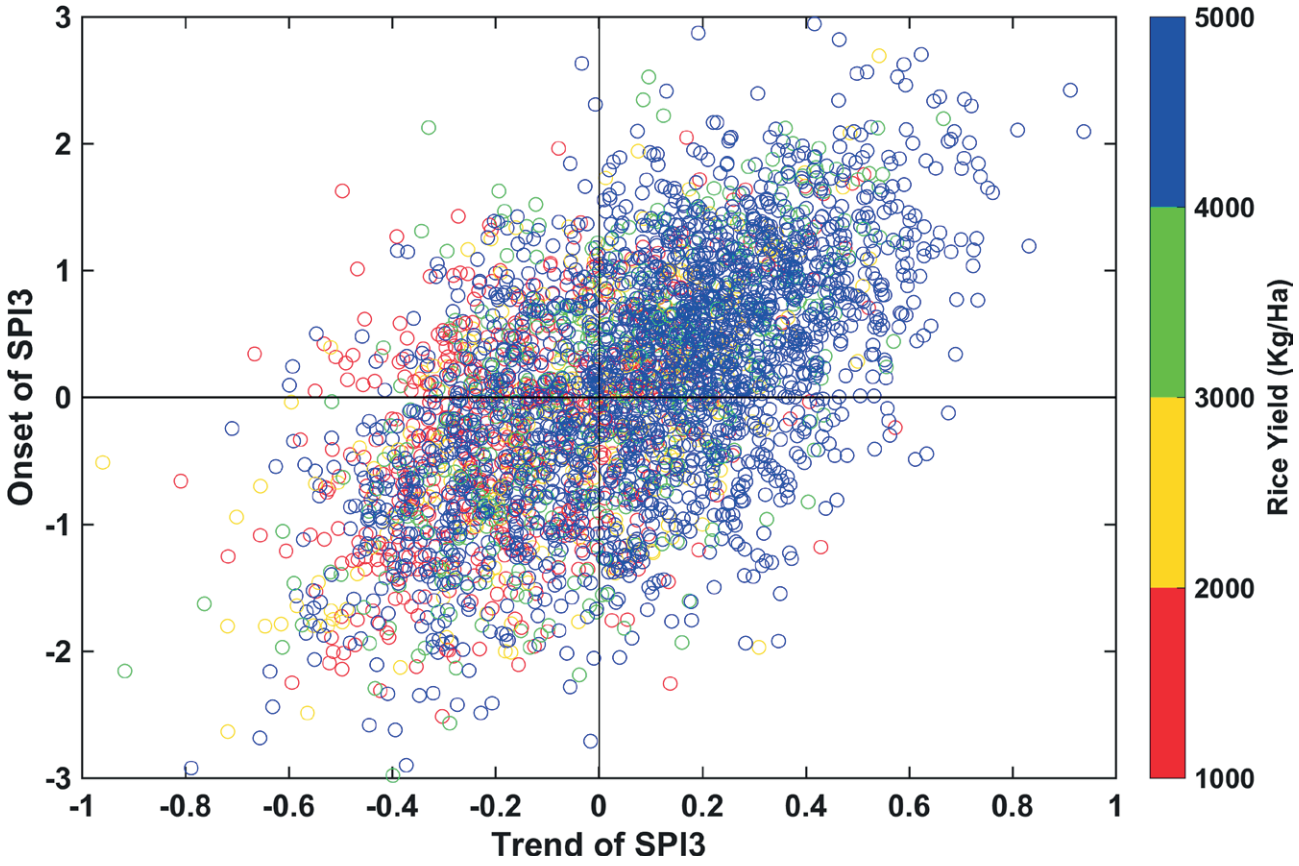

Figure 6. Rice yields are displayed in a Cartesian plot with the SPI3 onset value on the y-axis and the SPI3 trend on the x-axis. Positive SPI3 onset values correspond to wet conditions, whereas negative values indicate dryness. Similarly, a positive SPI3 trend represents rising moisture availability, while a negative trend reflects a decline. Quadrants represent onset–trend combinations: QI = wet/wetter, QII = wet/drier, QIII = dry/drier, QIV = dry/wetter. The color of the circle in the quadrat indicates different rice yields.

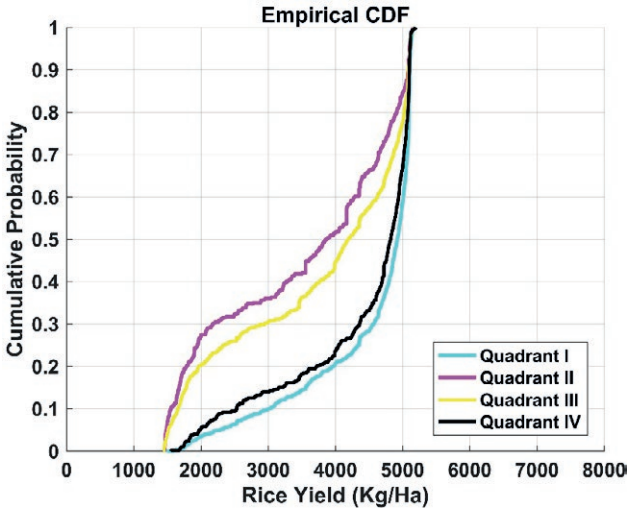

Figure 7. The CDF of rice yield for each quadrant.

Table 3. Criteria for rice drought levels

Quadrant	Sample (%) Rice yield < 2 ton/ha (a)	Probability of rice yield < 2 ton/ha (b)	Score (axb)	Drought level
I	15.194	0.034	0.005	Low
II	24.734	0.276	0.068	High
III	50.707	0.328	0.166	Very high
IV	9.364	0.130	0.012	Moderate

typically ranges from 50% to 80%. In the moderate category, accuracy varies between 40% and 70%, with reduced error bars indicating increased confidence. However, significant declines are observed in March and August, highlighting difficulties during the transitions between wet and dry seasons. The high category exhibits marginally higher accuracy (50-75%) compared to the moderate category, albeit with greater error margins. In the very high category, accuracy

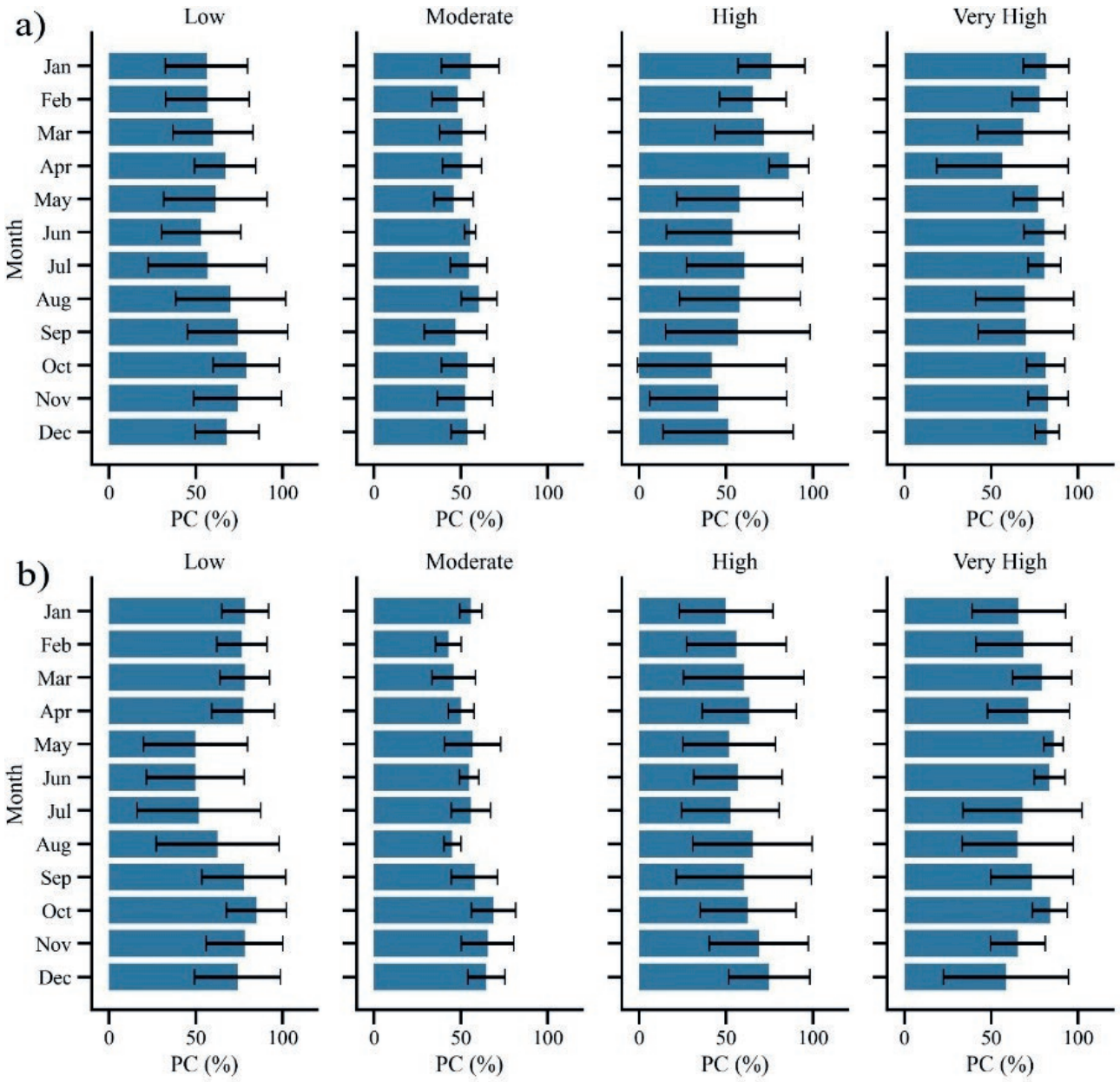

Figure 8. Accuracy of rice drought predictions for the 2014–2020 period in a) Indramayu and b) Bone.

ranges from 60% to 85%, peaking in June and July during the dry season. These findings suggest that the model is more effective in predicting severe droughts during the dry season, while its performance diminishes during the wet and transitional seasons.

Figure 8 (b) displays the efficacy of rice drought prediction in Bone. In the Low drought category, accuracies vary between 50% and 75%, with large error bars indicating high variability. In the Moderate drought category, accuracies range from 40% to 60%, with narrower error margins, suggesting a higher level of confidence. The model's accuracy for the High drought category ranges from 40% to 80%, with reduced performance observed during the wet season (October to December). This indicates challenges in accurately identifying severe drought events during the transitional dry–wet season. In the Very High category, accuracy improves across the months, ranging from 60% to 85%, suggesting enhanced performance. However, substantial uncertainty remains in predicting extreme drought conditions in April and

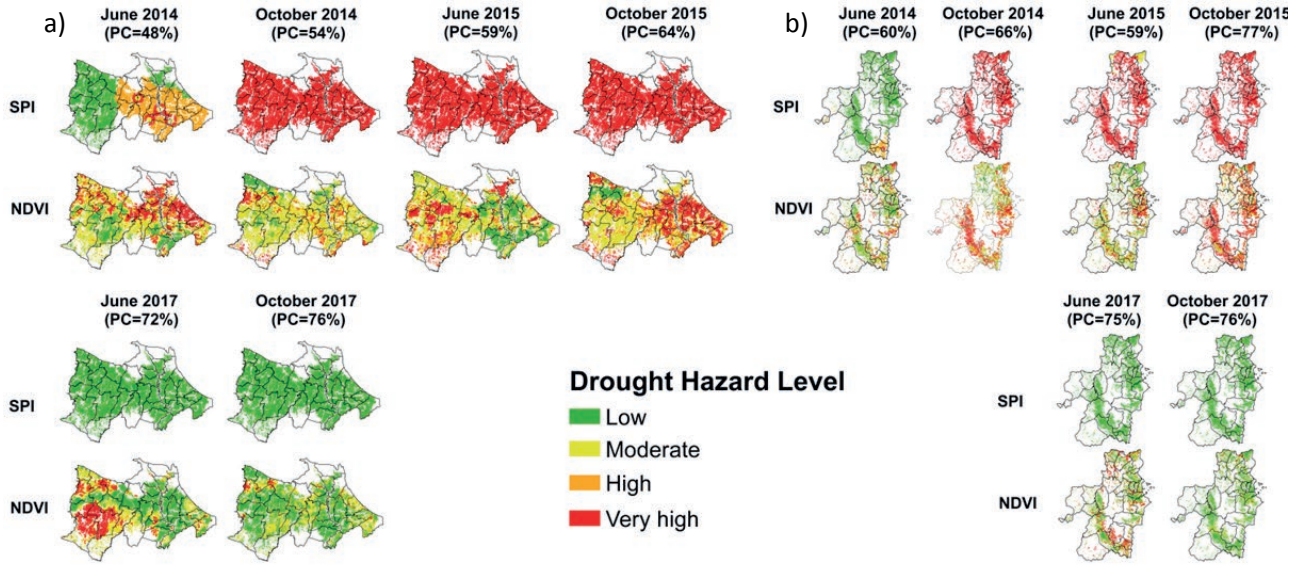

Figure 9. Map of the predicted and observed rice drought in a) Indramayu and b) Bone for June (DSP1) and October (DSP2) during 2014, 2015, and 2017, corresponding to Neutral, El Niño, and La Niña years. Shaded areas denote rice field regions, while color variations indicate the corresponding drought categories. The SPI row indicates predicted rice drought, while the NDVI row represents observed conditions.

September, highlighting challenges during transitions between the dry and wet seasons.

Figure 9 depicts the spatially predicted and observed rice drought for June (DSP1) and October (DSP2) in 2014, 2015, and 2017, corresponding to Neutral, El Niño, and La Niña years. The impact of ENSO on rice drought categories in the Indramayu and Bone regions shows a comparable pattern. During El Niño years, rice drought levels are typically higher than in Neutral years, whereas La Niña years generally exhibit lower levels.

Predictions for October (DSP2) in the Neutral year (2014) and the El Niño year (2015) indicate very high rice drought categories, with the highest PC at 64% for Indramayu and 76% for Bone. In the La Niña year (2017), predictions for June (DSP1) and October closely aligned with the observed low drought category, with the PC for both regencies ranging from 72% to 76%. Observations, however, revealed areas with varying hazard levels from low to high. Rice drought prediction for October shows higher accuracy compared to June, indicating improved model performance during the peak of the dry season. This discrepancy reflects the complexities of local conditions influencing vegetation resilience during drought periods.

DISCUSSION

Figure 5 highlights the link between SPI3 and rice yield anomalies. In Indramayu, prolonged severe negative SPI3 values are associated with reduced rice yields, as evidenced in 1982, 1991, and 1997. This aligns with the findings of Prabnakorn et al. (2018), which indicate that SPI values below -1 often lead to significant yield reductions. Furthermore, Rejekiningrum et al. (2022) emphasized that regions experiencing increased drought frequency and duration are likely to experience substantial agricultural losses, which underscores the sensitivity of rice cultivation in Indramayu to persistent climate stress. Conversely, in Bone, episodes of negative SPI3 tend to be shorter and less severe, reflecting milder drought conditions with relatively limited impacts on rice productivity. This divergence underscores the role of regional climatic variability in shaping drought risk and agricultural outcomes. It also suggests that while Indramayu requires more robust drought-mitigation strategies, Bone may benefit from adaptive practices that focus on maintaining resilience during shorter-term drought.

Figure 6 illustrates that rice yields exhibit a specific response to SPI3, particularly in relation to the onset and trends, and their progression throughout the growing season. Negative SPI3 values in the early growing season may hinder crop establishment, whereas moisture deficits during the reproductive phase often lead to pronounced yield reductions as a result of water stress during grain development (Ray et al., 2015). In contrast, positive SPI3 values reflect favorable moisture availability, which promotes crop growth and has the potential to enhance yields (Gebrehiwot et al., 2011; Forootan et al., 2019). Our

analysis strengthens earlier conclusions by indicating that SPI3 is effective not only in identifying drought occurrence but also in forecasting rice yield anomalies.

The accuracy of rice drought prediction varies across the four drought categories throughout the year, with higher accuracy observed in the low and very high drought categories. These observations align with the findings of Mohseni et al. (2021), who reported that satellite-based NDVI data, such as MOD13Q1, are effective in predicting both low and high drought events by clearly distinguishing between normal vegetation and stressed conditions. In contrast, the moderate drought category often shows reduced accuracy. This limitation arises because vegetation stress during moderate drought is relatively subtle, and the associated spectral changes may overlap with those observed under normal conditions. Consequently, NDVI alone may fail to discriminate intermediate drought intensities with sufficient precision (Zhang et al., 2016. Lee et al. (2021) further noted that incorporating additional variables, such as soil moisture or land surface temperature, enhances the accuracy of moderate drought detection by utilizing diverse datasets. Moreover, research using higher-resolution imagery, such as Landsat, has demonstrated improved accuracy in identifying severe droughts (Yang et al., 2023). Nevertheless, MOD13Q1 remains one of the most widely used products due to its temporal frequency and long historical record, even though its relatively coarse spatial resolution introduces challenges in capturing localized extreme drought events.

From an evaluation perspective, the PC method is widely used in drought monitoring because it provides an intuitive measure of correctly classified drought categories and offers a simple means of communicating forecast performance to stakeholders in early warning systems. However, PC has notable limitations, since missing an actual drought (miss) often carries more severe consequences than issuing a false alarm, leading to an overly optimistic view of forecast reliability. For this reason, PC is most effective when used in combination with additional skill scores that capture event-specific performance. Metrics such as the Heidke Skill Score, Cohen's Kappa, and the Brier Score offer more comprehensive evaluations of categorical forecasts, allowing for a more balanced assessment of model reliability (Mason, 2003; Wilks, 2019).

The discrepancy between drought predictions and NDVI observations in Indramayu during DSP2 (October) of the Neutral year 2014, as well as DSP1 (June) and DSP2 (October) of the El Niño year 2015 (Figure 9a), can largely be explained by the dominance of irrigation infrastructure in the western part of the regency. While the model-based predictions classified these periods into higher drought categories, NDVI values suggested a relatively low drought category in certain areas. This divergence highlights the buffering effect of irrigation systems, which can sustain vegetation health even under negative SPI3 conditions by providing a reliable water supply. (Xiao et al., 2023). Consequently, NDVI may underestimate drought severity in irrigated regions, as vegetation remains green and photosynthetically active despite underlying hydrological stress (Rembold et al., 2019; Satapathy et al., 2024).

In Bone, the accuracy of drought prediction is enhanced by its extensive rainfed rice fields, which enable SPI3 to effectively capture NDVI patterns. Unlike irrigated systems, rainfed agriculture is directly influenced by rainfall anomalies, linking meteorological drought indices and vegetation dynamics more apparent (Rojas et al., 2011; Chen et al., 2025). However, predictive accuracy decreases during transitional months, such as the shift between the dry and wet seasons, when rainfall patterns become highly variable and less predictable. This is often accompanied by a broad error margin, reflecting increased uncertainty in distinguishing between short-term dry spells and the onset of sustained drought conditions (AghaKouchak et al., 2015).

These findings underscore that in regions with extensive irrigation networks, NDVI may fail to fully capture the agricultural impacts of meteorological drought, leading to discrepancies between predicted drought categories and observed vegetation responses. This suggests that integrating additional variables, such as irrigation coverage, groundwater use, could improve the accuracy of drought assessments (He et al., 2022; Purnamasari et al., 2025). For policymakers, this implies that drought early warning systems should incorporate both climatic indicators and agricultural water management practices to provide more reliable information for decision-making.

The prediction accuracies obtained for both regions are nearly identical, indicating that data from Indramayu and Bone can generate predictions with comparable reliability. This finding supports the broader objective of developing a generalized model for application across Indonesia, where diverse rainfall regimes and agro-ecological conditions prevail. Furthermore, to enhance drought prediction accuracy, future research should prioritize integrating higher-resolution data with machine learning techniques, which could improve both the accuracy and reliability of predictions. Incorporating local irrigation practices into prediction models is crucial, as such practices can significantly mitigate the impacts of drought and lead to discrepancies between observed

NDVI and predicted rice drought. Finally, to improve the transferability of the model developed in this study, future work should emphasize validation across diverse regions, time periods, and climate regimes, thereby enabling a more comprehensive assessment of model accuracy and performance.

Several widely used data sources for operational SPI forecasts include the NOAA Climate Prediction Center, which issues global seasonal precipitation outlooks (NOAA, 2024); the ECMWF seasonal forecasting system, which provides ensemble-based precipitation predictions suitable for SPI calculation (ECMWF, 2023); the SPEIbase and Global Drought Observatory platforms, which disseminate SPI and related drought indices across varying time scales (GDO, 2024); and the BMKG's national seasonal rainfall forecasts, which are routinely available for Indonesia (BMKG, 2023). Although our study was retrospective, these forecast products offer a clear pathway for future operationalization, enabling real-time or anticipatory rice drought prediction and strengthening the applicability of our framework for practitioners and policymakers.

CONCLUSION

This study proposes a rice drought prediction model that employs the onset and trend of SPI3 as key predictors. The model was developed using data from two major rice-producing regions characterized by contrasting rainfall patterns. The onset of SPI3 refers to its value at the beginning of the planting season, while the SPI3 trend is defined as the gradient over four months from planting initiation to harvest. Rice yield predictions were generated one month prior to planting, providing an early warning of potential yield losses due to drought. Yield estimation within the model was conducted using a crop simulation approach, and drought predictions were validated against NDVI observations.

Our study highlights that the association between the onset and trend of SPI3 is strongly linked to rice yield outcomes. Specifically, lower yields tend to occur under negative SPI3 trends, reflecting drier-than-normal conditions during the growing season, whereas higher yields are generally associated with positive SPI3 trends, indicative of wetter conditions. This relationship underscores the utility of SPI3 not only as a drought indicator but also as a predictor of potential yield variability.

Overall, the results demonstrate that the prediction model performs more reliably in capturing severe drought conditions, particularly during the dry season, whereas its performance declines during wet and transitional periods. In both Indramayu and Bone, accuracies in the very high drought category are consistently higher, with accuracy ranges between 60-85%, indicating the model's strength in detecting extreme drought events. However, reduced accuracy and larger uncertainties during seasonal transitions highlight the challenges of predicting drought under highly variable climatic conditions. During El Niño years, rice drought categories are typically elevated compared to neutral years, with PCs ranging from 59% to 77%, whereas in La Niña years they correspond more closely with the observed low drought category, with PCs ranging from 72% to 76%.

The higher accuracy achieved for the very high rice drought category in this study is crucial for advancing rice drought prediction. Comparable prediction accuracies for Indramayu and Bone further support the feasibility of developing a generalized model applicable across Indonesia's diverse agroecological conditions. Nevertheless, accuracy decreases during transitional periods, highlighting the challenges of maintaining predictive reliability amid rapidly changing rainfall patterns. Incorporating local irrigation practices into the model is essential, as such practices can markedly alter drought impacts and explain discrepancies between observed NDVI and predicted rice drought. In addition, expanding validation across multiple regions, time periods, and climate regimes is essential to enhance the model's transferability and provide a thorough assessment of its accuracy, reliability, and overall performance under diverse agroclimatic conditions.

ACKNOWLEDGMENT

This study was partly supported by the Indonesian Agency for Agricultural Research and Development (Grant No. 83.3/PL.040/I.1/04/2016.K). We are grateful for the invaluable support provided by the Weather and Climate Prediction Laboratory, Bandung Institute of Technology.

REFERENCES

AghaKouchak A., Melton F.S., Teixeira J., Anderson M.C., Wardlow B.D., Hainet C.R., 2015. Remote sensing of drought: Progress, challenges and opportunities. Reviews of Geophysics, 53 (2): 452–480

Bhardwaj K., Shah D., Aadhar S., Mishra, 2020. Propagation of meteorological to hydrological droughts in India. Journal of Geophysical Research: Atmospheres, 125(22): e2020JD03345.

BMKG., 2023. Seasonal Climate Outlook. Indonesian Agency for Meteorology, Climatology, and Geophysics. https://www.bmkg.go.id

Boer R., Surmaini E., 2020. Economic benefits of ENSO information in crop management decisions: case study of rice farming in West Java, Indonesia. Theoretical and applied climatology, 139(3–4): 1435–1446.

BPS [Statistics Indonesia] (2024). Statistical Yearbook of Indonesia 2024 vol 52. BPS-Statistic Indonesia. 801p.

Chen Y., Wang Y., Wu C., Maniçoba A., Jardim R.F., Fang M., Yao L., Liu G., Xu Q., Chen L., Tang X., 2025. Drought-induced stress on rainfed and irrigated agriculture: Insights from multi-source satellite-derived ecological indicators. Agricultural Water Management, 37: 109249

D'Arrigo R.D., Wilson R., 2008. El Niño and Indian Ocean influences on indonesian drought : implication for forecasting rainfall and crop productivity. International Journal of Climatology, 28: 611–616.

Dai M., Huang S., Huang Q., Leng G., Guo Y., Wang L., Fang W., Li P., Zheng X., 2020. Assessing agricultural drought risk and its dynamic evolution characteristics. Agricultural Water Management, 231:1-12.

de Oliveira J.C., Epiphanio J.C.N., 2012. Noise reduction in MODIS NDVI time series data based on spatial-temporal analysis. In Proceeding of 2012 IEEE International Geoscience and Remote Sensing Symposium (pp. 2372-2375).

ECMWF., 2023. SEAS5*:* ECMWF Seasonal Forecasting System. European Centre for Medium-Range Weather Forecasts. https://www.ecmwf.int

FAO., 2012. Coping with water scarcity An action framework for agriculture and food security. FAO Water Reports. Food and Agriculture Organization of the United Nations. Viale delle Terme di Caracalla 00100 Rome, Italy

Forootan E., Khaki M., Schumacher M., Wulfmeyer V., Mehrnegar N., van Dijk A., et.al., 2019. Understanding the global hydrological droughts of 2003-2016 and their relationships with teleconnections. Science Total Environment, 650 (2): 2587–2604.

Gebrehiwot T., van der Veen A., Maathuis B., 2011. Spatial and temporal assessment of drought in the Northern highlands of Ethiopia. International Journal Applied Earth Observation, 13 (3): 309–321.

GDO., 2024. Global Drought Observatory. European Commission, Joint Research Centre. https://edo.jrc.ec.europa.eu/gdo

Hao Z., Singh V.P., 2015. Drought characterization from a multivariate perspective: A review. Journal of Hydrology, 527: 668–678.

He L., Tong L., Zhou Z., Gao T., Ding Y., Ding Y., Zhao Y., Fan W., 2022. A Drought Index: The Standardized Precipitation Evapotranspiration Irrigation Index. Water, 14(13): 2133.

Hendrawan V. S. A., Komori K., Kim W., 2023. Possible factors determining global-scale patterns of crop yield sensitivity to drought. PLoS ONE 18(2): e0281287

Hoogenboom G., Porter C.H., Shelia V., Boote K.J., Singh U., Pavan W., Oliveira F.A.A, Moreno-Cadena L.P., et al., 2023. Decision support system for sgrotechnology transfer (DSSAT) Version 4.8.2 (www.DSSAT.net). DSSAT Foundation, Gainesville, Florida, USA.

Jones J.W., Hoogenboom G., Porter C.H., Boote K.J. Batchelor W.D., Hunt L.A, Wilkens P.W., Singh U., Gijsman A.J., Ritchie, J.T., 2003. The DSSAT cropping system model. European Journal of Agronomi, 18: 235-265.

Lee S.J., Kim N., Lee Y.N., 2021. Development of integrated crop drought index by combining rainfall, land surface temperature, evapotranspiration, soil moisture, and vegetation index for agricultural drought monitoring. Remote Sensing 13(9): 1778.

Leng G., Hall J., 2019. Crop yield sensitivity of global major agricultural countries to droughts and the projected changes in the future. Science of The Total Environment Journal, 654: 811–821.

Li Q., Ye A., Wada Y., Zhang Y., Zhou J., 2024. Climate change leads to an expansion of global drought-sensitive area. Journal of Hydrology, 632: 1-9.

Mason I.B., 2012. Binary events. İn Jolliffe, I. T. and Stephenson, D.B (Eds). A practitioner's guide in atmospheric science (2 nd Edition). Oxford. Wiley & Blackwell.

McKee T.B., Doesken N.J., Kleist J., 1993. The relationship of drought frequency and duration to time-scale. In: Proceeding of The Eighth Conference on Applied Climatology 17-22 January 1993 Anaheim, California (Fort Collins: Colorado State University) p 6.

Mishra A.K., Singh V.P., 2010. A review of drought concepts. Journal of Hydrology, 391(1-2): 202-216.

Mohseni F., Sadr M.K., Eslamian S., Areffian A., Khoshfetrat A., 2021. Spatial and temporal monitoring of drought conditions using the satellite rainfall estimates and remote sensing optical and thermal measurements. Advances in Space Research, 67(12): 3942-3959.

Nanzad L., Zhang J., Tuvdendorj B., Nabil M., Zhang S., Bai Y., 2019. NDVI anomaly for drought 611 monitoring and its correlation with climate factors over Mongolia from 2000 to 2016. Journal of Arid Environment. 164 : 69–77

Naylor R.L., Battisti D.S., Vimont D.J., Falcon W.P., Burke, M.B., 2007. Assessing risks of climate variability and climate change for Indonesian rice agriculture. PNAS, 104(19): 7752–7757.

NOAA., 2024. Climate Prediction Center: Seasonal Climate Outlooks. National Oceanic and Atmospheric Administration. https://www.cpc.ncep.noaa.gov

Nurmi P., 2003. Recommendations on the verification of local weather forecasts. ECMWF Operations Department. 18p.

Pei Z., Fang S., Wang L., WangW., 2020. Comparative analysis of drought ındicated by the spı and speı at various timescales in ınner Mongolia, China. Water, 12: 925.

Prabnakorn S., Maskey S., Suryadi F.X., de Fraiture C., 2018. Rice yield in response to climate trends and drought index in the Mun River Basin, Thailand. Science Total Environment, 621: 108–119.

Purnamasari D., Teuling A.J., Weerts A.H., 2025. Identifying irrigated areas using land surface temperature and hydrological modelling: application to the Rhine basin. Hydrology and Earth System Sciences, 29: 1483–1503.

Rejekiningrum P., Apriyana Y., Sutardi, Estiningtyas W., Sosiawan H., Susilawati H.L., Hervani A., Alifia A.D., 2022. Optimising water management in drylands to increase crop productivity and anticipate climate change in Indonesia. Sustainability, 14: 11672.

Thapa S., Rudd J.C., Xue Q., Bhandari M., Reddy S. K., Jessup K.E., Liu S., Devkota R.N., Baker J., Baker, S., 2019. Use of NDVI for characterizing winter wheat response to water stress in a semi-arid environment. Journal of Crop Improvement, 33(5): 633–648.

Tsige D,T., Uddameri V., Forghanparast F., Hernandez E.A., Ekwaro-Osire S., 2019. Comparison of meteorologicaland agriculture-related drought indicators across Ethiopia. Water, 11:(11).

Ray D. K., Gerber J.S., MacDonald G.K., West P.C., 2015. Climate variation explains a third of global crop yield variability. Nature Communications. 6: 5989 https://doi.org/10.1038/ncomms6989

Rembold F., Meroni M., Urbano F., Csak G., Kerdiles H., Perez-Hoyos L.G., Leo O., Negre T., 2019. ASAP: A new global early warning system to detect anomaly hot spots of agricultural production for food security analysis, Agricultural Systems, 168 : 247–257.

Rojas O., Vrieling A., Rembold F., 2011. Assessing drought probability for agricultural areas in Africa with coarse resolution remote sensing imagery. Sensing of Environment, 115: 343–352.

Satapathy T., Dietrich J., Ramadas M., 2024. Agricultural drought monitoring and early warning at the regional scale using a remote sensing-based combined index. Environment Monitoring Assessment, 196: 1132.

Siswanto_S., Wardani K.K., Purbantoro B., Rustanto A., Zulkarnain F., Anggraheni E., Dewanti R., Nurlambang T., Dimyati M., 2022. Satellite-based meteorological drought indicator to support food security in Java Island. PLoS ONE, 17(6): e0260982.

Sunusi N., Auliana N.H., Jaya A.K., Siswanto, Herdian E.T., 2024. Mapping Meteorological Drought Periods in South Sulawesi Using the Standardized Precipitation Index with the Power Law Process Model. Journal of Environmental & Earth Sciences, 7(1): 438–456.

Surmaini E., Hadi T.W., Subagyono K., Puspito N.T., 2015. Early detection of drought impact on rice paddies in Indonesia by means of Niño 3.4 index. Theoriacl Applied Climatology, 121 (3–4): 669–684.

Surmaini E., Susanti E., Syahputra M.R., Hadi T.W., 2019. Exploring Standardized Precipitation Index for predicting drought on rice paddies in Indonesia. IOP Conference Series: Earth and Environmental Science, 303(1):012027

Surmaini E., Ramadhani F., Syahputra M.R., Dewi, E.R., Apriyana Y., 2020. Development of a paddy drought hazard forecasting system to cope with the impact of climate change. IOP Conf. Series: Earth and Environmental Science. 484: 012050

Wilks D. S., 2019. Statistical Methods in the Atmospheric Sciences (4th ed.). Amsterdam. Elsevier.

Wu B., Ma Z., Yan N., 2020. Agricultural drought mitigating indices derived from the changes in drought characteristics. Remote Sensing Environment, 244: 111813.

Xiao C., Zaehle S.,Yang H., Wigneron J.P., Schmullius C., Basto A., 2023. Land cover and management effects on ecosystem resistance to drought stress. Earth System Dynamics, 14: 1211–1237.

Xu Z., Wu Z., Shao, Q., He H., Guo X., 2023. From meteorological to agricultural drought: Propagation time and probabilistic linkages. Journal of Hydrology: Regional Studies, 46.

Yang Z., Huang Y., Duan Z., Tang J., 2023. Capturing the spatiotemporal variations in the gross primary productivity in coastal wetlands by integrating eddy covariance, Landsat, and MODIS satellite data: A case study in the Yangtze Estuary, China. Ecological Indicators, 149: 110154.

Zargar A., Sadiq R., Naser B., Khan F. I. 2011. A review of drought indices. Environmental Reviews, 19: 333–349.

Zhang J., Mu Q., Huang J., 2016. Assessing the remotely sensed Drought Severity Index for agricultural

drought monitoring and impact analysis in North China. Ecological Indicators, 63: 296-309.
Zinat M.R.M., Salam R., Badhan M.A., Islam A.R.M.T., 2020. Appraising drought hazard during Boro rice growing period in western Bangladesh. International Journal of Biometeorology, 64(10): 1687–1697.
Zipper S.C., Qiu J., Kucharik C.J., 2016. Drought effects on US maize and soybean production: Spatiotemporal patterns and historical changes. Environmental Research Letters, 11: 094021.
Zhou S., Yu B., Zhang Y., 2023. Global concurrent climate extremes exacerbated by anthropogenic climate change. Science Advances, 9 (10): eabo1638.

Italian Journal of Agrometeorology
Rivista Italiana di Agrometeorologia

Firenze University Press
https://riviste.fupress.net/index.php/IJAm

OPEN ACCESS

Citation: Deveci, H., Önler, B., & Erdem, T. (2025). Estimation of irrigation water requirements of sunflower under the context of climate change in TR21 Thrace Region. *Italian Journal of Agrometeorology* (2): 39-52. doi: 10.36253/ijam-2920

Received: August 24, 2024

Accepted: September 12, 2025

Published: December 31, 2025

Data Availability Statement: All relevant data are within the paper and its Supporting Information files.

Competing Interests: The Author(s) declare(s) no conflict of interest.

ORCID:
HD: 0000-0002-0143-2185
BÖ: 0000-0002-0928-595X
TE: 0000-0002-5887-9586

Estimation of irrigation water requirements of sunflower under the context of climate change in TR21 Thrace Region

Huzur Deveci[1,*], Buse Önler[2], Tolga Erdem[2]

[1] *Vocational School of Technical Sciences, Tekirdağ Namık Kemal University, Tekirdağ, Türkiye*
[2] *Faculty of Agriculture, Department of Biosystem Engineering, Tekirdağ Namık Kemal University, Tekirdağ, Türkiye*
*Corresponding author. E-mail: huzurdeveci@nku.edu.tr

Abstract. In order to use water resources efficiently and sustainably, it is very important to determine the impact of climate change on water resources accurately. For this purpose, reference evapotranspiration (ET_0), crop evapotranspiration (ET_c), irrigation water requirement (IWR) was determined with CROPWAT 8.0 using climate data obtained from HadGEM2-ES and MPI-ESM-MR model reference period (1971-2000) and future short (2031-2040) and long (2051-2060) periods RCP4.5 and RCP8.5 scenario outputs for sunflower in TR21 Thrace Region. Afterwards, the results obtained for the reference period and future periods are compared and evaluated. As a result, it is estimated that ET_0 values will increase by 6.3%-13.2% and 4.9%-26.9% in the upcoming short (2031-2040) and long (2051-2060) periods, respectively, compared to the reference period (1971-2000), and by 6.0%-13.0% and 3.4%-17.9% in the sunflower development period. ET_c is predicted to increase by 3.5%-12.0% in the short term and 2.4%-16.9% in the long term, compared to the reference period, and IWR values are predicted to vary between 0.3%-19.9% in the short term and -7.0%-20.8% in the long term. In the TR21 Thrace Region, it is estimated that the annual average ET_0, ET_0 during the sunflower development period, and sunflower water consumption will be negatively affected by climate change in the future periods (2031-2040, 2051-2060) and will increase compared to the reference period. It is anticipated that there will be increases and decreases in irrigation water demand; however, the general trend is towards an increase, and it has been determined that these increases will be greater than the decreases. This study will guide producers, managers, and decision makers in carrying out adaptation activities against the impact of climate change on water resources.

Keywords: CROPWAT 8.0, Crop water requirement, Reference evapotranspiration, Irrigation water requirement, *Helianthus annuus* L., Penman-Monteith.

1. INTRODUCTION

The impact of climate change on water resources is primarily due to changes in climate parameters, specifically changes in precipitation regimes and temperatures. Changes in temperatures affect crop evapotranspiration

(ET_c) rate, cloud characteristics, soil moisture, storm intensity, and snowfall and melting regimes. These changes occurring due to climate change can have very important consequences for the water cycle and water resources (RTMAFGDWM, 2020).

According to projections from various climate models based on different greenhouse gas emission scenarios, significant decreases in precipitation, water resources, and flows are expected over the next century, particularly for North Africa, the Mediterranean Basin, Türkiye, and the Middle East. There may be significant increases in surface air temperatures and evapotranspiration as well as extreme weather and climate events (Türkeş et al., 2013). Climate change reduces the availability and accessibility of water resources, increasing vulnerability and causing negative impacts on water-dependent sectors. Since Türkiye is in a semi-arid climate zone, it is of great importance to improve water quality, increase the amount of usable water, and ensure the sustainability of conservation and utilization balance (RTMEUCC, 2024).

Evaporation is an important component of the hydrological cycle, and knowing the water losses caused by evaporation within the scope of the hydrological cycle is an important issue in terms of water management and planning (Azlak, 2015). Evapotranspiration (ET) or ET_c, one of the most important parameters of the hydrological cycle, is used extensively in the project design of irrigation systems, preparation of irrigation programs, and hydrological studies. Therefore, accurate estimation of ET_c is important for water balance, environmental protection, design of irrigation systems, and water resources management. Insufficient and excessive irrigation in crop production negatively affects the soil, product, agricultural production input, and yield. In order to obtain quality and high-yield products, the most appropriate irrigation program must be created by taking into account plant water consumption (Bircan and Kızıl, 2021). Especially in Türkiye, which has an economy based on agriculture and where 70-75% of the water demand is generated by the agricultural sector, the management and planning of water is very important (Azlak, 2015).

Sunflower is one of the important agricultural products grown in Türkiye. Sunflower oil is the most common oilseed plant in Türkiye, as its share holds around 80-85% in vegetable oil consumption and 40% of its oil content. It should be increased to reduce the vegetable oil deficit. In Türkiye, sunflower oil is mainly produced in the Thrace Region and Konya. According to TURKSTAT (Turkish Statistical Institute) data, Tekirdağ (20.5%), Edirne (13.2%), Kırklareli (11.2%), Konya (10.5%), and Adana (8%) account for 63.5% of the oil sunflower cultivation area as of the 2021/2022 season. In terms of production, Tekirdağ ranks first with 18%, Konya 14.7%, Edirne 12.9%, Kırklareli 10.2%, and Adana 9.1% (Bozer, 2023). Therefore, the TR21 Thrace Region is a very potential region in terms of sunflower cultivation.

Some studies are using various models and Representative Concentration Pathways (RCP) scenarios for climate change predictions in Türkiye. These studies were conducted using HadGEM2-ES and MPI-ESM-MR models and RCP4.5 and RCP8.5 scenarios. These models were run using the RegCM4.3 Regional Climate Model, and outputs were produced with the RCP4.5 and RCP8.5 scenarios at ten-kilometer resolution (Akçakaya et al., 2013; Akçakaya et al., 2015; GDWM, 2016). Many studies have been conducted using these outputs. One of these is the "Impacts of Climate Change and Adaptation Strategies in TR21 Thrace Region" project carried out in the TR21 Thrace Region (Anonymous, 2019). With these outputs, climate predictions specific to the TR21 Thrace Region were made in ten-year periods, and evaluations were made for the region. At the same time, Deveci (2025) determined a great agreement between the monthly average temperature values obtained from the HadGEM2-ES, MPI-ESM-MR models, RCP4.5 and RCP8.5 scenario results, and the observed meteorological data, especially for the temperature data in the TR21 Thrace Region in the period 1915-2024. Therefore, these models and scenarios were preferred because they demonstrated consistency in the region and could be evaluated together with the studies conducted.

Several studies have been conducted around the world to determine the impact of climate change on reference evapotranspiration (ET_0) (Chaouche et al., 2010; Irmak et al., 2012; Fan et al., 2016; Dinpashoh et al., 2019; Ma et al., 2019; Sun et al., 2020; Li et al., 2022; Reta et al., 2024; Youssef et al., 2024). In Türkiye, reassessment of existing irrigation projects with FAO (Food and Agriculture Organization of the United Nations) criteria (Koç and Güner, 2005), the effect of climate change on seasonal plant water consumption (Bayramoğlu E., 2013), the effect of climate change on evaporation (Azlak, 2015), establishing an irrigation water program for eggplant (Kartal et al., 2019), determining the spatial variation of ET_0 (Yıldırım et al., 2019), development of an android-based application to be used in ET_0 calculation (Bircan and Kızıl, 2021), assessment of crop water requirements by using CROPWAT for sustainable water resources management in agriculture (Aydın-Kandemir and Yıldız, 2022), determining the impact of climate change on maize irrigation water requirements (Şen, 2023; Yetik and Şen, 2023) have been studied. In addition, studies have been car-

ried out on determining the impact of climate change on ET_0 in the Thrace Region (Deveci, 2015; Yıldırım, 2023; Yıldırım and Erdem, 2023; Deveci and Konukcu, 2024). These studies although the modeled region is the same, the reference period climate data, climate models' prediction scenarios, and predicted futures are different, and thus, different calculation methods were used. In addition to the previous studies conducted in the Thrace Region, these studies have diversified by predicting ET_0 in the future years with different climate models. In addition, the most important point that distinguishes this study from other studies is that, for the first time, the irrigation requirements of sunflower have been estimated for the future periods.

This study aims to estimate the change of ET_0, ET_c, and IWR in the future short (2031-2040) and long (2051-2060) periods compared to the reference period (1971-2000) by using HadGEM2-ES and MPI-ESM-MR model RCP4.5 and RCP8.5 scenario outputs for sunflower with CROPWAT 8.0 in TR21 Thrace Region. With the results obtained, the effect of climate change on irrigation water requirements in sunflower cultivation can be evaluated. Therefore, this study will guide producers, managers, and decision makers to carry out adaptation activities against the effects of climate change on water resources.

2. MATERIAL AND METHODS

2.1. Material

2.1.1. Study area

The research area is located in Türkiye. TR21 Thrace Region covers the provinces of Tekirdağ (TR211), Edirne (TR212), and Kırklareli (TR213). The surface area of the region (excluding lakes) is 18.665 km^2. Agricultural activities are intensively carried out in the region, and the proportion of land suitable for agriculture is quite high (TDA, 2010). The study area is shown in Figure 1.

2.1.2. Climate of the research area

A continental climate prevails in the inner part of the TR21 Thrace Region. The Marmara Sea coastline is under the influence of the Black Sea-Mediterranean climate. Winters are cool and rainy; summers are dry and hot. Long-term climate data of the research area are shown in Table 1. Accordingly, the province with the highest (19.8°C) and lowest (8.5°C) average temperature is Edirne. The highest total annual rainfall (601 mm) is also seen in Edirne.

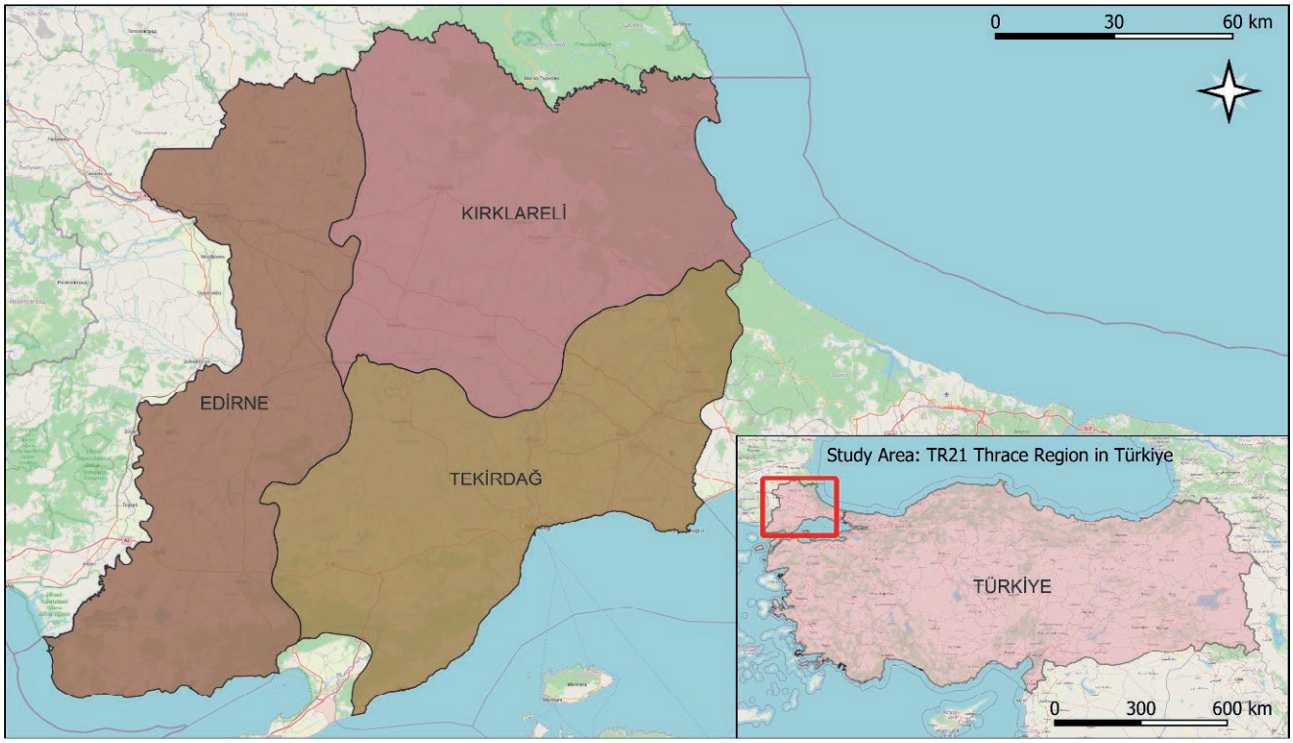

Figure 1. Geographical location of the study area (TR21 Thrace Region).

Table 1. Long-term monthly averages climate data (Edirne (1930–2023), Kırklareli (1959-2023), Tekirdağ (1940-2023)) (TSMS, 2024a; TSMS, 2024b; TSMS, 2024c).

Climate Parameters	Location	January	February	March	April	May	June	July	August	September	October	November	December	Avg./Tot.
Avg. Mean Temperature (°C)	Edirne	2.7	4.4	7.6	12.8	18.0	22.2	24.7	24.5	20.1	14.5	9.2	4.6	13.8
	Kırklareli	2.9	4.1	6.9	12.0	17.1	21.4	23.8	23.6	19.4	14.1	9.3	5.1	13.3
	Tekirdağ	4.9	5.5	7.3	11.7	16.7	21.1	23.7	23.9	20.3	15.7	11.3	7.3	14.1
Avg. Max. Temperature (°C)	Edirne	6.7	9.4	13.4	19.3	24.8	29.2	32.0	32.0	27.4	20.8	14.2	8.6	19.8
	Kırklareli	6.9	8.6	12.2	17.9	23.5	28.0	30.7	30.7	26.2	20.0	13.9	8.8	19.0
	Tekirdağ	8.1	9.0	11.0	15.7	20.6	25.3	28.1	28.3	24.5	19.5	14.8	10.5	18.0
Avg. Min. Temperature (°C)	Edirne	-0.5	0.5	2.9	7.1	11.7	15.5	17.4	17.3	13.5	9.3	5.3	1.4	8.5
	Kırklareli	0.1	1.0	3.0	7.1	11.6	15.6	17.8	17.8	14.1	9.8	5.9	2.3	8.8
	Tekirdağ	2.0	2.5	4.1	8.1	12.7	16.7	19.1	19.4	16.2	12.1	8.2	4.4	10.5
Avg. Daily Sunshine (hour)	Edirne	2.4	3.6	4.5	6.2	8.0	9.2	10.3	9.8	7.5	5.2	3.2	2.2	6.0
	Kırklareli	2.0	2.5	3.6	4.7	6.3	6.8	7.5	7.5	5.5	3.8	2.7	1.8	4.6
	Tekirdağ	2.8	3.4	4.2	6.0	7.4	8.5	9.4	8.4	6.8	4.9	3.2	2.5	5.6
Precipitation (mm)	Edirne	65.0	52.2	50.1	48.7	52.4	47.1	31.7	23.3	35.9	56.7	67.3	70.6	601.0
	Kırklareli	65.0	51.3	48.7	45.4	49.3	52.6	27.8	21.5	32.8	51.5	66.7	71.1	583.7
	Tekirdağ	68.0	54.5	53.4	42.1	37.2	38.3	23.8	15.5	32.7	60.2	74.3	80.0	580.0

TSMS: Turkish State Meteorological Service.

2.1.3. Climate data

The climate data used in the study include the climate data produced within the scope of the "Impact of Climate Change on Water Resources Project" carried out by the General Directorate of Water Management of the Ministry of Forestry and Water Affairs of the Republic of Türkiye and obtained to be used in the "Climate Change Impacts and Adaptation Strategies in the TR21 Thrace Region" project (GDWM, 2016; Anonymous, 2019). Within the scope of the "Impact of Climate Change on Water Resources Project", the RegCM4.3 regional climate model was run simultaneously for Türkiye using the outputs of three global models (HadGEM2-ES, MPI-ESM-MR, CNRM-CM5.1) selected from the CMIP5 (Coupled Model Intercomparison Project Phase 5) archive. Since the resolutions of the climate and earth system models reach hundreds of kilometers and there are uncertainties in these model outputs, dynamic downscaling was performed with the RegCM4.3 Regional Climate Model within the scope of the project. The data used in this study are the outputs of the HadGEM2-ES and MPI-ESM-MR models and the RCP4.5 and RCP8.5 scenarios. The period covers the reference period (1971-2000), short (2031-2040), and long (2051-2060) period data.

2.1.4. Plant data

The crop parameters of sunflower were defined in detail for each growth stage to ensure accurate estimation of irrigation water requirements within the CROPWAT 8.0 model. These include growth period durations, crop coefficients (K_c), rooting depth, critical depletion fraction, and yield response factor (k_y). The values were obtained from national agricultural guidelines and FAO sources and applied at the provincial level, allowing for the modeling of regional variability. The crop characteristics of sunflower are presented in Table 2.

2.1.5. Soil data

In the study, a single soil type defined as "medium texture" in the CROPWAT 8.0 database was used to represent average field conditions across the TR21 Region. The selected soil profile reflects loamy soil properties, with moderate water holding capacity and infiltration characteristics, as shown in Table 3.

2.1.6. CROPWAT 8.0 model

CROPWAT 8.0 is developed by the Land and Water Development Division of FAO. It can be downloaded and used free of charge (FAO, 2024b). CROPWAT helps

Table 2. The crop characteristics of sunflower for Edirne, Kırklareli, and Tekirdağ.

Crop Parameters		Edirne	Kırklareli	Tekirdağ	Reference
Crop Development Period (days)	Initial	25	25	25	(RTMAFGDARP, 2017)
	Development	30	30	30	(RTMAFGDARP, 2017)
	Mid-Season	60	60	60	(RTMAFGDARP, 2017)
	Late-Season	30	30	30	(RTMAFGDARP, 2017)
Crop Coefficient (K_c)	Initial	0.38	0.36	0.40	(RTMAFGDARP, 2017)
	Mid-Season	1.14	1.12	1.11	(RTMAFGDARP, 2017)
	Late-Season	0.34	0.32	1.31	(RTMAFGDARP, 2017)
Rooting Depth (m)	Initial	0.30	0.30	0.30	(FAO, 2024a)
	Late-Season	0.90	0.90	0.90	(Erdem, 2001)
Sowing Date		15 April	15 April	15 April	(RTMAFGDARP, 2017)
Vegetation Duration (days)		145	145	145	(RTMAFGDARP, 2017)
Critical Depletion (Fraction)		0.5	0.5	0.5	(Steduto et al., 2012)
Yield Response Factor (k_y)		1.0	1.0	1.0	(Steduto et al., 2012)

RTMAFGDARP: Republic of Türkiye Ministry of Environment, Urbanization and Climate Change.

Table 3. Soil properties.

Soil Parameters	Values
Total available soil moisture (mm/m)	140.0
Maximum rain infiltration rate (mm/day)	40.0
Maximum rooting depth (cm)	900
Initial soil moisture depletion (%)	0

to calculate ET_0, ET_c, IWR, and scheme water demand. It develops irrigation schedules under various management conditions. Furthermore, it estimates rainfed production and drought effects. The program calculates ET_0 using the FAO Penman-Monteith method (Allen et al., 1998).

CROPWAT 8.0 program works using the following climate, plant, and soil parameters:

- Climate parameters (minimum temperature (°C), maximum temperature (°C), humidity (%), rainfall (mm), wind speed (m/sec), sunshine hours (hours),
- Crop parameters (planting date (days), crop development period (days), crop coefficient (K_c), rooting depth (m), critical depletion, yield response factor (k_y),
- Soil parameters (total available soil moisture (mm/m), maximum rain infiltration rate (mm/day), maximum rooting depth (cm), initial soil moisture depletion (%).

2.2. Method

In this study, monthly climate data for the reference period (1971-2000) and two future projection periods (2031-2040 and 2051-2060) were separately entered into the CROPWAT 8.0 software. The data were derived from the HadGEM2-ES and MPI-ESM-MR models under RCP4.5 and RCP8.5 scenarios. This approach allowed the evaluation of potential changes in sunflower irrigation water requirements under varying climate scenarios and time frames.

In CROPWAT 8.0, ET_0 was calculated using the FAO Penman-Monteith method. Based on ET_0 and K_c values defined for each growth stage of sunflower, ET_c was estimated. Effective rainfall (P_{eff}) was calculated using the USDA (United States Department of Agriculture) method, and IWR was determined by subtracting P_{eff} from ET_c (Deveci et al., 2025).

2. RESULTS

In this study, annual average ET_0, ET_0 during the sunflower growing period, ET_c, and IWR were evaluated. For these calculations, climate data obtained from the HadGEM2-ES and MPI-ESM-MR models, reference period (1971-2000) and future short (2031-2040) and long (2051-2060) periods under the RCP4.5 and RCP8.5 scenarios were used.

2.1. Evaluation of annual average ET_0

ET_0 is predicted to increase in three locations in both models and both scenarios compared to the reference period (Edirne (4.9%-26.9%), Kırklareli (5.3%-18.3%), and Tekirdağ (5.7%-17.5%)) (Table 4, Figure 2). The highest ET_0 was predicted in Edirne in the period

Table 4. HadGEM2-ES and MPI-ESM-MR model annual average ET_0 values change for the reference period (1971-2000) and future periods (2031-2040, 2051-2060) in sunflower.

Location	Future Periods	Deviation from the reference period (1971-2000) (%)			
		HadGEM2-ES Model		MPI-ESM-MR Model	
		RCP4.5	RCP8.5	RCP4.5	RCP8.5
Edirne	2031-2040	8.3	10.9	6.7	7.9
	2051-2060	18.0	26.9	4.9	9.0
Kırklareli	2031-2040	10.2	13.2	7.7	9.5
	2051-2060	14.0	18.3	5.3	9.0
Tekirdağ	2031-2040	9.9	11.7	6.3	9.1
	2051-2060	12.9	17.5	5.7	8.9

2051-2060 (3.54 mm/day) because of the HadGEM2-ES model under the RCP8.5 scenario, and the lowest ET_0 was predicted in Tekirdağ in the period 2051-2060 (2.70 mm/day) because of the MPI-ESM-MR model RCP8.5 scenario (Figure 2). The largest change compared to the reference period was predicted in Edirne in the period 2051-2060 (26.9%) because of the HadGEM2-ES model RCP8.5 scenario, and the smallest change was predicted in Edirne in the period 2051-2060 (4.9%) because of the MPI-ESM-MR model RCP8.5 scenario (Table 4).

In this part of the study, the accuracy of HadGEM2-ES and MPI-ESM-MR model monthly ET_0 values covering 30 years for the reference period 1971-2000 was evaluated. For this purpose, the ET_0 values obtained from the reference period climate data were compared with the ET_0 values calculated and published monthly for each province in Türkiye covering a long period of 30 years in the "Guide to Plant Water Consumption of Irrigated Crops in Türkiye" published by the General Directorate of Agricultural Research and Policies and State Hydraulic Works (RTMAFGDARP, 2017). In this guide, ET_0 values were prepared by using quality-controlled 30-year daily climate data from 259 meteorological stations of the General Directorate of Meteorology throughout Türkiye. Parameters such as minimum, maximum, and average temperature, relative humidity, insolation time, insolation intensity, precipitation, and wind speed were taken into account in the preparation of the guide, missing data were completed by Allen et al. (1998) and solar radiation data were organized according to ASCE-EWRI (2004) principles. In this framework, monthly average ET_0 values covering 30 years for Edirne, Tekirdağ, and Kırklareli provinces were obtained from the guide and compared with the values calculated with 30-year reference data of HadGEM2-ES and MPI-ESM-MR models, and a high level of agreement was found (Figure 3). For

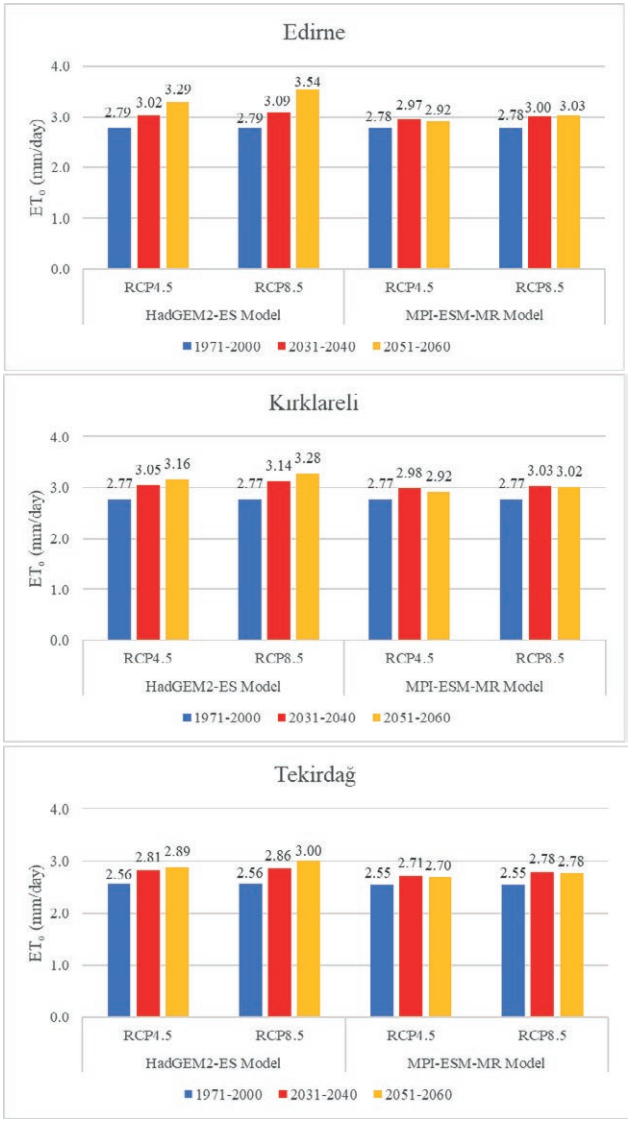

Figure 2. Daily average ET_0 values (mm/day) for the reference (1971-2000) and future periods (2031-2040, 2051-2060) according to HadGEM2-ES and MPI-ESM-MR climate models.

the correlation coefficients, it was calculated as 0.995 for Edirne, 0.987 for Kırklareli, and 0.987 for Tekirdağ in the HadGEM2-ES model. In the MPI-ESM-MR model, it was calculated as 0.995 for Edirne, 0.994 for Kırklareli, and 0.984 for Tekirdağ. In addition, the difference between the annual total ET_0 values was 13.2% (Edirne), 6.6% (Kırklareli), and 4.1% (Tekirdağ) in the HadGEM2-ES model, while it was 13.0% (Edirne), 6.6% (Kırklareli), and 3.8% (Tekirdağ) in the MPI-ESM-MR model. These findings show that both model reference data used in the study overlap to a large extent with the 30-year ET_0 values calculated with measured climate data for the region

and that the data obtained from the models can be used reliably.

2.2. Evaluation of ET_0 during the sunflower vegetation period

In general, ET_0 (during the sunflower vegetation period) in the TR21 Thrace Region is projected to increase in both models, scenarios, and periods compared to the reference period (Table 5, Figure 4). This increase was predicted to be between 3.4%-16.7% in Edirne, 3.9%-17.9% in Kırklareli and 4.7%-17.6% in Tekirdağ (Table 5). During the sunflower growing period, the highest ET_0 was predicted in Edirne in the period 2051-2060 (5.06 mm/day) because of the HadGEM2-ES model RCP8.5 scenario, and the lowest ET_0 was predicted in Tekirdağ in the period 2051-2060 (3.97 mm/day) because of MPI-ESM-MR model RCP8.5 scenario (Figure 2). In addition, the largest change compared to the reference period was predicted in Kırklareli in the period 2051-2060 (17.9%) because of HadGEM2-ES model RCP8.5 scenario and the smallest change was predicted in Edirne in the period 2051-2060 (3.4%) because of MPI-ESM-MR model RCP8.5 scenario (Table 5).

Figure 3. Comparison of monthly ET_0 values obtained from 30-year observed data with HadGEM2-ES and MPI-ESM-MR model reference data.

2.3. Evaluation of ET_c of (Sunflower)

ET_c in the TR21 Thrace Region is predicted to increase in both models, both scenarios, and both periods compared to the reference period (Table 6, Figure 5). This increase is projected to be between 2.4%-15.8% in Edirne, 3.1%-16.9% in Kırklareli, and 3.5%-15.6% in Tekirdağ (Table 6). The highest ET_c was predicted in Edirne for the period 2051-2060 (698.4 mm/season) because of the HadGEM2-ES model RCP8.5 scenario, while the lowest ET_c was predicted in Tekirdağ for the period 2051-2060 (533.8 mm/season) because of the MPI-ESM-MR model RCP8.5 scenario (Figure 5). The largest change compared to the reference period was predicted in Kırklareli in the period 2051-2060 (16.9%) because of the HadGEM2-ES model RCP8.5 scenario, and the smallest change was predicted in Edirne in the period 2051-2060 (2.4%) because of the MPI-ESM-MR model RCP8.5 scenario (Table 6).

2.4. Evaluation of IWR

IWR is predicted to increase in the period 2051-2060 in Edirne, Kırklareli, and Tekirdağ in the RCP4.5

Table 5. HadGEM2-ES and MPI-ESM-MR model ET_0 values change for the reference period (1971-2000) and future periods (2031-2040, 2051-2060) in the sunflower vegetation period.

Location	Future Periods	Deviation from the reference period (1971-2000) (%)			
		HadGEM2-ES Model		MPI-ESM-MR Model	
		RCP4.5	RCP8.5	RCP4.5	RCP8.5
Edirne	2031-2040	7.5	10.5	6.1	7.8
	2051-2060	11.3	16.7	3.4	7.7
Kırklareli	2031-2040	9.5	13.0	7.1	9.1
	2051-2060	14.1	17.9	3.9	8.1
Tekirdağ	2031-2040	9.8	11.6	6.0	9.2
	2051-2060	13.2	17.6	4.7	8.1

Figure 4. HadGEM2-ES and MPI-ESM-MR model ET_0 values for the reference period (1971-2000) and future periods (2031-2040, 2051-2060) for sunflower in the vegetation period.

scenario in the MPI-ESM-MR model. In addition, in Tekirdağ, the same model predicted a decrease in the RCP8.5 scenario for the same period and an increase in all other forecasts (Table 7). This change is projected to be between -5.3%-17.5% in Edirne, -7.0%-20.8% in Kırklareli, and -3.3%-17.9% in Tekirdağ (Table 7). The highest IWR occurred in Edirne in the period 2051-2060 (587.1 mm/season) because of the HadGEM2-ES model RCP8.5 scenario, and the lowest IWR occurred in Tekirdağ in the period 2051-2060 (389.1 mm/season) because of the MPI-ESM-MR model RCP4.5 scenario (Figure 6). In addition, the largest

Table 6. HadGEM2-ES and MPI-ESM-MR model ET_c values change for the reference period (1971-2000) and future periods (2031-2040, 2051-2060) in the sunflower vegetation period.

Location	Future Periods	Deviation from the reference period (1971-2000) (%)			
		HadGEM2-ES Model		MPI-ESM-MR Model	
		RCP4.5	RCP8.5	RCP4.5	RCP8.5
Edirne	2031-2040	7.3	9.7	3.8	8.1
	2051-2060	11.4	15.8	2.4	6.0
Kırklareli	2031-2040	9.6	12.0	5.2	10.4
	2051-2060	13.8	16.9	3.1	6.3
Tekirdağ	2031-2040	8.4	9.9	3.5	9.4
	2051-2060	12.5	15.6	3.6	6.5

change compared to the reference period was projected in Kırklareli in the period 2051-2060 (20.8%) because of HadGEM2-ES model RCP8.5 scenario and the smallest change was projected in Kırklareli in the period 2051-2060 (-7.0%) because of MPI-ESM-MR model RCP8.5 scenario (Table 7).

3.5. General evaluation

The general evaluation of the results is presented in Table 8. Accordingly, it is predicted that the annual average ET_0 will vary between 2.70-3.54 mm/day in the TR21 Thrace Region, and ET_0 will vary between 3.97-5.06 mm/day during the sunflower growing period. The change in annual average ET_0 compared to the reference period was estimated to be 4.9%-26.9%, and the change in ET_0 compared to the reference period during the sunflower growing period was estimated to be 3.4%-17.9%. ET_c for sunflower was predicted to vary between 533.8-698.4 mm/season in the modeled periods, and this change was predicted to be 2.4%-16.9% compared to the reference period. IWR is predicted to vary between 389.1-587.1 mm/season, and this change is predicted to be -7.0%-20.8% in both models, both scenarios, and both periods compared to the reference period.

In TR21 Thrace Region, annual average ET_0, ET_0 during the sunflower growing period, and sunflower evapotranspiration (ET_c) are estimated to be negatively affected by climate change and to increase compared to the reference period. It is estimated that ET_0 values will increase by 6.3%-13.2% and 4.9%-26.9% in the upcoming short (2031-2040) and long (2051-2060) periods, respectively, compared to the reference period (1971-2000), and by 6.0%-13.0% and 3.4%-17.9% in the sunflower development period, respectively. ET_c is pre-

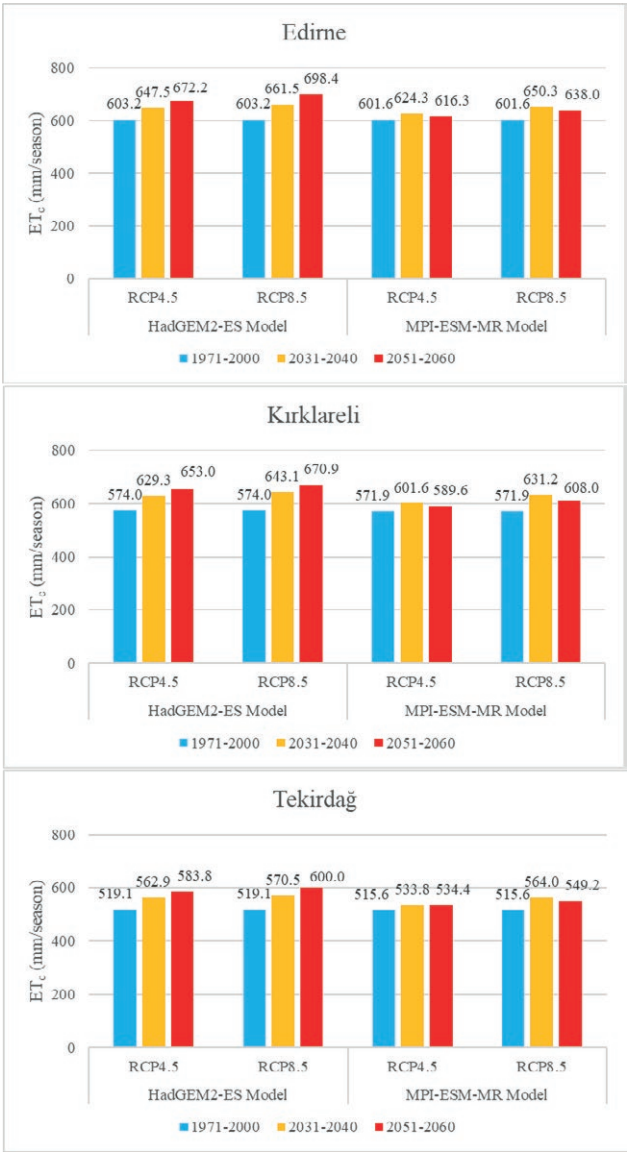

Figure 5. HadGEM2-ES and MPI-ESM-MR model ET_c values for the reference period (1971-2000) and future periods (2031-2040, 2051-2060) for sunflower.

dicted to increase by 3.5%-12.0% in the short term and 2.4%-16.9% in the long term, compared to the reference period. It is anticipated that there will be increases and decreases in irrigation water demand. Because it has been determined that IWR values will vary between 0.3%-19.9% in the short term and -7.0%-20.8% in the long term. However, the general trend is towards an increase, and it has been determined that these increases will be greater than the decreases.

Table 7. HadGEM2-ES and MPI-ESM-MR model IWR values change for the reference period.

Location	Future Periods	Deviation from the reference period (1971-2000) (%)			
		HadGEM2-ES Model		MPI-ESM-MR Model	
		RCP4.5	RCP8.5	RCP4.5	RCP8.5
Edirne	2031-2040	10.8	10.4	4.0	15.8
	2051-2060	17.1	17.5	-5.3	1.5
Kırklareli	2031-2040	14.1	13.6	6.3	19.9
	2051-2060	20.8	19.2	-7.0	1.5
Tekirdağ	2031-2040	11.3	12.3	0.3	12.3
	2051-2060	17.9	17.0	-3.3	-0.1

3. DISCUSSION

In the "Impacts of Climate Change and Adaptation Strategies in TR21 Thrace Region" project carried out in the region, climate assessments were made in ten-year periods (Anonymous, 2019). Accordingly, it is predicted that there will be temperature increases in both models and scenarios in Edirne, Kırklareli, and Tekirdağ in the short (2031-2040) and long (2051-2060) periods, and periodic increases and decreases in precipitation. Possible temperature increases are projected to vary between 1.08°C and 2.90°C, while the change in precipitation is projected to be between -13.70 and 11.46 mm (Hanedar et al., 2019). In this study, it is predicted that the annual average ET_0 will vary between 2.70 and 3.54 mm/day in the TR21 Thrace Region, and ET_0 will vary between 3.97 and 5.06 mm/day during the sunflower growing period. The change in annual average ET_0 compared to the reference period is estimated to be 4.9%-26.9%, and the change in ET_0 compared to the reference period during the sunflower growing period is estimated to be 3.4%-17.9%. In another study conducted in the region, Deveci and Konukcu (2024) evaluated the reference (1961-1990) and future A2 SRES scenario outputs of the ECHAM5 General Circulation Model in Pınarbaşı Basin in the Thrace Region and predicted an average temperature increase of 0.12°C between 2016-2025, 1.43°C between 2046-2055 and 3.05°C between 2076-2085 compared to the model reference years (1970-1990). It is also predicted that total precipitation will increase by 60 mm between 2016-2025 (9%), total precipitation will decrease by 91 mm between 2046-2055 (14%), and total precipitation will decrease by 78 mm between 2076-2085 (12%). In 2012, an experiment was conducted and it was estimated that while the average ET_0 values were 3.0 mm/day in 2012, they would increase to 3.2 mm/day (+7%) between 2016-2025, 3.6 mm/day (+20%) between 2046-

Figure 6. HadGEM2-ES and MPI-ESM-MR model IWR values for the reference period (1971-2000) and future periods (2031-2040, 2051-2060) for sunflower.

2055 and 4.0 mm/day (+33%) between 2076-2085. In addition, when compared with the reference period (1970-1990), ET_0 values change by 9% and 21% in the medium 2046-2055 and long 2076-2085 terms, respectively. Even though the reference periods, future periods, forecast models, and scenarios used in these studies are different, the results of this research support each other. In addition, De Oliveira et al. (2021) stated that the ET_0 value, which is an important component in calculating the water requirement of plants, can be affected by climate change. Arabi and Candoğan (2022) estimated ET_0 values for 18 meteorological stations in the Marmara Region using monthly climate data between 1990 and 2020 and found statistically significant increasing trends in ET_0 values in Edirne, Kırklareli, and Tekirdağ. These results and the results found in this study are in the same direction. When other studies conducted in Türkiye are evaluated, it is estimated that ET_0 increases with temperature increases in the Çukurova Region (Şen, 2023; Yetik and Şen, 2023). In the study conducted by Anlı (2014) for the Southeastern Anatolia region, the change in ET_0 values over time was investigated, and it was determined that there were significant increasing trends in ET_0 values. Selçuk (2021) calculated the monthly ET_0 values for the years 1959-2019 using the FAO Penman-Monteith method, using the climate data of 17 meteorological stations within the borders of Malatya province, and revealed that increasing temperature values increased Malatya ET_0 values by 3%. In the worldwide studies, Irmak et al. (2012) found that at reference (potential) evapotranspiration (ET_{ref}), precipitation, and relative humidity were significantly ($P<0.05$) inversely correlated, while mean temperature, maximum temperature, vapor pressure deficit, solar radiation and net radiation values had significant and positive correlations. Goyal (2004), in his study on long-term climate data for 32 years (1971-2002) in Rajasthan (India), determined that there would be a 14.8% increase in total ET with a 20% increase in temperature (maximum 8°C). As a result, all these studies are in line with the conclusion that the annual average ET_0 and ET_0 values during the sunflower growing period will increase with the predicted climate change in the region.

Şen et al. (2008) predicted a decrease in effective precipitation and thus in water resources in the Seyhan Basin, but an increase in plant water requirements. Although climatic factors are not the sole determinant of sunflower yield, they have significant effects on yield, and according to the results of the analysis, it was determined that temperature and humidity parameters have a significant effect on sunflower yield (Gürkan et al., 2016). In this study, sunflower ET_c was predicted to vary between 533.8-698.4 mm/season during the modeled periods, and this change could be 2.4%-16.9% compared to the reference period. Together with the predicted temperature increases in the region (1.08°C-2.90°C), this situation was considered as probable. Similarly, Deveci et al. (2025) determined that ET_c would increase with temperature increases in wheat and canola in the same region, even though the plants were different.

In this study, IWR was predicted to change between 389.1-587.1 mm/season, and this change was predicted to be -7.0%-20.8% in both models, both scenarios, and both periods compared to the reference period. It is pre-

Table 8. General evaluation of ET_0, ET_0 (sunflower vegetation period), ET_c (sunflower), and IWR.

	Values		Deviation from the reference period (1971-2000) (%)	
	Max.	Min.	Max.	Min.
ET_0 (annual average)	Edirne HadGEM2-ES RCP8.5 2051-2060 3.54 mm/day	Tekirdağ MPI-ESM-MR RCP8.5 2051-2060 2.70 mm/day	Edirne HadGEM2-ES RCP8.5 2051-2060 %26.9	Edirne MPI-ESM-MR RCP8.5 2051-2060 %4.9
ET_0 (sunflower vegetation period)	Edirne HadGEM2-ES RCP8.5 2051-2060 5.06 mm/day	Tekirdağ MPI-ESM-MR RCP8.5 2051-2060 3.97 mm/day	Kırklareli HadGEM2-ES RCP8.5 2051-2060 %17.9	Edirne MPI-ESM-MR RCP8.5 2051-2060 %3.4
ET_c (sunflower)	Edirne HadGEM2-ES RCP8.5 2051-2060 698.4 mm/season	Tekirdağ MPI-ESM-MR RCP8.5 2051-2060 533.8 mm/season	Kırklareli HadGEM2-ES RCP8.5 2051-2060 %16.9	Edirne MPI-ESM-MR RCP8.5 2051-2060 %2.4
IWR	Edirne HadGEM2-ES RCP8.5 2051-2060 587.1 mm/season	Tekirdağ MPI-ESM-MR RCP4.5 2051-2060 389.1 mm/season	Kırklareli HadGEM2-ES RCP8.5 2051-2060 %20.8	Kırklareli MPI-ESM-MR RCP8.5 2051-2060 -%7.0

dicted that there will be increases and decreases in irrigation water demand; the general trend is in the direction of increase, and proportionally, these increases will be more than the amount of decrease. In the MPI-ESM-MR model, it is estimated that there will be a decrease in Edirne (-5.3%), Kırklareli (-7%) and Tekirdağ (-3.3%) in the period 2051-2060 in the RCP4.5 scenario and also in Tekirdağ in the same model, same period RCP8.5 scenario (-0.1%), and an increase in all other forecasts (Table 7). Looking at the 3 situations that draw attention as a decrease, it is estimated that the temperature will increase by 1.36°C in Edirne, 1.34°C in Tekirdağ and 1.34°C in Kırklareli, and precipitation will increase by 5.71 mm in Edirne, 9.75 mm in Tekirdağ and 11.46 mm in Kırklareli (Hanedar et al., 2019). Therefore, it is seen that there is a close change in temperatures. Increases in precipitation were observed during this period. Precipitation is more decisive. Therefore, the decrease in IWR with increases in precipitation was considered normal. In fact, it is interpreted that these precipitations probably occurred during the development period of the plant, and the need for irrigation water is likely to decrease.

The calculated IWR values represent the net water requirement of the crop, independent of the irrigation method and application efficiency. However, the efficiency of irrigation systems used in practice can significantly affect the actual amount of water applied in the field. For instance, while the application efficiency of traditional surface irrigation methods is typically around 30–40%, it may reach 55–70% in furrow irrigation and 90–95% in drip irrigation systems (Qureshi et al., 2015; Yara, 2024). Therefore, even if similar IWR values are estimated for different regions, the total volume of water that needs to be applied in the field can vary depending on the irrigation method used. Similar findings in the literature have emphasized that irrigation methods play a critical role in meeting increased or altered water demands under the influence of climate change (Lakhiar et al., 2024).

Overall, the findings of this study are largely consistent with both regional and national literature, indicating that climate change directly affects irrigation water requirements, and the magnitude of this effect varies depending on local climatic conditions, precipitation patterns, and the irrigation techniques employed.

4. CONCLUSIONS

In this study, the effect of climate change on the irrigation water requirement of sunflower in the TR21 Thrace Region was modeled. As a result, in this study, annual average ET_0, ET_0 during the sunflower growth period, and sunflower evapotranspiration in the TR21 Thrace Region were predicted to be negatively affected by climate change and to increase compared to the reference period. Decreases in IWR are predicted only in the MPI-ESM-MR Model, it is estimated that there will be a decrease in Edirne (-5.3%), Kırklareli (-7%) and Tekirdağ (-3.3%) in the period 2051-2060 in the RCP4.5 scenario and also in Tekirdağ in the same model, same period RCP8.5 scenario (-0.1%), and an increase in all other forecasts and the general trend is upward. Increases in

IWR are expected to proportionally outweigh decreases. Accurately determining the impact of climate change on ET_0, ET_c, and IWR is crucial for designing irrigation systems and preparing irrigation programs. These results suggest that the currently widespread rainfed sunflower cultivation in the TR21 Thrace Region may become insufficient under future climate conditions, potentially necessitating the use of supplementary irrigation. Therefore, the efficient, planned, and sustainable management of regional water resources is of great importance. In this context, the findings may serve as a guide for producers, irrigation planners, and policymakers in developing adaptation strategies to climate change.

REFERENCES

Akçakaya A., Eskioğlu O., Atay H., Demir Ö., 2013. Climate Change Projections for Türkiye With New Scenarios. Meteorology General Directorate Printing House, Türkiye. https://mgm.gov.tr/FILES/iklim/IKLIM_DEGISIKLIGI_PROJEKSIYONLARI.pdf

Akçakaya A., Sümer U.M., Demircan M., Demir Ö., Atay H., Eskioğlu O., Gürkan H., Yazıcı B., Kocatürk A., Şensoy S., Bölük E., Arabacı H., Açar Y., EKİCİ M., Yağan S., Çukurçayır F., 2015. Türkiye Climate Projections with New Scenarios and Climate Change TR2015-CC. https://www.mgm.gov.tr/FILES/iklim/iklim-degisikligi-projeksiyon2015.pdf

Allen R.G., Pereira L.S., Raes D., Smith M., 1998. Crop evapotranspiration-Guidelines for computing crop water requirements-FAO Irrigation and drainage paper 56. Rome, Italy, 300 (9): D05109.

Anlı A.S., 2014. Temporal variation of reference evapotranspiration (ET_0) in Southeastern Anatolia Region and meteorological drought analysis through RDI (Reconnaissance Drought Index) method. Journal of Agricultural Sciences, 20 (2014): 248-260. https://doi.org/10.15832/tbd.82527

Anonymous. 2019. Climate Change Impacts and Adaptation Strategies in the TR21 Thrace Region. Tekirdag Namık Kemal University, Tekirdağ, Türkiye. https://www.iklimtrak.com/FileUploads/ProjectOutput/ProjectOutput_2505151205144.pdf

Arabi C., Candoğan B.N., 2022. Spatial and temporal change of reference crop evapotranspiration in Marmara Region. International Journal of Agriculture and Wildlife Science, 8 (2): 268-281. https://doi.org/10.24180/ijaws.1080376

ASCE-EWRI 2004. The ASCE Standardized Reference Evapotranspiration Equation. Technical Committee report to the Environmental and Water Resources Institute of the American Society of Civil Engineers from the Task Committee on Standardization of Reference Evapotranspiration. 173 p.

Aydın-Kandemir F., Yıldız D., 2022. Assessment of crop water requirements by using cropwat for sustainable water resources management in agriculture (Akhisar-Manisa, Turkey). International Journal of Water Management and Diplomacy, 1 (5): 5-20.

Azlak M., 2015. Possible Effects of Climate Change on Evaporation. MSc. Thesis. İstanbul Technical University, İstanbul.

Bayramoğlu E., 2013. Evapotranspiration seasonal effects of climate change in Trabzon: the Penman-Monteith Method. Kastamonu University Journal of Forestry Faculty, 13 (2): 300-306.

Bircan N., Kızıl Ü., 2021. Development of an android-based application to be used in the calculation of reference evapotranspiration. COMU Journal of Agriculture Faculty, 9 (2): 247-257. https://doi.org/10.33202/comuagri.970742

Bozer P. 2023. Sunflower Status-Forecast Report 2023. Republic of Türkiye Ministry of Agriculture and Forestry Agricultural Economic and Policy Development Institute. https://arastirma.tarimorman.gov.tr/tepge/Belgeler/PDF%20Durum-Tahmin%20Raporlar%C4%B1/2023%20Durum-Tahmin%20Raporlar%C4%B1/Ay%C3%A7i%C3%A7e%C4%9Fi%20Durum-Tahmin%20Raporu%202023-392%20TEPGE.pdf

Chaouche K., Neppel L., Dieulin C., Pujol N., Ladouche B., Martin E., Salas D., Caballero Y., 2010. Analyses of precipitation, temperature and evapotranspiration in a French Mediterranean region in the context of climate change. Comptes Rendus. Géoscience, 342 (3): 234-243. https://doi.org/10.1016/j.crte.2010.02.001

De Oliveira R.G., Valle Júnior L.C.G., da Silva J.B., Espíndola D.A.L.F., Lopes R.D., Nogueira J.S., Curado L.F.A., Rodrigues T.R., 2021. Temporal trend changes in reference evapotranspiration contrasting different land uses in southern Amazon basin. Agricultural water management, 250: 106815. https://doi.org/10.1016/j.agwat.2021.106815

Deveci H., 2015. Modelling the Effect of Climate Change on Surface Water Resources, Soil Water Profile and Plant Yield in Thrace Region. Ph.D. Thesis. Namık Kemal University, Türkiye.

Deveci H., 2025.Determination of the accuracy of average temperature values obtained from different climate models in TR21 Thrace Region. In: 9th International Conference on Global Practice of Multidisciplinary Scientific Studies, Havana, Cuba. https://www.

izdas.org/_files/ugd/614b1f_c300ca6abbdf45db9aed0060cde06741.pdf

Deveci H., Konukcu F., 2024. Modeling the Effect of Climate Change on Evapotranspiration in the Thrace Region. Atmosphere, 15 (10): 1188. https://doi.org/10.3390/atmos15101188

Deveci H., Önler B., Erdem T., 2025. Modeling the effects of climate change on the irrigation water requirements of wheat and canola in the TR21 Thrace Region using CROPWAT 8.0. Frontiers in Sustainable Food Systems, 9. https://doi.org/10.3389/fsufs.2025.1563048

Dinpashoh Y., Jahanbakhsh-Asl S., Rasouli A., Foroughi M., Singh V., 2019. Impact of climate change on potential evapotranspiration (case study: west and NW of Iran). Theoretical and Applied Climatology, 136: 185-201. https://doi.org/10.1007/s00704-018-2462-0

Erdem T., 2001. Evapotranspiration of sunflower for Tekirdağ conditions. Journal of Agricultural Sciences, 7 (2): 62-68. https://doi.org/10.1501/Tarimbil_0000000623

Fan J., Wu L., Zhang F., Xiang Y., Zheng J., 2016. Climate change effects on reference crop evapotranspiration across different climatic zones of China during 1956–2015. Journal of Hydrology, 542: 923-937. https://doi.org/10.1016/j.jhydrol.2016.09.060

FAO 2024a. Food and Agriculture Organization. Sunflower. https://www.fao.org/land-water/databases-and-software/crop-information/sunflower/en/

FAO 2024b. Food and Agriculture Organization. CropWat. https://www.fao.org/land-water/databases-and-software/cropwat/en/

GDWM 2016. General Directorate of Water Management. Impact of climate change on water resources project project final report. ttps://www.tarimorman.gov.tr/SYGM/Belgeler/iklim%20de%C4%9Fi%C5%9Fikli%C4%9Finin%20su%20kaynaklar%C4%B1na%20etkisi/Iklim_NihaiRapor.pdf

Goyal R., 2004. Sensitivity of evapotranspiration to global warming: a case study of arid zone of Rajasthan (India). Agricultural water management, 69 (1): 1-11. https://doi.org/10.1016/j.agwat.2004.03.014

Gürkan H., Bayraktar N., Bulut H., Koçak N., Eskioğlu O., Demircan M., 2016.Analyzing of the potential impact of climate change on yield of sunflower (Helianthus annuus L.): example of the Marmara Region. In: XII. National Agricultural Economics Congress, Isparta, Türkiye.

Hanedar A., Ferat Ç., Erdem G., Konukcu F., Altürk B., Albut S., 2019. TR21 Region Climate Assessment: Current Situation and Projections, in: F. Konukcu, et al. (Eds.), Effects of Climate Change and Adaptation Strategies in TR21 Thrace Region, Tekirdağ Namık Kemal University, Tekirdağ. pp. 1-22.

Irmak S., Kabenge I., Skaggs K.E., Mutiibwa D., 2012. Trend and magnitude of changes in climate variables and reference evapotranspiration over 116-yr period in the Platte River Basin, central Nebraska–USA. Journal of Hydrology, 420: 228-244. https://doi.org/10.1016/j.jhydrol.2011.12.006

Kartal S., Çolak Y.B., Gönen E., Özfidaner M., 2019. Using CROPWAT program for irrigation scheduling of eggplant in Tarsus Region. Turkish Journal of Agricultural and Natural Sciences, 6 (2): 332-342.

Koç A., Güner Ü., 2005. Reassessment of existing irrigation projects with fao criteria: TavasPlain example. Dumlupınar University Science Institute Journal, 9: 93-106.

Lakhiar I.A., Yan H., Zhang C., Wang G., He B., Hao B., Han Y., Wang B., Bao R., Syed T.N., Chauhdary J.N., Rakibuzzaman M., 2024. A Review of Precision Irrigation Water-Saving Technology under Changing Climate for Enhancing Water Use Efficiency, Crop Yield, and Environmental Footprints. Agriculture, 14 (7): 1141.

Li Y., Qin Y., Rong P., 2022. Evolution of potential evapotranspiration and its sensitivity to climate change based on the Thornthwaite, Hargreaves, and Penman–Monteith equation in environmental sensitive areas of China. Atmospheric Research, 273: 106178. https://doi.org/10.1016/j.atmosres.2022.106178

Ma Z., Yan N., Wu B., Stein A., Zhu W., Zeng H., 2019. Variation in actual evapotranspiration following changes in climate and vegetation cover during an ecological restoration period (2000-2015) in the Loess Plateau, China. Science of the Total Environment, 689: 534-545. https://doi.org/10.1016/j.scitotenv.2019.06.155

Qureshi A.L., Gadehi M.A., Mahessar A.A., Memon N.A., Soomro A.G., Memon A.H., 2015. Effect of drip and furrow irrigation systems on sunflower yield and water use efficiency in dry area of Pakistan. American-Eurasian Journal of Agricultural & Environmental Sciences, 15 (10): 1947-1952. https://doi.org/10.5829/idosi.aejaes.2015.15.10.12795

Reta B.G., Hatiye S.D., Finsa M.M., 2024. Crop water requirement and irrigation scheduling under climate change scenario, and optimal cropland allocation in lower kulfo catchment. Heliyon, 10 (10): e31332. https://doi.org/10.1016/j.heliyon.2024.e31332

RTMAFGDARP 2017. Republic of Türkiye ministry of agriculture and forestry general directorate of

agricultural research and policies. Plant water consumption of irrigated plants in Türkiye. https://www.tarimorman.gov.tr/TAGEM/Belgeler/yayin/Tu%CC%88rkiyede%20Sulanan%20Bitkilerin%20Bitki%20Su%20Tu%CC%88ketimleri.pdf

RTMAFGDWM 2020. Republic of Türkiye Ministry of Agriculture and Forestry General Directorate of Water Management. Climate Change and Adaptation https://www.tarimorman.gov.tr/SYGM/Belgeler/iklim%20de%C4%9Fi%C5%9Fikli%C4%9Finin%20su%20kaynaklar%C4%B1na%20etkisi/iklimkitap2020.pdf

RTMEUCC 2024. Republic of Türkiye Ministry of Environment, Urbanization and Climate Change. Climate Change Adaptation Strategy and Action Plan (2024-2030). https://iklim.gov.tr/db/turkce/icerikler/files/%C4%B0klim%20De%C4%9Fi%C5%9Fikli%C4%9Fine%20Uyum%20Stratejisi%20ve%20Eylem%20Plan_%202024-2030.pdf

Selçuk E.B., 2021. Evaluation of the Impact of Global Warming and Climate Change on Temperature and Reference Evapotranspiration: the Case of Malatya Province. MSc. Thesis. İnönü University, Türkiye.

Steduto P., Hsiao T.C., Fereres E., Raes D., 2012. Crop yield response to water. FAO Rome, Italy.

Sun J., Wang G., Sun X., Lin S., Hu Z., Huang K., 2020. Elevation-dependent changes in reference evapotranspiration due to climate change. Hydrological Processes, 34 (26): 5580-5594. https://doi.org/10.1002/hyp.13978

Şen B., 2023. Determining the changing irrigation demands of maize production in the cukurova plain under climate change scenarios with the CROPWAT model. Water, 15 (24): 4215. https://doi.org/10.3390/w15244215

Şen B., Topcu S., Giorgi F., Xunqiang B., Kanıt E., Dalkılıç T., 2008.Climate Change and Agricultural Water in Seyhan Basin Effects on Use. In: TMMOB 2nd Water Policy Congress, Ankara, Türkiye.

TDA 2010. Thrace Development Agency. TR21 Thrace Regional Plan Tekirdağ, Edirne, Kırklareli 2010. https://www.trakyaka.org.tr/upload/Node/33265/xfiles/tr21_trakya_2010-2013.pdf

TSMS 2024a. Turkish State Meteorological Service. Long-term monthly averages climate data https://www.mgm.gov.tr/veridegerlendirme/il-ve-ilceler-istatistik.aspx?m=EDIRNE

TSMS 2024b. Turkish State Meteorological Service. Long-term monthly averages climate data https://www.mgm.gov.tr/veridegerlendirme/il-ve-ilceler-istatistik.aspx?m=KIRKLARELI

TSMS 2024c. Turkish State Meteorological Service. Long-term monthly averages climate data https://www.mgm.gov.tr/veridegerlendirme/il-ve-ilceler-istatistik.aspx?m=TEKIRDAG

Türkeş M., Şen Ö.L., Kurnaz L., Madra Ö., Şahin Ü. 2013. Recent Developments in Climate Change: IPCC 2013 Report. Sabancı University, İstanbul Policy Center. https://ipc.sabanciuniv.edu/Content/Images/CKeditorImages/20200327-02035048.pdf

Yara 2024. Producing more, with less: Water use efficiency in irrigation. https://www.yara.com/knowledge-grows/water-use-efficiency-in-irrigation/#:~:text=Drip%20irrigation%20systems%2C%20for%20example,can%20reach%20up%20to%2095%25

Yetik A.K., Şen B., 2023. Evaluation of the impacts of climate change on irrigation requirements of maize by CROPWAT Model. Gesunde Pflanzen, 75 (4): 1297-1305. https://doi.org/10.1007/s10343-022-00751-x

Yıldırım E.A., 2023. Investigation of climate change in Tekirdag conditions on reference evapotranspiration. MSc. Thesis. Tekirdağ Namık Kemal University, Türkiye.

Yıldırım E.A., Erdem T., 2023. Investigation of the effect of climate change on reference evapotranspiration in Tekirdağ, Türkiye. Revista de Climatología, 23: 35-45. https://doi.org/10.59427/rcli/2023/v23.35-45

Yıldırım Y.E., Taş İ., Özaydın K.A., 2019. Determination of spatial variation of reference evapotranspiration case study of Gediz Basin. Soil Water Journal: 153-161. https://doi.org/10.21657/topraksu.655582

Youssef M.A., Peters R.T., El-Shirbeny M., Abd-ElGawad A.M., Rashad Y.M., Hafez M., Arafa Y., 2024. Enhancing irrigation water management based on ET_0 prediction using machine learning to mitigate climate change. Cogent Food & Agriculture, 10 (1): 1-17. https://doi.org/10.1080/23311932.2024.2348697

Italian Journal of Agrometeorology
Rivista Italiana di Agrometeorologia

Firenze University Press
https://riviste.fupress.net/index.php/IJAm

OPEN ACCESS

Citation: Morbidini, F., Locatelli, S., Raimondi, G., Barbera, A. C., Iurato, A., Nicoletto, C., & Maucieri, C. (2025). Nocturnal transpiration of tomato under deficit irrigation in greenhouse conditions. *Italian Journal of Agrometeorology* (2): 53-63. doi: 10.36253/ijam-3656

Received: July 14, 2025

Accepted: November 20, 2025

Published: December 31, 2025

Data Availability Statement: All relevant data are within the paper and its Supporting Information files.

Competing Interests: The Author(s) declare(s) no conflict of interest.

ORCID:
FM: 0009-0002-4586-1202
SL: 0000-0003-1187-7716
GR: 0000-0001-9046-8309
ACB: 0000-0002-7963-5150
AI: 0009-0006-4029-6995
CM: 0000-0003-4004-6612

Nocturnal transpiration of tomato under deficit irrigation in greenhouse conditions

Francesco Morbidini[1], Silvia Locatelli[1], Giorgia Raimondi[1,*], Antonio C. Barbera[2], Antonella Iurato[2], Carlo Nicoletto[1], Carmelo Maucieri[1]

[1] *Department of Agronomy, Food, Natural Resources, Animals and Environment – DAFNAE, University of Padua, Agripolis Campus, Viale dell'Università 16, Legnaro, PD, Italy*
[2] *Department of Agriculture, Food and Environment (Di3A) – University of Catania, Via S. Sofia 100, 95123, Catania, Italy*
*Corresponding author. E-mail: giorgia.raimondi@unipd.it

Abstract. Nocturnal transpiration (E) can reduce water productivity by causing water loss during a period without photosynthetic activity. This study quantifies tomato nocturnal E under greenhouse conditions, comparing two irrigation managements (full irrigation – FI vs. Deficit irrigation – DI) and four fertilization treatments (raw compost vs. sieved compost vs. mineral vs. no fertilization), addressing a key gap in understanding potential inefficiencies in crop water use. Physiological and environmental parameters were monitored weekly from transplanting to harvesting at four different hours each day (06:00, 12:00, 18:00, and 24:00). At harvest, fruit yield, quality, and water productivity were assessed. Only irrigation significantly affected E, with FI plants exhibiting higher daytime E rates (+11–16%) than DI. Stomatal conductance varied by time but was not influenced by irrigation. Nocturnal E persisted at ~12–13% of daytime rates, indicating residual stomatal opening. Under FI, E positively correlated with leaf temperature and vapor pressure deficit, while under DI, E was more influenced by environmental temperature, reflecting tighter environmental control under water stress. Neither irrigation nor fertilization significantly affected total (on average 64.1 Mg ha^{-1}) or marketable fruit yield (about 77.5% of total yield). Water productivity was significantly higher under DI (+14.7%) than FI (21.5 kg m^{-3}). DI also increased fruit dry matter content (+6.5%) and slightly lowered fruit pH without affecting total soluble solids, titratable acidity, or electrical conductivity.

Keywords: transpiration, stomatal conductance, water productivity, fruits' quality, fruits' yield.

HIGHLIGHTS

- Nighttime transpiration was ~12–13% of daytime, unaffected by irrigation management
- Deficit irrigation improved water productivity by 14.7% without yield loss
- Deficit irrigation increased fruits dry matter without altering other quality traits

1. INTRODUCTION

Water is a critical and increasingly limited resource for agricultural production, directly affecting both crop growth and yield. However, the increase of water productivity (WP) remains a major challenge, particularly in the face of climate change, growing food demand, and the increasing frequency of drought events (FAO, 2021; IPCC, 2022; Borin, 2023). Among the physiological processes involved in plant water use, transpiration (E) plays a fundamental role in leaf temperature (T_{leaf}) regulation and gas exchange, ensuring the uptake of CO_2 necessary for photosynthesis (Taiz and Zeiger, 2015). Stomata regulate the exchange of gases between the leaf's internal air spaces and the atmosphere, playing a crucial role in balancing CO_2 uptake for photosynthesis with the prevention of excessive water loss. Due to this dual function, they have become a key target in strategies aiming to enhance WP in crops (Nguyen et al., 2023). However, under suboptimal environmental conditions, stomatal behavior can result in unproductive water loss. For instance, stomata may remain partially open during periods of water stress to support photosynthesis, leading to a significant reduction in WP (Flexas et al., 2013). While traditional strategies have focused on steady-state stomatal conductance (gsw), recent attention to stomatal kinetics and responsiveness offers promising alternatives to enhance WP without compromising carbon assimilation (Nguyen et al., 2023).

Efficient irrigation systems aim to align water supply with plant water demand to maximize productivity. Irrigation is commonly based on reference evapotranspiration (ET_0) – which depends on environmental variables such as solar radiation, air temperature, vapor pressure deficit (VPD), and crop coefficient (Kc) (Pereira et al., 2025). However, this simple approach can fall short of capturing crop-specific physiological responses and developmental stages, needing adjustment, for example, considering the deficit irrigation (DI) management (Gong et al., 2020). To overcome this limitation, crop E models that incorporate factors such as leaf area index (LAI), stomatal resistance, and crop development stage have been proposed (Choi and Shin, 2020). Quantifying crop evapotranspiration (ET_c) has thus become essential for implementing more targeted and water-efficient irrigation strategies (Sharma and Bhambota, 2022).

Since E is closely linked to plant physiology, it can serve as a reliable indicator of crop growth and development. For this reason, designing irrigation strategies based on E models has become an increasingly important approach to improve irrigation efficiency (Jo et al., 2021). Various methodologies have been developed to estimate E, including the Penman–Monteith, Stanghellini, and Priestley–Taylor models, or to measure E through experimental approaches using soil water balance (Strati et al., 2018), gsw via porometers (Toro et al., 2019), sap flow (Lascano et al., 2016), and weighing lysimeters (Choi and Shin, 2020).

Despite these advances, comparatively little attention has been given to the substantial water losses that occur during the night. Recent evidence suggests that nocturnal E, though not associated with carbon assimilation, may account for a considerable fraction of daily water loss. Across a wide range of C_3 and C_4 plant species, nighttime E has been reported to range from 5% to 15% of daytime E rates, with values reaching as high as 30% under specific environmental conditions (Caird et al., 2007a; Fricke, 2019).

Carbon exchange and water vapor loss through E represent the two major mass flow processes in plants during the day. Interestingly, both continue at night to some extent through partially open stomata (Fricke, 2019). Nighttime E has also been observed in crops grown under artificial lighting and in arid field conditions, suggesting that nighttime E is both widespread and environmentally persistent (Resco de Dios et al., 2016; Fricke, 2019).

The physiological role of nocturnal E remains debated. However, Fricke (2019) suggests that it may offer several benefits, including the maintenance of hydraulic conductivity, facilitation of nutrients transport, and preservation of leaf water potential. Nighttime water loss may also facilitate respiratory CO_2 release through open stomata, a process essential for leaf expansion, particularly under stress conditions such as drought and salinity (Fricke, 2019). Under these circumstances, leaf expansion at night may represent a more efficient use of absorbed water compared to daytime, contributing to stress acclimation mechanisms. In *Solanum lycopersicum* (tomato), for instance, Lanoue et al. (2017) observed a modest but measurable increase in nighttime E (from 22:00 to 06:00), despite the absence of nocturnal lighting. Although this effect was less pronounced than in *Eustoma grandiflorum* (lisianthus), the results suggest that tomato exhibits circadian regulation of gsw. Notably, despite similar photosynthetic rates, tomato plants acclimated to red-white and red-blue LED lighting showed a reduction in overall water use efficiency by 25% and 31%, respectively, compared to those grown under high-pressure sodium (HPS) lamps. These findings imply that nocturnal E can substantially impact WP, especially under artificial lighting conditions. From an agronomic perspective, nocturnal water loss can lower WP by consuming irrigation resources without contributing to biomass

accumulation and carbon assimilation. Nevertheless, variation in nighttime E among species and genotypes suggests opportunities for genetic selection. A survey of wild and cultivated tomato species showed a range of nighttime E from 8% to 33% of daytime values, highlighting substantial intra- and interspecific variability and breeding potential (Caird et al., 2007b).

Despite the economic importance of tomato, quantitative assessments of nocturnal E in this species remain limited, and no threshold values have been proposed for breeding purposes. In particular, the occurrence of nocturnal E that do not contribute to biomass formation may represent a hidden inefficiency in the plant's water balance.

This study addresses this gap by quantifying nighttime water loss in greenhouse-grown tomato under different fertilization and irrigation management, also assessing the quanti-qualitative tomato response.

2. MATERIALS AND METHODS

2.1. Experimental site and materials

The study was conducted in a tunnel greenhouse at the "L. Toniolo" experimental farm of the University of Padova (45°21'00" N, 11°57'02" E; 7 m a.s.l.) from June to September 2022. The climate of the area is classified as sub-humid, with an average annual temperature of 13.5 °C. The average annual precipitation (1994–2021) is 830 mm, but evapotranspiration typically exceeds precipitation from April to September by approximately 260 mm (Berti et al., 2014). The soil is classified as Fluvi-Calcaric Cambisol (CMcf) with a silty loam texture (IUSS Working Group WRB, 2014). It has a field capacity and wilting point of 34% (v/v) and 13.5% (v/v), respectively, a bulk density of 1.45 Mg m^{-3}, and a slightly alkaline pH (approximately 8).

2.2. Experimental layout

Before transplanting, two soil tillage operations were performed using a rotary tiller. Fertilization was applied between the two tillage operations, followed by the installation of a drip irrigation system and the transplanting of seedlings. One polyethylene drip line was installed for each tomato row. The drip lines (16 mm diameter) had in-line drippers inserted along the pipe at 0.5 m spacing, with a discharge of 1.1 L h^{-1}. Tomato (HEINZ 1281 F1 - Furia Seed) transplanting took place on June 14, 2022, with a planting density of 2.5 plants m^{-2}, whereas harvesting on September 27, 2022.

Table 1. Chemical properties of compost used

Element	Content
Total N	2.0 %
Total C	22.4%
P	6373 mg kg^{-1}
K	26549 mg kg^{-1}
Cd	0.74 mg kg^{-1}
Cr	36.96 mg kg^{-1}
Cu	104.64 mg kg^{-1}
Pb	37.37 mg kg^{-1}
Zn	247.55 mg kg^{-1}

The irrigation volume was determined using soil moisture sensors (Teros 10 - METER Group, Inc., Pullman, WA, USA) placed at three different depths (20 cm, 40 cm, and 60 cm). Irrigation was applied when in the soil layer explored by the plants' roots, remained the 60% of the available water, restoring soil moisture to field capacity. The seasonal irrigation volume was measured using a water meter.

The experiment followed a split-plot design, with two irrigation management as the main factor (plots of 45 m × 4 m each) and five levels of fertilization as the second factor (subplots of 7.5 m × 4 m each), for a total of 10 plots. The main factor included irrigation at 100% ET_c (FI) (for a total irrigation volume of 320 mm) and at 75% ET_c (DI) (for a total irrigation volume of 240 mm). The fertilization factor included mineral fertilization, raw compost, fractionated compost (<2 mm), and a control without fertilization. The amount of fertilizers applied provided 150 kg N ha^{-1}, 100 kg P_2O_5 ha^{-1}, and 200 kg K_2O ha^{-1} to the crop. The characteristics of the compost used in the experiment are reported in Table 1.

2.3. Tomato monitoring

From June 28 to September 6, 2022, physiological (E, gsw, quantum yield of photosystem II - PhiPS2, VPD_{leaf}, T_{leaf}) and environmental (T_{ref}) parameters were manually measured weekly in six plants per plot using a porometer-fluorometer (LI-600, LI-COR Biosciences, Lincoln, NE, USA). Measurements were taken at four different hours of the day (06:00, 12:00, 18:00, and 00:00). The choice to measure six plants per plot was made to allow the assessment of 60 plants (six plants across ten plots) within approximately one hour, thereby minimizing the potential influence of time on the measured parameters. Additionally, leaves' chlorophyll content (SPAD index) was measured at 12:00 using a portable chlorophyll-meter (SPAD-502, Minolta, Japan).

On September 13, 2022, three plants per plot were sampled to determine the fruit quality by measuring dry matter content after oven drying at 65 °C, total soluble solids (TSS) content (°Brix), electrical conductivity, and pH. Yield was quantitatively assessed two weeks later, on September 27, 2022, by harvesting five plants per plot. At the end of the growing season the WP was calculated using the following equation:

$$WP = \frac{Cumulative \quad fruits \quad production \quad (kgha^{-1})}{Irrigation \quad volume \quad (m^3ha^{-1})}$$

2.4. Statistical analyses

Descriptive statistics were calculated for all datasets to assess the main characteristics of the data distribution. The normality and homoscedasticity of residuals were evaluated using the Shapiro-Wilk test (Shapiro & Wilk, 1965) and the Bartlett test (Snedecor & Cochran, 1989). When these assumptions were not satisfied, Z-score normalization was applied (Cheadle et al., 2003).

A linear model was fitted using the 'lm()' function in R software (Bates et al., 2015) to evaluate E as a function of irrigation regime and sampling hour, including their interaction, across the full dataset. The same approach was used to assess crop yield, WP, and fruits' quality-related parameters – dry matter content, TSS content, electrical conductivity, and pH – as functions of irrigation and sampling hour, including their interaction, using the complete dataset.

Post hoc analyses were conducted using the 'emmeans' package (Lenth et al., 2021) to estimate marginal means, in combination with the 'rstatix' or 'multcomp' packages (Kassambara, 2019), applying the Sidak method for multiple comparisons.

The correlation between all variables analyzed and T was examined by calculating Spearman's rank correlation coefficients using the R function 'cor' with method = "Spearman".

3.RESULTS AND DISCUSSION

3.1. Crop's physiological traits

The analysis of fertilization and irrigation effects revealed that neither fertilization nor the interaction between the two factors significantly influenced E and gsw. Therefore, based on these results, we focused exclusively on irrigation, excluding fertilization from subsequent analyses.

Considering the entire growing cycle, we observed that E varied significantly over time and between irrigation regimes. The analysis of the irrigation management × sampling hour interaction across the full dataset revealed significant effects on E (Figure 1). At 12:00, the highest E rates were recorded, with FI showing signifi-

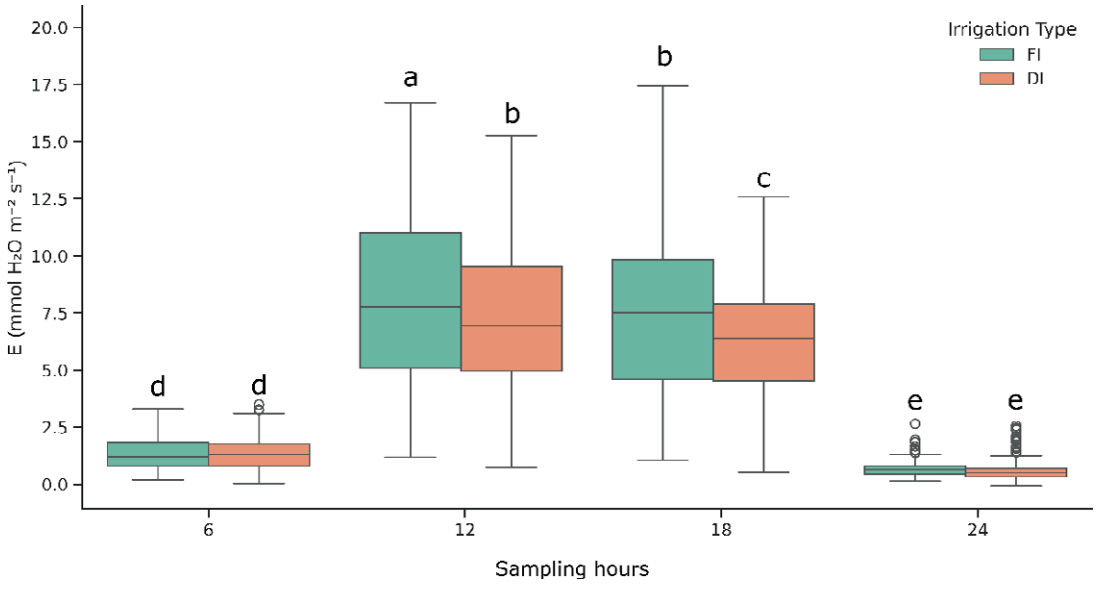

Figure 1. Crop transpiration (E) (mmol H2O m-2 s-1) (A) measured in two irrigation management, one with s with 100% ET_c irrigation (FI) and the other with 75% ET_c irrigation (DI) assessed at four sampling hours (6:00 – 6, 12:00 - 12, 18:00 - 18, and 24:00 - 24). Different lowercase letters indicate significant differences between irrigation managements (p-value ≤ 0.05). The box shows the quartiles of the dataset, while the whiskers extend to show the rest of the distribution.

cantly higher values (+11.1%) than the DI. At 12:00 the solar radiation usually peaks as well as the VPD, which might have driven stomatal opening and E, as previously suggested (Grossiord et al., 2020). The higher E observed in FI might have been related to the greater water availability and higher gsw (Chaves et al., 2002).

By 18:00, E decreased in both irrigation managements, although it was still significantly higher in FI (+15.8%) than DI. This finding is consistent with the natural decline in light intensity and air temperature. The higher values registered in FI, confirm the relationship between E and water supply even in the afternoon. Throughout the daytime, as reported in literature (Flexas et al., 2006), DI might have induced partial stomatal closure to conserve water, thereby reducing E rate. In addition, the higher relative difference at 18:00 than 12:00 might suggest a cumulative effect of water stress over the day under DI.

No significant effect was instead monitored during the night measurements (6:00 and 24:00) when E was low, but consistently above zero, confirming the findings of previous studies (Caird et al., 2007a; Resco de Dios et al., 2016). The absence of treatment effects at night may suggest that the two compared irrigation managements in our experimental greenhouse conditions have less impact on stomatal behavior during nocturnal periods. On average across the growing season, nighttime measurements showed that E at 06:00 was 1.4 times higher than at 24:00, reaching 0.5 mmol H_2O m^{-2} s^{-1}. This might be related to a pre-dawn stomatal opening in anticipation of light, as suggested by the findings of Resco et al. (2009).

On average, the daytime E values (12:00 and 6:00) were 7.7 mmol H_2O m^{-2} s^{-1} and 6.8 mmol H_2O m^{-2} s^{-1} for FI and DI managements, respectively. The nighttime E values were the 12.0% and 12.9% of the daytime E values for FI and DI managements, respectively. Our findings agree with Caird et al. (2007b), who measured with a portable photosynthesis system a nocturnal E of 10% of maximal daytime E. The observed nighttime water loss represents a substantial amount of water being lost without simultaneous carbon fixation through photosynthesis. Although this reduction in WP was observed, further physiological assessments are needed to determine possible positive effects, such as lower $T_{leaf,}$ that may enable faster and more effective recovery from daytime stress, particularly under DI management.

The gsw was significantly influenced by the sampling time, but not by the irrigation management (Table 2). This suggests that the differences observed in E were not only or primarily due to stomatal behavior. It reached its peak at 12:00, with a value of 0.75 mmol H_2O m^{-2} s^{-1}. It then decreased by about 25% at 18:00, 75% at 06:00, and 87.5% at 24:00. The higher gsw registered at 12:00, followed by 18:00, confirms the maximal stomatal opening under optimal light conditions, which might explain the corresponding peak in E. The gsw decrease registered at 18:00 coincides with the decrease in E, reinforcing that stomatal aperture is the primary driver of daytime E variation (Flexas et al., 2006). The values of gsw registered at 6:00 and 24:00 reflect a slight residual stomatal conductance corresponding to the non-zero E registered. These findings align with studies showing that nocturnal gsw, while low, can be physiologically meaningful and may contribute to hydraulic redistribution, nutrient uptake, or cooling (Caird et al., 2007b; Resco de Dios et al., 2019).

Table 2. Crop physiological parameters: stomatal conductance (gsw) (mmol H_2O m^{-2} s^{-1}) and quantum yield of photosystem II – (PhiPS2) measured in all treatments at the same four different sampling hours (6:00; 12:00; 18:00; 24:00). Different lowercase letters indicate significant differences between treatments (p-value ≤ 0.05).

Sampling hours	Physiological parameters	
	gsw	PhiPS2
6:00	0.20 c	0.77 ab
12:00	0.75 a	0.71 b
18:00	0.58 b	0.71 b
24:00	0.07 d	0.81 a

PhPS2 was significantly affected by the hours, exhibiting the highest values at 24:00 (0.81) and the lowest at 12:00 and 18:00 (0.71). Intermediate values were recorded at 6:00, which did not differ significantly from those at 12:00 and 18:00 (Table 2). No significant differences were found among managements for the leaf SPAD values (56 on average).

3.2. Physiological parameters' correlation

The correlation matrices for both night (18:00, 24:00) and day hours (6:00, 12:00) in the two irrigation managements are presented in Figure 2. Only significant correlations ($p < 0.05$) are described below. E was significantly positively correlated with gsw under both FI and DI managements during both daytime and nighttime. The results are consistent with previous studies showing that increased gsw facilitates water vapor loss from the leaf surface, thereby enhancing plants' E (Flexas et al., 2012).

Similarly, a recent study (Savvides et al., 2022) documented a positive relationship between gsw and E under water-stress conditions, although they observed lower E values under DI, a trend not detected in the pre-

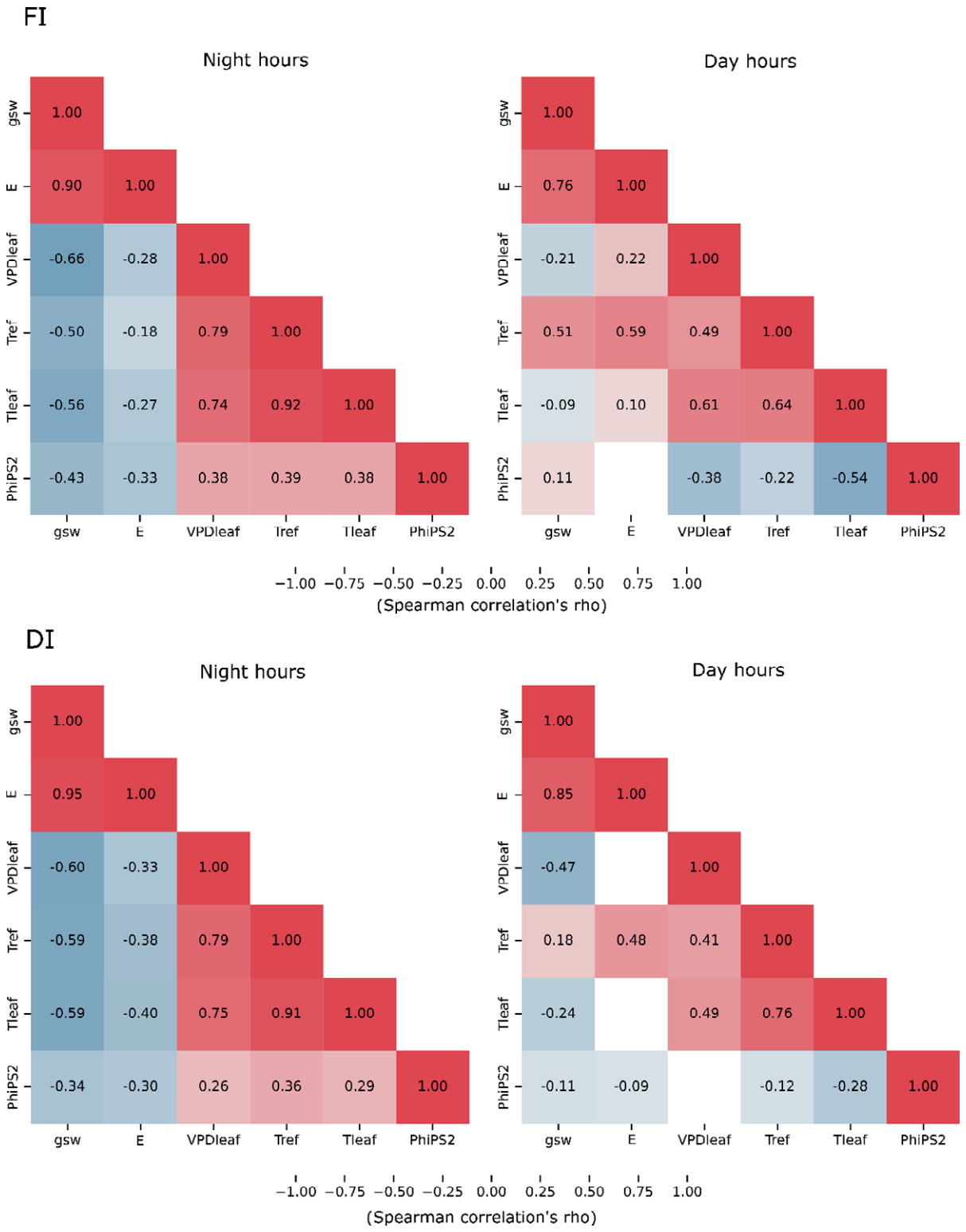

Figure 2. Spearman correlation heatmap showing relationships between all analyzed variables (stomatal conductance – gsw; chlorophyll fluorescence – PhiPS2; reference temperature – Tref; leaf temperature – Tleaf; vapor pressure deficit - VPD) and transpiration (E) within the 100% ET_c irrigation management (FI) and the 75% ET_c irrigation management (DI), assessed at night (6:00h, 24:00h) and day (12:00, 18:00h) sampling hours. Statistical differences are marked with * ($p < 0.05$). rho-values are displayed in different colors, and the blank space indicate the absent of statistically significant correlations.

sent study. Although gsw typically decreases at night, the positive nocturnal relationship between gsw and E observed in this study may be explained by residual E, as it did not drop to zero. This pattern aligns with the findings of Caird et al. (2007b). In the nighttime, E was also significantly negatively correlated with VPD_{leaf} under both irrigation managements. This suggests that nocturnal E was more strongly controlled by residual stomatal behavior than by atmospheric water demand. At nighttime, E was significantly negatively correlated with T_{leaf} and T_{ref}. During daytime, E was positively correlated with T_{leaf} under FI and with T_{ref} under both irrigation managements. Additionally, E and VPD_{leaf} were significantly negatively correlated at nighttime under both irrigation managements, while a positive correlation was observed under FI during daytime. The correlations between E and T_{leaf}, T_{ref}, and VPD_{leaf} highlight the role of E in regulating plant thermal balance and vapor pressure dynamics. As reported, E rate drives evaporative cooling, which might affect T_{leaf} (Gates, 1968). During the night period, without solar radiation input, T_{leaf} is mainly influenced by T_{ref}, and E-induced evaporative cooling should be minimal. However, in the present study, plants exhibited a non-zero nocturnal E (with related incomplete stomatal closure), which might have caused water loss, consistently with previous observations (Coupel-Ledru et al., 2016), promoting slight evaporative cooling and thereby lowering T_{leaf} (Caird et al., 2007b). This is consistent with the observed strong positive correlations between T_{ref} and T_{leaf} during the night under both FI and DI conditions, suggesting that T_{ref} might determine T_{leaf} at night. At the same time, the cooling effect on T_{leaf} caused by residual nocturnal E lowers VPD_{leaf}, since VPD_{leaf} depends on air temperature, T_{leaf}, and ambient humidity, as described by Monteith and Unsworth (2013). Indeed, nocturnal VPD_{leaf} was strongly positively correlated with both T_{ref} and T_{leaf}, reinforcing the idea that T_{leaf} plays a key role in nocturnal vapor pressure dynamics in greenhouse conditions (Caird et al., 2007a; Coupel-Ledru et al., 2016). Thus, the nocturnal E, by promoting leaf cooling, might have led to a lower VPD_{leaf}, explaining the observed negative E-VPD_{leaf} correlation under both FI and DI.

During the day, the dynamics shift due to incoming solar radiation, which significantly increases T_{leaf}. Under FI, high E through open stomata enhances evaporative cooling, helping to counteract heat buildup (Gates, 1968; Jones, 1999). Across the diurnal cycle E and T_{leaf} are often positively covarying because they share a common driver (increased solar radiation and air temperature): during the midday radiation peak both T_{leaf} and E can rise together even though E acts to reduce T_{leaf} relative to the no-transpiration case. This distinction between causal effect (evaporative cooling) and covariation (common forcing by radiation and air temperature) helps explain E–T_{leaf} positive correlations. Moreover, as daytime temperatures rise and humidity drops, VPD_{leaf} increases, and well-watered plants can respond by increasing stomatal opening, thus sustaining high E. This pattern explains the positive E-VPD_{leaf} correlation observed during daytime under FI. In well-watered, non-stressed conditions, stomata behave passively, responding directly to the evaporative demand driven by increasing VPD rather than actively regulating to conserve water, as described by Monteith (1995) and Jones (2014). In this context, the positive correlations of VPD_{leaf} with T_{ref} and T_{leaf} observed under FI further support the role of air temperature increases in driving vapor pressure dynamics during the day. Additionally, the strong positive correlation between T_{ref} and T_{leaf} during the daytime under FI highlights that T_{leaf} was largely controlled by T_{ref}, even under well-watered conditions.

Regarding T_{ref}, the absence of correlation with E under FI conditions indicates that when water is not limiting, temperature alone is not sufficient to influence E. This suggests that, also under FI, E might be controlled by stomatal and internal plant hydraulic factors by higher extent than external temperatures alone, as reported for water-limited conditions (Chaves et al., 2002; Medrano et al., 2002) where E is primarily regulated by stomatal responses and internal hydraulic constraints (e.g., xylem conductance, water potential), much more than being a direct reaction to external factors like temperature or VPD. Under DI conditions, plants tend to close their stomata to conserve water. This reduces evaporative cooling, making the relationship between E and T_{leaf} weaker, as registered in the present study where it didn't result statistically significant. Instead of helping cool the leaf, E might become more influenced by the T_{ref}. This is consistent with the observed positive correlations between T_{ref} and E and the strong positive T_{ref}–T_{leaf} correlation under daytime DI conditions, suggesting a tighter environmental control of T_{leaf} and E rates under water deficit. Under DI, plants can be more sensitive to factors like T_{ref} and VPD_{leaf}, which might explain the significant relationships between T_{ref} and E, consistently with the findings of Patakas et al. (2005) reporting that when soil water is limited, plants cannot maintain full stomatal control, making E more tightly linked to external environmental factors like T_{ref} and VPD_{leaf}, especially during daytime when evaporative demand is highest.

E was negatively correlated with PhiPS2 in both irrigation managements during nighttime and in DI during daytime. At night, while the E decreases, in both

irrigation managements, PhiPS2 might have undergone basal photochemical and repair activities as previously observed by Flexas et al. (2004) and Baker (2008). Under DI, water stress conditions might have altered photosynthetic efficiency, including the regulation of electron transport rates and photochemical efficiency (Flexas et al., 2004). During daytime, under DI, the negative correlation between E and PhiPS2 might reflect how limited CO_2 uptake under water-limited conditions, together with the light energy, might have caused photochemical impairments, including reduced PhiPS2, as demonstrated in previous studies (Flexas et al., 2004; Chaves et al., 2009; Lawlor and Tezara, 2009). Differently, under FI, adequate water availability might have maintained photosynthetic efficiency, preventing a significant PhiPS2 relationship.

3.3. Crop yield and water productivity

Neither fertilization and irrigation, nor their interaction had a statistically significant effect on total fruits yield, which showed an overall average of 64.1 Mg ha^{-1}. These results are consistent with those reported by Bekele (2017), who found that a 25% reduction in irrigation volume did not significantly affect tomato yield, while improving water productivity.

In the present study, the proportion of marketable yield remained high and comparable between irrigation managements, with values of 77.6% under FI and 77.4% under DI. This suggests that a moderate reduction in irrigation did not compromise fruit yield (Nigatu et al., 2024). Similar findings were reported by Patanè et al. (2011), who demonstrated that DI strategies, including a 50% reduction in ET_c applied during part or all of the growing season, did not significantly reduce the marketable yield. Conversely, Lahoz et al. (2016) observed that DI at 75% of ET_c led to a 28.2% reduction in water use but also resulted in a 16.4% decrease in marketable yield.

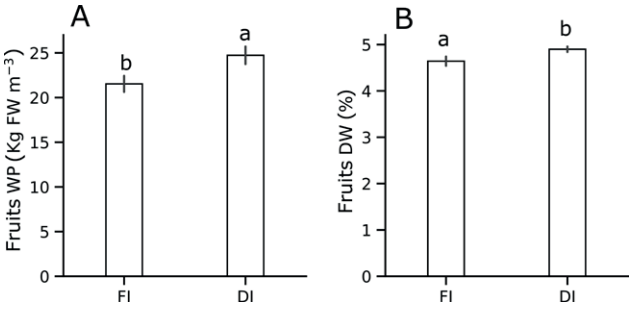

Figure 3. Average fruits' water productivity (WP) (kg FW m-3) ± SE (A), and average fruits' dry weight (DW) (%) ± SE (B) measured in two experimental managements with 100% ET_c irrigation (FI) and the 75% ET_c irrigation (DI). Different lowercase letters indicate significant differences between managements (n = 5; p-value ≤ 0.05, Sidak post-hoc test).

Fruits' production was significantly enhanced under DI, with a 14.7% increase compared to FI (21.5 kg m^{-3}) (Figure 3A). A similar trend was reported by Gragn et al. (2023), who noted a progressive increase in WP as irrigation levels decreased from 100% to 50% ET_c. In their study, the highest WP (20.4 kg m^{-3}) was achieved at 50% ET_c, while the lowest (12.0 kg m^{-3}) was recorded at 100% ET_c, which was statistically comparable to 75% ET_c.

3.4. Marketable fruits' quality

The application of DI increased the fruits dry matter content (+6.5%) compared to the FI, which recorded 4.9% (Figure 3B). This parameter is particularly relevant for the tomato processing industry, as lower fruit water content is associated with improved processing efficiency (Xu et al., 2024). Instead, no statistically significant differences were observed between irrigation managements for TSS, titratable acidity, or electrical conductivity, with average values of 4.2 °Brix, 6.16, and 4.24 µS/cm, respectively. However, fruits pH was slightly but consistently lower under DI (4.1) than under FI (4.3). Previous studies have highlighted the potential of regulated DI to enhance fruit quality in processing tomato by increasing TSS and other compositional attributes (Xu et al., 2024). For instance, Lahoz et al. (2016) reported an 8.4% increase in TSS and a 2.4% rise in the Hunter a/b ratio, an indicator of improved fruit redness, under DI. However, they did not observe significant changes in pH, contrasting with the slight decrease detected in our study. Our results agree with the findings of Zhang et al. (2017), who found no significant differences in TSS between 70% and 100% ET_c irrigation managements, with values ranging from 5.78% to 5.62%. Their findings suggest that moderate water reductions can conserve resources without compromising key fruit quality traits. These improvements are particularly important for the processing sector, as elevated TSS levels contribute to increased product yield and reduced processing costs (Johnstone et al., 2005).

4. CONCLUSIONS

Nocturnal E in tomato plants, although of low magnitude, was consistently detected at 24:00 and 06:00 under both FI and DI, indicating that nocturnal water loss is not negligible. This residual E, likely driven by incomplete stomatal closure, represents a hidden compo-

nent of the crop's water balance. Its potential physiological roles, such as contributing to nocturnal leaf cooling, warrant further investigation.

Irrigation management significantly affected daytime E but not nocturnal values. FI resulted in higher E and gsw during peak irradiance (12:00 and 18:00), reflecting passive stomatal behavior under high atmospheric evaporative demand. In contrast, DI induced partial stomatal closure and reduced E, particularly in the afternoon, showing greater dependence on T_{ref} due to limited stomatal control.

DI improved WP by 14.7% without reducing yield. Furthermore, DI enhanced fruit dry matter content by 6.5%, an important quality attribute for processing tomato, without negatively affecting TSS, acidity, or electrical conductivity. These results highlight the potential of moderate water-saving irrigation strategies to improve WP and fruit quality without yield penalties.

ACKNOWLEDGMENTS

This experiment was supported by the project "Deficit irrigation del pomodoro da industria nell'areale veneto" (prot. BIRD 227047) funded by the University of Padova - Department of Agronomy Food Natural resources Animals and Environment (DAFNAE).

REFERENCES

Baker, N. R. (2008). Chlorophyll fluorescence: a probe of photosynthesis in vivo. Annu. Rev. Plant Biol., 59(1), 89-113.

Barbour, M. M., & Buckley, T. N. (2007). The stomatal response to evaporative demand persists at night in Ricinus communis plants with high nocturnal conductance. Plant, Cell & Environment, 30(6), 711-721.

Bekele, S. (2017). Response of tomato to deficit irrigation at Ambo, Ethiopia. Journal of Natural Sciences Research, 7(23).

Berti, A., Tardivo, G., Chiaudani, A., Rech, F., & Borin, M. (2014). Assessing reference evapotranspiration by the Hargreaves method in north-eastern Italy. Agricultural Water Management, 140, 20-25.

Borin, M. (2023). A wise irrigation to contribute to integrated water resource management. Italian Journal of Agrometeorology, (2), 5-19.

Caird, M. A., Richards, J. H., & Donovan, L. A. (2007a). Nighttime stomatal conductance and transpiration in C3 and C4 plants. Plant Physiology, 143(1), 4–10. https://doi.org/10.1104/pp.106.092940

Caird, M.A., Richards, J.H., & Hsiao, T.C. (2007b). Significant transpirational water loss occurs throughout the night in field-grown tomato. Functional Plant Biology, 34(3), 172–177.

Chaves, M. M., Pereira, J. S., Maroco, J., Rodrigues, M. L., Ricardo, C. P. P., Osório, M. L., Carvalho, I., Faria, T., Pinheiro, C. (2002). How plants cope with water stress in the field? Photosynthesis and growth. Annals of botany, 89(7), 907.

Chaves, M. M., Flexas, J., & Pinheiro, C. (2009). Photosynthesis under drought and salt stress: regulation mechanisms from whole plant to cell. Annals of botany, 103(4), 551-560.

Cheadle, C., Vawter, M. P., Freed, W. J., & Becker, K. G. (2003). Analysis of microarray data using Z score transformation. The Journal of molecular diagnostics, 5(2), 73-81.

Choi, Y. B., & Shin, J. H. (2020). Development of a transpiration model for precise irrigation control in tomato cultivation. Scientia Horticulturae, 267, 109358.

Coupel-Ledru, A., Lebon, E., Christophe, A., Gallo, A., Gago, P., Pantin, F., ... & Simonneau, T. (2016). Reduced nighttime transpiration is a relevant breeding target for high water-use efficiency in grapevine. Proceedings of the National Academy of Sciences, 113(32), 8963-8968.

FAO (2021). The State of the World's Land and Water Resources for Food and Agriculture – Systems at breaking point. Food and Agriculture Organization of the United Nations.

Flexas, J., Bota, J., Cifre, J., Mariano Escalona, J., Galmés, J., Gulías, J., Medrano, H. (2004). Understanding down-regulation of photosynthesis under water stress: future prospects and searching for physiological tools for irrigation management. Annals of applied Biology, 144(3), 273-283.

Flexas J., Bota J., Galmés J., Medrano H. & Ribas-Carbó M. (2006). Keeping a positive carbon balance under adverse conditions: responses of photosynthesis and respiration to water stress. Physiologia Plantarum, 127, 343–352.

Flexas, J., Barbour, M. M., Brendel, O., Cabrera, H. M., Carriquí, M., Díaz-Espejo A., Douthe C., Dreyer E., Juan F. P., Gago J., Gallé A., Galmés J., Kodama N., Medrano H., Niinemets Ü., Peguero-Pina J. J., Pou A., Ribas-Carbó M., Tomás M., Tosens T., Warren, C. R. (2012). Mesophyll diffusion conductance to CO2: an unappreciated central player in photosynthesis. Plant Science, 193, 70-84.

Flexas J., Niinemets Ü., Gallé A., Barbour M.M., Centritto M., Diaz-Espejo A., Medrano H. (2013) Diffu-

sional conductances to CO_2 as a target for increasing photosynthesis and photosynthetic water-use efficiency. Photosynthesis Research, 117, 45–59.

Fricke, W. (2019). Night-time transpiration – favouring growth? Trends in Plant Science, 24(4), 311–317.

Gates, David Murray. "Energy exchange in the biosphere." (1968): 33-43.

Gong, X., Qiu, R., Sun, J., Ge, J., Li, Y., & Wang, S. (2020). Evapotranspiration and crop coefficient of tomato grown in a solar greenhouse under full and deficit irrigation. Agricultural Water Management, 235, 106154.

Gragn, T., Mamo, A., & Wolde, O. (2023). Evaluation of tomato (Solanum Lycopersicum L.) response to deficit irrigation at Adola District, Guji Zone, Southern Ethiopia. Science Research, 11(5), 117-122.

Grossiord, C., Buckley, T. N., Cernusak, L. A., Novick, K. A., Poulter, B., Siegwolf, R. T. W., Sperry, J. S., & McDowell, N. G. (2020). Plant responses to rising vapor pressure deficit. New Phytologist, 226(6), 1550-1566

IPCC (2022). Climate Change 2022: Impacts, Adaptation and Vulnerability. Working Group II Contribution to the Sixth Assessment Report of the Intergovernmental Panel on Climate Change.

IUSS Working Group, (2014). World reference base for soil resources 2014. International soil classification system for naming soils and creating legends for soil maps.

Jo, W. J., & Shin, J. H. (2021). Development of a transpiration model for precise tomato (*Solanum lycopersicum* L.) irrigation control under various environmental conditions in greenhouse. Plant Physiology and Biochemistry, 162, 388-394.

Johnstone, P. R., Hartz, T. K., LeStrange, M., Nunez, J. J., & Miyao, E. M. (2005). Managing fruit soluble solids with late-season deficit irrigation in drip-irrigated processing tomato production. HortScience, 40(6), 1857-1861.

Jones, H. G. (1999). Use of infrared thermometry for estimation of stomatal conductance as a possible aid to irrigation scheduling. Agricultural and forest meteorology, 95(3), 139-149.

Jones, H. G. (2014). *Plants and microclimate: a quantitative approach to environmental plant physiology*. Cambridge university press.

Lahoz, I., Pérez-de-Castro, A., Valcárcel, M., Macua, J. I., Beltrán, J., Roselló, S., & Cebolla-Cornejo, J. (2016). Effect of water deficit on the agronomical performance and quality of processing tomato. Scientia Horticulturae, 200, 55-65.

Lanoue, J., Leonardos, E. D., Ma, X., & Grodzinski, B. (2017). The Effect of Spectral Quality on Daily Patterns of Gas Exchange, Biomass Gain, and Water-Use-Efficiency in Tomatoes and Lisianthus: An Assessment of Whole Plant Measurements. Frontiers in Plant Science, 8, 1076. https://doi.org/10.3389/fpls.2017.01076

Lascano, R. J., Goebel, T. S., Booker, J., Baker, J. T., & Gitz III, D. C. (2016). The stem heat balance method to measure transpiration: Evaluation of a new sensor. Agricultural Sciences, 7(9), 604-620.

Lawlor, D. W., Tezara, W. (2009). Causes of decreased photosynthetic rate and metabolic capacity in water-deficient leaf cells: a critical evaluation of mechanisms and integration of processes. Annals of botany, 103(4), 561-579.

Medrano, H., Escalona, J. M., Bota, J., Gulías, J., & Flexas, J. (2002). Regulation of photosynthesis of C3 plants in response to progressive drought: stomatal conductance as a reference parameter. Annals of botany, 89(7), 895-905.

Monteith, J.L. (1995). "A reinterpretation of stomatal responses to humidity." Plant, Cell & Environment, 18(4), 357–364.

Monteith, J.L., Unsworth, M.H. (2013). Principles of Environmental Physics (4th ed.). Academic Press.

Nguyen, T. B. A., Lefoulon, C., Nguyen, T. H., Blatt, M. R., & Carroll, W. (2023). Engineering stomata for enhanced carbon capture and water-use efficiency. Trends in Plant Science, 28(11), 1290-1309.

Nigatu, B., Getu, D., Getachew, T., & Getaneh, B. (2024). Effect of irrigation regime on yield component and water use efficiency of tomato at Ataye irrigation scheme, Ataye Ethiopia. Italian Journal of Agrometeorology, (2), 89-100.

Patakas, A., Noitsakis, B., & Chouzouri, A. (2005). Optimization of irrigation water use in grapevines using the relationship between transpiration and plant water status. Agriculture, Ecosystems & Environment, 106(2-3), 253-259.

Patanè, C., Tringali, S., & Sortino, O. (2011). Effects of deficit irrigation on biomass, yield, water productivity and fruit quality of processing tomato under semi-arid Mediterranean climate conditions. Scientia Horticulturae, 129(4), 590-596.

Resco, V., Hartwell, J., & Hall, A. (2009). Ecological implications of plants' ability to tell the time. Ecology letters, 12(6), 583-592.

Resco de Dios, V., Loik, M. E., Smith, R., Aspinwall, M. J., & Tissue, D. T. (2016). Genetic variation in circadian regulation of nocturnal stomatal conductance enhances carbon assimilation and growth. Plant, Cell & Environment, 39(1), 3-11.

Sánchez-Rodríguez, E., Rubio-Wilhelmi, M. M., Cervilla, L. M., Blasco, B., Rios, J. J., Rosales, M. A., Rome-

ro, L., & Ruiz, J. M. (2010). Genotypic differences in some physiological parameters symptomatic for oxidative stress under moderate drought in tomato plants. Plant Science, 178(1), 30–40. https://doi.org/10.1016/j.plantsci.2009.10.002

Pereira, L.S., Allen, R.G., Paredes, P., López-Urrea, R., Raes, D., Smith, M., Kilic, A. & Salman, M. 2025. Crop evapotranspiration – Guidelines for computing crop water requirements. Second edition, revised 2025. FAO Irrigation and Drainage Paper, No.56 Rev.1. Rome, FAO. https://doi.org/10.4060/cd6621en

Savvides, A. T., Trouvelot, S., Ruelle, P., & Villemant, C. (2022). Challenging the water stress index concept — A synthesis of plant gas-exchange responses under drought and salinity. *Plant, Cell & Environment*, 45(8), 2302-2319.

Sharma, V., & Bhambota, S. (2022). Strategies to Improve Crop-Water Productivity. In Food, Energy, and Water Nexus: A Consideration for the 21st Century (pp. 149-172). Cham: Springer International Publishing.

Strati, V., Albéri, M., Anconelli, S., Baldoncini, M., Bittelli, M., Bottardi, C., Mantovani, F. (2018). Modelling soil water content in a tomato field: proximal gamma ray spectroscopy and soil–crop system models. Agriculture, 8(4), 60.

Toro, G., Flexas, J., & Escalona, J. M. (2019). Contrasting leaf porometer and infra-red gas analyser methodologies: an old paradigm about the stomatal conductance measurement. Theoretical and Experimental Plant Physiology, 31(4), 483-492.

Xu, J., Li, X., Wan, W., Zhu, X., Li, C., Zhao, X., Pang, S., Diao, M. (2024). Impact of regulated deficit irrigation on the dynamics of quality changes in processing tomato fruits during ripening. Agricultural Water Management, 304, 109068.

Zhang, H., Xiong, Y., Huang, G., Xu, X., & Huang, Q. (2017). Effects of water stress on processing tomatoes yield, quality and water use efficiency with plastic mulched drip irrigation in sandy soil of the Hetao Irrigation District. Agricultural Water Management, 179, 205-214.

Italian Journal of Agrometeorology
Rivista Italiana di Agrometeorologia

Firenze University Press
https://riviste.fupress.net/index.php/IJAm

OPEN ACCESS

Citation: Sarvina, Y., & Mansyah, E. (2025). Quantifying the effect of ENSO on Mangosteen yield using multi-year data in Indonesia. *Italian Journal of Agrometeorology* (2): 65-77. doi: 10.36253/ijam-3511

Received: May 28, 2025

Accepted: July 8, 2025

Published: December 31, 2025

Data Availability Statement: All relevant data are within the paper and its Supporting Information files.

Competing Interests: The Author(s) declare(s) no conflict of interest.

ORCID:
YS: 0000-0002-9185-2596
EM: 0000-0003-2161-4006

Quantifying the effect of ENSO on Mangosteen yield using multi-year data in Indonesia

Yeli Sarvina[1,*], Ellina Mansyah[2]

[1] *Research Center for Climate and Atmospheric, National Research and Innovation Agency (BRIN), Jl. Raya Puspiptek 60, Tangerang Selatan 15310, Indonesia*
[2] *Research Center for Horticulture, Indonesian Agency for Research and Innovation (BRIN), Jl. Raya Jakarta-Bogor KM 46, Cibinong, Kab. Bogor – 16915, Indonesia*
*Corresponding author. E-mail: yeli002@brin.go.id

Abstract. The El Niño–Southern Oscillation (ENSO) is a major driver of inter-annual climate variability in Indonesia and has significant implications for agricultural productivity. Mangosteen (*Garcinia mangostana*), a perennial tropical fruit and one of Indonesia's key export commodity, is highly sensitive to climate fluctuations. Understanding how ENSO affects mangosteen production is critical for developing climate-informed cultivation strategies. This study investigates the impact of ENSO on mangosteen production dynamics in Indonesia using provincial-scale data from 1997 to 2020, including the number of harvested plants, yield, and total annual production. The Oceanic Niño Index (ONI) was used to classify each year into El Niño, La Niña, or Neutral phases. Number of harvested plants, yield and production during El Niño and La Niña years were then compared to those of neutral years to assess ENSO-related impacts. Results show that the impact of ENSO on mangosteen varies across different regions of Indonesia. Generally, the number of harvested plants increased during El Niño years but declined during La Niña years. In contrast, yield is generally lower in both El Niño and La Niña years compared to neutral years in most production centre area except in Bali- Nusa Tenggara and Maluku- Papua. Overall production increased slightly (1–12%) during El Niño but dropped significantly (2–40%) during La Niña, indicating that excessive rainfall during La Niña has a more detrimental effect on mangosteen yields than drought during El Niño. These findings highlight the importance of ENSO monitoring as a basis for climate risk management in perennial fruit crops. Early warning systems and adaptive measures, such as irrigation planning for dry years and drainage infrastructure for wet years, are essential to mitigate ENSO-related production losses.

Keywords: ENSO, Mangosteen, climate variability, rainfall, economic loss.

HIGHLIGHTS

- The effects of ENSO on mangosteen differ across various regions in Indonesia
- Mangosteen yields decline during both El Niño and La Niña, with La Niña except in Bali- Nusa Tenggara and Maluku- Papua. While annual

production increase slightly in El- Niño Year (1-12 %) and drop during La-Niña (2-40%)
- El Niño increases harvested plant numbers, slightly boosting total production despite lower yields.
- ENSO monitoring and adaptive measures (e.g., irrigation in dry years, drainage in wet years) are critical to reduce climate-related losses.

INTRODUCTION

The mangosteen (*Garcinia mangostana L.*) is one of Indonesia's leading horticultural commodity with high potential to contribute to national economic development, public health, and rural livelihoods. It is rich in minerals and vitamins particularly vitamin C (Aizat et al., 2019; Ansori et al., 2020; Ovalle-Magallanes et al., 2017) and contains xanthones in its rind, which have been identified for their antioxidant, anti-inflammatory, anticancer, and cardiovascular health benefits (Ansori et al., 2022; Kalick et al., 2023; Nauman & Johnson, 2022). In 2023, Indonesia exported 42.8 thousand tons of mangosteen, generating USD 112 thousand in foreign exchange (Ministry of Agriculture, 2024). This makes mangosteen the second-largest contributor to fruit-based foreign exchange income. Given its economic and health benefits, sustainable production of mangosteen is crucial to improving societal well-being.

Despite Indonesia's favourable agroclimatic conditions and genetic diversity with 14 registered cultivars mangosteen productivity remains low, only reaching 5–8 tons/ha, compared to Thailand's 10 tons/ha (Directorate General of Horticulture, 2021). Climate is one of the most influential abiotic factors affecting mangosteen development (Jaroensutasinee et al., 2023; Raju et al., 2024; Sayruamyat et al., 2021) . Climate affects flowering, pollination, fruit formation, pest and disease attacks, as well as fruit production and quality (Apiratikorn et al., 2012; Jaroensutasinee et al., 2023b; Mansyah, 2009; Ounlert et al., 2017). Studies have shown that climatic variability accounts for nearly one-third of plant growth and productivity (Leng et al., 2016; Ray et al., 2015). However, the impacts of specific climatic phenomena on mangosteen yield and quality remain underexplored (Tengsetasak et al., 2024). The sustainability of production in Indonesia requires support from various research and development efforts on mangosteen, particularly in increasing production and controlling pests and diseases affecting mangosteen (Mansyah et al., 2013).

Indonesia's climate is strongly influenced by interannual variability, particularly the El Niño–Southern Oscillation (ENSO) (Aldrian & Susanto, 2003; Arrigo & Wilson, 2008; Hendrawan et al., 2019; Hidayat & Ando, 2018) and Indian Ocean Dipole (IOD) (Mulyana, 2002; Nur'utami & Hidayat, 2016). ENSO refers to the recurring pattern of climate variability in the eastern Pacific Ocean, marked by sea surface temperature anomalies (SSTA) and changes in sea level. The warming of sea surface temperatures indicates an El Niño event, while the cooling signifies a La Niña event. El Niño typically delays the onset of the rainy season and extends the dry season in Indonesia ((El Ramija et al., 2021; Hidayati & Chrisendo, 2010; Iskandar et al., 2019; Karuniasa & Pambudi, 2022; Nugraheni et al., 2024a; Sidauruk et al., 2023). Conversely, La Niña tends to bring an earlier onset of the rainy season and a shorter dry season (Alhadid & Budi Nugroho, 2024; Endah Ardhi Ningrum Abdullah et al., n.d.; Harahap et al., 2023; Hidayat et al., 2018; Nugraheni et al., 2024b; Supari et al., 2018)

ENSO has been shown to affect flowering periods and harvest dynamics in tropical fruit crops, including mangosteen (Sarvina & Sari, 2018) (Apiratikorn et al., 2014). With increasing occurrences of extreme ENSO events due to climate change (Chen et al., 2024; Xie et al., 2022), understanding their impact on mangosteen production is essential for developing adaptive agricultural strategies.

This study aims to assess the influence of interannual climate variability focusing on ENSO on the production dynamics of mangosteen in Indonesia. The findings are expected to support climate-smart mangosteen farming through the development of cultivation calendars and adaptive agronomic planning.

MATERIALS AND METHODS

This study uses mangosteen production data, specifically the number of haversted plant and yield all provinces across regions in Indonesia for the period 1997–2020. The data were obtained from the Central Bureau of Statistics (BPS), compiled in the Indonesian Fruit and Vegetable Statistics Book. The ENSO indicator used in this study was the Oceanic Niño Index (ONI), covering the same period as the available production data. This data was obtained from the National Oceanic and Atmospheric Administration (NOAA) and downloaded from the website http://www.cpc.ncep.noaa.gov/products/. The ONI represents a three-month running average of sea surface temperature (SST) anomalies in the Niño 3.4 region (5°N–5°S, 120°–170°W). Sea surface temperature in the Niño 3.4 region is a widely recognized indicator of variability

that significantly affects Indonesia (Hidayat et al., 2018; Surmaini et al., 2015)). The ONI data is used to identify years of La Niña and El Niño years.

The data on the harvested plants and yield were grouped according to the years of Neutral, El Niño, and La Niña events. This method has been widely used to examine the influence of ENSO on agricultural commodity production (Cirino et al., 2015; Cobon et al., 2016; Ramirezrodrigues et al., 2014; Sarvina & Sari, 2018) . This approach is known as the anomaly approach. The ENSO years selected include El Niño and La Niña events with moderate, strong, and very strong intensities. For each year, the average values were calculated. The number of harvested plants and yield during El Niño and La Niña years were compared to those in neutral years, providing information on the increase or decrease in production during El Niño and La Niña compared to neutral conditions. Furthermore, the increases and decreases in the number of harvested plants and yield were mapped spatially to identify the regions experiencing the greatest changes in production thus identifying the most impacted areas.

RESULTS

The uneven distribution of mangosteen production in Indonesia highlights a concentration in Java and Sumatra, with limited expansion to other regions. This spatial limitation is compounded by the predominance of traditional cultivation practices, where mangosteen is often grown in home gardens with minimal inputs and without standardized agronomic management, resulting in generally low yields and quality. Figure 1 illustrates the number of harvested mangosteen plants across major islands during different ENSO phases. Analytical results indicate that La Niña events are associated with a reduction in the number of harvested plants across most islands, reflecting possible negative impacts of excess rainfall or prolonged wet conditions on flowering and fruiting processes. However, Maluku and Papua deviate from this trend, showing a notable increase in productive trees during La Niña, which may be attributed to differing agroecological conditions or adaptive local cultivation practices.

In contrast, El Niño years generally correspond with a higher number of productive trees compared to Neu-

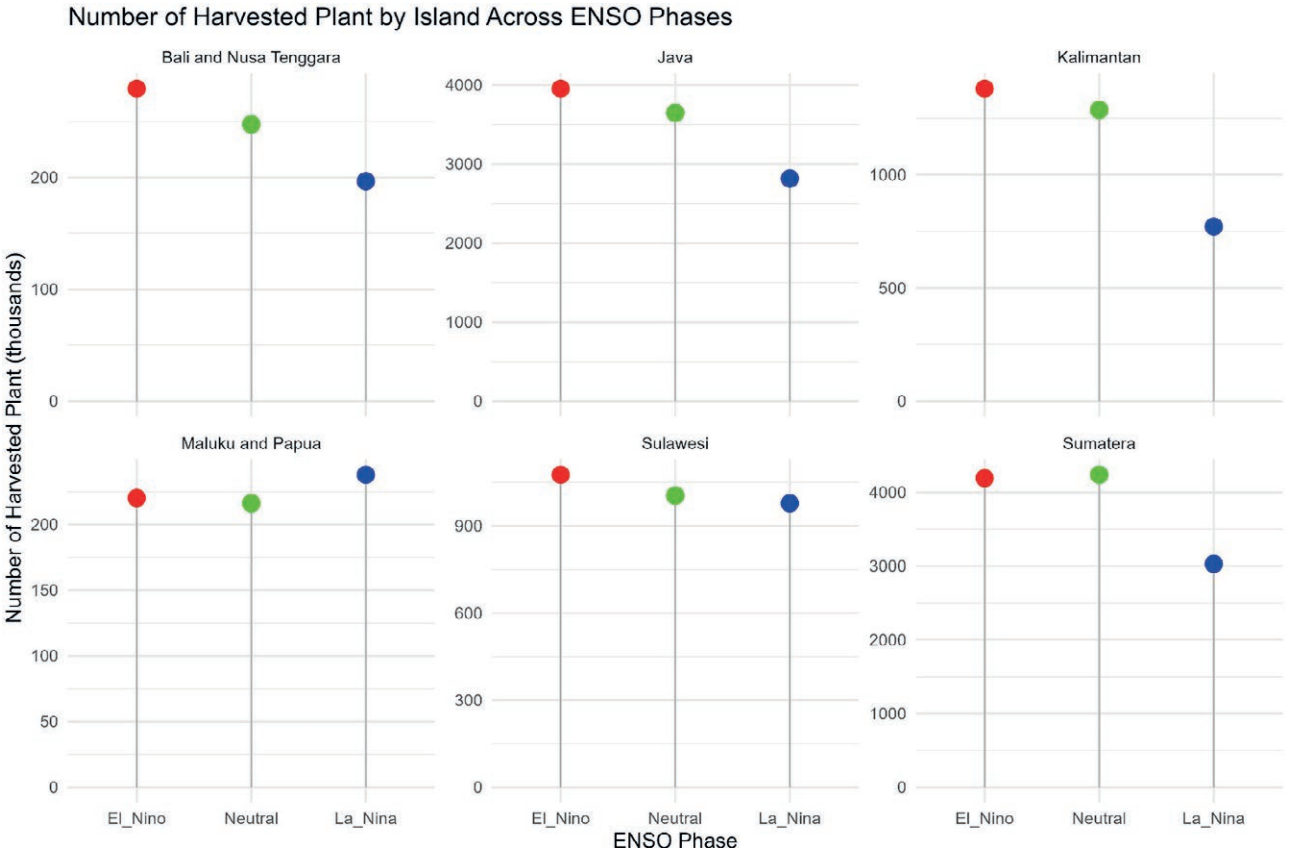

Figure 1. The number of Harvested Plants per Island/group Island.

tral years, potentially due to drier conditions favouring flowering induction in mangosteen, which is known to respond positively to stress prior to fruiting. The only exception is Sumatra, where a slight decline in number harvested plant was recorded during El Niño years, suggesting regional variability in mangosteen response to climatic stressors. These findings underscore the importance of understanding regional responses to ENSO variability for improving adaptive strategies in mangosteen cultivation across Indonesia.

The yield of mangosteen during Neutral, El Niño, and La Niña years in Indonesia is presented in a boxplot in Figure 2. The highest mangosteen yield in Indonesia is found in Java and Sumatra, ranging between 60–70 kg/tree, while the lowest productivity is found in Kalimantan, Maluku, and Papua, at below 50 kg/tree. This indicates that in eastern Indonesia, the crop has not yet been cultivated optimally. There is still significant potential to increase productivity, thus further research and studies on productivity improvement are needed.

The differing patterns of yield increase and number of harvested plants during El Niño and La Niña events affect mangosteen production patterns. Changes in mangosteen production during El Niño and La Niña years are presented in Figure 3, which shows that, in general, mangosteen production in Indonesia increased during El Niño years, except in Sumatra. Conversely, during La Niña years, production generally decreased, except in Maluku and Papua. During El Niño years, production increased by approximately 1–12%, while during La Niña years, production declined by 2–40%.

The distribution map of production changes during La Niña and El Niño years by province is presented in Figure 4. During La Niña years, it is observed that most provinces in Java, Kalimantan, and Sumatra experienced a decline in production. These regions are the main mangosteen production centers in the country thus production declines in these areas can trigger substantial national level supply fluctuations. The regions with the largest decline in production during La Niña years are Kalimantan, Sumatra, and Java. The regions where production increased during El Niño years are Java, Bali, and Nusa Tenggara.

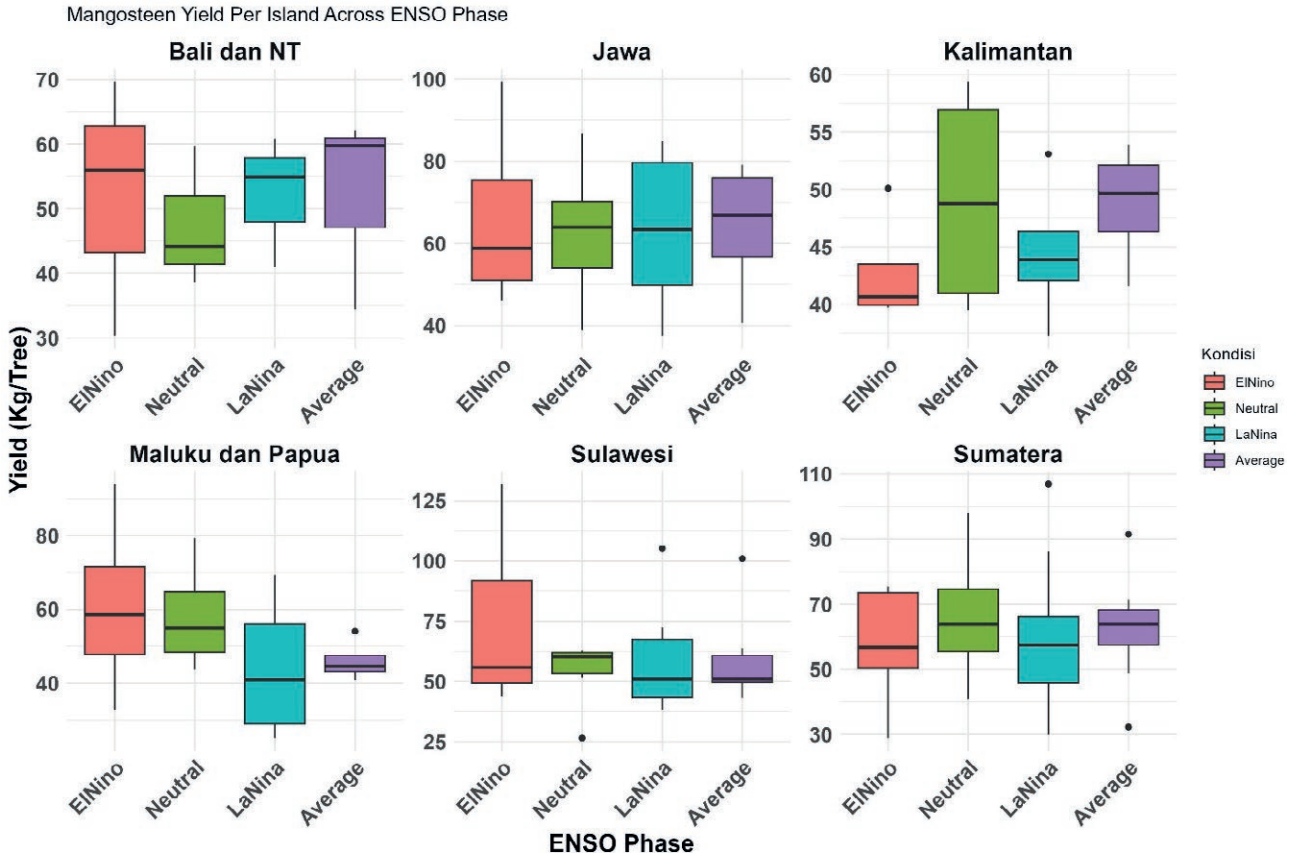

Figure 2. Boxplot of mangosteen yield (kg/tree) per island during each ENSO phase.

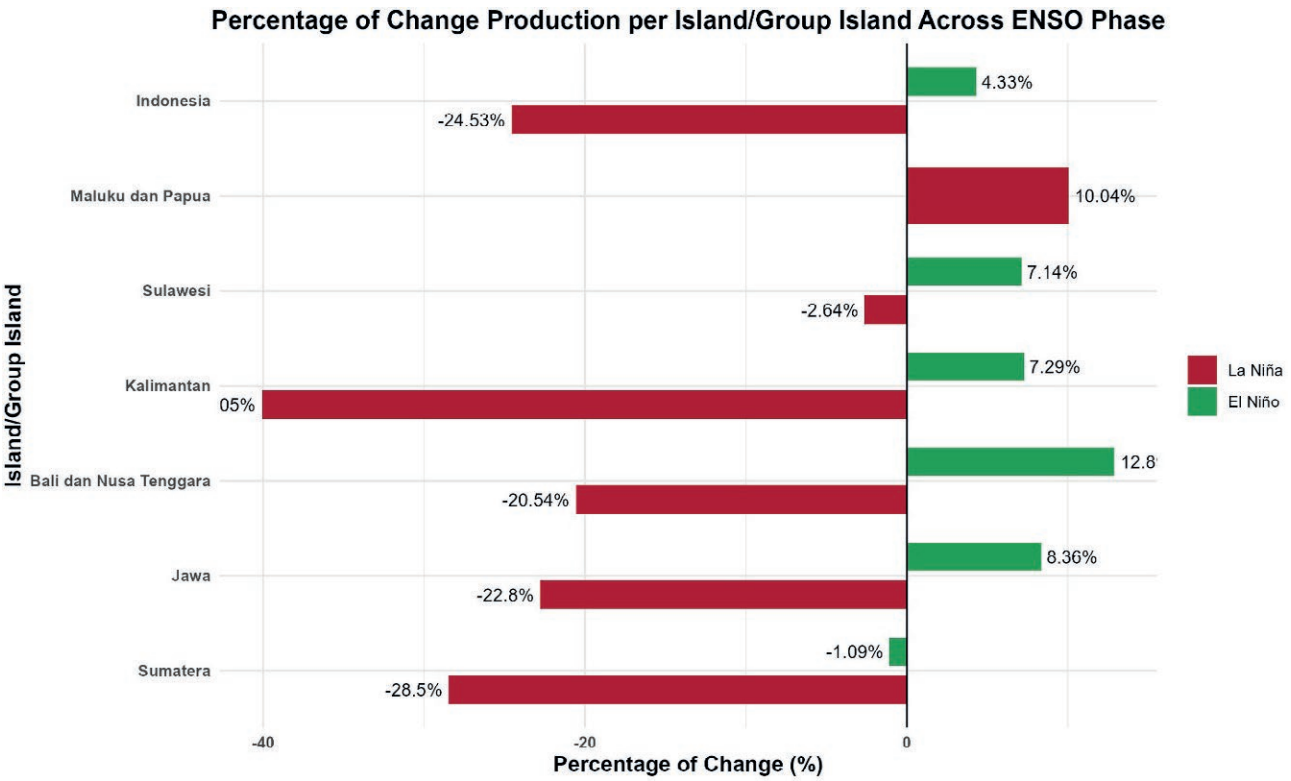

Figure 3. Changes in mangosteen production during El Niño and La Niña years.

Figure 5 illustrates the spatial distribution of yield changes during El Niño and La Niña years. In general, areas experiencing yield declines during El Niño years include most parts of Sumatra, Java, and Kalimantan. In contrast, during La Niña years, yield reductions predominantly occurred in Central and Eastern Java, Eastern and Central Sumatra, Eastern and Western Kalimantan, Southern Sulawesi, and Papua.

Differences in rainfall during El Niño, neutral, and La Niña years are presented in Figure 6. The selected years are 2015 for El Niño (very strong), 2013 for neutral, and 2010 for La Niña (moderate). In 2015, the very strong El Niño event led to a significant reduction in rainfall across Indonesia, with most regions receiving less than 2000 mm of annual rainfall. In contrast, during the moderate La Niña year of 2010, increased rainfall was observed, resulting in wetter conditions across much of the country.

DISCUSSION

ENSO phases significantly influence production: during El Niño, there is a general increase in the number of harvested plants in regions like Java, Bali, and Nusa Tenggara, leading to a national production rise of about 4.3%, although Sumatra sees a slight decline. In contrast, La Niña causes a decrease in harvested plants and yield in major producing regions, particularly Java, Sumatra, and Kalimantan, resulting in a 24.5% national production drop. Regional patterns vary: Maluku and Papua show increased productive trees during La Niña and higher productivity during El Niño, while Bali and Nusa Tenggara experience increased productivity in both El Niño and La Niña years. Spatial analysis confirms La Niña's widespread negative impact and El Niño's more localized yet potentially beneficial effects.

Mangosteen requires a dry period to induce flowering (Lu & Chacko, 2000; Ounlert et al., 2017; Salakpetch & Nagao, 2006) . Water stress can trigger flowering by altering the hormonal balance within the plant, such as changes in gibberellin, cytokinin, and abscisic acid (ABA) levels, as well as an increase in the carbon-to-nitrogen ratio in the shoots. Water stress suppresses vegetative growth, and an adequate dry period stimulates floral induction (Anisworth, 2006). Rainfall for optimal growth totals 1,500–2,500 mm per year, with 7–10 wet months (rainfall >100 mm/month) and 2–4 dry months (rainfall <50 mm/month) (Nuraini et al., 2022)

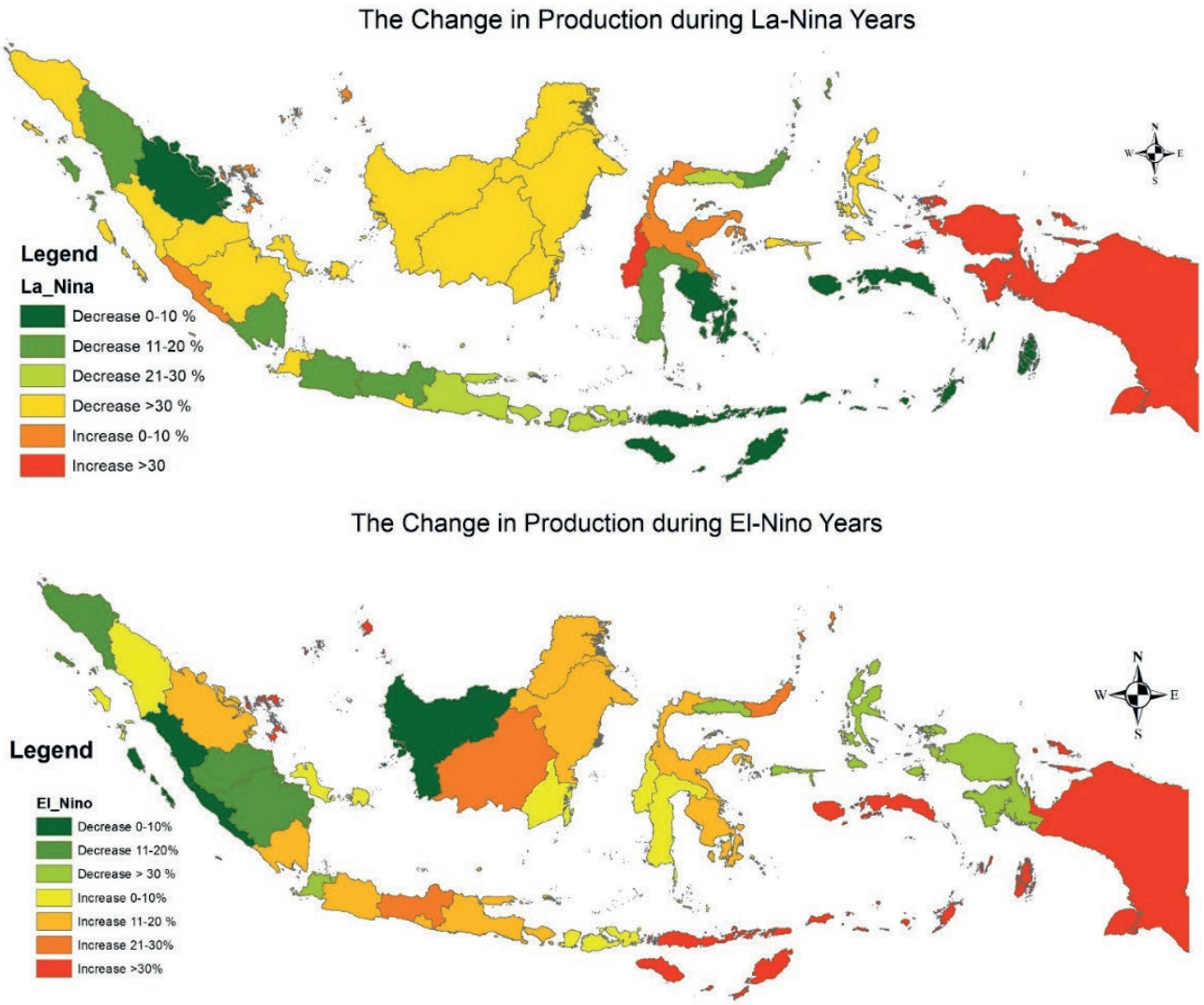

Figure 4. Map of change of mangosteen production during La-Nina (top) and El-Nino (bottom).

Insufficient dry periods caused by high rainfall intensity, such as during La Niña events disrupt the flowering induction process. This disruption is one of the main factors contributing to the decline in the number of harvested plants of mangosteen during La Niña years. This finding is consistent with field research conducted by (Nidyasari et al., 2018), which reported that mangosteen trees failed to flower and produce fruit due to excessive rainfall, reaching 301–400 mm/month. A decrease in rainfall and a delayed onset of the rainy season disrupts production. During El Niño years, the dry period is sufficiently long to induce flowering, which leads to a higher number of harvested plants compared to neutral years.

A different pattern is observed in Maluku and Papua, where the number of harvested plants is higher during La Niña years compared to El Niño years. This can be explained by the fact that Maluku has a rainfall pattern that is the opposite of the general rainfall pattern in most parts of Indonesia (Aldrian and Susanto, 2003). Meanwhile, in Sumatra, the number of harvested plants during El Niño years is lower than in neutral years, possibly because rainfall in this region is influenced not only by ENSO but also by the IOD (Nur'utami & Hidayat, 2016))

During both El Niño and La Niña years, a decline in yield occurred across all major mangosteen-producing regions, such as Sumatra and Java. The same pattern was also observed in Kalimantan, Maluku, and Papua. In El Niño years, although the number of harvested plants was higher compared to neutral years, the continuous decrease in rainfall disrupted flowering and

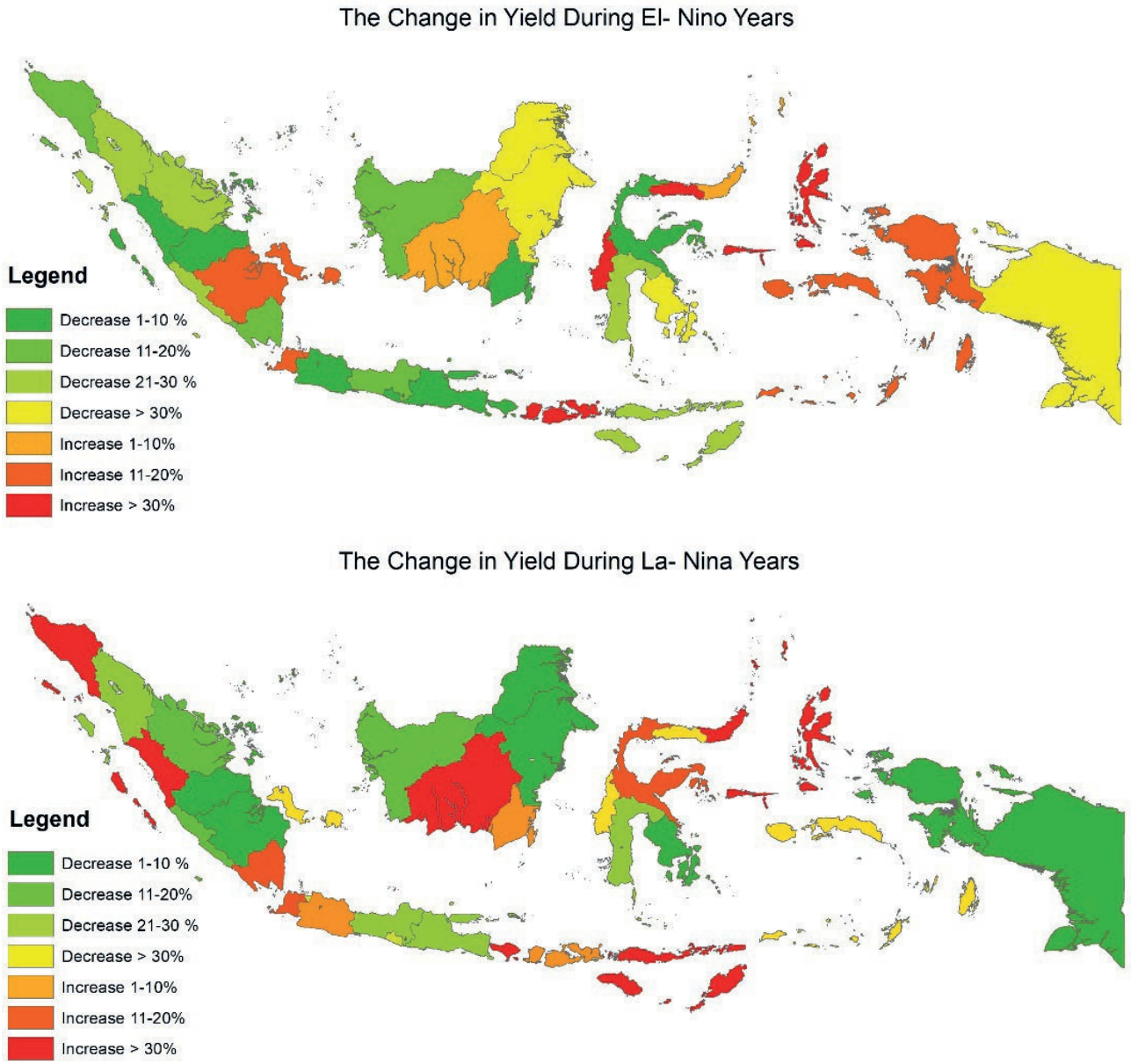

Figure 5. Map of change Mangosteen yield during La Niña and El Niño years.

fruit development. After flower formation, adequate irrigation is needed to ensure that the flowers develop into fruit. Since rainfall during El Niño years is lower than normal, Water scarcity due to drought can significantly impede the physiological processes involved in fruit growth and development, resulting in reduced fruit size and diminished yield. This is consistent with the findings of Jaroensutitas Asinee (2023) and Salakpetch et al. (2006), which showed that off-season mangosteen fruits, developing under warmer and drier conditions, had less developed pericarps, resulting in significantly lower fresh weight and smaller fruit size. Off-season trees also produced fewer flowers and fruits per branch, indicating limited resources for fruit development and leading to smaller fruits, fewer blossoms, and increased fruit drop.

In La Niña years, the decline in production was due not only to the lower number of harvested plants caused by the lack of dry stress but also to the high rainfall, which can lead to flower and fruit drop, thereby affecting mangosteen yields. Furthermore, mangosteen is a plant that does not tolerate waterlogging. The roots of the mangosteen plant lack root hairs, which are crucial

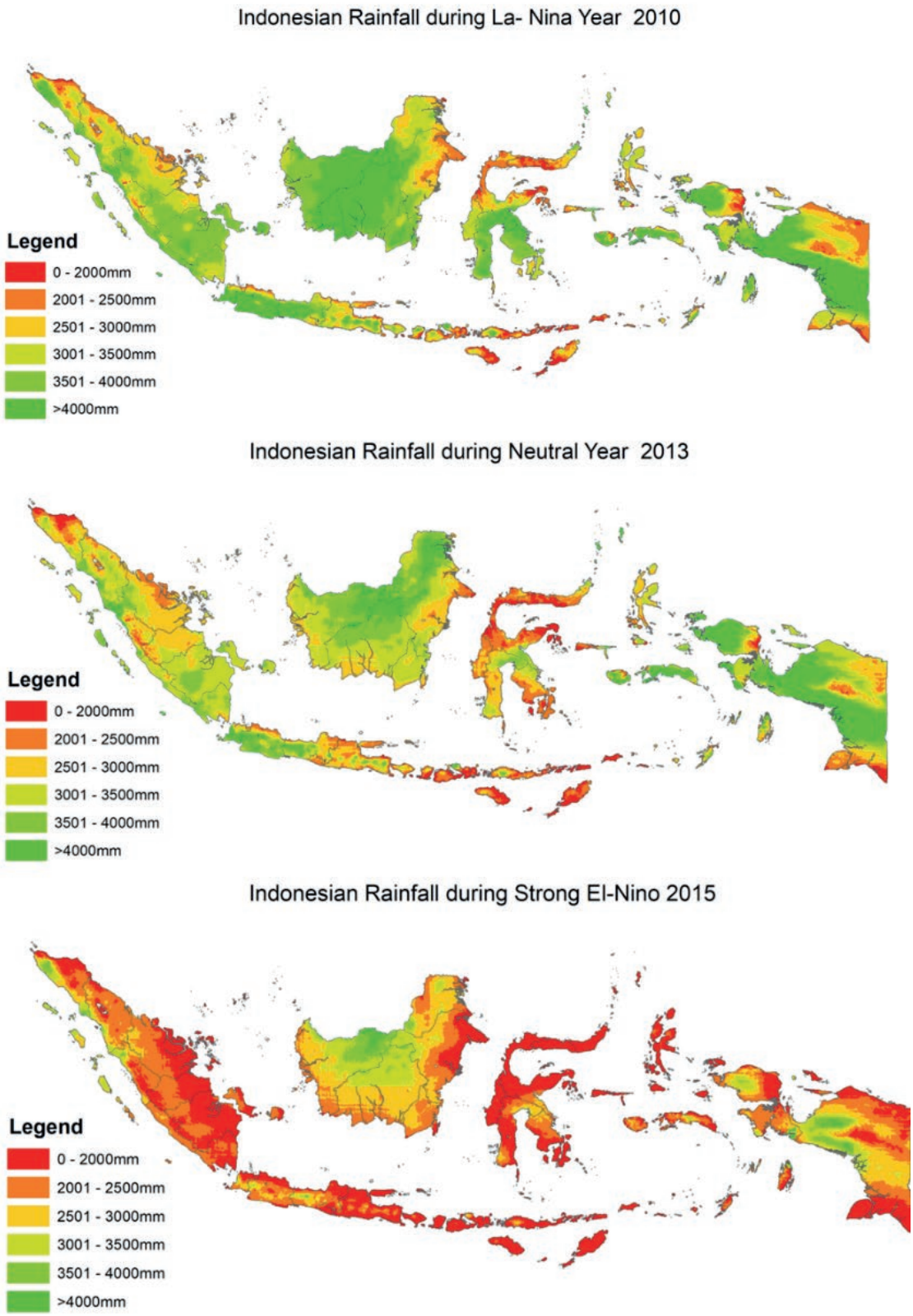

Figure 6. Indonesian Rainfall during El Niño(2015), Neutral (2013) and La-Niña (2010) (DataSource : CHIRSP data: https://data.chc.ucsb.edu/products/CHIRPS-2.0/)

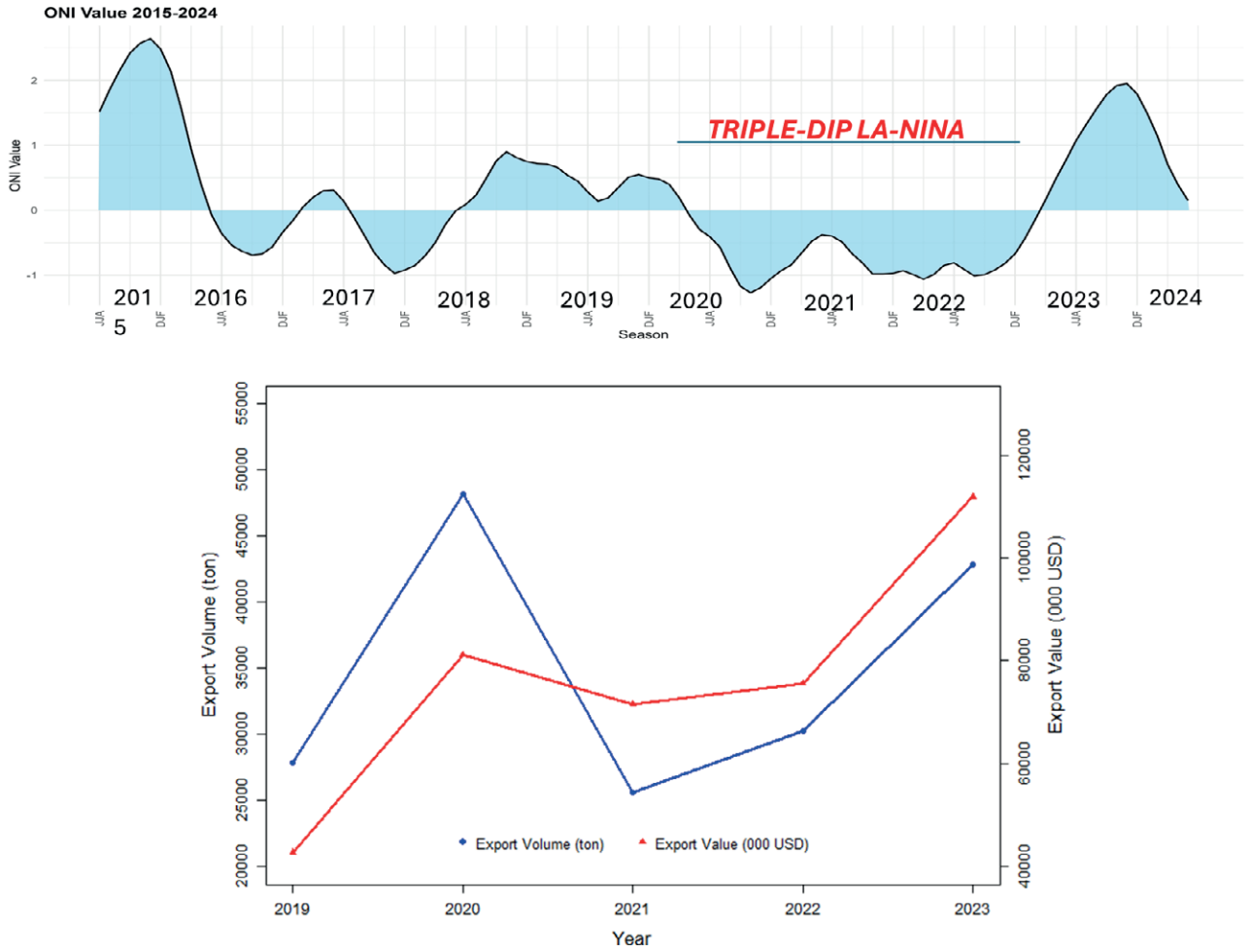

Figure 7. Export volume and value of Manggosteen fo 2019- 2023 (source : Ministry of Agriculture Republic Indonesia, 2024) and NOAA, 2025).

for efficient absorption of water and nutrients. Additionally, the plant exhibits a low photosynthetic rate and a slow rate of cell division at the shoot meristem (Wiebel et al., 1992). These physiological limitations make mangosteen highly sensitive to environmental stress. Consequently, both drought and excess water can severely hinder its growth and reduce fruit production.

Mangosteen Yield in the Bali and Nusa Tenggara regions shows a different pattern compared to other areas, where yield during neutral years is lower than in El Niño and La Niña years. Bali and Nusa Tenggara have relatively low rainfall compared to other regions in Indonesia. The climate types in West Nusa Tenggara (NTB) and East Nusa Tenggara (NTT) include C3, D3, D4, and E4 (Oldeman et al., 1980; Susanti et al., 2021; Tasiyah et al., 2024). During La Niña years, increased rainfall may contribute to higher yield. Meanwhile, the rise in yield during El Niño years is likely since the decrease in rainfall does not occur during the flowering and fruit development stages. However, this hypothesis requires further investigation using more detailed data.

The changes in total mangosteen production shown in Figure 3 indicate that during La Niña years, there was a significant decline in production, especially in key mangosteen-producing regions such as Sumatra and Java. During El Niño years, production increased despite lower yield compared to neutral years, due to a higher number of harvested plants in those years. However, the increase during El Niño was lower than the decrease during La Niña. According to the Directorate of Horticultural (2025), in 2010 when Indonesia's climate was disrupted by a moderate intensity La Niña, the production of vegetables and fruits was severely affected, leading to shortages that triggered price hikes. Fruit production declined by 35–75%, while vegetable production fell to only 20–25% of normal levels.

The impact of reduced mangosteen production in key producing areas disrupts the supply needed to meet market demand. This impact can be seen, for example, in the sharp decline in Indonesia's mangosteen export volume in 2021 and 2022 because of the Triple Dip La Niña, a rare climatic phenomenon characterized by the continuation or recurrence of La Niña conditions over three successive years, which lasted from mid-2020 to early 2023 (Figure 7). The export volume in 2021 declined by nearly 50% compared to that in 2020. This clearly demonstrates that ENSO had a significant economic impact on the mangosteen trade system in Indonesia.

The results of this study suggest that the ENSO index at moderate to strong intensities can serve as an early warning tool for policymakers in developing preventive measures for mangosteen cultivation management. ENSO forecasts issued by various global climate research institutions can be used as essential references for cultivation planning. Several adaptive measures can be considered, including the provision of irrigation systems during El Niño years to mitigate drought risks, and the construction of adequate drainage systems during La Niña years to prevent excessive water accumulation that could damage crops. In addition, it is important to develop technologies that allow artificial drought stress induction during wetter years, enabling flower initiation to still occur. During high rainfall La Niña years, the application of hormones or enzymes that strengthen flowers and fruits is also necessary to prevent drop caused by extreme weather conditions. For instance, (Lerslerwong et al., 2013) can extend harvest period by chemical control.

CONCLUSIONS

ENSO has been shown to significantly affect rainfall patterns in Indonesia. El Niño events are associated with reduced rainfall, while La Niña events tend to increase rainfall across the region. ENSO influences the dynamics of mangosteen production In Indonesia.The number of harvested plant decreases during La Niña years and increases during El Niño years in most regions of Indonesia except Sumatera. In general, productivity during both El Niño and La Niña years is lower compared to neutral years except Bali- Nusa Tenggara and Maluku-Papua. Annual total production tends to increase during El Niño years and decrease during La Niña years, with the decline in production during La Niña being greater than that during El Niño.

REFERENCES

Aizat, W. M., Jamil, I. N., Ahmad-Hashim, F. H., & Noor, N. M. (2019). Recent updates on metabolite composition and medicinal benefits of mangosteen plant. *PeerJ*, *7*. https://doi.org/10.7717/peerj.6324

Aldrian, E., & Susanto, D. R. (2003). Identification of three dominant rainfall regions within Indonesia and their relationship to sea surface temperature. *International Journal of Climatology*, *23*(12), 1435–1452.

Alhadid, at, & Budi Nugroho, A. (2024). The Study of Triple-Dip La Nina Phenomenon (2020-2023) and Its Impact on Atmospheric Dynamics and Rainfall in The Indonesian Region. *Science and Education*, *3*, 707–716. https://cds.climate.copernicus.eu.

Anisworth, C. (2006). *Flowering and its Manipulation* (J. Roberts, D. Evans, Imaseki, & J. K. C. Rose, Eds.). Blackwell Publishing.

Ansori, A. N. M., Fadholly, A., Hayaza, S., Susilo, R. J. K., Inayatillah, B., Winarni, D., & Husen, S. A. (2020). A review on medicinal properties of mangosteen (Garcinia mangostana L.). *Research Journal of Pharmacy and Technology*, *13*(2), 974–982. https://doi.org/10.5958/0974-360X.2020.00182.1

Ansori, A. N. M., Kharisma, V. D., Parikesit, A. A., Dian, F. A., Probojati, R. T., Rebezov, M., Scherbakov, P., Burkov, P., Zhdanova, G., Mikhalev, A., Antonius, Y., Pratama, M. R. F., Sumantri, N. I., Sucipto, T. H., & Zainul, R. (2022). Bioactive Compounds from Mangosteen (Garcinia mangostana L.) as an Antiviral Agent via Dual Inhibitor Mechanism against SARS-CoV-2: An In Silico Approach. *Pharmacognosy Journal*, *14*(1), 85–90. https://doi.org/10.5530/pj.2022.14.12

Apiratikorn, S., Sdoodee, S., Lerslerwong, L., & Rongsawat, S. (2012). The impact of climatic variability on phenological change, yield and fruit quality of mangosteen in Phatthalung province, southern Thailand. *Kasetsart Journal - Natural Science*, *46*(1), 1–9.

Apiratikorn, S., Sdoodee, S., & Limsakul, A. (2014). Climate-related changes in tropical-fruit flowering phases in Songkhla province, Southern Thailand. *Research Journal of Applied Sciences, Engineering and Technology*, *7*(15), 3150–3158. https://doi.org/10.19026/rjaset.7.654

Arrigo, R. D., & Wilson, R. (2008). El nino and indian ocean influences on Indonesian drought :implication for forecasting rainfall and crop productivity. *International Journal of Climatology*, *28*, 611–616. https://doi.org/10.1002/joc

Chen, Z., Li, L., Wang, B., Fan, J., Lu, T., & Lv, K. (2024). The impact of global warming on ENSO

from the perspective of objective signals. *Atmospheric Research*, *299*. https://doi.org/10.1016/j.atmosres.2023.107176

Cirino, P. H., Féres, J. G., Braga, M. J., & Reis, E. (2015). Assessing the impacts of ENSO-related weather effects on the Brazilian agriculture. *Procedia Economics and Finance*, *24*(15), 146–155. https://doi.org/10.1016/S2212-5671(15)00635-8

Cobon, D. H., Ewai, M., Inape, K., & Bourke, R. M. (2016). Food shortages are associated with droughts, floods, frosts and ENSO in Papua New Guinea. *AGSY*, *145*, 150–164. https://doi.org/10.1016/j.agsy.2016.02.012

Directorate General of Horticulture. 2025. Sekolah Lapang Iklim Hortikultura Antisipasi Dampak Perubahan Iklim. Tabloid Sinar Tani. https://tabloidsinartani.com/detail/indeks/komoditi/2691-sekolah-lapang-iklim-hortikultura---antisipasi-dampak-perubahan-iklim (May 2025)

Directorate General of Horticulture. (2021). *Buku Lapang Budidaya Manggis (Field Guide to Mangosteen Cultivation)*. Directorate General of Horticulture.

El Ramija, K., Sudrajat, A., Irwandi, H., & Ariantono, J. Y. (2021). Influence of El Niño 2015/2016 on Climate Variability and Production of Main Crops in Langkat Regency. *Agromet*, *35*(2), 98–107. https://doi.org/10.29244/j.agromet.35.2.98-107

Endah Ardhi Ningrum Abdullah, S., Klimatologi Kelas Jawa Tengah, S. I., & Siliwangi, J. (n.d.). *Dampak dan Tingkat Resiko La Nina Terhadap Penambahan Curah Hujan di Jawa Tengah (The Impact and Risk Levels of La Nina on Increasing Rainfall IN Central Jawa)*. *15*(1), 1–7. https://doi.org/10.46824/megasains.8e9xwd36

Harahap, W. N., Yuniasih, B., & Gunawan, S. (2023). Dampak La Nina 2021-2022 terhadap Peningkatan Curah Hujan. *AGROISTA : Jurnal Agroteknologi*, *7*(1), 26–32. https://doi.org/10.55180/agi.v7i1.364

Hendrawan, I. G., Asai, K., Triwahyuni, A., & Lestari, D. V. (2019). The interanual rainfall variability in Indonesia corresponding to El Niño Southern Oscillation and Indian Ocean Dipole. *Acta Oceanologica Sinica*, *38*(7), 57–66. https://doi.org/10.1007/s13131-019-1457-1

Hidayat, R., & Ando, K. (2018). Rainfall Variability Over Indonesia and Its Relation to ENSO/IOD: Estimated Using Jra-25/Jcdas. *Agromet*, *28*(1), 1. https://doi.org/10.29244/j.agromet.28.1.1-8

Hidayat, R., Juniarti, M. D., & Ma'Rufah, U. (2018). Impact of la Niña and la Niña Modoki on Indonesia rainfall variability. *IOP Conference Series: Earth and Environmental Science*, *149*(1). https://doi.org/10.1088/1755-1315/149/1/012046

Hidayati, R., & Chrisendo, D. N. (2010). Prediction Of Planting Date And Growing Period Using Sea Surface Temperature (Sst) Anomalies In Nino 3.4 For Indramayu District. *J.Agromet*, *24*(2), 1–8. http://journal.ipb.ac.id/index.php/agromet

Iskandar, I., Lestrai, D. O., & Nur, M. (2019). Impact of El Niño and El Niño Modoki Events on Indonesian Rainfall. *Makara Journal of Science*, *23*(4), 217–222. https://doi.org/10.7454/mss.v23i4.11517

Jaroensutasinee, K., Jaroensutasinee, M., & Boonsanong, P. (2023a). Climatic Factor Differences and Mangosteen Fruit Quality between On-and Off-Season Productions. *Emerging Science Journal*, *7*(2), 578–588. https://doi.org/10.28991/ESJ-2023-07-02-020

Jaroensutasinee, K., Jaroensutasinee, M., & Boonsanong, P. (2023b). Climatic Factor Differences and Mangosteen Fruit Quality between On-and Off-Season Productions. *Emerging Science Journal*, *7*(2), 578–588. https://doi.org/10.28991/ESJ-2023-07-02-020

Kalick, L. S., Khan, H. A., Maung, E., Baez, Y., Atkinson, A. N., Wallace, C. E., Day, F., Delgadillo, B. E., Mondal, A., Watanapokasin, R., Barbalho, S. M., & Bishayee, A. (2023). Mangosteen for malignancy prevention and intervention: Current evidence, molecular mechanisms, and future perspectives. *Pharmacological Research*, *188*. https://doi.org/10.1016/j.phrs.2022.106630

Karuniasa, M., & Pambudi, P. A. (2022). The analysis of the El Niño phenomenon in the East Nusa Tenggara Province, Indonesia. *Journal of Water and Land Development*, *52*, 180–185. https://doi.org/10.24425/jwld.2022.140388

Leng, G., Zhang, X., Huang, M., Asrar, G. R., & Leung, L. R. (2016). The role of climate covariability on crop yields in the conterminous United States. *Nature*, *6*(September), 1–11. https://doi.org/10.1038/srep33160

Lerslerwong, L., Rugkong, A., Imsabai, W., & Ketsa, S. (2013). The harvest period of mangosteen fruit can be extended by chemical control of ripening-A proof of concept study. *Scientia Horticulturae*, *157*, 13–18. https://doi.org/10.1016/j.scienta.2013.03.027

Lu, P., & Chacko, E. K. (2000). Effect of water stress on mango flowering in low latitude tropics of Northern Australia. *Acta Horticulturae*, *509*, 283–289. https://doi.org/10.17660/actahortic.2000.509.31

Mansyah, E. (2009). Pengaruh curah hujan terhadap getah kuning pada buah manggis (Garcinia angostana L.) (The effect of rain fall on gamboge disorder of mangosteen fruit (Garcinia mangostana L.). In A. D. Susila, D. Winarso, & Poerwanto R (Eds.), *Seminar Ilmiah Perhimpunan Hortikultura Indones1a.*

(pp. 594–600). https://www.researchgate.net/publication/288834736

Mansyah, E., Muas, I., Jawal A.S, M., & Affandi. (2013). The Research for Supporting Sustainable Mangosteen (Garcinia mangostana L.) Production. *International Journal on Advanced Science, Engineering and Information Technology*, *3*(1), 16–22. https://doi.org/10.18517/ijaseit.3.1.269

Ministry of Agriculture. (2024). *Statistik Pertanian 2024 (Agricultural Statistics 2024)*. Center for Agricultural Data and Information System Ministry of Agriculture.

Mulyana, E. (2002). Pengaruh dipole mode terhadap curah hujan di Indonesia. *Jurnal Sains & Teknologi Modifikasi Cuaca*, *3*(1), 39–43.

Nauman, M. C., & Johnson, J. J. (2022). The purple mangosteen (Garcinia mangostana): Defining the anticancer potential of selected xanthones. *Pharmacological Research*, *175*. https://doi.org/10.1016/j.phrs.2021.106032

Nidyasari, R. S., Akmal, H., & Sri Ariyanti, N. (2018). Karakterisasi Morfologi dan Anatomi Tanaman Manggis dan Kerabatnya (Garcinia spp.) di Taman Buah (Mekarsari Morphological and Anatomical Characterization of Mangosteen Plants and Its Relatives (Garcinia spp.) in Mekarsari Fruit Garden). *Jurnal Sumber Daya Hayati*, *4*(1), 12–20. http://biologi.ipb.ac.id/jurnal/index.php/jsdhayati

Nugraheni, M., Zakaria, A., Wahono, E. P., Kusumastuti, D. I., & Herison, A. (2024a). Rainfall Patterns in Indonesian Provinces During El-Nino and La-Nina: FFT and Lomb Periodogram Analysis. *MEDIA KOMUNIKASI TEKNIK SIPIL*, *30*(2), 157–165. https://doi.org/10.14710/mkts.v30i2.65646

Nugraheni, M., Zakaria, A., Wahono, E. P., Kusumastuti, D. I., & Herison, A. (2024b). Rainfall Patterns in Indonesian Provinces During El-Nino and La-Nina: FFT and Lomb Periodogram Analysis. *MEDIA KOMUNIKASI TEKNIK SIPIL*, *30*(2), 157–165. https://doi.org/10.14710/mkts.v30i2.65646

Nuraini, F., Fajarsari, I. M., Rosita, D., & Cahyani, E. N. (2022). *Profil Manggis Mendukung Ekspor*. Kementerian Pertanian.

Nur'utami, M. N., & Hidayat, R. (2016). Influences of IOD and ENSO to Indonesian Rainfall Variability: Role of Atmosphere-ocean Interaction in the Indopacific Sector. *Procedia Environmental Sciences*, *33*, 196–203. https://doi.org/10.1016/j.proenv.2016.03.070

Oldeman, L. R., Las, I., & Muladi. (1980). *The Agroclimatic Maps of Kalimantan, Maluku, Irian Jaya and Bali, West and East Nusa Tenggara* (Vol. 60). Central Research Institute for Agriculture.

Ounlert, P., Sdoodee, S., & Tongkhow, P. (2017). *The mangosteen flowering date model in Nakhon Si Thammarat province, southern Thailand*. *18*(1), 176–184. https://doi.org/10.5513/JCEA01/18.1.1876

Ovalle-Magallanes, B., Eugenio-Pérez, D., & Pedraza-Chaverri, J. (2017). Medicinal properties of mangosteen (Garcinia mangostana L.): A comprehensive update. In *Food and Chemical Toxicology* (Vol. 109, pp. 102–122). Elsevier Ltd. https://doi.org/10.1016/j.fct.2017.08.021

Raju, C., Pazhanivelan, S., Perianadar, I. V., Kaliaperumal, R., Sathyamoorthy, N. K., & Sendhilvel, V. (2024). Climate Change as an Existential Threat to Tropical Fruit Crop Production; a Review. In *Agriculture (Switzerland)* (Vol. 14, Issue 11). Multidisciplinary Digital Publishing Institute (MDPI). https://doi.org/10.3390/agriculture14112018

Ramirez-rodrigues, M. A., Asseng, S., Fraisse, C., Stefanova, L., & Eisenkolbi, A. (2014). Climate risk management tailoring wheat management to ENSO phases for increased wheat production in Paraguay. *Climate Risk Management*, *3*, 24–38. https://doi.org/10.1016/j.crm.2014.06.001

Ray, D. K., Gerber, J. S., Macdonald, G. K., & West, P. C. (2015). Climate variation explains a third of global crop yield variability. *Nature Communications*, *6*, 1–9. https://doi.org/10.1038/ncomms6989

Salakpetch, S., & Nagao, M. A. (2006). *Soil Moisture Stress and Irrigation Management Promote Mangosteen (Garcinia mangostana L.) Flowering*.

Sarvina, Y., & Sari, K. (2018). Dampak ENSO Terhadap Produksi dan Puncak Panen Durian di Indonesia (ENSO Impacts on Production and Peak Harvest Season of Durian in Indonesia). *Dampak ENSO Terhadap Produksi Dan Puncak Panen Durian Di Indonesia (ENSO Impacts on Production and Peak Harvest Season of Durian in Indonesia)*, *41*(2), 149–158. https://doi.org/10.2017/jti.v41i2.7829

Sayruamyat, S., Praneetvatakul, S., Vijitsrikamol, K., Potchanasin, C., Thamthanakoon, N., & Pananurak, P. (2021). Orchardists' Needs for the Development of Technology and Innovation Lecturer, Department of Agricultural and Resource Economics 2*. *Journal of Business, Economics and Communications*, *17*(1), 136–151.

Sidauruk, M., Juni Risma Saragih, H., Tri Utomo, S., & Widodo, P. (2023). Rainfall Variability In East Kalimantan From Impact Of El Nino And La Nina To Effort Disaster Prevention To Support National Security. *International Journal of Progressive Sciences and Technologies (IJPSAT*, *38*(2), 431–440. https://origin.cpc.ncep.noaa.gov

Supari, Tangang, F., Salimun, E., Aldrian, E., Sopaheluwakan, A., & Juneng, L. (2018). ENSO modulation of seasonal rainfall and extremes in Indonesia. *Climate Dynamics*, *51*(7–8), 2559–2580. https://doi.org/10.1007/s00382-017-4028-8

Surmaini, E., Hadi, T. W., Subagyono, K., & Puspito, N. T. (2015). Early detection of drought impact on rice paddies in Indonesia by means of Niño 3.4 index. *Theoretical and Applied Climatology*, *121*(3–4), 669–684. https://doi.org/10.1007/s00704-014-1258-0

Susanti, E., Surmaini, E., Pramudia, A., Heryani, N., Estiningtyas, W., Suciantini, S., & Apriyana, Y. (2021). Pemutakhiran Peta Sumberdaya Agroklimat Indonesia untuk Mendukung Perencanaan Pertanian. *Jurnal Tanah Dan Iklim*, *45*(1), 47. https://doi.org/10.21082/jti.v45n1.2021.47-58

Tasiyah, L. A., Sutriono, R., & Silawibawa, I. P. (2024). Analisis Tipe iklim Berdasarkan Curah Hujan Pada Beberapa Kecamatan di Kabupaten Lombok Barat. *Journal of Soil Quality and Management 1*(1), 67–72. https://jsqm.unram.ac.id/index.php/jsqm/article/view/169

Tengsetasak, P., Tongkoom, K., Yomkerd, J., Susawaengsup, C., Khongdee, N., Chatsungnoen, T., Dangtungee, R., & Bhuyar, P. (2024). Sustainable Strategies for Fresh Mangosteen: Adapting to Climate Challenges. In *Earth Systems and Environment*. Springer Science and Business Media Deutschland GmbH. https://doi.org/10.1007/s41748-024-00512-y

Wiebel, J., Downton, W. J. S., & Chacko, E. K. (1992). Influence of applied plant growth regulators on bud dormancy and growth of mangosteen (*Garcinia mangostana L.*). In *Scientia Horticulturae* (Vol. 52).

Xie, X., Huang, P., Zhou, S., & Zhang, J. (2022). Changes in ENSO-driven Hadley circulation variability under global warming. *Atmospheric Research*, *274*. https://doi.org/10.1016/j.atmosres.2022.106220

Italian Journal of Agrometeorology
Rivista Italiana di Agrometeorologia

Firenze University Press
https://riviste.fupress.net/index.php/IJAm

OPEN ACCESS

Citation: Muter, S. A., Al-Jiboori, M. H., & Al-Timimi, Y. K. (2025). An assessment of the correlation between rainfall and the Normalized Difference Vegetation Index (NDVI) over Iraq. *Italian Journal of Agrometeorology* (2): 79-94. doi: 10.36253/ijam-3069

Received: November 2, 2024

Accepted: July 18, 2025

Published: December 31, 2025

Data Availability Statement: All relevant data are within the paper and its Supporting Information files.

Competing Interests: The Author(s) declare(s) no conflict of interest.

ORCID:
SAM: 0000-0002-6728-9609
MHA-J: 0000-0002-0816-3918
YKA-T: 0000-0002-3902-8719

An assessment of the correlation between rainfall and the Normalized Difference Vegetation Index (NDVI) over Iraq

Sara Ali Muter*, Monim H. Al-Jiboori, Yaseen K. Al-Timimi

Department of Atmospheric Sciences, College of Science, Mustansiriyah University, Baghdad, Iraq
*Corresponding author. E-mail: sara.a.atmsc@uomustansiriyah.edu.iq

Abstract. The Normalized Difference Vegetation Index (NDVI) is one of the earliest spectral indices developed to monitor vegetation dynamics and assess changes over time. Climatic conditions, particularly rainfall, play a significant role in shaping the distribution and density of vegetation, especially in urban and semi-arid environments. The study aims to use remote sensing techniques to find out how dense vegetation cover is in Iraq, how it has changed over time, and how NDVI and rainfall are related. We applied the NDVI to 264 monthly satellite photos from NASA's MODIS sensor, captured between 2000 and 2021. The study looked at changes in NDVI and rainfall data over the same period to find trends in the two variables throughout space and time. The results showed that vegetation cover changed a lot over the years of the study. Climate variables, especially rainfall, directly affected whether vegetation grew or shrank. There was a modest positive link between NDVI and rainfall, with a correlation coefficient 0.5. This means that more rain usually means more vegetation growth and activity. The data also showed that the NDVI values were greater in the northern and eastern Iraq than in the southern and western parts. This was because the north has many mountains and a fairly humid climate. Over time, the vegetation in the central region slowly decreased because of urban growth and less rain. These findings show how important it is to combine NDVI and rainfall data for effective management of land and water resources and to find locations with more potential for farming.

Keywords: rainfall, vegetation, NDVI, MODIS, temporal and spatial analysis, Iraq.

HIGHLIGHTS

1. NDVI was analyzed to assess vegetation dynamics in Iraq from 2000 to 2021 using 264 MODIS satellite images.
2. The study reveals a clear relationship between rainfall and vegetation density, with a correlation coefficient of 0.5.
3. Changes in vegetation cover correspond to climatic variations, showing greater density in the northern and eastern regions.
4. NDVI has increased slightly over the years, suggesting improved vegetation or changing land use patterns.

5. The results help identify areas suitable for agriculture and water resource management.

1. INTRODUCTION

Vegetation cover is a key component of ecosystems, reflecting the land's health and response to climatic conditions, particularly rainfall. Because of this, it can impact health, the environment, and the economy. Because of this, scientists keep an eye on plant life all around the world (Zheng, 2021). NASA satellites have been making maps of Earth's land surfaces since 2000. These maps show the amount of vegetation on the land. These satellites always go around the Earth, collecting information about the oceans, the air, and the land (Mustafa, 2020). The satellites can also watch what living things do. Satellite images are useful when available to anyone who wants to look at them (Deagan et al., 2023).

NASA Earth Observations (NEO) aims to provide accessibility to global satellite imagery. This will let anyone study and download data from NASA's Earth Observation System satellites (Almamalachy et al., 2020). There are more than 50 different worldwide datasets that give daily, weekly, and monthly snapshots in a variety of formats (Helali et al., 2022). The loss of vegetation cover in Iraq is a major environmental problem caused by things like drought, too much grazing, and the growth of cities (Guo et al., 2021). Also, when plants die, the soil becomes weaker and more likely to be eroded by wind, which makes dust storms more likely to happen. These events make the air quality worse and put people's health at risk (Naif et al., 2020). The association between the Normalised Difference Vegetation Index (NDVI) and rainfall is very similar to how the seasons and weather fluctuate in the area (Jaber et al., 2020). Rain is a big reason why plants flourish, especially in areas that are semi-arid or desert. Rainfall makes more water accessible in the soil, which helps plants develop faster. The greater NDVI value shows that the plants are growing. Because Iraq has a semi-arid and arid environment, its agricultural areas depend a lot on rain that falls every year (Al-Hasn, 2024).

Many studies have been written about how NDVI changes over time and how it relates to rainfall. For example, Al-Hasn (2024) looked at the link between rainfall and NDVI in Syria from 2012 to 2022 and found a good correlation of R=0.7. Naif et al. (2020) used Landsat satellite pictures to map the NDVI in Baghdad twice a year from 2008 to 2013 and again in 2019. The study looked at how NDVI changed during the growing seasons in connection to two weather conditions: air temperature and rain. The results showed a substantial link between the NDVI-based patterns of plant development and the climate data collected throughout the current growing seasons. Muhammad and Hassoun (2023) used NDVI data from 1992 to 1999 to compare rainfall in Sulaymaniyah and how it affected plant cover. Their research showed that the most rain in 1992 (5 mm) helped plants expand, whereas the least rain in 1999 (4 mm) made plants cover less ground.

Al-Daoudi and Al-Timimi (2024) used NDVI data from MODIS to examine how Iraq's plant cover changed between 2000 and 2023. The study examined important years (2004, 2009, 2014, 2019, and 2023) and compared them to the baseline year of 2000. The results showed that April 2019 had the most vegetation, with 51.2%, while 2000 had 14.5%. The lowest coverage occurred in 2009, with only 14% of the area covered. Hatem et al. (2024) investigated the impact of drought on Iraq's vegetation from 2000 to 2022, using remote sensing (RS) using the NDVI index. The analysis identified 2000, 2008, 2009, 2010, 2012, and 2022 as the years most affected by drought. Landsat images revealed the lowest vegetation percentages in 2000, 2008, 2009, and 2010, with values of 3.35, 4.98, 5.40, and 5.11%, respectively. Similarly, MODIS data indicated the lowest vegetation cover percentages 11.12, 11.26, 12.58, 13.02, and 14.44% in years 2008, 2000, 2009, 2012, and 2022, respectively. Al Rukabie et al. (2024) examined the influence of monthly precipitation on surface water area, vegetation area (represented by the Normalized Difference Vegetation Index, NDVI), and potential evapotranspiration across two years (2018 and 2021) in Baghdad, Iraq. The Thornthwaite aridity index was employed to evaluate annual aridity and categorize the climate during these years. In 2021, a lack of precipitation resulted in no discernible link in arid climates, whereas in 2018, semi-arid climates had a positive non-linear correlation between precipitation and MNDWI and NDVI areas, alongside a negative correlation with PET.

The research problem focuses on examining the correlation between vegetation cover density and rainfall fluctuations in the region from 2000 to 2021. Utilizing RS and geographic information systems (GIS), this paper aims to quantify the strength of this relationship. Given the study area's temporal and spatial variability in rainfall, understanding this connection is crucial for assessing the effect of rainfall on vegetation cover density and its subsequent changes. This study highlights the crucial importance of RS, especially the NDVI, as an effective tool for early warning systems related to agricultural drought.

2. MATERIALS AND METHODS

2.1. Study area

The Republic of Iraq is the area of study. It is in the southwestern part of Asia. It is located in the northern hemisphere's subtropical latitudes, when summer temperatures are very high (Abdulkareem and Nemah, 2021). The country is between 29.5° and 37.5°N and 38.45° and 48.45°E of the Greenwich Meridian (Al-Lami et al., 2023). Iraq covers a surface area of 435,052 km² and has a coastline stretching 58 km. The country's climate and thermal characteristics are significantly influenced by its primary bodies of water, the Arabian Gulf and the Mediterranean Sea (Muter, 2024). It shares direct land borders with six neighbouring countries: Iran, Jordan, Kuwait, Saudi Arabia, Syria, and Turkey (Nassif et al., 2024) (see Fig. 1). Iraq has a Mediterranean climate, ranging from semi-arid (highlands) to arid (lowlands), with dry and hot summers and cool winters (Abdul Jabbar and Abdulkareem, 2021). Iraq experiences a continental subtropical climate characterized by four distinct seasons. The average annual temperature is 0°C in winter and 51°C in summer (Gaznayee et al., 2022). Rainfall falls seasonally from November to May, with an average annual rainfall of 150 mm in the south and 900 mm in the northeast. According to (Kadhum et al. 2022), the average wind speed in the research area was 3.6 m/s. The amount of vegetation in Iraq changes from the northern mountainous parts to the centre and southern areas, which have less vegetation. This change has an impact on the country's biological variety and farming systems (Mzuri et al., 2021).

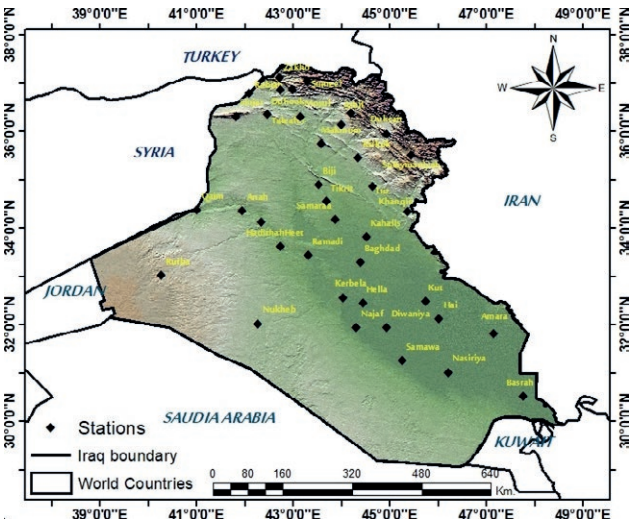

Figure 1. Study area and spatial distribution of meteorological stations. (Muter et al., 2024).

2.2. Data sources

2.2.1. Ground stations

Monthly rainfall data for the period 2000-2021, obtained from the Iraq Meteorological and Seismological Organization (IMOS), were used to determine the average rainfall covering 38 rainfall stations in the study area. The details of these stations by geographical coordinates are presented in Table 1.

2.2.2. Satellite images

Satellite data were used to identify the NDVI values and the spatial distribution of vegetation cover during the study period using ArcMap 10.4.1 software. NASA's Earth satellite used MODIS (Land/Aqua) satellite data to make NDVI images for the years 2000 to 2021. For this study, 264 monthly satellite images were downloaded and analyzed, with 22 images covering the entire study area used for each year of the study period. The study examined the temporal and spatial variations of the NDVI index and its responses to rainfall, using satellite observation from the last two decades in Iraq. The use of MODIS NDVI data instead of higher-resolution alternatives can be justified based on several factors. MODIS provides continuous NDVI data from 2000 to the present, with regular updates. MODIS with spatial resolution (500 m or 1 km) is suitable for large-scale regional studies. If the purpose of the study is to analyze general trends and large-scale changes in a country such as Iraq, MODIS resolution is sufficient and less complex to manage. MODIS data is small, making it faster and easier to analyze. MODIS provides composite data that reduces the effect of clouds. In arid or semi-arid regions, such as Iraq, where seasonal clouds can occur, MODIS data may be more appropriate.

2.3. Methodology

2.3.1. Rainfall

Rainfall maps for the research area were generated utilising annual rainfall data from 38 climate stations within the ArcGIS 10.4.1 framework, employing the Kriging tool from the Spatial Analyst extension. Kriging is a geostatistical interpolation technique that estimates unknown values based on known data points, providing a more precise spatial prediction. It accounts for both the distance and the degree of variation between points to predict values at unmeasured locations. The general equation for the Kriging method (Goovaerts, 2019) is

Table. 1. Geographic coordinates for study area. (Ministry of Transport, IMOS).

Station No.	Station Name	Latitude (Degree)	Longitude (Degree)	Altitude (m)
1	Emadiah	37.05N	43.29E	1236
2	Sumeel	36.86N	42.85E	250
3	Rabiah	36.48N	042.06E	382
4	Tel-Afer	36.22N	042.29E	373
5	Sinjar	36.19N	041.50E	476
6	Ducan	36.12N	44.92E	276
7	Zakho	37.08N	042.41E	442
8	Duhook	36.52N	043.00E	276
9	Salahaddin	36.37N	044.13E	1088
10	Mosul	36.19N	043.09E	223
11	Erbeel	36.09N	044.00E	420
12	Makhmoor	35.45N	043.36E	270
13	Sulaimaniya	35.33N	045.27E	853
14	Kirkuk	35.28N	044.24E	331
15	Baiji	34.56N	043.29E	150
16	Tuz	34.53N	044.39E	220
17	Tikrit	34.34N	043.42E	107
18	Ana	34.28N	041.57E	150
19	Al-Kaem	34.23N	041.01E	178
20	Kanaqin	34.18N	045.26E	202
21	Samaraa	34.11N	043.53E	75
22	Haditha	34.04N	042.22E	140
23	Al-Khalis	33.50N	044.32E	44
24	Heet	33.38N	043.45E	58
25	Ramadi	33.27N	043.9E	48
26	Baghdad	33.14N	044.14E	34
27	Rutbah	33.02N	040.17E	615
28	Karbalaa	32.37N	044.01E	29
29	Kut	32.30N	045.49E	19
30	Hella	32.27N	044.27E	27
31	Kut-Al-Hai	32.10N	046.03E	15
32	Nukaib	32.02N	042.15E	305
33	Najaf	32.01N	44.20E	53
34	Diwaniya	31.59N	044.59E	20
35	Amarah	31.51N	047.10E	9
36	Semawa	31.18N	045.16E	6
37	Nasiriya	31.05N	046.14E	3
38	Basra	30.34N	047.47E	2

$$(x) = \lambda_1 * Z(x_1) + \lambda_2 * Z(x_2) + \ldots + \lambda_n * Z(x_n) \quad (1)$$

Where Z(x) is the estimated value at the unknown location. $Z(x_1)$، $Z(x_2)$، ... $Z(x_n)$ are the known values at the surrounding locations. λ_1, λ_2, ... λ_n are the Kriging weights assigned to each known value. n is the number of known points.

The Kriging method was chosen for spatial interpolation because of its strong geostatistical basis and its ability to provide accurate predictions in areas where the data distribution is irregular, such as rainfall. Kriging surpasses simpler interpolation algorithms in accuracy by taking into account the spatial autocorrelation among data points. This renders it particularly advantageous for analysing environmental phenomena, where spatial variations are significant. This method effectively produces smooth, precise maps of spatial distribution, which are crucial for environmental investigations requiring accurate visual representation. According to Katipotoğlu (2022), Kriging can assist decrease estimation mistakes by providing a variance map. This map indicates areas where the data is less reliable and aids in making more informed judgements regarding data interpretation and analysis.

2.3.2. NDVI

NDVI indicates the size and vigour of vegetation in a specific location. It is utilised in remote sensing and Geographic Information Systems (GIS). (Li et al. 2021) assert that NDVI is calculated using aerial or satellite imagery to assess plant health and density. NDVI was first referenced in 1973, coinciding with the development of near-infrared (NIR) sensors for satellites (Rousta, 2022). The index is determined by the extent to which green plants reflect near-infrared light and absorb visible red light (Zhang, 2018). NDVI values range from -1.0 to 1.0. They are determined by calculating the difference between near-infrared reflectance and red reflectance relative to the sum of both bands. Negative values typically indicate snow-covered areas, clouds, or water bodies, while values approaching 1.0 represent dense forested regions (Muhammad et al., 2023).

$$NDVI = (NIR — Red) / (NIR + Red) \quad (2)$$

Where RED and NIR (near infrared) are the spectral bands measured in the near infrared and red wavebands, respectively. A simple understanding of NDVI values is that a value greater than 0.6 would indicate healthy vegetation, and a value less than 0.6 but greater than 0 would indicate unhealthy vegetation. Values less than 0 can be water (Al-Khudhairy and Al-Timimi, 2021). Table 2 represents NDVI value variations according to surface coverage. Because of its stability, NDVI is an effective measure of vegetation that allows meaningful comparisons of interannual variations in vegetation growth and activity. The higher these ratios are, the more actively the plant grows (Al-Mazban, 2023). The territory of Iraq was defined using satellite imagery based on the administrative boundaries established by IMOS, and the NDVI satellite pictures were classed use ArcGIS.

Table 2. The values of the Normalized Difference Vegetation Index (Mahdi et al., 2024).

Vegetation cover type	Categories
Non-existent	>0
Low density	0.2-0.0
Medium density	0.7-0.3
Dense	1-0.8

Table 3. Classification of Pearson Coefficient Correlation (Hamad et al., 2022).

R	Correlation level
0.00	No correlation
0.00-0.25	Very weak correlation
0.25-0.50	Enough correlation
0.50-0.75	Strong correlation
0.75-0.99	Very strong correlation
1.00	Perfect correlation

2.3.3. Statical analysis

Two different statistical analysis approaches have been used. The first is the Pearson correlation coefficient, which is defined as a statistical measure that expresses the degree and strength of the relationship between the two variables used in this study. Table 3 shows the classifications of this factor, which will be adopted to clarify the relationship between the two variables whose relationship is being studied (Hamad et al., 2022). The second is a trend line, which is a line drawn above the highs or below the lows to show the dominant direction of the data. The more points there are to connect, the stronger the trend line becomes (Al-Jasani and Abdullah, 2023). A line in charts is used to indicate the direction of data over a given period. It is plotted on the graph to illustrate a general trend, which may show an increase, decrease, or stability in the data (Abdulla, 2019). This line can be used to predict future values. A trend line can tell if the health of the vegetation is improving, deteriorating, or remaining constant (Wang et al., 2020).

2.3.4. Spatial pattern analysis using Moran's Index (I)

This study employed spatial correlation analysis to examine the distribution of climate and environmental variables, determining whether they are clustered, randomly dispersed, or diverging. The Global Moran's Index was employed, a recognized method for assessing the spatial correlation of the values of the studied phenomenon across several locations. It aids individuals in comprehending the distribution of environmental and meteorological variables, such as precipitation and vegetation cover, within a region. It can also assist in determining whether elements are uniformly distributed within a specific area. It corroborates the results of other studies, such as elucidating the correlation between NDVI and rainfall, and furnishes a scientific foundation for comprehending the region's environmental and climatic impacts. This equation (Wang et al., 2020) is utilized to calculate the Moran index:

$$\mathrm{I} = \frac{n}{\sum W_{ij}} * \frac{\sum\sum W_{ij}\left(Xi-\bar{X}\right)\left(Xj-\bar{X}\right)}{\sum\left(Xi-\bar{X}\right)^{2}} \quad (3)$$

Where I: is the Moran's index, which measures spatial correlation. n: is the number of geographical locations (pixels or climate stations). Xi and Xj are the values of the variable (such as rainfall or NDVI) at locations i and j. $\bar{X}$ is the arithmetic mean of values across all locations. W_{ij} is the spatial weight matrix that determines the relationship between different geographic locations.

If I > 0, it shows a clustered pattern with values that are comparable to one another. If I < 0.05, it suggests a dispersed pattern with surrounding values differing from one another. I=0 suggests a random distribution, which means there is no discernible spatial structure.

2.3.5. Variogram assessment (Model Validation sections)

The variogram model is a statistical model that describes how spatial values vary with distance. Kriging uses frequencies to assess the link between geographically spread points in the field and enhance prediction accuracy. Kriging results may be erroneous or unreliable in the absence of frequency analysis. To confirm the accuracy of the Kriging model employed in this study, a frequency analysis was conducted to determine the spatial relationship between points. The empirical frequencies were generated in ArcGIS and then fitted to the semivariogram model. The frequencies model had the best match to the data, with extracted values for Nugget, Range, and Sill aligning with the geographic structure. The model was cross-validated to ensure the accuracy of the estimations and the efficacy of Kriging in producing high-quality maps. The following Fig. 2 incorporates the steps that were followed in this research.

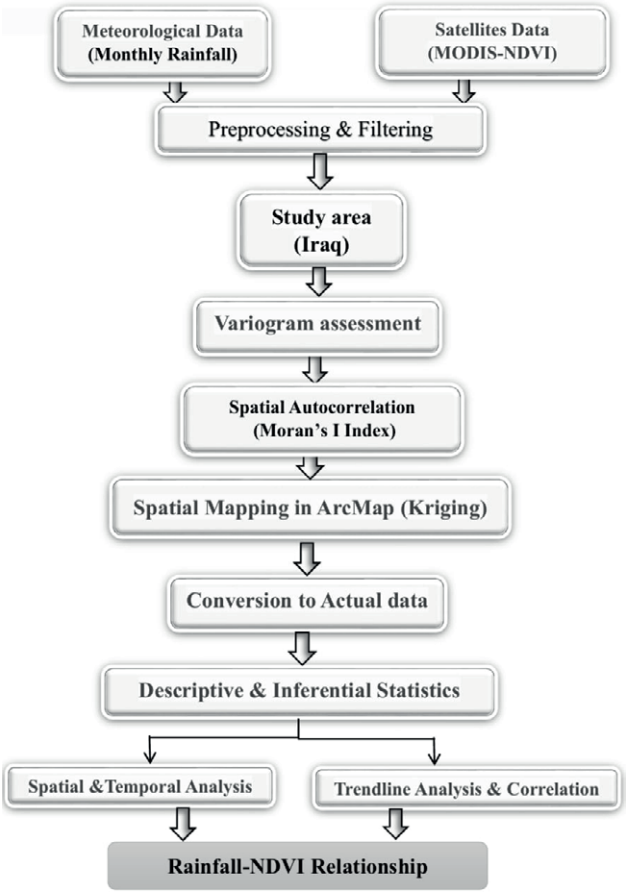

Figure 2. Workflow of the adopted methodology for assessing the spatio-temporal relationship between rainfall and NDVI using GIS and remote sensing techniques.

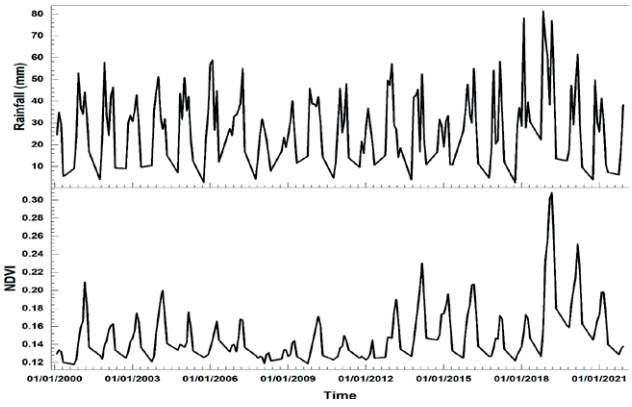

Figure 3. Temporal variation of NDVI and rainfall (2000–2021). The values represent monthly averages spatially aggregated across 38 meteorological stations distributed across the country.

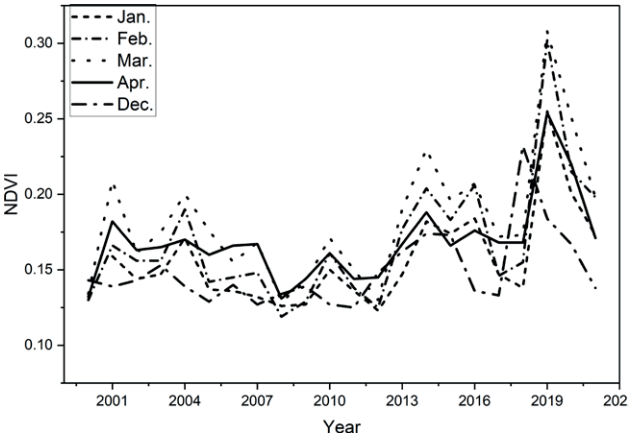

Figure 4. Monthly Normalized Difference Vegetation Index trends for the period 2000-2021.

3. RESULTS AND DISCUSSION

3.1. Temporal analysis

Fig. 3 illustrates the temporal analysis of NDVI and rainfall in the study area from 2000 to 2021. The data demonstrates a clear correlation, showing that years with lower rainfall levels typically correspond to decreased NDVI values. This time series is particularly evident in 2008, which stands out as a drought year due to the significant decline in both rainfall and NDVI. The values range between 0.152 (2008) and 0.308 (2019). It can be seen that most years have low NDVI values, indicating low vegetation density. The NDVI increased significantly in 2019 (0.308) and 2020 (0.250), indicating that the vegetation density in these years was moderate. This may be the result of favorable environmental factors, such as increased rainfall or improved weather conditions. The years with the lowest NDVI values were 2000 (0.11) and 2008 (0.15). During these times, conditions such drought or little rain are unfavorable for plantation.

Fig. 4 shows how Iraq's Normalized Difference Vegetation Index (NDVI) changes monthly from 2000 to 2021. It focuses on January through April, the best months for plants to thrive. The NDVI has a distinct seasonal pattern: it goes up during the wet season (November to April) and down during the dry season (May to October). NDVI readings are usually highest between February and April when the weather is best for growth because it rains more and the temperatures are moderate. However, Table 4 shows they drop significantly during the summer months (June to August).

The results showed that the vegetation cover changed significantly during the study period. Perhaps, in addition to man-made pressures, the main reason is the natural changes caused by successive droughts. NDVI

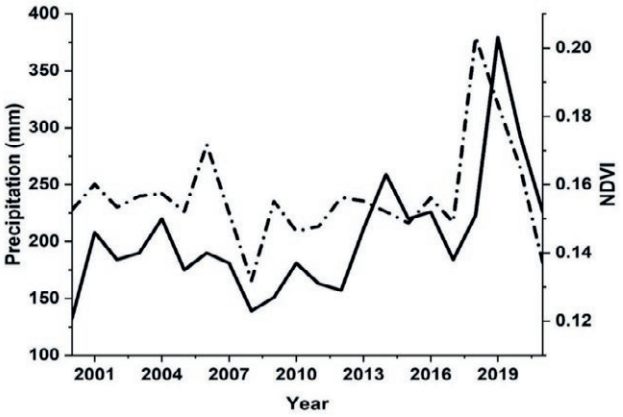

Figure 5. Temporal patterns of rainfall and NDVI for (2000-2021).

values increased over time, especially between 2018 and 2019, reaching 0.35, which may indicate unusually wet periods or improved vegetation growth conditions during those years or new agricultural projects. Conversely, in early years (2000–2010), values appear to follow a fairly consistent seasonal pattern, while later years show greater variability, possibly reflecting the effects of climate change or changes in land management, which may indicate unusually wet periods or improved vegetation growth conditions during those years.

Fig. 5 shows the time series of rainfall and the NDVI during 22 years. It can be observed that there is a correlation between rainfall and NDVI, meaning that as rainfall increases, NDVI values rise accordingly. It is also evident that 2018 experienced a significant amount of rainfall, as the graph displays a substantial increase in rainfall that year, marking the highest recorded during the specified period. An increase in rainfall is associated with an increase in NDVI values, indicating a positive effect of rainfall on vegetation. It can also be observed that periods of reduced rainfall coincide with a decrease in the NDVI index. The results showed that the lowest NDVI value, 0.152, occurred in 2008. This year marked the driest period, with the lowest recorded rainfall of 165 mm. In contrast, the highest NDVI value, 0.308, was observed in 2019. This year also had the highest rainfall rate, representing one of the peak records during the study period.

Fig. 6 shows the Normalized Difference Vegetation Index (NDVI) values for 38 locations in Iraq. The total distribution of NDVI demonstrates a definite pattern that reflects Iraq's prevalent environmental and climatic effects. The graphic illustrates that the highest NDVI values are centered in the northern regions, gradually decreasing towards the center and south. Stations in the north have high NDVI readings, reaching 0.35. The northern regions have comparatively significant rainfall amounts compared to the rest of Iraq, ranging from 400 to 900 mm annually. Temperatures are lower than in southern locations, allowing soil moisture to be retained for longer periods of time. Stations in the center, on the other hand, show lower values as rainfall rates gradually decrease to 120 mm per year, diminishing the

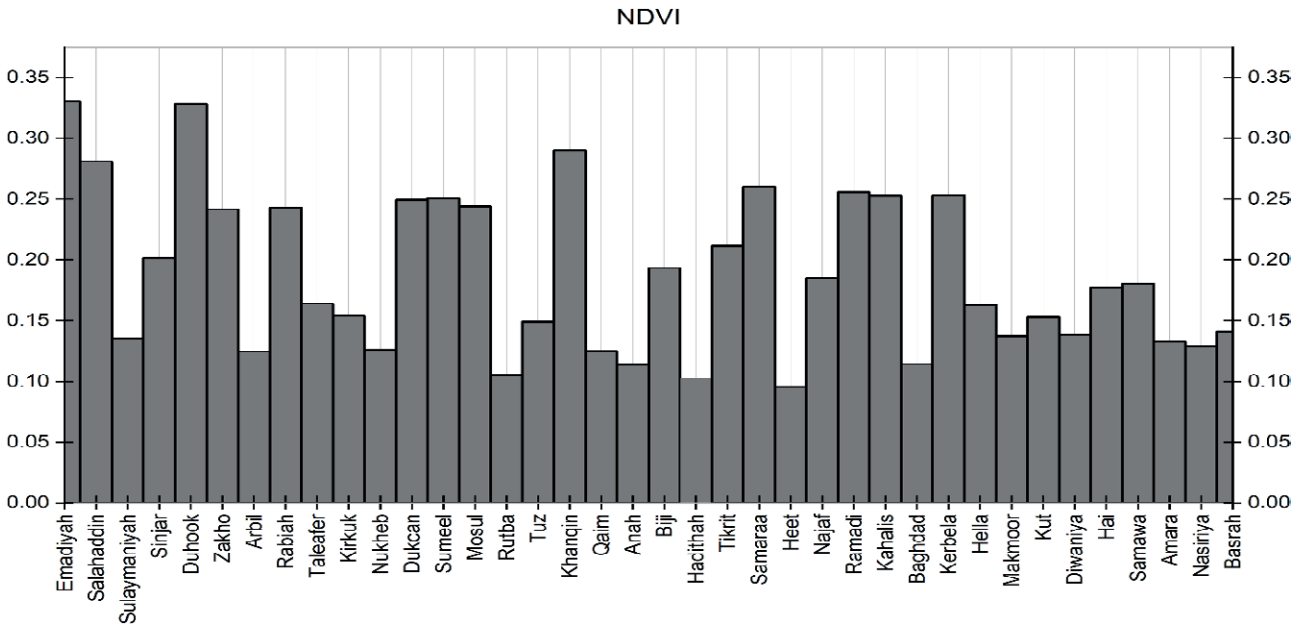

Figure 6. Spatial distribution of NDVI across the study stations from north to southern of Iraq.

availability of natural water for plant development. The Tigris and Euphrates rivers sustain vegetation, but urban growth and seasonal crops lessen natural vegetation density in these places. The southern sections are classified as semi-arid to desert, with annual rainfall below 100 mm, which is insufficient to maintain natural vegetation. High temperatures, which can exceed 50°C in the summer, cause rapid water evaporation, which limits plant development. Soils in the southern regions are salinized and drought-prone due to little rainfall and high evaporation rates, resulting in lower NDVI values. The graph depicts a strong gradient in NDVI values from north to south across Iraq, indicating climatic and environmental differences.

Table 4 summarizes the average values of NDVI and rainfall for each station for the duration of the study, providing a nuanced understanding of the dynamic response of vegetation to rainfall variations. Based on this table, Emadiah has the highest NDVI value (0.33) with a mean rainfall of 606.2 mm. This suggests that areas with dense vegetation are generally associated with higher rainfall levels. In comparison, Duncan, which has the highest rainfall (624.41 mm), shows a slightly lower NDVI value (0.249). This indicates that while rainfall significantly promotes vegetation growth, NDVI is not solely dependent on rainfall and can be influenced by other factors, such as soil type, temperature, and type of vegetation cover.

Table 4. Properties of stations rainfall & NDVI used in this study for the period (2000-2021).

Station No.	St. name	NDVI	Rainfall (mm)
1	Emadiah	0.33	606.2
2	Sumeel	0.251	434.23
3	Rabiah	0.243	339.23
4	Tel-Afer	0.164	308.82
5	Sinjar	0.201	331.82
6	Ducan	0.249	624.41
7	Zakho	0.242	526.22
8	Duhook	0.328	487.52
9	Salahaddin	0.281	451.56
10	Mosul	0.244	358.41
11	Erbeel	0.124	392.87
12	Makhmoor	0.137	292.7
13	Sulaimaniya	0.135	595.7
14	Kirkuk	0.154	337.8
15	Baiji	0.193	194.44
16	Tuz	0.149	269.56
17	Tikrit	0.211	162.64
18	Ana	0.114	124.32
19	Al-Kaem	0.125	118.8
20	Kanaqin	0.29	287.51
21	Samaraa	0.26	153.19
22	Haditha	0.103	115.9
23	Al-Khalis	0.253	171.77
24	Heet	0.096	110.47
25	Ramadi	0.256	107.51
26	Baghdad	0.114	120.47
27	Rutbah	0.105	106.13
28	Karbalaa	0.253	90.32
29	Kut	0.153	139.2
30	Hella	0.163	105.72
31	Kut-Al-Hai	0.177	131.11
32	Nukaib	0.126	76.17
33	Najaf	0.185	94.2
34	Diwaniya	0.138	101.95
35	Amarah	0.133	173.63
36	Semawa	0.18	99.12
37	Nasiriya	0.129	119.93
38	Basra	0.141	126.49

3.2. Spatial distribution

Fig. 7 shows a comparison of the Kriging and IDW methods using scatter plots that show measured data from remote sensing images (for NDVI) at specific known locations. The Ordinary Kriging interpolation is used to make the forecast values for places where there are no direct measurements. After comparing them, Kriging was chosen for a variety of reasons. Kriging is a more complex and in-depth investigation of spatial relationships that uses advanced interpolation techniques. It is based on geostatistical analysis, geographical relationships, and spatial variation, which means that spatial patterns are analyzed in more depth than just interpolated data. Fig. 7 (left) shows that the points are closely distributed, indicating that the predicted values are very close to measured values. The relationship between them is completely linear, indicating that the IDW leads to a homogeneous interpolation of the data with small variations. As for Fig. 7 (right), the points follow the main trend line but with a clear distribution, which means that kriging shows a more complex response to the data, as it can handle trends and spatial variations. IDW, although it provides accurate results, does not take into account spatial relationships, such as location variation. Kriging shows a greater ability to capture spatial patterns because it is more complex than IDW, and this allows it to better handle spatial trends. Since this study looks at differences in space and time and tries to find out how rainfall and NDVI are related across Iraq, it is essential to use a geostatistical method to account for

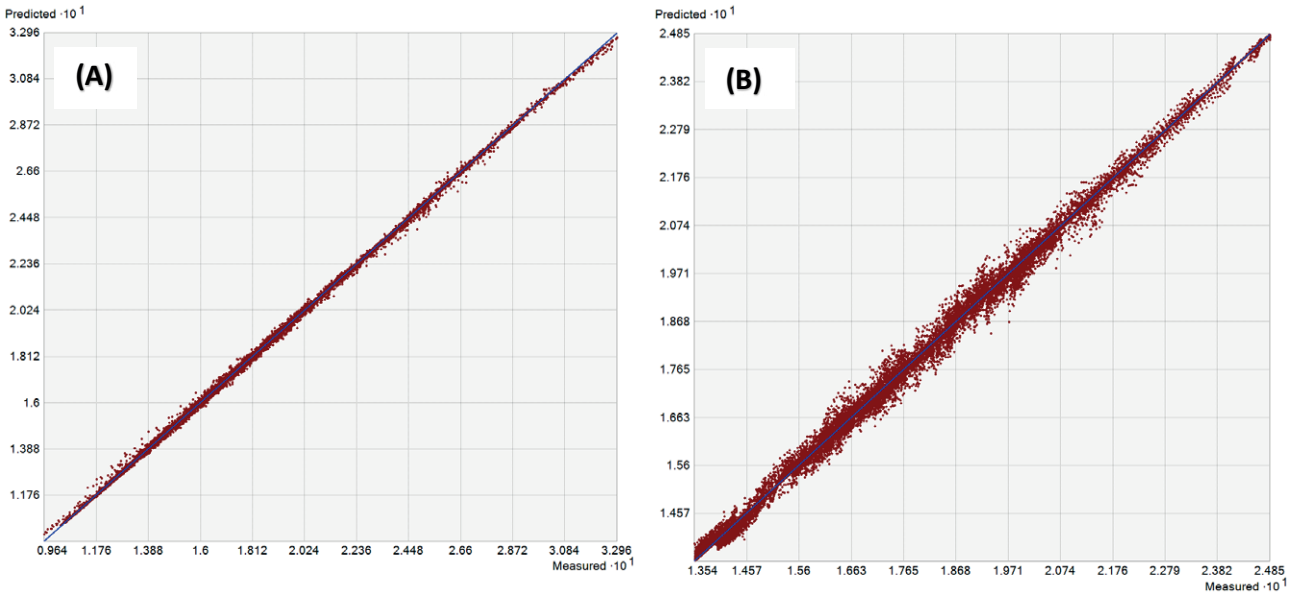

Figure 7. Comparison of spatial interpolation methods, (A): IDW and (B): Kriging using predicted vs. measured values analysis for NDVI.

both. Geographic factors, such as terrain, have a significant effect on rainfall. NDVI shows how vegetation responds to available moisture but doesn't necessarily show how much rain fell. The researchers used the Kriging interpolation method to better understand how this relationship changes over space. Kriging is a way to guess values in locations where we don't have measurements by using the connections between known data points. This practice makes it easier to get a fuller and accurate picture of the variables being researched.

As shown in Fig. 8, the spatial distribution of NDVI values was analyzed using the semivariogram model to assess the degree of spatial autocorrelation of vegetation cover. The semivariogram indicates that the nugget effect is approximately 0.00347, suggesting a low level of random variation or measurement error, possibly due to sensor noise or local-scale heterogeneity not captured at the resolution used. The partial sill, estimated as 0.00135, reflects the structured spatial variance, whereas the range of approximately 4.35 degrees denotes the spatial extent beyond which NDVI values are no longer spatially correlated. A stable semivariogram model was fitted to the experimental data, resulting in a reasonable fit, as evidenced by the alignment of the binned empirical values with the fitted model curve. The spatial pattern was discovered to be isotropic, meaning that spatial dependency in NDVI values is consistent in all directions. These findings indicate the presence of a distinct spatial structure in NDVI data, hence confirming the use of geostatistical interpolation techniques such conventional Kriging for spatial prediction. The geographical dependence seen within the specified range allows for credible interpolation of vegetation cover in unsampled areas, resulting in more accurate and meaningful environmental evaluations and land cover monitoring.

In this research, the spatial interpolation of both rainfall and NDVI was performed using the ordinary Kriging method, which is widely recognised for its effectiveness in modeling spatial continuity. The spherical semivariogram model was chosen because it matched the data's spatial pattern the best, shown by having the lowest Root Mean Square Error (RMSE) in the cross-validation process. The semivariogram model parameters were as follows: Nugget: 0.00347, Sill: 0.00135, Range: 4.3526. These values indicate a moderate spatial dependency among the data points.

Fig. 9 presents the spatial distribution patterns of both rainfall and NDVI across the study area. These maps allow for a visual comparison between the two variables and help identify potential zones where higher or lower values might correspond. It offers a spatial context that supports further statistical analysis of their relationship. The NDVI map shows that the northern and eastern parts of Iraq have higher vegetation cover than the southern and western parts. This distribution makes sense with the geography since the northern part contains mountains and a humid environment. Figure 9B shows how rain falls over the country. The northern and eastern parts of Iraq get more rain than the southern and western parts (Muter et al., 2025). The weather

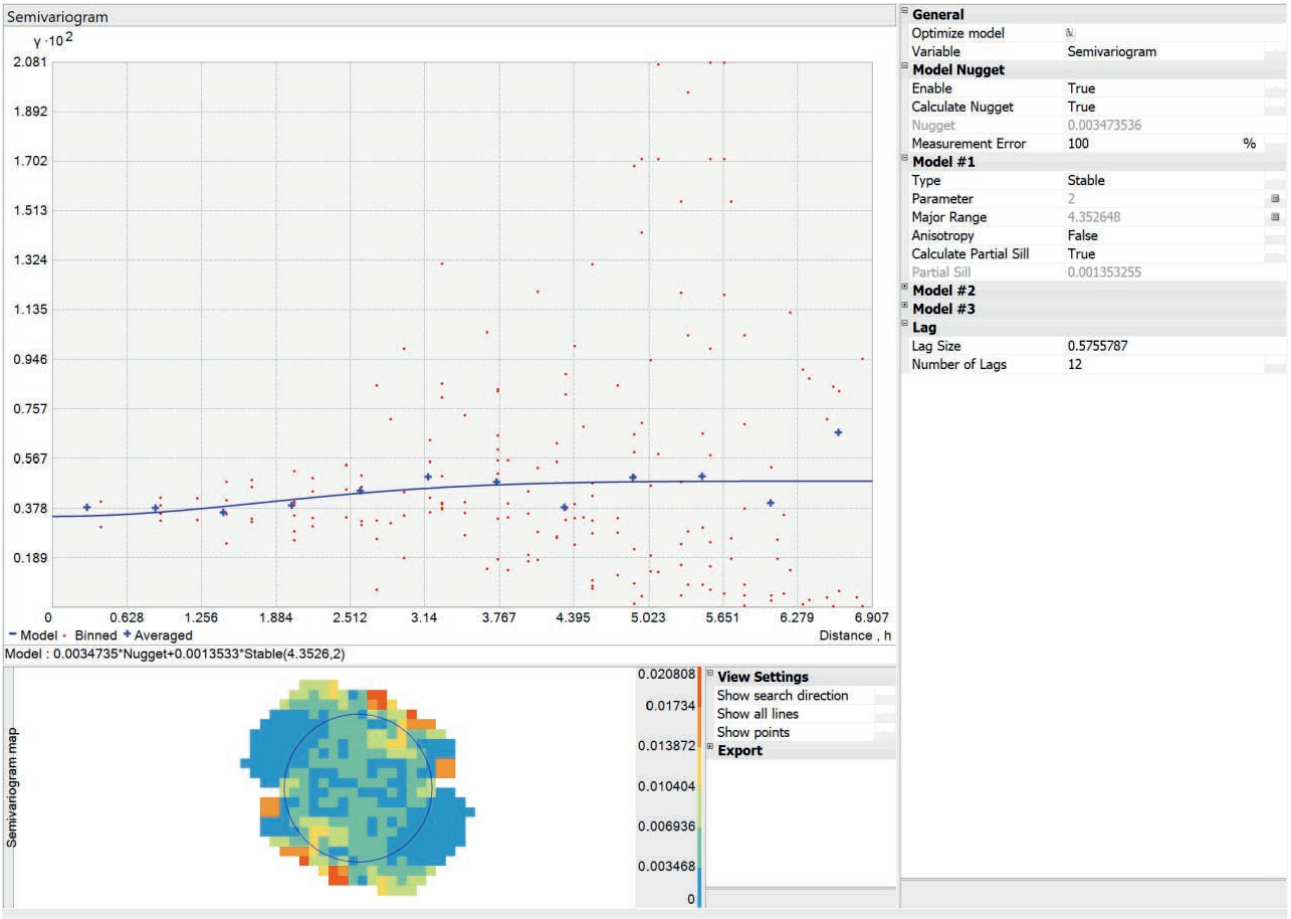

Figure 8. Experimental and fitted semi-variogram of NDVI for spatial variability analysis.

of Iraq is like this; however, the northern part has a humid environment since the mountains are so high. It looks like the areas with a lot of rain on this map match up well with the areas with a lot of plants on the NDVI map. This means that rain is a big part of figuring out how dense the vegetation is in Iraq.

3.3. Spatial correlation analysis of rainfall and NDVI using Moran's Index

The purpose of this analysis is to examine the regional pattern of rainfall and the NDVI using Moran's I, a statistical metric that indicates whether the spatial values of a given variable are randomly distributed, clustered, or scattered. Fig. 10 illustrates the spatial correlation analysis of both rainfall and NDVI using Moran's model. This analysis uses statistical values (Moran's I, Z-score, and p-value) to assess whether the spatial distribution is associated or random. Moran's I for rainfall is 0.711, showing significant geographical clustering of rainfall. The Z-score value of 11.578 indicates that the spatial distribution of rainfall is not random. The statistical significance level (p-value) was zero, which is a very low statistical value (<0.01), well below 0.01, confirming that this clustered pattern is not the result of chance but rather reflects the influence of climatic and geographical factors on rainfall distribution in the study area. The spatial maps reveal a clear grouping of heavy rainfall and dry areas close together, indicating that climatic systems have a substantial influence on rainfall distribution. Rainfall distribution appears to be clustered rather than random. There is a strong spatial association between neighbouring values, as stations with high rainfall rates tend to be close, and stations with low rainfall rates tend to be close.

This demonstrates the impact of climatic and geographical conditions. In terms of spatial distribution, Moran's I for the NDVI index was 0.175, which is a comparatively low value when compared to rainfall, showing that the natural vegetation index clusters less spatially.

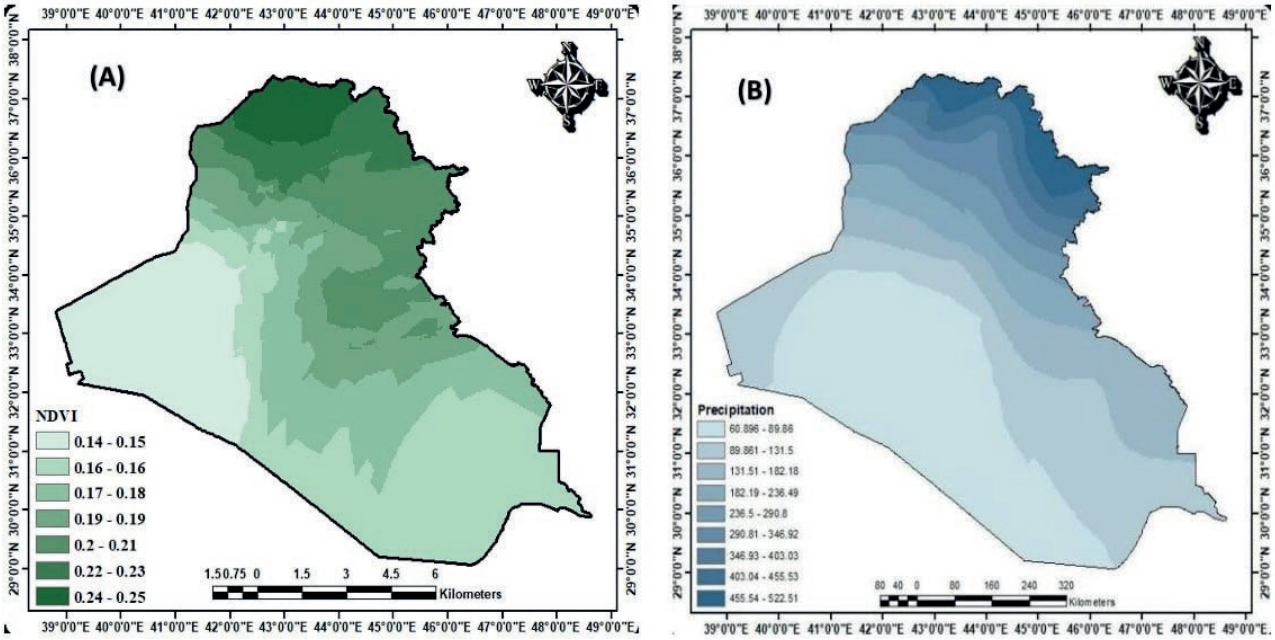

Figure 9. Spatial pattern of (A): Normalized Difference Vegetation Index and (B) rainfall for (2000-2021).

Variables	Rainfall	NDVI
Moran's I	0.711	0.175
Z-score	11.578	2.528
P-value	0.000000	0.011460

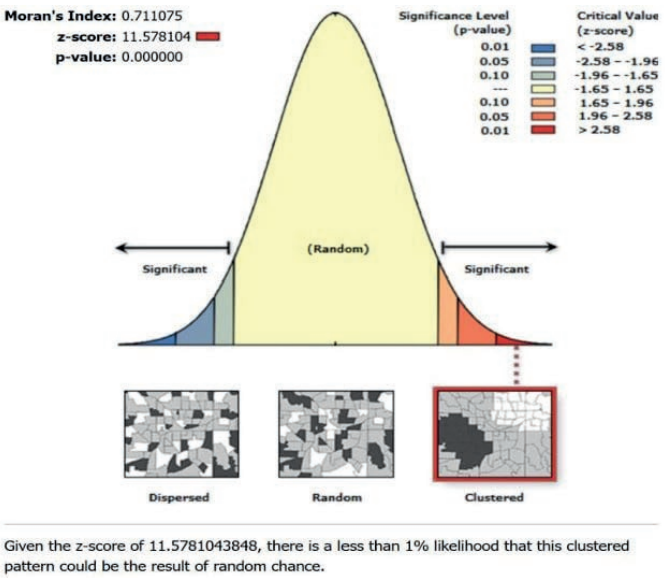

Figure 10. Spatial autocorrelation analysis of rainfall and NDVI using Moran's I Index.

The Z-score of 2.528 was low but still within the statistically significant range, showing some clustering but not as strong as rainfall. The statistical significance level (p-value) was 0.011460, less than 0.05, indicating that this clustered pattern is not due to chance. These extra elements could make it more changeable and less clear than the rainfall distribution. The NDVI index doesn't cluster as strongly as rainfall does in space. This is because other things, like soil type, land use, human involvement, and artificial irrigation, can alter vegetation cover without affecting rainfall. The Moran's rainfall index is much higher than the natural vegetation index, which means that rainfall is more evenly spread out over space.

The natural vegetation index is more spread out, which shows the area's ecological and human activity diversity. When looking at how climate and vegetation

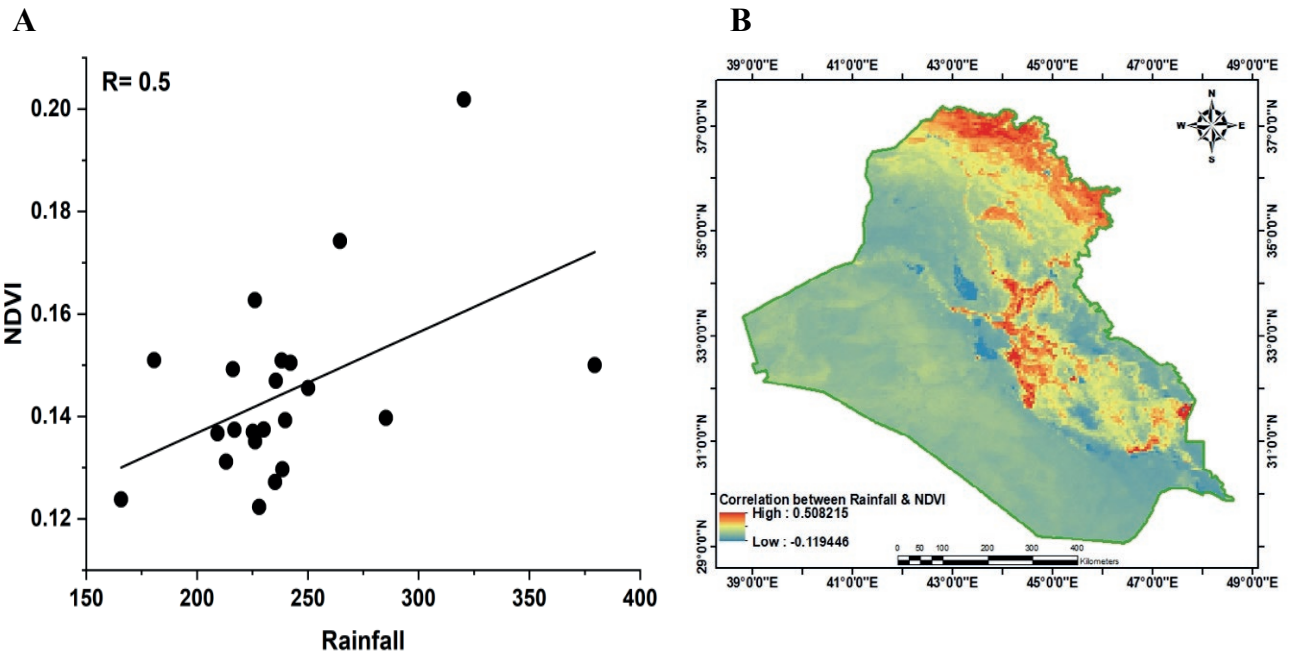

Figure 11. (A) represents the annual of correlation, and (B) is spatial distribution of NDVI and rainfall (mm).

cover are associated in the context of environmental and climate changes, it might be helpful to tell the two distribution patterns apart. This study helps us learn more about the link between climate and vegetation cover. This lets us figure out how climate change affects ecosystems and how to take care of the environment.

Fig. 11A shows the yearly relationship between NDVI and rainfall. The link between vegetation index and rainfall depends a lot on how the weather changes in a certain area and how it affects plant development. The correlation coefficient between rainfall and the vegetation index is 0.5. This means that there is a fairly positive association between the two variables, but it is not strong enough to be a reliable predictor of how one variable would behave in respect to the other. Since the correlation coefficient is positive, this indicates that the relationship between the two variables is a direct relationship. That is, when one variable increases, the other variable is likely to increase as well. Since the dispersion between values, the relationship between the two variables is not perfect. This means that in addition to rainfall, there are other factors that affect vegetation, such as temperature, soil quality, and human interventions (such as agriculture and urbanization).

Figure 11B shows how rainfall and NDVI in Iraq have changed during the past 22 years. So, this map shows us how much rain influences plant growth in different parts of Iraq. Over the past ten years, Iraq has had a lot of droughts and rain that has changed a lot (Muter et al., 2024). This could change how rainfall and NDVI relate to each other in space. There is a good link between NDVI and rainfall. These places are mostly in northern Iraq, a hilly region known for heavy rain and thick vegetation. Areas with more rain have higher NDVI values, meaning the vegetation cover is denser. It can be seen how rivers affect NDVI because green spots occur along riverbanks when there is water. This map emphasizes the importance of rainfall in determining vegetation density in Iraq. This map can be used as a tool for planning water and agricultural resource management in Iraq. Low values represent areas with a weak or negative relationship between rainfall and NDVI. These areas are concentrated in the southern and western regions, where rainfall is lower and the environment is drier; the relationship between rainfall and NDVI may be weaker where rainfall is scarce and vegetation cover is less dense. Negative values may indicate areas where vegetation thrives in the absence of rainfall, thereby elucidating the reliance on alternative water sources such as irrigation or groundwater.

From 2000 to 2021, irrigated agriculture grew in various parts of Iraq, especially in the south. These actions may have lessened the effect of low rainfall on NDVI, which could explain why the link between rainfall and vegetation is different. The wars and conflicts that Iraq went through at that time changed the way

people used land, which changed the vegetation cover. For instance, the Ducan station, which gets an average of 624.41 mm of rain and has an NDVI of 0.249, may be linked to thick vegetation. On the other hand, stations with minimal rainfall, such Nukhaib (76.17 mm), had low NDVI values of 0.126. The stations are spread out over different areas, which means that the amount of rain and NDVI varies from one area to another. Local factors including plant habitat, soil, and climate have an effect on this diversity.

This study effectively elucidates the relationship between vegetation cover and rainfall across various terrains and climates. Conversely, Al-Hasn (2024) examines the impact of drought on vegetation cover in arid regions, providing further insights into environmental issues in both nations. The little correlation between rainfall and NDVI in Iraq, in contrast to recent regional studies (Al-Hasn, 2024), may result from a combination of environmental, topographical, climatic, and anthropogenic factors. The climate in Iraq is diverse, encompassing deserts, semi-arid regions, and agricultural areas. The majority of these locations are situated in arid or semi-arid environments, where vegetation exhibits minimal responsiveness to rainfall. In arid regions, vegetation relies on the moisture present in the soil. Plants in these regions have adapted to harsh conditions, hence they have a diminished response to precipitation compared to flora in temperate regions. Rainfall in Iraq is irregular both spatially and temporally, typically occurring within a brief duration throughout the winter and spring seasons.

Human activities such as unsustainable agriculture, deforestation, and urbanization have weakened the relationship between NDVI and rainfall. Iraq suffers from a shortage of freshwater and the reduced flow of its main rivers (Tigris and Euphrates) due to dams and regional water policies. The limited availability of surface water and groundwater makes plants more dependent on these sources than on rainfall, resulting in a weak relationship between NDVI and rainfall. The variety of soil types in Iraq affects the soil's ability to store and use water. Climate change and rising temperatures in Iraq are increasing evaporation rates, reducing the impact of rainfall on soil moisture and plant growth.

4. CONCLUSION

The geographical distribution of sites analyzed in this study highlights notable differences in rainfall and NDVI across various regions of Iraq. A positive relationship is evident between rainfall and NDVI, with a correlation coefficient of 0.5, but the relationship is not perfectly linear, and variations can be seen between different locations. This indicates that while increased rainfall generally enhances vegetation abundance and activity, other factors also influence these variables. Regions in the north and east, characterized by higher rainfall, typically support denser vegetation compared to the drier south and west, a pattern consistent with Iraq's geographical reality, where the northern areas have mountainous terrain and a more humid climate. The study identified 2018 as an anomalous year, marked by the heaviest rainfall in recent years, which sparked further research interest. A lag was observed in the vegetation's response to rainfall, as plants require time to grow following rainfall. There were clear seasonal changes in vegetation. NDVI was highest in February, March, and April and lowest in the summer months in June, July, and August. The year with the least rain was 2008, with an NDVI value of 0.152 and 165 mm. The year with the most rain was 2019, with an NDVI value of 0.308 and one of the highest rainfall rates of the research period. The study also shows how helpful maps can be for designing farms since they help farmers find regions where crops grow well based on how much rain falls there. These maps can also be helpful in climate change studies since they show how vegetation and rainfall patterns change over time in different areas. Also, combining NDVI with RS provides a cheap way to keep an eye on vegetation cover in Iraq, which helps with managing natural resources. Finally, MODIS satellite photos worked well for finding global drought indicators, which made it possible to figure out how bad a drought was in places without ground-based measurements.

The amount and distribution of rainfall have big effects on farming, managing water resources, and planning for the environment. This is because stations with more rainfall are more likely to have lush vegetation and higher agricultural production. In contrast, areas with lower rainfall may face water scarcity and drought issues. Rainfall has a distinct clustered spatial pattern that reflects climatic and geographic effects, with wet and dry areas clearly converging. However, the NDVI score has a less defined regional distribution because of additional natural and anthropogenic influences. The substantial difference between Moran's I for rainfall (0.711) and NDVI (0.175) suggests that rainfall has a more uniform spatial distribution than vegetation, which is more variable due to non-climatic variables. It was observed that rainfall exhibits a more homogeneous spatial pattern, whereas the NDVI is influenced by multiple factors, resulting in a less uniform spatial pattern.

ACKNOWLEDGEMENTS

The authors would like to express their sincere gratitude to Mustansiriyah University for their continuous support and for providing an academic environment that fostered their research. My appreciation also extends to the Iraqi Meteorological Organization and Seismology (IMOS), Ministry of Transport, for providing essential meteorological data that contributed to this study. Additionally, I would like to thank NASA for supplying the Terra MODIS NDVI dataset.

REFERENCES

Abdulla H.J., 2019. Manifestations of climate change in Baghdad Area. Al-Mustansiriyah J. Sci., 30 (4): 39-42. DOI: https://doi.org/10.23851/mjs.v30i4.657

Almamalachy Y.S., Al-Quraishi A.M.F., Moradkhani H., 2020. Agricultural Drought Monitoring Over Iraq Utilizing MODIS Products. In: Al-Quraishi, A., Negm, A. (eds) Environmental Remote Sensing and GIS in Iraq. Springer Water. Springer, Cham. https://doi.org/10.1007/978-3-030-21344-2_11

Abdul Jabbar A.M., Abdulkareem A.K., 2021. Predicted the Cumulative Annual Rainfall in Iraq using SDSM Modal. Al-Mustansiriyah J. Sci., 32(2): 11-17. https://doi.org/10.23851/mjs.v32i2.977

Abdulkareem I.H, Nemah H.A., 2021. Variation of Weather Elements during Different Seasons in Iraq. Journal of Engineering Science and Technology, 16 (6): 5000-5012. https://dx.doi.org/10.1088/1755-1315/1223/1/012002

Al-Khudhairy A.A., Al-Timimi Y.K., 2021. Analysis of the LST and Vegetation Indices relationship using Landsat-8 data in Duhok Governorate, Iraq. Al-Mustansiriyah J. Sci., 32, (4). DOI: http://doi.org/10.23851/mjs.v32i4.1012

Al-Jasani N.A.A., Abdullah H.N.N., 2023. Geographical analysis of the variation of the standard vegetation index "NDVI" and its characteristics in the Najaf Governorate for the summer season. Anbar University Journal of Human Sciences, 1: 327-350. http://search.mandumah.com/Record/1386106

Al-Lami A. M., Khaleed O. L., Ahmed M. M., 2023. Assessment of some Bioclimatic Indices using RayMan Model for Baghdad-Iraq. IOP Conf. Ser.: Earth Environ. Sci. 1223, 012019. https://doi.org/10.1088/1755-1315/1223/1/012019

Al-Mazban M.T.Q., 2023. The impact of climatic changes on the vegetation cover difference index in eastern Maysan governorate. Journal of Education College Wasit University, 50 (1): 271-281. https://doi.org/10.31185/eduj.Vol50.Iss1.3433

Al-hasn R., 2024. Studying correlation between rainfall and NDVI/MODIS for Time Series (2012–2022) in Arid Region in Syria. Environmental Sciences Proceedings 29, 1: 58. https://doi.org/10.3390/ECRS2023-16704

Al-Daoudi A.S., Al-Timimi Y.K., 2024. Monitoring of Iraq Vegetation Dynamics Using MODIS Data From 2000-2023. IOP Conference Series: Earth and Environmental Science, 1371 (2): 1755-1315. https://dx.doi.org/10.1088/1755-1315/1371/2/022033

Al Rukabie J. S. A., Naif S. S., Al-Jiboori M. H., 2024. Quantitative Impact of Monthly Precipitation on Urban Vegetation, Surface Water and Potential Evapotranspiration in Baghdad Under Wet and Dry Conditions. Nature Environment and Pollution Technology, 23:4, 2383-2389. https://doi.org/10.46488/NEPT.2024.v23i04.041

Deagan E. M., Al-Jiboori M.h., 2023. The Relationship of CLWC and Rainfall to the Synoptic Cases of Two Case Studies Over Iraq. IOP Conf. Series: Earth and Environmental Science, 1262: 082038. https://doi.org/10.1088/1755-1315/1262/8/082038

Goovaerts, P., 2019. Geostatistical estimation methods: Kriging. In P. Bogaert, M. Saïd, & P. Goovaerts (Eds.), Geostatistics for Environmental Applications: 221–244. Springer. https://doi.org/10.1007/978-3-030-17860-4_16

Guo E., Wang Y., Wang C., Sun Z., Bao Y., Mandula N., Jirigala B., Bao Y., Li H., 2021. NDVI Indicates Long-Term Dynamics of Vegetation and Its Driving Forces from Climatic and Anthropogenic Factors in Mongolian Plateau. Remote Sensing 13, 4: 688. https://doi.org/10.3390/rs13040688

Gaznayee H.A, Al-Quraishi A.M.F., Karrar M., and Coen R., 2022. A Geospatial Approach for Analysis of Drought Impacts on Vegetation Cover and Land Surface Temperature in the Kurdistan Region of Iraq. Water, 14, (6): 927. https://doi.org/10.3390/w14060927

Hamad A. I., Ali A. B., Hassoon A. F. 2022. Climate change and its effect on water and vegetation cover over sharp regions using GIS techniques. AIP Conf. Proc. 2398 (1): 020055. https://doi.org/10.1063/5.0097668

Helali J., Asaadi S., Jafarie T., Habibi M., Salimi S., Momenpour S.E., Shahmoradi S., Hosseini S.A., Hessari B., Saeidi V., 2022. Drought monitoring and its effects on vegetation and water extent changes using remote sensing data in Urmia Lake watershed, Iran. Journal of Water and Climate Change, 13 (5): 2107–2128. https://doi.org/10.2166/wcc.2022.460

Hatem I., Alwan I., Ziboon A., Kuriqi A., 2024. Assessment of agricultural drought in Iraq employing Landsat and MODIS imagery. Open Engineering, 14(1): 20220583. https://doi.org/10.1515/eng-2022-0583

Jaber S.H., Al-Saadi L.M., Al-Jiboori M.H., 2020. Spatial Vegetation growth and its relation to seasonal temperature and precipitation in Baghdad. Int. J. Agricult. Stat. Sci., 16 (1), 2021-2026. https://connectjournals.com/03899.2020.16.2021

Kadhum J.H., Al-Zuhairi M.F., Hashim A.A., 2022. Synoptic and dynamic analysis of few extreme rainfall events in Iraq. Earth Syst. Environ. 8: 4939–4952. https://doi.org/10.1007/s40808-022-01419-1

Katipoğlu O.M., 2022. Spatial analysis of seasonal rainfall using various interpolation methods in the Euphrates basin, Turkey. Acta Geophys. 70: 859–878. https://doi.org/10.1007/s11600-022-00756-0

Li P. J., Wang M., Liu Z., Xue A., Bagherzadeh M. Liu., 2021. Spatial-Temporal Variation Characteristics of NDVI and its Response to Climate on the Loess Plateau from 1985 to 2015. CATENA 203: 105331. https://doi.org/10.1016/j.catena.2021.105331

Mustafa Y.T., 2020. Spatiotemporal Analysis of Vegetation Cover in Kurdistan Region-Iraq using MODIS Image Data. J. Appl. Sci. Technol., 1: 01-07. https://doi.org/10.38094/jastt119

Mzuri R.T, Omar A.A., Mustafa Y.T., 2021.Spatiotemporal Analysis of Vegetation Cover and Its Response to Terrain and Climate Factors in Duhok Governorate, Kurdistan Region, Iraq. Iraqi Geological Journal, 54(1A). https://doi.org/10.46717/igj.54.1A.10Ms-2021-01-31

Muhammad R.A, Abbas A., Hussein S., 2023. Land cover changes in the Musayyib area-Babylon using remote sensing data and geographic information systems, Midad AL-Adab Refereed Quarterly Journal, 30: (3), Article 14. https://digitalcommons.aaru.edu.jo/midad/vol30/iss3/14

Muhammad B. J., Hassoun I. S., 2023. Rainfall and its impact on vegetation cover within Sulaymaniyah Governorate: (A comparative study for the period between (1992-1999). Journal of Educational and Human Sciences, 24: 125-44. https://doi.org/10.33193/JEAHS.24.2023.365

Muter S.A, Al-Timimi Y.K., Al-Jiboori M.H., 2024. Analysis of Temporal and Spatial Drought Characteristics in Iraq Using the Standard Rainfall Index (SPI). IOP Conference Series: Earth and Environmental Science, Pollution and Ecology, 1371. https://doi.org/10.1088/1755-1315/1371/2/022032

Mahdi Z.S., Abu-ALShaeer M.J., Al-Jiboori M.H., 2024. Quanti-native relationships among potential evapotranspiration, surface water, and vegetation in an urban area (Bagh-dad). Italian Journal of Agrometeorology (2): 81-88. https://doi.org/10.36253/ijam-2557

Muter S.A, Al-Jiboori M.H., Al-Timimi Y.K. 2025. Assessment of Spatial and Temporal Monthly Rainfall Trend over Iraq. Baghdad Science Journal; 22: 3, Article 17. DOI: https://doi.org/10.21123/bsj.2024.10367

Naif S.S., Mahmood D.A., Al-Jiboori M.H., 2020. Seasonal normalized difference vegetation index responses to air temperature and rainfall in Baghdad. Open Agriculture, 5, (1): 631-637. https://doi.org/10.1515/opag-2020-0065

Nassif W.G., Al-Ataby I.K., Al-Taai O.T., 2024. Impact of Soil Temperature and rainfall on Vegetation Cover Over Selected Stations in Iraq. Asian Journal of Water, Environment and Pollution, 21 (1): 25-33. https://doi.org/10.3233/AJW240005

Othman A.A., Shihab A.T., Al-Maamar A.F., Al-Saady Y.I., 2020. Monitoring of the Land Cover Changes in Iraq. Environmental Remote Sensing and GIS in Iraq. Springer Water. Springer, Cham. https://doi.org/10.1007/978-3-030-21344-2_8

Rousta I., Moniruzzaman M., Olafsson H., Zhang H., Baranowski P., Tkaczyk P., Lipińska H., Kępkowicz A., Krzyszczak J., 2022. Investigation of the Vegetation Coverage Dynamics and its Relation to Atmospheric Patterns in Kabul River Basin in Afghanistan. Pure and Applied Geophysics, 179: 3075-3094. https://doi.org/10.1007/s00024-022-03044-6

Wang J., Ouyang J., Zhang M. 2020. Spatial distribution characteristics of soil and vegetation in a reclaimed area in an opencast coalmine. CATENA, 195, 104773. https://doi.org/10.1016/j.catena.2020.104773

Zhang H., Chang J., Zhang L., Wang Y., Li Y., Wang X., 2018. NDVI dynamic changes and their relationship with meteorological factors and soil moisture. Environ Earth Sci, 77 (582). https://doi.org/10.1007/s12665-018-7759-x

Zheng K., Tan L., Sun Y., Wu Y., Duan Z., Xu Y., Gao C., 2021. Impacts of climate change and anthropogenic activities on vegetation change: Evidence from typical areas in China. Ecological Indicators; 126 (107648): 1470-160X. https://doi.org/10.1016/j.ecolind.2021.107648

Italian Journal of Agrometeorology
Rivista Italiana di Agrometeorologia

Firenze University Press
https://riviste.fupress.net/index.php/IJAm

OPEN ACCESS

Citation: Ammoniaci, M., Voltarelli, M., Biagi, M., Cascella, F., Carapelli, C., Zombardo, A., Puccioni, S., Storchi, P., & Perria, R. (2025). Impact of climate change effects on grapevine through a multi-year analysis in the Chianti Classico Area (Italy). *Italian Journal of Agrometeorology* (2): 95-105. doi: 10.36253/ijam-3493

Received: May 12, 2025

Accepted: December 17, 2025

Published: December 31, 2025

Data Availability Statement: All relevant data are within the paper and its Supporting Information files.

Competing Interests: The Author(s) declare(s) no conflict of interest.

ORCID:
MA: 0000-0003-0658-6981
MV: 0009-0006-0623-0300
AZ: 0000-0003-1613-9667
SP: 0000-0002-8653-7620
PS: 0000-0001-7534-5634
RP: 0000-0002-4591-4370

Impact of climate change effects on grapevine through a multi-year analysis in the Chianti Classico Area (Italy)

Marco Ammoniaci[1,*], Matteo Voltarelli[1,3], Massimiliano Biagi[2], Fabio Cascella[2], Claudio Carapelli[2], Alessandra Zombardo[1], Sergio Puccioni[1], Paolo Storchi[1], Rita Perria[1]

[1] *CREA—Council for Agricultural Research and Economics, Research Centre for Viticulture and Enology, Viale Santa Margherita, 80, 52100 Arezzo, Italy*
[2] *Barone Ricasoli S.p.A. Società Agricola, Piazza Goldoni, 2 – 50123 Firenze, Italy*
[3] *University of Cagliari, Department of Life and Environmental Sciences, University Campus, S.P. Monserrato-Sestu Km 0.700, Monserrato, 09042, Cagliari, Italy*
*Corresponding author. E-mail: marco.ammoniaci@crea.gov.it

Abstract. Recent years have been increasingly characterized by the prevalence of extreme weather events due to climate change. Among these events, record-high temperatures and extended periods of drought are challenging the conventional viticulture techniques across many traditional grapevine-producing districts worldwide. The present study analyzes the data recorded over 16 years (2008-2023) in Chianti Classico, a renowned area in Tuscany (Italy) whose economy is based not only on the wine trade but also on the induced effects generated, such as wine tourism. The analysis correlated the historical climate patterns with the analytical profiles of the grapes at harvest. The results highlighted how increasing temperatures lead to an anticipation of the harvest date and, accordingly, a significant variation in grape chemical characteristics. This advance is linked mainly to achieving specific sugar concentrations in relation to the winery's oenological objectives. As a result, organic acids and the phenolic fraction, along with their extractability, play a less decisive role and remain uncontrolled, potentially making the transformation process more challenging to manage.

Keywords: grape quality, time series analysis, ripening trends, Growing Degree Days (GDDs), Sangiovese.

1. INTRODUCTION

The rise in temperatures on land, in the atmosphere, and in the oceans, combined with the retreating of snow and glaciers, which in turn contribute to rising sea levels, makes it hard to deny the phenomenon of global warming (IPCC, 2015). As these changes in the environmental balance challenge the sustainability of agriculture, valuable crops such as grapevines are not spared. Climate change, in fact, poses a risk to the cultivation of this plant in traditional growing areas and to the entire wine sector that depends on

it (Al-Ghussain, 2019; Aydinalp and Cresser, 2008; Ortiz et al., 2021; Reidmiller et al., 2018). *Vitis vinifera* L., with 80 million tonnes produced annually over 7.3 million Hectares is the third most valuable agricultural product worldwide (OIV, 2020). *Vitis vinifera* (L.) is a remarkably resilient species, demonstrating impressive adaptability to extremely different climatic conditions (Duchêne, 2016). This plant, through human intervention (i.e., cultivar and clone selections, grafting, and agricultural practices), has been shaped over the centuries to thrive in different environments. The species of the genus *Vitis* that are of agricultural interest, thanks to their phenotypic plasticity, can be cultivated over a wide range of latitudes (50 °N to 40 °S), in 93 different countries and up to altitudes exceeding 3,000 meters (OIV, 2017; Van Leeuwen et al., 2024).

According to the current predicted possible climatic scenarios, the future is likely to hold a shift in terms of cultivation areas, with new regions becoming suitable for grape cultivation and others potentially at risk of being abandoned (Cameron et al., 2022; de Cortazar Atauri et al., 2017; Duchêne and Schneider, 2005; Van Leeuwen et al., 2019). As the novel climatic conditions move along the described pattern, grapevine phenology is altered, and while the length of the stages tends to remain constant, an anticipation of their occurrence is observed. Numerous studies have examined this phenomenon (Koch and Oehl, 2018; Dalla Marta et al., 2010; Tomasi et al., 2011), correlating climatic data with vine phenological stages across various production areas over the years, arriving at similar conclusions. Since the harvest date is primarily determined by the desired technological maturity of the grapes, climatic changes have resulted in an average advancement of 2-3 weeks in most wine-growing regions compared to past decades.

The current climate change in viticulture also has a strong impact on the vines' physiological behavior during the vegetative season and, consequently, on the biochemical profile of the grapes (Van Leeuwen & Darriet, 2016). As a matter of fact, the vines spend part of the hot season under multiple abiotic stresses, with consequent impact on grape quality, as the latter is strictly linked to the environmental conditions (Drappier et al., 2019; Jackson and Lombard, 1993). An increased cluster exposure to solar radiation and a moderate water deficit can be desirable to boost the accumulation of polyphenols and aromatic compounds in the berries (Rienth et al., 2021; Van Leeuwen et al., 2022; Zarrouk et al., 2016). On the other hand, the adaptation of the plants to irregular hot and dry conditions might result in shrunk canopies and reduced photosynthetic activity, associated with withered clusters, possible sunburn damage and altered grape's analytical profile (Cataldo et al., 2023; De Orduna, 2010; De Rességuier et al., 2023; Keller et al., 2016; Rustioni et al., 2023; Scholasch and Rienth, 2019). In particular, the worst effects of extended exposure of grapes to intense solar radiation and heat are lower acidic profiles, increased sugar accumulation (resulting in higher alcoholic content), and a general decoupling of phenological and technological maturity (Arrizabalaga et al., 2018; Kliewer, 1977; Mori et al., 2007).

Indeed, anthocyanins and sugar accumulation are closely linked during the early stages of ripening, but when the temperature gets over 35 °C, a significant slowdown in the biosynthesis of phenolic substances is often observed (Bergqvist et al., 2001; Gambetta and Kurtural, 2021; Pastore et al., 2017; Spayd et al., 2002). In most cases, when clusters are under intense heat, a delay in the onset of anthocyanin accumulation occurs, but once started, the rate of anthocyanin synthesis and accumulation remains constant (Sadras and Moran, 2012). Because of these unbalanced metabolic processes, when berries are long exposed to extreme temperatures, visible differences in berry size and color may be observed on the opposite sides of the clusters (Castellarin (a), et al., 2007; Castellarin (b), et al., 2007; Hernández-Montes et al., 2021). As the water stress reaches a specific threshold, the plant closes its leaf stomata to prevent damage from excessive water losses, consequently limiting the CO_2 intake and the photosynthetic activity (Flexas et al., 1998; Medrano et al., 2003). As this occurs, sugar accumulation in berries is also impaired (Intrigliolo and Castel, 2010). However, under these conditions, berry growth is severely restricted as well, resulting musts display higher total final sugar concentration (Dai et al., 2009; Gambetta et al., 2020) due to a reduced berry weight. In this condition, to compensate for the energy deficit the plant speeds up the malate metabolism, causing a consumption of malic acid as fuel for the cells. As this happens, total acidity decreases, and pH rises in the musts at harvest (Hewitt et al., 2023; Sweetman et al., 2009; Van Leeuwen et al., 2009). Finally, water deficit may also advance the onset of sugar accumulationGiven the complex responses of *Vitis vinifera* at both plant and fruit levels, accurately assessing future possible scenarios for growing regions is crucial for planning mitigation strategies, as grape and wine production often represent the foundation of many agricultural communities. This study focuses on the shifts in grapevine ripening timing over the past 16 years in Chianti Classico, a key Italian wine district producing an average of 36 million bottles per year and valued at over 1 billion euros (Nesto and Di Savino, 2016). Focusing on Sangiovese, the Tuscan most emblematic variety, this research aims to assess

the impact of rising temperatures on harvest timing and grape quality. By analyzing climatic trends, the findings will provide insights into preserving the distinctive characteristics of Sangiovese and suggest adaptive strategies for sustainable viticulture and enhanced wine production in this prestigious wine-growing area.

2. MATERIALS AND METHODS

2.1. Vineyard conditions

The study was carried out in the Chianti Classico district (Tuscany, Italy), in a 22 ha vineyard (43 ° 23 ‘ 02 “N, 11 ° 26 ‘ 04 “E, 320 meters a.s.l.) of Sangiovese (grafted on 110 Richter rootstock), over a 16-year period, from 2008 to 2023. The vineyard is located at the Barone Ricasoli Farm, the largest winery of the Chianti Classico district, having 240 ha of vineyards, displaying the pedological and climatological characteristics best suited for quality wine production. The farm has undergone several studies over the years, resulting in the creation of a zoning map. Moreover, the vineyard selected is the one closest to the weather control unit and has also been zoned, ensuring that all its soil characteristics are well-documented. The vines of the experimental vineyard are spaced 2.00 m between and 0.80 m within the rows, with parallel NW - SE orientation and an average 6 ° slope. The vines are trained on a vertical shoot positioned trellis, with spur cordon pruning (2 buds per spur, 4 spurs per vine). The soil has a clay-loam texture with high stoniness (up to 40 % limestone fragments) and a high calcium carbonate content (20-30 %). It has moderate water retention capacity, fast internal drainage due to rock fragments, low organic matter and nitrogen content, and a pH of 8.1-8.3. According to WRB classification, it is a Skeletic Calcaric Cambisol (Costantini, 2013).

2.2. Weather data

The area has a predominantly temperate climate with hot-dry summer (Peel et al., 2007), characterized by wet winters and dry summers, with temperatures ranging from warm to extremely hot. During the growing seasons from 2008 to 2023, climate data were collected using an automated control unit (METOS ® by Pessl Instruments) located near the experimental vineyard. The parameters measured included daily maximum temperature (°C), daily average temperature (°C), daily minimum temperature (°C), and daily precipitation (mm), covering the period from April 1 to October 31, the conventional growing season for vines. Based on this data, the Growing Degree Days (GDDs) were calculated using the method described by (Winkler, 1974), with a temperature threshold of 10 °C. Essentially, GDDs represent the cumulative daily temperatures above a certain threshold that support active vine growth during the vegetative season. For each year, the focus was set on the growing period leading up to the Day Of Harvest (DOH, according to the Day-of-year calendar), assessing the GDDs from April 1 to the DOH, which varies in each single vintage (Table 1).

2.3. Grape maturity parameters

Every year, at DOH, 15 samples constituted of 200 berries each were randomly collected in the experimental vineyard and screened to assess the analytical parameters of the grape. Half of the berries were manually pressed, and the obtained juice was analyzed to assess the technological parameters: reducing sugars, pH, and total acidity. Analyses were directly performed on the filtered must samples using Fourier Transform Near-Infrared Spectrometry (FT-NIR) with the WineScan FT 120 system (Foss Italia S.r.l., Italy). All the above-mentioned parameters need to fall into specific ranges dictated by the Chianti Classico D.O.C.G. production regulations, in order to the wine to present the typical sensorial profile and claim the appellation. The second half of the samples were analyzed as described by Ribéreau-Gayon et al. (1965) and Saint Cricq de Gaulejac et al. (1998) to determine phenolic maturity indices: Total Anthocyanins, Extractable Anthocyanins, and the Cellular Maturity Index. All these indices are related to the phenolic composition of the wines allow to evaluate both their quantity and color. In detail, Total Anthocyanins are obtained by analyzing an extract prepared with a highly acidic buffer (pH 1.00) and represent the total anthocya-

Table 1. Harvest day expressed as day of the year (DOH) and reported as conventional month and day, for the period of the years 2008-2023.

Year	2008	2009	2010	2011	2012	2013	2014	2015	2016	2017	2018	2019	2020	2021	2022	2023
DOH	276 10/02	268 09/25	271 09/28	264 09/21	276 10/02	269 09/26	273 09/30	260 09/17	268 09/24	264 09/21	269 09/26	269 09/26	261 09/17	265 09/22	257 09/14	262 09/19

nin content in the berries, expressed in mg/L of must. Extractable Anthocyanins, also expressed in mg/L of must, refer to the amount of anthocyanins measured in an extract obtained with a buffer at pH 3.20, similar to that of the wine. This fraction represents the bulk of pigments that are subject to the technological winemaking process. The Cellular Maturity Index reflects the ability of the berry skin to release anthocyanins and was determined using the following ratio:

$$Cellmaturityindex(\%) = \frac{\text{TotalAnthocyanins} - \text{ExtractableAnthocyanins}}{\text{TotalAnthocyanins}} \times 100$$

Given the structure of the formula, lower index values correspond to a higher proportion of extractable anthocyanins, indicating a more advanced maturity stage.

2.4. Data analysis

The data collected and organized were analysed using the R program (R Core Team, 2023, https://www.R-project.org/) inside RStudio environmental. To evaluate the interactions between both weather and oenological parameters, a statistical analysis was performed using Pearson correlation coefficient (r) and evaluated its p-value. These two values together allow to understand how strong the relationship between two variables is, and whether it is statistically significant. These statistical results are shown within the graphs developed through the graphical tool ggplot2 (Wickham and Wickham, 2016).

3. RESULTS

3.1. Weather conditions

The data processed from the weather station (Table 2) between April 1 and October 31 in 2008-2023 shown an average GDDs accumulation of 1907. The year with the lowest GDDs was 2010, with a total of 1605, while the highest was recorded in 2022, with 2136 GDDs. Over the same period, rainfall averaged 414 mm, with the lowest amount of water fed occurring in 2011 at 213 mm and the highest in 2016 at 586 mm. Events of temperatures dropping below 0 °C after 1st April (after bud burst) occurred in the following years: 2012 (2 days), 2015 (2 days), 2017 (2 days), 2020 (3 days), 2021 (4 days), 2022 (5 days), and 2023 (3 days), with all occurrences happening in the first half of April. The increasing frequency of late frosts after 1st April could increased the risk of damage to the newly sprouted vegetation. Additionally, GDDs data processed specifically from April to harvest day, revealed an average GDDs accumulation of 1692. Lowest annual GDDs over the years occurred in 2010 (1501 GDDs), and the highest was in 2017 (1842 GDDs). Mean precipitation for this period was 301 mm, with the lowest value in 2020 and the highest in 2010 with 135 mm 450 mm respectively. An additional metric of interest for long-term grape analysis was the frequency of days with temperatures exceeding 35 °C, which averaged 17 days per year.

As shown in Figure 1, the correlation between the year and the GDDs from April to October ($r = 0.71$, p-value < 0.01), suggested that, over the years, there had been a significant increase in the heat units accumulated during the growing season. With the rise in temperatures over the years, a direct correlation was observed between the year and the number of days with temperatures exceeding 35 °C ($r = 0.56$, p-value < 0.05). The significant correlation between the year and the DOH was explained by the fact that as the years progressed, the harvest dates occured in advance ($r = -0.65$, p-value < 0.01), indicating a significant tendency. Despite the progressively earlier harvest, which reduced the number of days from April 1 to harvest, GDDs at DOH continued to increase ($r = 0.49$, p-value > 0.05).

Table 2. Climate parameters 2008 - 2023. Growing Degree Days (GDDs) from April 1 to October 31, and from April 1 to the DOH; Rainfall (mm) from April 1 to October 31, and from April 1 to the DOH; Yearly number of days with maximum temperatures exceeding 35 °C (T max > 35 °C).

Year	2008	2009	2010	2011	2012	2013	2014	2015	2016	2017	2018	2019	2020	2021	2022	2023	Average
GDDs from 1 April to 31 October	1763	1883	1605	1880	1917	1749	1748	1959	1877	2064	2076	1975	1913	1904	2136	2070	1907
Rainfall (mm) from 1 April to 31 October	476	411	523	213	474	539	399	429	586	421	417	325	261	219	477	460	414
GDDs from April to DOH	1600	1715	1501	1663	1758	1545	1555	1731	1685	1842	1831	1746	1714	1694	1831	1666	1692
Rainfall (mm) from April to DOH	393	316	450	157	308	304	382	273	435	408	345	247	135	181	199	282	301
Yearly number of days Tmax > 35 °C	9	13	1	12	23	6	0	25	3	40	7	21	19	20	37	31	17
Yearly number of days Tmin < 0 °C	0	0	0	0	2	0	0	5	0	2	0	0	3	4	5	3	1.5

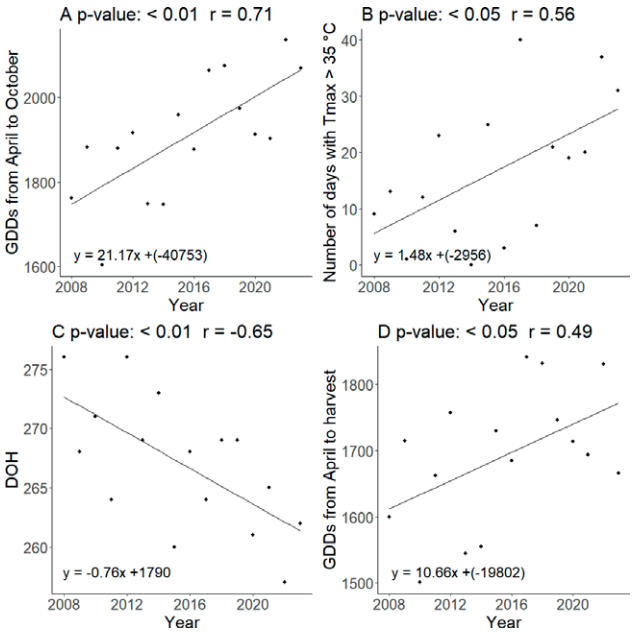

Figure 1. Relationship among Year with Growing Degree Days (GDDs) from April to October (A), number of days with Temperature max > 35 °C (B), day of harvest (DOH) (C) and GDDs from April to harvest (D).

3.2. Berry composition

As shown in Table 3, the oenological parameters obtained from grape samples collected at the DOH presented the following average values: reducing sugars, 234 g/L; pH, 3.27; and total acidity, 6.57 g/L. The year 2011 exhibited notably high levels of reducing sugars and low pH values, while 2016 and 2020 showed high levels of both sugars and pH. In contrast, the 2014 season recorded the lowest mean sugar concentration (209 g/L) and pH (3.13), along with the highest total acidity value (8.30 g/L). On the contrary, the lowest total acidity (5.20 g/L) was observed in 2020. Total Anthocyanin levels averaged 1093 mg/L, while Extractable Anthocyanins averaged 644 mg/L, resulting in a mean extractability of 41 %. Significant variations in anthocyanin levels were observed, with the higher concentrations noted in 2011, 2016, and 2020, while the lower levels were recorded in 2012, 2014, and 2017.

In Figure 2, although the correlation between reducing sugars and DOH was not statistically significant (p value = 0.07), it emerged that reducing sugars decreased as DOH increased, with a near-significant trend. The reducing sugars shown no statistically significant correlations with the other variables considered. A significant negative correlation was found between total acidity and GDDs (r = -0.62, p-value <0.05). For pH, both a positive trend over the years (r = 0.64, p-value <0.01) and with the GDDs (r = 0.55, p-value <0.05) are observed, while a significant negative correlation was found with DOH (r = -0.50, p-value <0.05).

As illustrated in Figure 3, there was no correlation among Total Anthocyanins and the other parameters considered. Anyway, the extractable anthocyanins presented a significant correlation only with the DOH (r = -0.57, p-value <0.05), showing a decrease as this variable increased and indicating that a later harvest reduced the amount of Extractable Anthocyanins. Despite these results, a significant correlation was found between the Cell Maturity Index and DOH (r = 0.51, p-value <0.05), showing an increase with later harvest dates and decreasing GDDs at harvest (r = -0.52, p-value <0.05). This indicated that a late harvest promoted higher cellular maturation, while greater heat accumulation could reduce it.

4. DISCUSSION

The increasing frequency of enduring high temperatures and heat waves determines a growing economic impact on cultivated species, including *Vitis vinifera*.. In the area of investigation, Chianti Classico, a leading wine-growing district in the Italian panorama, the impact on grape quality (reducing sugar, acidity, pH, anthocyanins) in Sangiovese (the main black-berried cultivar in Italy) was evaluated over 16 consecutive growing seasons, from 2008 to 2023. The study here proposed helps to define what the possible future scenarios might be. Results highlight a significant rise in temperatures during the considered growing seasons (GDDs from April 1st to October 31th), with an average of 1649 GDDs from 2008 to 2012, leading to a 8 days advance in the harvest date compared to the period from 2019 to 2023, which had an average of 1729 GDDs. Along with the correlation between years and the increase in GDDs, there is an increase in days with extreme temperatures (>35 °C). To counter this trend, harvest is increasingly anticipated, which helps maintain relatively constant levels of total soluble solids and total phenolics at harvest. On the other hand, late frosts became more frequent after the 1st April , hence, late pruning was carried out to delay the vegetative awakening of the vines, without significantly compromising yield or grape quality (Poni et al., 2022).

Despite, GDDs show a tendency to continue to increase at DOH. This finds justification on the fact that temperature has a controversial effect on plant and cluster's metabolism, where sugar and organic acids are both subject to anabolic and catabolic processes accord-

Table 3. Oenological parameters measured in the grape samples collected from 2008 to 2023. Reducing sugars (g/L), pH, Total acidity (g/L tartaric acid), Total Anthocyanins (mg/L), Extractable Anthocyanins (mg/L), and Cell Maturity Index (%).

Year	Reducing sugars (g/L)	pH	Total acidity (g/L tartaric acid)	Total Anthocyanins (mg/L)	Extractable Anthocyanins (mg/L)	Cell Maturity Index (%)
2008	220	3.20	7.20	1162	516	56
2009	219	3.19	6.30	1199	613	49
2010	235	3.20	6.94	1059	643	45
2011	252	3.21	6.60	1289	891	31
2012	223	3.28	5.98	736	426	42
2013	228	3.22	6.87	1129	585	48
2014	210	3.13	8.30	817	478	41
2015	230	3.26	7.08	1002	659	34
2016	252	3.42	5.74	1583	873	45
2017	251	3.23	6.59	754	593	21
2018	243	3.37	6.49	1123	698	38
2019	238	3.30	6.37	933	565	39
2020	261	3.41	6.41	1359	842	38
2021	232	3.21	6.21	1066	557	48
2022	234	3.46	5.20	1140	678	40
2023	225	3.34	6.92	1112	689	38
Average	235	3.27	6.57	1093	644	41

ingly to the temperature's range. Sugar accumulation is indeed most efficient in the range of 22 - 28 °C but comes to a complete stop when 35 °C is reached (Keller, 2020). Grapes directly exposed to extreme heat and solar radiation may experience a blockage in sugar accumulation, although berries in the shade remain active (Kliewer and Lider, 1968). In general, extreme heat interrupts ripening, slows physiological processes and extends the time required to reach maturity. Rising GDDs at DOH, combined with heat-induced interruptions, complicate ripening management by increasing thermal accumulation during the growing period, disrupting the balance between metabolic and ripening processes. Reducing sugars remain the main decision parameter to start the harvest, as supported by the relatively constant levels over time. This decision, however, often comes at the expense of other analytical parameters of the grapes.

For the above-described earlier occurrence of the date of harvest, a reduction of the total acidity measured on must is observed, when compared with GDDs at DOH. Also measured a higher pH as sun-exposed berries tend to have a significantly lower amount of malate (Kliewer and Lider, 1968; Reynolds et al., 1986). This phenomenon is likely to be caused by the reduced photochemical activity of the plants under heat stress, and the consequent use of malic acid as a source of energy by the plant (Ribéreau-Gayon et al., 2021). These increasing pH levels in the berries are likely to rise further, with potential impacts on the typicity of the final wine, as the number of extreme-heat-days continue to grow.

Concerning total anthocyanins in the musts, final concentrations have shown to remain relatively stable. Is indeed acquired that intense heat may decouple the onset of phenolics and sugar accumulation but, once started, phenolics synthesis might catch up. The lack of association between the total anthocyanin contents and the other parameters detected can be therefore explained by the fact that total phenolic substances are influenced more by genetics rather than by climate except in the case of prohibitive environmental conditions. This fact is supported by other authors who have correlated the phenological stages to a constant amount of GDDs in different grape cultivars (Zapata et al., 2015). In this respect, it was significant to observe that the general trend of grapes harvested earlier produced musts with higher amounts of extractable phenolic compounds due to the possible effects of the intense heat and light exposure on berry tissues. Anthocyanin production peaks at an optimal berry temperature of approximately 30 °C but declines when temperatures exceed 35 °C (Kliewer, 1977; Spayd et al., 2002). Prolonged exposure to excessive heat and excessive light radiation can induce oxidative stress, which not only inhibits anthocyanin synthesis but also contributes to its degradation (Mori et al., 2007). The Cell Maturity

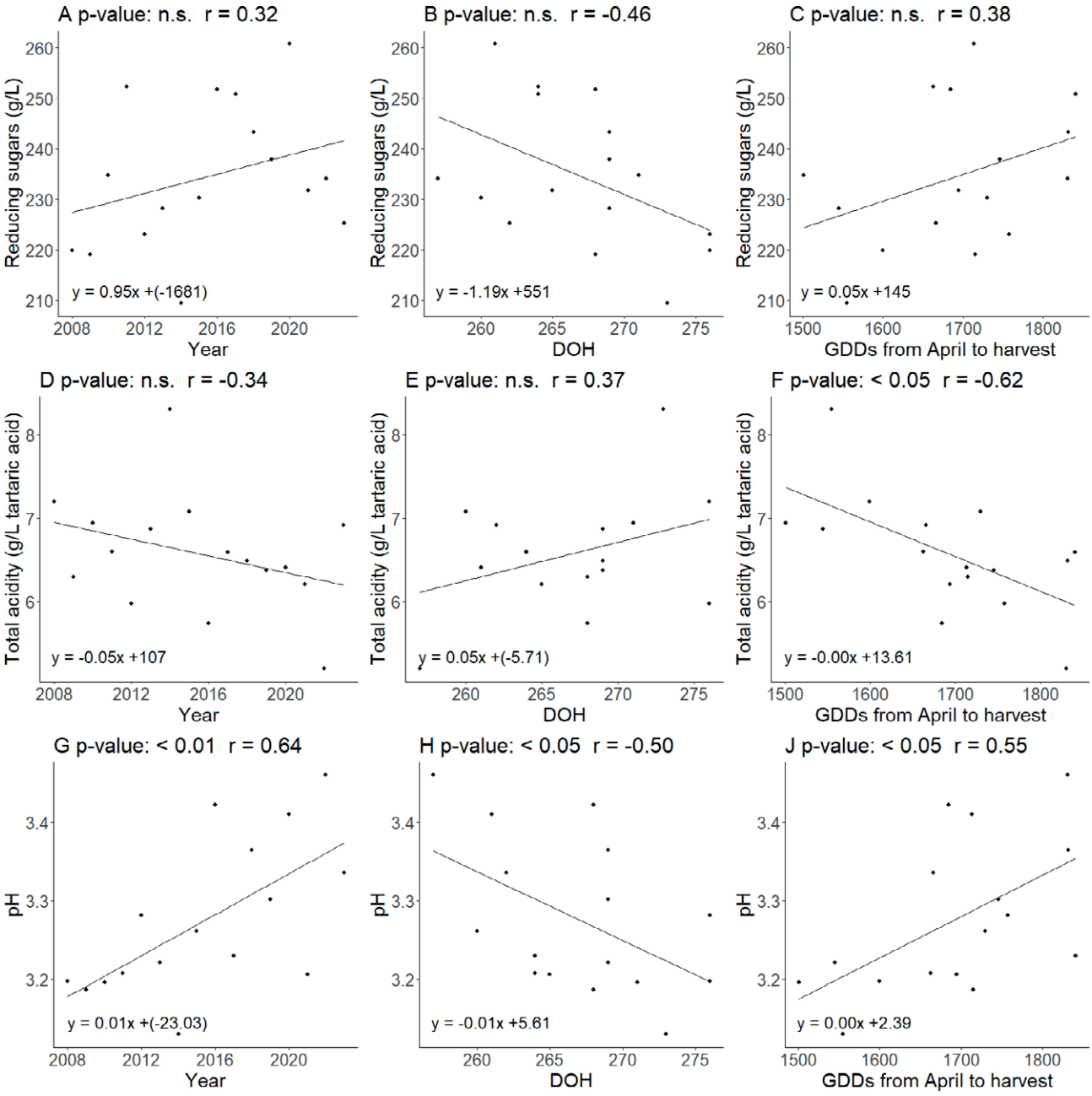

Figure 2. Relationship among reducing sugars (g/L) with year (A day of harvest (DOH) (B), and Growing Degree Days (GDDs) (C) from April to harvest, among total acidity (g/L tartaric acid) with year (D), DOH (E), and GDDs from April to Harvest (F) and among pH with year (G), DOH (H) and GDDs from April to harvest (J).

Index confirms that the percentage of extractable anthocyanins is higher in the grapes harvested earlier. Moreover, the significant correlation between GDDs to harvest highlights the influence of climate on grape maturity. This supports the observation that warmer conditions during the vegetative growth phase led to higher extractable anthocyanin percentages.

5. CONCLUSION

The data collected over a prolonged period, 16 years (2008 – 2023), analyzed in this study allow us to conclude that there is evidence of an overall increase in temperatures during the grapevine growing season, leading, in general, to an earlier harvest date within every year. Events of

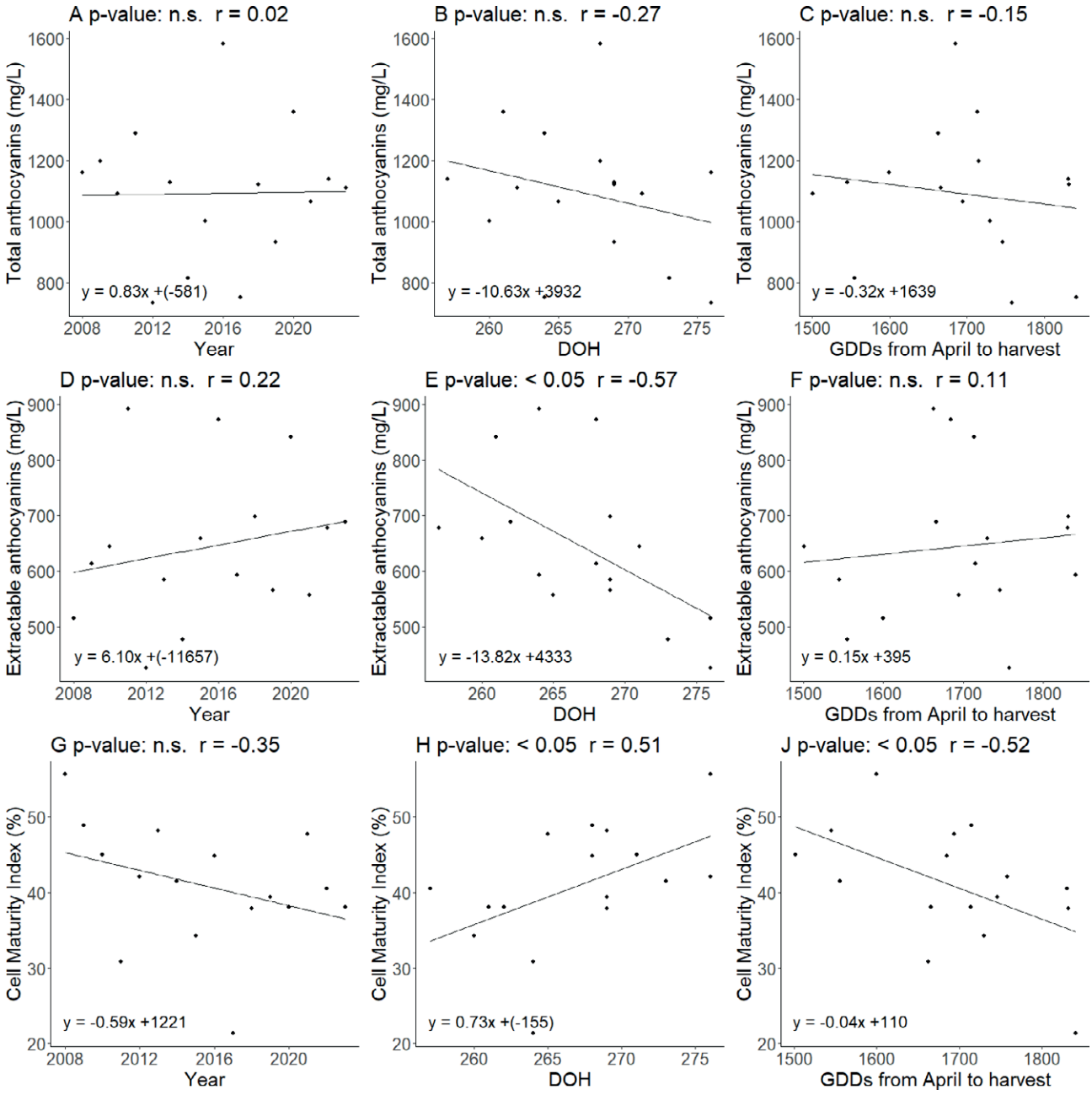

Figure 3. Relationship among total anthocyanins (mg/L) with year (A), day of harvest (DOH) (B), and Growing Degree Days (GDDs) from April to Harvest (C), among extractable anthocyanins (mg/L) with year (D), DOH (E), and GDDs from April to harvest (F) and among Cell Maturity Index (%) with year (G), DOH (H) and GDDs from April to harvest (J).

extreme heat are also occurring with increasing frequency. Sugar level remains the main factor in determining the harvest day for a winery, while total acidity has been decreasing over the years. While the grape total anthocyanin content has not significantly changed over time, the concentrations of extractable anthocyanins increased, likely due to the grapes experiencing more thermal stress.

Advance the harvest impacts the balance of sugars, acidity, and aromas, altering the wines' flavour profile, and at the same time, it brings on logistical and economic challenges, such as managing seasonal labour and adapting production cycles.

Although the advancement of the harvest in response to the accelerated plant's metabolism is main-

ly driven by the need to maintain constant the sugar level, to predict a future scenario remains difficult as extreme-heat-days are also occurring more frequently. As plant physiological processes are an articulated system, and different metabolic pathways get involved in response to combined stresses, is rightful to assume, as one of the possible scenarios, that extreme heat events may prevent further advancements delaying the ripening by halting photochemical activity. This underscores the complex relationship between climate change and agricultural practices, emphasizing the need for sustainable farming methods (e.g., optimized irrigation, canopy management, shading nets, reflective clays) and ongoing research to address these challenges while preserving the wine sector's quality and stability.

ACKNOWLEDGEMENTS

The authors want to thank the property and the technicians of "Barone Ricasoli S.p.A. - Società Agricola" for their support in the experimental activity conducted within the winery vineyards.

REFERENCES

Al-Ghussain, L. (2019). Global warming: review on driving forces and mitigation. *Environmental Progress and Sustainable Energy*, *38*(1), 13–21). John Wiley and Sons Inc. https://doi.org/10.1002/ep.13041

Arrizabalaga, M., Morales, F., Oyarzun, M., Delrot, S., Gomès, E., Irigoyen, J. J., Hilbert, G. & Pascual, I. (2018). Tempranillo clones differ in the response of berry sugar and anthocyanin accumulation to elevated temperature. *Plant Science*, *267*, 74–83. https://doi.org/10.1016/j.plantsci.2017.11.009

Aydinalp, C. & Cresser, M. S. (2008). The effects of global climate change on agriculture. *American-Eurasian Journal of Agricultural & Environmental Sciences*, *3*(5), 672–676.

Bergqvist, J., Dokoozlian, N. & Ebisuda, N. (2001). Sunlight exposure and temperature effects on berry growth and composition of Cabernet Sauvignon and Grenache in the Central San Joaquin Valley of California. *American Journal of Enology and Viticulture*, *52*(1), 1–7. https://doi.org/10.5344/ajev.2001.52.1.1

Cameron, W., Petrie, P. R. & Barlow, E. W. R. (2022). The effect of temperature on grapevine phenological intervals: Sensitivity of budburst to flowering. *Agricultural and Forest Meteorology*, *315*, 108841. https://doi.org/10.1016/j.agrformet.2022.108841

Castellarin, S. D., Matthews, M. A., Di Gaspero, G. & Gambetta, G. A. (2007). Water deficits accelerate ripening and induce changes in gene expression regulating flavonoid biosynthesis in grape berries. *Planta*, *227*, 101–112. https://doi.org/10.1007/s00425-007-0598-8

Castellarin, S. D., Pfeiffer, A., Sivilotti, P., Degan, M., Peterlunger, E. & Di Gaspero, G. (2007). Transcriptional regulation of anthocyanin biosynthesis in ripening fruits of grapevine under seasonal water deficit. *Plant, Cell & Environment*, *30*(11), 1381–1399. https://doi.org/10.1111/j.1365-3040.2007.01716.x

Cataldo, E., Eichmeier, A. & Mattii, G. B. (2023). Effects of Global Warming on Grapevine Berries Phenolic Compounds—A Review. *Agronomy*, *13*(9), 2192.

IPCC, 2014: Climate Change 2014: Synthesis Report. Contribution of Working Groups I, II and III to the Fifth Assessment Report of the Intergovernmental Panel on Climate Change [Core Writing Team, R.K. Pachauri and L.A. Meyer (eds.)]. IPCC, Geneva, Switzerland, 151 pp.

Costantini E.A.C. (ed), 2013. Oltre la zonazione. Beyond zoning. Tre anni di studio al Castello di Brolio / A three years study at Castello di Brolio. Firenze: Edizioni Polistampa.

Dai, Z. W., Vivin, P., Robert, T., Milin, S., Li, S. H. & Génard, M. (2009). Model-based analysis of sugar accumulation in response to source–sink ratio and water supply in grape (Vitis vinifera) berries. *Functional Plant Biology*, *36*(6), 527–540. https://doi.org/10.1071/FP08284

Dalla Marta, A., Grifoni, D., Mancini, M., Storchi, P., Zipoli, G. & Orlandini, S. (2010). Analysis of the relationships between climate variability and grapevine phenology in the Nobile di Montepulciano wine production area. Journal of Agricultural Science, *148*(6), 657–666. https://doi.org/10.1017/S0021859610000432

de Cortazar Atauri, I. G., Duchêne, E., Destrac, A., Barbeau, G., De Rességuier, L., Lacombe, T., Parker, A. K., Saurin, N. & Van Leeuwen, C. (2017). Grapevine phenology in France: from past observations to future evolutions in the context of climate change. *Oeno One*, *51*(2), 115–126. https://doi.org/10.20870/oeno-one.2017.51.2.1622

De Orduna, R. M. (2010). Climate change associated effects on grape and wine quality and production. *Food Research International*, *43*(7), 1844–1855.

De Rességuier, L., Pieri, P., Mary, S., Pons, R., Petitjean, T. & Van Leeuwen, C. (2023). Characterisation of the vertical temperature gradient in the canopy reveals increased trunk height to be a potential adaptation to climate change. *Oeno One*, *57*(1), 41–53. https://doi.org/10.20870/oeno-one.2023.57.1.5365

Drappier, J., Thibon, C., Rabot, A. & Geny-Denis, L. (2019). Relationship between wine composition and temperature: Impact on Bordeaux wine typicity in the context of global warming. *Critical Reviews in Food Science and Nutrition*, *59*(1), 14–30. https://doi.org/10.1080/10408398.2017.1355776

Duchêne, E. (2016). How Can Grapevine Genetics Contribute to the Adaptation to Climate Change? OENO One, 50, 113-124. https://doi.org/10.20870/oeno-one.2016.50.3.98

Duchêne, Eric & Schneider, C. (2005). Grapevine and climatic changes: a glance at the situation in Alsace. *Agronomy for Sustainable Development*, *25*(1), 93–99. https://doi.org/10.1051/agro:2004057

Flexas, J., Escalona, J. M. & Medrano, H. (1998). Down-regulation of photosynthesis by drought under field conditions in grapevine leaves. *Functional Plant Biology*, *25*(8), 893–900. https://doi.org/10.1071/PP98054

Focus, O. I. V. (2017). Distribution of the world's grapevine varieties. *International Organisation of Vine and Wine*, 54.

Gambetta, G. A., Herrera, J. C., Dayer, S., Feng, Q., Hochberg, U. & Castellarin, S. D. (2020). The physiology of drought stress in grapevine: towards an integrative definition of drought tolerance. *Journal of Experimental Botany*, *71*(16), 4658–4676. https://doi.org/10.1093/jxb/eraa245

Gambetta, G. A. & Kurtural, S. K. (2021). Global warming and wine quality: are we close to the tipping point? *Oeno One*, *55*(3), 353–361. https://doi.org/10.20870/oeno-one.2021.55.3.4774

Hernández-Montes, E., Zhang, Y., Chang, B.-M., Shcherbatyuk, N. & Keller, M. (2021). Soft, sweet, and colorful: Stratified sampling reveals sequence of events at the onset of grape ripening. *American Journal of Enology and Viticulture*, *72*(2), 137–151. https://doi.org/10.5344/ajev.2020.20050

Hewitt, S., Hernández-Montes, E., Dhingra, A. & Keller, M. (2023). Impact of heat stress, water stress, and their combined effects on the metabolism and transcriptome of grape berries. *Scientific Reports*, *13*(1), 9907. https://doi.org/10.1038/s41598-023-36160-x

Intrigliolo, D. S. & Castel, J. R. (2010). Response of grapevine cv.'Tempranillo'to timing and amount of irrigation: water relations, vine growth, yield and berry and wine composition. *Irrigation Science*, *28*, 113–125. https://doi.org/10.1007/s00271-009-0164-1

Jackson, D. I. & Lombard, P. B. (1993). Environmental and management practices affecting grape composition and wine quality-a review. *American Journal of Enology and Viticulture*, *44*(4), 409–430. https://doi.org/10.5344/ajev.1993.44.4.409

Keller, M. (2020). *The science of grapevines*. Academic press.

Keller, M., Romero, P., Gohil, H., Smithyman, R. P., Riley, W. R., Casassa, L. F. & Harbertson, J. F. (2016). Deficit irrigation alters grapevine growth, physiology, and fruit microclimate. *American Journal of Enology and Viticulture*, *67*(4), 426–435. https://doi.org/10.5344/ajev.2016.16032

Kliewer, W. M. (1977). Effect of high temperatures during the bloom-set period on fruit-set, ovule fertility, and berry growth of several grape cultivars. *American Journal of Enology and Viticulture*, *28*(4), 215–222. https://doi.org/10.5344/ajev.1977.28.4.215

Kliewer, W. M. & Lider, L. A. (1968). Influence of cluster exposure to the sun on the composition of Thompson Seedless fruit. *American Journal of Enology and Viticulture*, *19*(3), 175–184. https://doi.org/10.5344/ajev.1968.19.3.175

Koch, B. & Oehl, F. (2018). Climate Change Favors Grapevine Production in Temperate Zones. *Agricultural Sciences*, *9*(3), 247–263. https://doi.org/10.4236/as.2018.93019

Medrano, H., Escalona, J. M., Cifre, J., Bota, J. & Flexas, J. (2003). A ten-year study on the physiology of two Spanish grapevine cultivars under field conditions: effects of water availability from leaf photosynthesis to grape yield and quality. *Functional Plant Biology*, *30*(6), 607–619. https://doi.org/10.1071/FP02110

Mori, K., Goto-Yamamoto, N., Kitayama, M. & Hashizume, K. (2007). Loss of anthocyanins in red-wine grape under high temperature. *Journal of Experimental Botany*, *58*(8), 1935–1945. https://doi.org/10.1093/jxb/erm055

Nesto, B. & Di Savino, F. (2016). *Chianti Classico: The Search for Tuscany's Noblest Wine*. (Univ of California Press, Ed.).

Ortiz, A. M. D., Outhwaite, C. L., Dalin, C. & Newbold, T. (2021). A review of the interactions between biodiversity, agriculture, climate change, and international trade: research and policy priorities. *One Earth*, *4*(1), 88–101. https://doi.org/10.1016/j.oneear.2020.12.008

Pastore, C., Dal Santo, S., Zenoni, S., Movahed, N., Allegro, G., Valentini, G., Filippetti, I. & Tornielli, G. B. (2017). Whole plant temperature manipulation affects flavonoid metabolism and the transcriptome of grapevine berries. *Frontiers in Plant Science*, *8*, 929. https://doi.org/10.3389/fpls.2017.00929

Peel, M. C., Finlayson, B. L. & Mcmahon, T. A. (2007). Hydrology and Earth System Sciences Updated world map of the Köppen-Geiger climate classification. In *Hydrol. Earth Syst. Sci* (Vol. 11). www.hydrol-earth-syst-sci.net/11/1633/2007/

Poni, S., Sabbatini, P. & Palliotti, A. (2022). Facing spring frost damage in grapevine: recent developments and the role of delayed winter pruning–a review. *American Journal of Enology and Viticulture*, *73*(4), 211–226. https://doi.org/10.5344/ajev.2022.22011

Reidmiller, D. R., Avery, C. W., Easterling, D. R., Kunkel, K. E., Lewis, K. L. M., Maycock, T. K. & Stewart, B. C. (Eds.). (2018). *Impacts, Risks, and Adaptation in the United States: The Fourth National Climate Assessment, Volume II*. https://doi.org/10.7930/NCA4.2018

Reynolds, A. G., Pool, R. M. & Matiick, L. R. (1986). Influence of cluster exposure on fruit composition and wine quality of Seyval blanc grapes. *Vitis*, *25*, 85–95. https://doi.org/10.5073/vitis.1986.25.85-95

Ribéreau-Gayon, P., Glories, Y., Maujean, A. & Dubourdieu, D. (2021). *Handbook of Enology, volume 2: The chemistry of wine stabilization and treatments*. John Wiley & Sons.

Rienth, M., Vigneron, N., Darriet, P., Sweetman, C., Burbidge, C., Bonghi, C., Walker, R. P., Famiani, F. & Castellarin, S. D. (2021). Grape Berry Secondary Metabolites and Their Modulation by Abiotic Factors in a Climate Change Scenario–A Review. In *Frontiers in Plant Science* (Vol. 12). Frontiers Media S.A. https://doi.org/10.3389/fpls.2021.643258

Rustioni, L., Altomare, A., Shanshiashvili, G., Greco, F., Buccolieri, R., Blanco, I., Cola, G. & Fracassetti, D. (2023). Microclimate of grape bunch and sunburn of white grape berries: effect on wine quality. *Foods*, *12*(3), 621.

Sadras, V. O. & Moran, M. A. (2012). Elevated temperature decouples anthocyanins and sugars in berries of Shiraz and Cabernet Franc. *Australian Journal of Grape and Wine Research*, *18*(2), 115–122. https://doi.org/10.1111/j.1755-0238.2012.00180.x

Scholasch, T. & Rienth, M. (2019). Review of water deficit mediated changes in vine and berry physiology: consequences for the optimization of irrigation strategies. *Oeno One*. https://doi.org/10.20870/oeno-one.2019.53.3.2407

Spayd, S. E., Tarara, J. M., Mee, D. L. & Ferguson, J. C. (2002). Separation of sunlight and temperature effects on the composition of Vitis vinifera cv. Merlot berries. *American Journal of Enology and Viticulture*, *53*(3), 171–182. https://doi.org/10.5344/ajev.2002.53.3.171

Sweetman, C., Deluc, L. G., Cramer, G. R., Ford, C. M. & Soole, K. L. (2009). Regulation of malate metabolism in grape berry and other developing fruits. *Phytochemistry*, *70*(11–12), 1329–1344. https://doi.org/10.1016/j.phytochem.2009.08.006

Tomasi, D., Jones, G. V, Giust, M., Lovat, L. & Gaiotti, F. (2011). Grapevine phenology and climate change: relationships and trends in the Veneto region of Italy for 1964–2009. *American Journal of Enology and Viticulture*, *62*(3), 329–339. https://doi.org/10.5344/ajev.2011.10108

O.I.V. (2020). *2020 Wine production—OIV first estimates*. International Organisation of Vine and Wine Paris.

Van Leeuwen, C., Barbe, J. C., Darriet, P., Destrac-Irvine, A., Gowdy, M., Lytra, G., Marchal, A., Marchand, S., Plantevin, M., Poitou, X., Pons, A. & Thibon, C. (2022). Aromatic maturity is a cornerstone of terroir expression in red wine. *Oeno One*, *56*(2), 335–351. https://doi.org/10.20870/oeno-one.2022.56.2.5441

Van Leeuwen, C. & Darriet, P. (2016). The Impact of Climate Change on Viticulture and Wine Quality. *Journal of Wine Economics*, *11*(1), 150–167. https://doi.org/10.1017/jwe.2015.21

Van Leeuwen, C., Destrac-Irvine, A., Dubernet, M., Duchêne, E., Gowdy, M., Marguerit, E., Pieri, P., Parker, A., De Resseguier, L. & Ollat, N. (2019). An update on the impact of climate change in viticulture and potential adaptations. *Agronomy*, *9*(9), 514. https://doi.org/10.3390/agronomy9090514

Van Leeuwen, C., Sgubin, G., Bois, B., Ollat, N., Swingedouw, D., Zito, S. & Gambetta, G. A. (2024). Climate change impacts and adaptations of wine production. *Nature Reviews Earth & Environment*, *5*(4), 258–275. https://doi.org/10.1038/s43017-024-00521-5

Van Leeuwen, C., Trégoat, O., Choné, X., Bois, B., Pernet, D. & Gaudillère, J.-P. (2009). Vine water status is a key factor in grape ripening and vintage quality for red Bordeaux wine. How can it be assessed for vineyard management purposes? *Oeno One*, *43*(3), 121–134. https://doi.org/10.20870/oeno-one.2009.43.3.798

Wickham, H. & Wickham, H. (2016). *Data analysis*. Springer.

Winkler, A. J. (1974). *General viticulture*. University of California Press.

Zapata, D., Salazar, M., Chaves, B., Keller, M. & Hoogenboom, G. (2015). Estimation of the base temperature and growth phase duration in terms of thermal time for four grapevine cultivars. *International Journal of Biometeorology*, *59*, 1771–1781. https://doi.org/10.1007/s00484-015-0985-y

Zarrouk, O., Brunetti, C., Egipto, R., Pinheiro, C., Genebra, T., Gori, A., Lopes, C. M., Tattini, M. & Chaves, M. M. (2016). Grape ripening is regulated by deficit irrigation/elevated temperatures according to cluster position in the canopy. *Frontiers in Plant Science*, *7*, 1640. https://doi.org/10.3389/fpls.2016.01640

RIGOROUS PEER REVIEW
Each submission to IJAm is subject to a rigorous quality control and peer-review evaluation process before receiving a decision. The initial in-house quality control check deals with issues such as competing interests; ethical requirements for studies involving human participants or animals; financial disclosures; full compliance with IJAm's data availability policy, etc.
Submissions may be returned to authors for queries, and will not be seen by our Editorial Board or peer reviewers until they pass this quality control check.
Each paper is subjected to critical evaluation and review by Field Editors with specific expertise in the different areas of interest and by the members of the international Editorial Board.

OPEN ACCESS POLICY
The Italian Journal of Agrometeorology provides immediate open access to its content. Our publisher, Firenze University Press at the University of Florence, complies with the Budapest Open Access Initiative definition of Open Access: By "open access", we mean the free availability on the public internet, the permission for all users to read, download, copy, distribute, print, search, or link to the full text of the articles, crawl them for indexing, pass them as data to software, or use them for any other lawful purpose, without financial, legal, or technical barriers other than those inseparable from gaining access to the internet itself. The only constraint on reproduction and distribution, and the only role for copyright in this domain is to guarantee the original authors with control over the integrity of their work and the right to be properly acknowledged and cited. We support a greater global exchange of knowledge by making the research published in our journal open to the public and reusable under the terms of a Creative Commons Attribution 4.0 International Public License (CC-BY-4.0). Furthermore, we encourage authors to post their pre-publication manuscript in institutional repositories or on their websites prior to and during the submission process and to post the Publisher's final formatted PDF version after publication without embargo. These practices benefit authors with productive exchanges as well as earlier and greater citation of published work.

COPYRIGHT NOTICE
Authors who publish with IJAm agree to the following terms:
Authors retain the copyright and grant the journal right of first publication with the work simultaneously licensed under a Creative Commons Attribution 4.0 International Public License (CC-BY-4.0) that allows others to share the work with an acknowledgment of the work's authorship and initial publication in IJAm.
Authors are able to enter into separate, additional contractual arrangements for the non-exclusive distribution of the journal's published version of the work (e.g., post it to an institutional repository or publish it in a book), with an acknowledgment of its initial publication in this journal.
Authors are allowed and encouraged to post their work online (e.g., in institutional repositories or on their website) prior to and during the submission process, as it can lead to productive exchanges, as well as earlier and greater citation of published work (See The Effect of Open Access).

PUBLICATION FEES
Unlike many open-access journals, the Italian Journal of Agrometeorology does not charge any publication fee.

WAIVER INFORMATION
Fee waivers do not apply at Firenze University Press because our funding does not rely on author charges.

PUBLICATION ETHICS
Responsibilities of IJAm's editors, reviewers, and authors concerning publication ethics and publication malpractice are described in IJAm's Guidelines on Publication Ethics.

CORRECTIONS AND RETRACTIONS
In accordance with the generally accepted standards of scholarly publishing, IJAm does not alter articles after publication: "Articles that have been published should remain extant, exact and unaltered to the maximum extent possible". In cases of serious errors or (suspected) misconduct IJAm publishes corrections and retractions (expressions of concern).

Corrections
In cases of serious errors that affect or significantly impair the reader's understanding or evaluation of the article, IJAm publishes a correction note that is linked to the published article. The published article will be left unchanged.

Retractions
In accordance with the "Retraction Guidelines" by the Committee on Publication Ethics (COPE) IJAm will retract a published article if:
- there is clear evidence that the findings are unreliable, either as a result of misconduct (e.g. data fabrication) or honest error (e.g. miscalculation)
- the findings have previously been published elsewhere without proper crossreferencing, permission or justification (i.e. cases of redundant publication)
- it turns out to be an act of plagiarism
- it reports unethical research.
- An article is retracted by publishing a retraction notice that is linked to or replaces the retracted article. IJAm will make any effort to clearly identify a retracted article as such.

If an investigation is underway that might result in the retraction of an article IJAm may choose to alert readers by publishing an expression of concern.

ARCHIVING
IJAm and Firenze University Press are experimenting a National legal deposition and long-term digital preservation service.

SUBMITTING TO IJAm
Submissions to IJAm are made using FUP website. Registration and access are available at: https://riviste.fupress.net/index.php/IJAm/submission
For more information about the journal and guidance on how to submit, please see https://riviste.fupress.net/index.php/IJAm/index

Principal Contact
Simone Orlandini, University of Florence
simone.orlandini@unifi.it

Support Contact
Alessandro Pierno, Firenze University Press
alessandro.pierno@unifi.it

GUIDE FOR AUTHORS
1. Manuscript should refer to original researches, not yet published except in strictly preliminary form.
2. Articles of original researches findings are published in Italian Journal of Agrometeorology (IJAm), subsequent to critical review and approval by the Editorial Board. External referees could be engaged for particular topics.
3. Three types of paper can be submitted: original paper, review, technical note. Manuscript must be written in English. All pages and lines of the manuscript should be numbered.
4. First Name, Last Name, position, affiliation, mail address, telephone and fax number of all the Co-Authors are required. Corresponding Authors should be clearly identified.
5. The abstract should be no longer than 12 typed lines.
6. Full stop, not comma, must be used as decimal mark (e.g. 4.33 and not 4,33).
7. Figures, tables, graphs, photos and relative captions should be attached in separate files. All images must be vector or at least 300 effective ppi/dpi to ensure quality reproduction.
8. Captions should be written as: Fig. x – Caption title, Tab. x – Caption title. Images should be referred to in the text as (Fig. x), (Tab. x).
9. Proof of the paper (formatted according to the Journal style) will be sent to the Corresponding Author for proof reading just one time. Corrections can be made only to typographical errors.
10. All the references in the text must be reported in the "References" section and vice-versa. In the text, only the Author(s) last name must be present, without the name or the first letter of the name (e.g. "Rossi, 2003" and not "Federico Rossi, 2003" or "F. Rossi, 2003"). If two authors are present, refer to them as: "Bianchi and Rossi, 2003" in the text (do not use "&" between the surnames). If more than two Authors are present, refer to them as: "Bianchi et al., 2003" in the text.
For journals, references must be in the following form:
Bianchi R., Colombo B., Ferretti N., 2003. Title. Journal name, number: pages.
For books:
Bianchi R., Colombo B., Ferretti N., 2003. Book title. Publisher, publishing location, total number of pages pp.
Manuscripts "in press" can be cited.

BECOME A REVIEWER
Peer review is an integral part of the scholarly publishing process. By registering as a reviewer, you are supporting the academic community by providing constructive feedback on new research, helping to ensure both the quality and integrity of published work in your field. Once registered, you may be asked to undertake reviews of scholarly articles that match your research interests. Reviewers always have the option to decline an invitation to review and we take care not to overburden our reviewers with excessive requests.
You must login before you can become a reviewer.
If you don't want to be a reviewer anymore, you can change your roles by editing your profile.

COMPETING INTERESTS
You should not accept a review assignment if you have a potential competing interest, including the following:
- Prior or current collaborations with the author(s)
- You are a direct competitor
- You may have a known history of antipathy with the author(s)
- You might profit financially from the work

Please inform the editors or journal staff and recuse yourself if you feel that you are unable to offer an impartial review.
When submitting your review, you must indicate whether or not you have any competing interests.

Italian Journal of Agrometeorology

Rivista Italiana di Agrometeorologia

n. 2 – 2025

Table of contents